

Molecular mechanisms regulating neurogenesis in the developing mouse cerebral cortex

PhD Thesis

Fakultät für Biologie
der Ludwig-Maximilians-Universität München

Prepared at the Helmholtz Center Munich
German Research Center for Environmental Health (GmbH) – Institute of Stem
Cell Research in the group of Prof. Dr. Magdalena Götz

Luisa Pinto
Munich, August 2008

Examiners of the thesis

1. Prof. Dr. Magdalena Götz
2. Prof. Dr. Mark Hübener
3. Prof. Dr. Benedikt Grothe
4. PD. Dr. Angelika Böttger

The thesis was submitted in the 14th of August, 2008

The day of oral examination was in the 28th of November, 2008

1 Table of content

1	Table of content	2
2	Abstract	9
3	Introduction	11
3.1	Progenitor cells and neuron production in the CNS	11
3.1.1	Population heterogeneity in CNS development	11
3.1.2	Forebrain development and regionalization	12
3.1.3	Radial glia progenitors in the forebrain	13
3.1.4	Radial glial cells as committed progenitors	15
3.1.5	Generation of neurons from two different types of progenitors ..	16
3.1.6	Neuronal production timing and specification during brain development	18
3.1.7	Transcriptional regulators of cell fate in the developing forebrain	19
3.1.8	Isolation of functionally distinct progenitor subsets by FACS ...	20
3.1.9	Adult neurogenesis from astroglia in mammals	21
3.2	The transcription factor AP2 γ	23
3.2.1	AP2 family of transcription factors	23
3.2.2	Expression and functions of AP2 γ in the developing and adult mouse	24
4	Abbreviations	26
5	Material and Methods	28
5.1	Animals	28
5.2	Genotyping of mice	28
5.3	Fixation of mouse brains and cryosections	29
5.4	Immunostaining	30
5.5	<i>In situ</i> hybridization	31
5.6	Cell culture	31
5.6.1	Cortex dissection and dissociation	31
5.6.2	Clonal analysis and overexpression <i>in vitro</i>	32
5.6.3	Neurospheres cultures	32
5.6.4	Dual-luciferase reporter assay	33
5.7	Fluorescence activated cell Sorting (FACS) and cell cycle analysis ...	33

5.8	RNA isolation and microarray analysis	34
5.9	Molecular biology	36
5.9.1	Plasmids and viral production	36
5.9.2	Transformation into chemically competent E.coli	38
5.9.3	DNA-purification	38
5.9.4	DNA restriction digest	39
5.9.5	Vector dephosphorylation	39
5.9.6	Ligation	39
5.10	PCR	39
5.11	cDNA synthesis and real-time PCR analysis	40
5.12	<i>In vivo</i> injections	40
5.12.1	<i>In utero</i> injections	40
5.12.2	Beads injections	41
5.13	BrdU labelling <i>in vivo</i>	41
5.14	Data analysis	41
5.14.1	Quantification of fluorescence intensity at the confocal microscope	41
5.14.2	Clonal analysis	42
5.14.3	Quantification of PH3-positive cells	42
5.14.4	Interkinetic nuclear migration quantifications	42
5.14.5	Cortical neuronal layers measurements	42
5.14.6	Statistics	43
5.15	Materials	43
5.15.1	Kits	43
5.15.2	Medium	43
5.15.3	Primers	43
5.15.4	Plasmids and vectors	46
5.15.5	Primary antibodies	47
5.15.6	Secondary antibodies	47
5.15.7	Solutions	48
6	Results	49
6.1	Lineage analysis at the transcriptome level – new insights into functionally distinct radial glial subtypes	49
6.1.1	Separation of distinct radial glia-derived lineages	49

6.1.2	Prospective isolation of distinct radial glia progenitor subtypes .	51
6.1.3	Transcriptome analysis of distinct radial glial lineages	53
6.1.4	Transcriptome analysis of distinct radial glial subtypes	55
6.1.5	Clustering analysis of differential gene expression in subtypes of E14 radial glial cells	58
6.1.5.1	GFP ^{low} /prominin+ enriched mRNAs	58
6.1.5.2	GFP ^{high} /prominin+ enriched mRNAs	59
6.1.6	Cell surface genes identified for distinct radial glial subtypes ...	59
6.1.7	Summary of the transcriptome and lineage of distinct radial glia subsets isolated at mid-neurogenesis	60
6.1.8	Characterization of cortical radial glial cells at the end of neurogenesis	61
6.1.9	Comparison of primary radial glial subsets with radial glia derived from embryonic stem cells	63
6.2	Expression and function of the transcription factor AP2 γ in a subset of cortical radial glia	64
6.2.1	AP2 γ expression in the developing and adult mouse cerebral cortex	64
6.2.2	AP2 γ expression in the adult mouse brain	65
6.2.3	AP2 γ expression in the primate and human cortex	66
6.2.4	AP2 γ deletion in the developing cortex causes decrease in the number of neurons and misspecification of basal, but not apical progenitors at mid-neurogenesis	67
6.2.5	Transcriptome analysis of AP2 γ ^{-/-} cortices at mid-neurogenesis	70
6.2.6	Cell death of basal progenitors in the AP2 γ ^{-/-} cortex	73
6.2.7	Defects in neuron generation and basal progenitor specification in the AP2 γ ^{-/-} cortex at the end of neurogenesis	73
6.2.8	AP2 γ deletion reduces upper layer neuron generation	74
6.2.9	Defects in layers II/III callosal projection neurons in the adult AP2 γ ^{-/-} occipital cortex	76
6.2.10	Functional defects in visual acuity in the AP2 γ ^{-/-} mice	77
6.2.11	AP2 γ overexpression increases the generation of basal progenitors	78
6.2.12	Molecular mechanisms regulating AP2 γ in the cortex	80

7	Figures and Tables	82
	Figure 1: Subtypes of progenitors present in the embryonic mammalian cortex during development	83
	Figure 2: Distinct subsets of radial glial cells in the dorsal and ventral telencephalon	85
	Figure 3: Astrocytic heterogeneity in the adult mammalian brain	86
	Figure 4: Schematic representation of the genomic fragment and protein structure of the transcription factor AP2 γ	87
	Figure 5: FACS isolation and clonal analysis of distinct radial glia-derived lineages	88
	Figure 6: Neurospheres forming capacity of distinct radial glia-derived lineages .	90
	Figure 7: Isolation and characterization of distinct radial glial subsets	91
	Figure 8: Generation of Tbr2-positive clones by distinct subsets of radial glial cells	93
	Figure 9: RT-PCR analysis of differentially expressed genes between distinct subsets of radial glia	94
	Figure 10: Summary of the transcriptome of GFP+(high and low) and GFP+(high and low)/prominin+ sorted cells	96
	Figure 11: <i>In situ</i> hybridization of mRNAs with differential expression levels in the GFP ^{high} /GFP ^{low} and GFP/prominin double positive radial glia subsets	97
	Figure 12: Hierarchical clustering of overlapping genes differentially expressed between GFP ^{high} /GFP ^{low} fractions and GFP/prominin double positive fractions isolated from E14 cortex	98
	Figure 13: Prospective isolation of neurogenic radial glia from E14 cortex by staining of p75, CD83 and Flrt2 cell surface markers.....	99
	Figure 14: Summary of the lineage analysis of GFP+(high and low) and GFP+(high and low)/prominin+ sorted cells	100
	Figure 15: Characterization of cortical radial glial cells at the end of neurogenesis (E18)	101
	Figure 16: Hierarchical clustering of genes differentially expressed between E18 GFP+/prominin+ and E14 GFP/prominin radial glia subsets	102
	Figure 17: <i>In situ</i> hybridization of mRNAs with differential expression levels between E18 GFP+ and E14 GFP+ fractions of sorted cells	103

Figure 18: Comparison of the expression profile of ES cell-derived radial glia and subsets of radial glia sorted at different developmental stages	104
Figure 19: AP2 γ expression in the mouse brain	105
Figure 20: AP2 γ expression in the adult mouse brain	106
Figure 21: AP2 γ expression in the adult neural stem cells in the SEZ and their progeny in the olfactory bulb (OB).....	107
Figure 22: AP2 γ expression in the E80 primate cortex	108
Figure 23: AP2 γ expression in the human occipital cortex at 20-22 gestational weeks	109
Figure 24: AP2 γ deletion by Emx1::Cre in the mouse cerebral cortex	110
Figure 25: Neuron and progenitor identity in the AP2 γ ^{-/-} cortex at E12	111
Figure 26: Apical progenitor identity in the cerebral cortex of AP2 γ ^{-/-} mice at mid-neurogenesis (E14)	112
Figure 27: Neuron defects in the cerebral cortex of AP2 γ ^{-/-} mice at E14	113
Figure 28: Cell division defects and misspecification of basal progenitors in the AP2 γ ^{-/-} cortex at E14	114
Figure 29: Interkinetic nuclear migration in the AP2 γ ^{-/-} cortex at E14	116
Figure 30: Heat map representing the genes significantly regulated between E14 WT and AP2 γ ^{-/-} cortices at intermediate-caudal regions	117
Figure 31: Transcriptome analysis and basal progenitor defects in the AP2 γ ^{-/-} cortex at E14	118
Figure 32: Cell death of basal progenitors in the AP2 γ ^{-/-} cortex at E14	119
Figure 33: Neuron and progenitor identity in the AP2 γ ^{-/-} cortex at the end of neurogenesis (E17)	120
Figure 34: Neurogenesis in the cerebral cortex of AP2 γ ^{-/-} mice	121
Figure 35: Upper layer neuron defects in the adult AP2 γ ^{-/-} cortex	123
Figure 36: Defects in layers II/III callosal projection neurons in the adult AP2 γ ^{-/-} cortex	124
Figure 37: Bead injections in the occipital cortex of adult AP2 γ ^{-/-} mice	125
Figure 38: Visual performance of WT and AP2 γ ^{-/-} adult mice	126
Figure 39: AP2 γ overexpression of E14 cortical cells <i>in vitro</i>	127
Figure 40: AP2 γ overexpression <i>in vivo</i> in the developing cortex	128
Figure 41: Upstream and downstream targets of AP2 γ in the developing cortex	129
Figure 42: Regulation of AP2 γ by Mash1 and Ngn2 in the developing cortex ...	130

Figure 43: Molecular mechanisms regulating AP2 γ in the cortex	131
Table 1: Differentially expressed genes between subsets of radial glia excluding and including their progeny	132
Table 2: mRNAs differentially expressed in the GFP ^{low/high} but absent in the GFP/Prominin sorted cells	136
Table 3a: mRNAs differentially expressed in the GFP ^{low} but absent in the GFP ^{low} /Prominin sorted cells	137
Table 3b: mRNAs differentially expressed in the GFP ^{high} but absent in the GFP ^{high} /Prominin sorted cells	138
Table 4: Cell surface genes significantly expressed in the distinct subsets of radial glial cells	139
Table 5: Differentially expressed genes between subsets of radial glia at mid-neurogenesis and radial glia at the end of neurogenesis	140
Table 6: Transcriptome analysis of E14 WT and AP2 γ ^{-/-} cortices	144
Table 7: Visual performance of adult WT and AP2 γ ^{-/-} mice	146
8 Discussion	147
8.1 Lineage analysis at the transcriptome level – new insights into functionally distinct radial glial subtypes	147
8.1.1 Novel insights into radial glial lineages in the developing cortex – direct versus indirect neurogenesis	148
8.1.2 Molecular mechanisms regulating direct versus indirect neurogenesis in the developing cortex	149
8.1.3 Radial glial subsets are comparable to ES cell derived radial glia	151
8.1.4 Novel insights into the transcriptome of distinct radial glial lineages at mid-neurogenesis	152
8.1.4.1 Transcripts enriched in the subset of radial glia directly generating neurons	152
8.1.4.2 Transcripts enriched in the largely self-renewing radial glial subset	153
8.1.4.3 Novel transcripts expressed in both radial glial lineages during development and maintained in the progenitors of the adult brain	155
8.1.5 Novel insights into transcriptional changes in radial glial cells at	

	the end of neurogenesis	156
8.2	Expression and function of the transcription factor AP2 γ in a subset of cortical radial glia	158
	8.2.1 The role of AP2 γ in the specification and cell survival of basal progenitors	158
	8.2.2 Maintenance of the embryonic lineage of progenitors expressing AP2 γ in the adult brain	160
	8.2.3 AP2 γ -/- phenotype reveals specific molecular program for upper layer neuron generation	161
	8.2.4 AP2 γ acts in a region-specific manner in the cortex	162
	8.2.5 Functional relevance of the regulation of upper layer neuron numbers by AP2 γ	163
	8.2.6 Phylogenetic considerations on the regulation of upper layer neurons by AP2 γ	165
9	References	167
10	Acknowledgements	182
11	Curriculum vitae	183

2 Abstract

Radial glial cells are a widespread non-neuronal cell type in the developing central nervous system (CNS) of all vertebrates. In the cortex, distinct subsets of radial glial cells coexist that are either multipotent or specified towards the generation of neurons or glial cells (Malatesta et al., 2000). Radial glial cells in the cerebral cortex are also the source of a second type of neurogenic progenitors, called basal progenitors. However, whether the generation of basal progenitors occurs in a stochastic manner or whether a specific lineage of radial glial cells is specified towards the generation of these progenitors has not been previously known. To identify functionally distinct lineages of cortical radial glial cells, I developed a new strategy using fluorescence-activated cell sorting (FACS) to isolate them and study their progeny. I isolated radial glial cells by FACS from a transgenic mouse line in which green fluorescent protein (GFP) expression is under the control of the human GFAP promoter. Strikingly, GFP intensity was correlated with cell fate. Selective enrichment of cells with a higher GFP intensity separated a largely non-neurogenic from a neurogenic (low GFP-intensity) subsets of radial glial cells. Notable differences on the progeny of these distinct sets of radial glia were found. The neurogenic radial glial cells subset generated neurons directly and those that are largely non-neurogenic also gave rise to a small proportion of Tbr2-positive basal progenitors that are then neurogenic. Thus, this last subset comprises an indirect neurogenic population of radial glial cells present in the developing cortex. Microarray analysis of these distinct sets of radial glial cells revealed profound differences in their gene expression. Genes related to gliogenesis, proliferation and cell-cycle regulation were expressed at higher levels in the largely non-neurogenic set of radial glia while genes related to neurogenesis, cell adhesion, neurotransmitter secretion and axon guidance were expressed mostly in the neurogenic subset. Moreover, the set of genes expressed at higher levels in the neurogenic radial glia was down-regulated at later stages (cortical radial glia at E18). Thus, this analysis reveals differences at the transcriptional level between direct neurogenic and largely non-neurogenic radial glial cells, supporting their intrinsic lineage differences. The functional analysis of a key fate determinant for neurogenesis from radial glia discovered in this transcriptome analysis will also be presented. This gene is the transcription factor AP2 γ which was expressed at significantly higher levels in radial glial cells generating basal progenitors. AP2 γ is restricted to the ventricular zone (VZ)/subventricular zone (SVZ) regions of the developing cerebral cortex in the entire nervous system and is also highly expressed in primate and human cortical progenitors. Its genetic deletion within the mouse cerebral cortex results in the molecular misspecification of basal progenitors with decreased

levels of Tbr2 and Math3 expression, as well as their overproliferation associated with increased cell death specifically in the occipital cortex. This causes a reduction in upper layer neuron generation with intriguing functional defects in visual acuity. Gain-of-function studies also revealed the important role of AP2 γ for the adequate specification and development of basal progenitors in the cerebral cortex, while apical progenitors were not affected by the loss- and gain-of-function of this transcription factor.

Thus, I show for the first time the prospective isolation of distinct radial glia subtypes in the mouse developing cortex demonstrated at the molecular and functional level.

3 Introduction

3.1 Progenitor cells and neuron production in the CNS

3.1.1 Population heterogeneity in CNS development

The central nervous system (CNS) represents the largest part of the nervous system, including the brain and the spinal cord. The basic patterning of the CNS is highly conserved throughout vertebrate species and during evolution. The CNS originates from the neural plate, a specialised region of the ectoderm - the outermost of the three germ layers. During embryonic development, the neural plate folds forming the neural tube. The internal cavity of the neural tube will give rise to the ventricular system and the regions of the neural tube will differentiate progressively into transversal systems. Initially, the whole neural tube will differentiate into two major subdivisions: brain and spinal cord. The brain will consecutively differentiate into prosencephalon and brainstem. Posteriorly, the prosencephalon will be subdivided into telencephalon and diencephalon, and the brainstem into mesencephalon and rhombencephalon. Finally, the telencephalon gives rise to the neocortex dorsally and the basal ganglia ventrally with the cavity becoming the lateral ventricles.

Throughout development of the CNS, cellular or even sub-cellular heterogeneity in progenitor cells is a basic concept underlying the cellular diversity in the adult organism. Even before fertilization, the egg cell is pre-patterned into an animal and a vegetal pole which are determined to later on give rise to the different germ layers in a defined manner (Gardner and Davies, 2003). The fate of one specific cell type and its progeny can be determined either by its local environment (non-cell autonomous) which may provide different signals to the cell as it may be pre-specified by a cell-internal program of gene expression (cell-autonomous). Thus, the existence of phenotypic heterogeneity in clonal populations of mammalian cells can be a consequence of extrinsic and intrinsic factors. Initially, identical cells may become different because they encounter different local microenvironments that induce adaptive responses. Heterogeneity between cells may also result from asymmetric segregation of intrinsic fate determinants during cell division that differently affect the fate of the daughter cells.

Population heterogeneity and lineage restriction is conserved in all organisms up to higher vertebrates, being an important concept in development. During development of the CNS, diverse cell types need to be generated. Different studies show evidence for a hierarchical fate restriction. In most CNS regions multipotent progenitors are sequentially more and more

restricted during development to generate a specific cell type (Desai and McConnell, 2000). Towards this end, distinct subsets of progenitor cells appear to specialize to the production of one of the three major cell-types - neurons, oligodendrocytes or astrocytes. Such a lineage restriction also allows regulating the number of specific cell-types generated at specific developmental stages by amplifying the number of their immediate progenitors. Taken together, to unravel the molecular regulation of lineage restriction and population heterogeneity is important to understand the molecular mechanisms acting in functionally distinct subsets of progenitors.

3.1.2 Forebrain development and regionalization

Early steps in CNS patterning are largely conserved, and studies primarily performed in chick, fish, frog and mouse are beginning to unravel the mechanisms by which the forebrain is induced and patterned. The forebrain arises from the anterior neuroectoderm during gastrulation, and by the end of somitogenesis it comprises the dorsally positioned telencephalon and eyes, the ventrally positioned hypothalamus, and the more caudally located diencephalon (Lupo et al., 2006). Prior to and during gastrulation, anterior-posterior (A-P) pattern starts to emerge within the embryo and neural induction occurs. In regions of the embryo protected from the influence of caudalizing signals, this neural tissue forms the prospective forebrain. The patterning of the neural plate along the A-P axis has been proposed to occur via planar signals, that is, signals traveling through the plane of the neuroepithelium (Ruiz i Altaba, 1998).

Signalling molecules, such as Fgfs, Wnts, Retinoic Acid (RA), Nodals, and bone morphogenic proteins (Bmps) have been proposed as caudalizing factors (Munoz-Sanjuan and A, 2001), and the combinatorial activity of several pathways is required to establish early A-P pattern (Haremake et al., 2003; Kudoh et al., 2002). For example, several Wnts are expressed in the cortical hem and are involved in hippocampal development (Grove and Fukuchi-Shimogori, 2003). Others, such as Wnt7b and Wnt8b show different expression patterns in the neocortex (Kim et al., 2001a). Moreover, Wnt receptors, such as Fz-8, and Wnt antagonists, such as SFRP-1, are expressed in the early neocortex (E10.5–12.5) in a restricted fashion (Kim et al., 2001b). It is therefore thought that Wnt function could contribute to neocortical patterning. Indeed, Wnt activity has been implicated in planar patterning in insects and in dorso-ventral specification of the mouse telencephalon (Backman et al., 2005; Mlodzik, 1999).

In the last years, several studies have been done to understand the intrinsic regionalization of the embryonic dorsal telencephalon, which may be related to the formation of distinct functional areas in the adult neocortex. In this context, the posterior/occipital region of the neocortex is generally directed to the processing of visual information. In contrast, more anterior - rostral regions constitute association areas. Several intrinsic fate determinants play important roles in rostral-occipital regionalization. For example, the homeobox gene family of transcription factors comprises important factors for embryonic patterning. Mutation of the homeobox gene *Emx2* has been shown to result in mispatterning of the neocortex (Bishop et al., 2000; Mallamaci et al., 2000). This observation is interesting as *Emx1* and *Emx2* are part of a relatively small number of genes that show specific expression in the dorsal telencephalon (Gulisano et al., 1996). Moreover, *Emx2* is expressed in a graded fashion in the progenitors of the cortical neuroepithelium, with highest levels posteriorly (Mallamaci et al., 1998). Mice lacking *Emx2* show a compression of the visual cortex as determined by the extent of innervation of lateral geniculate nucleus (LGN) axons (Bishop et al., 2000; Mallamaci et al., 2000). However, most area-specific markers tested are still expressed in their normal fashion, but shifted. A similar result, but with opposite polarity, has been suggested for mutations in the homeobox gene *Pax6*. *Pax6* mutant mice (small eye mice – *Sey/Sey*) were suggested to have compressed anterior areas as measured by thalamocortical axonal tracings and region-specific gene expression (Bishop et al., 2000). Thus, *Emx2* and *Pax6* may be involved in the proportioning of areas, a process that could be important for the plasticity of areal borders. Nevertheless, in the absence of either *Emx2* or *Pax6*, the cerebral cortex forms and is molecularly distinguishable from adjacent structures. Interestingly, however, the deletion of both *Emx2* and *Pax6* from the cerebral cortex leads to its transformation into striatum (Muzio et al., 2002). Taken together, these results reveal that regional specification in the developing neocortex is initiated by the graded expression of specific transcription factors. How these are translated into the formation of distinct and highly specified cortical areas, however, is less well understood.

3.1.3 Radial glia progenitors in the forebrain

The adult CNS is composed of different neuronal and glial cell types that are generated from heterogeneous progenitor populations during development. A remaining crucial question in neural development is how different these progenitor populations are at the molecular level and which intrinsic signals may regulate this heterogeneity. To get new insights into intrinsic

fate determinants regulating progenitor heterogeneity, I studied the transcriptome of progenitor subtypes - radial glial cells (RGCs)- in the developing forebrain.

RGCs are a widespread non-neuronal cell type in the CNS of all vertebrates analyzed so far and are the progenitors of nearly all glial cells and projecting neurons in the mammalian cortex (Campbell and Götz, 2002; Götz et al., 2002; Kriegstein and Götz, 2003; Malatesta et al., 2000; Noctor et al., 2001; Pinto and Gotz, 2007). This cell type shows a well characterized radial morphology, defined by two long radial processes extending from the apical surface, where they contact the ventricle, to the basal surface where they contact the basal lamina. The cell bodies of RGCs are located in the ventricular zone (VZ) (Bentivoglio and Mazzarello, 1999; Cameron and Rakic, 1991). These RGCs are born from the neuroectoderm and share several morphological and molecular characteristics with neuroepithelial progenitor cells (NEPs) - the cell type they arise from by embryonic day (E) 10 (Götz and Huttner, 2005; Pinto and Gotz, 2007) (Fig. 1a). Moreover, RGCs maintain certain NEPs features in terms of morphology (apico-basal polarity, radial processes spanning the neural wall, connecting by apical junctions and forming gap junctions) and gene expression (nestin, RC1, RC2) (Bennett et al., 2003; Bittman et al., 1997; Chanas-Sacre et al., 2000; Hartfuss et al., 2001; Misson et al., 1988a; Mori et al., 2005). However, only RGCs express the astroglia proteins BLBP, GLAST, S100 β , GFAP, vimentin, GS, TNC and contain glycogen granules - all of these features they share with reactive astrocytes and neural stem cells in the adult brain but not with quiescent astrocytes (Doetsch et al., 1999b; Doetsch et al., 2002; Fawcett and Asher, 1999; Ridet et al., 1997; Seri et al., 2004; Seri et al., 2001; Temple and Alvarez-Buylla, 1999). Therefore, RGCs can be clearly distinguished from NEPs based on molecular and ultrastructural criteria. Notably however, molecular markers have not been identified so far that would allow the discrimination between RGCs and reactive astrocytes. Furthermore, the expression of these markers is not homogenous in all RGCs existent in the CNS (Hartfuss et al., 2001; Pinto and Gotz, 2007; Pinto et al., 2008), and cell populations expressing distinct markers only partially overlap.

NEPs and RGCs also undergo interkinetic nuclear migration (Sauer, 1935b). While going through the G1 and S-phase of their cell cycle, these cells translocate their nuclei from the ventricular surface to the subventricular zone (SVZ), they return during G2 to the ventricular zone (VZ) and undergo mitosis at the ventricular surface (Sauer, 1935b). This process is –in a different manner- also performed by NEPs. Interkinetic nuclear migration of NEPs covers the entire distance from the ventricular to the pial surface and back which clearly distinguishes them from RGCs (Götz and Huttner, 2005; Misson et al., 1988b).

3.1.4 Radial glial cells as committed progenitors

As RGCs constitute the majority of the progenitors during neurogenesis in the brain, this suggested that they may actively and directly contribute to the generation of neurons. The first hint to focus more in possible functions of this specialized cell type was their proliferating activity during neurogenesis (from E12-E18), that turned out to be very important to start considering radial glia as progenitor cells (Hartfuss et al., 2001; Malatesta et al., 2000; Noctor et al., 2001). The cellular mechanisms of neuron production from RGCs have then been studied in the recent years. Using *in vitro* clonal analysis of RGCs purified by fluorescence activated cell sorting (FACS), it was first demonstrated that RGCs are neuronal progenitors during neurogenesis (at E14 and E16), giving rise mostly to neuronal clones and to a small proportion of non-neuronal clones (Malatesta et al., 2000). This analysis showed that a small proportion of RGCs is bipotent and thus capable to generate neurons and astrocytes. After the period of neurogenesis, at E18, RGCs lose the capacity to generate neurons and exclusively generates astrocytes. These *in vitro* studies apart from the direct evidence of a neurogenic role of radial glia also bring us evidences for the existence of radial glia heterogeneity during mouse brain development. Furthermore, the neurogenic potential of RGCs was demonstrated *in vivo* using fate mapping methods. In the first fate-mapping studies, all progenitor cells were labelled by fluorescent dyes (DiI) or non-specific viral vectors. Later on, labelling was performed by retroviral vectors carrying a reporter gene, such as GFP, which is incorporated into the dividing cell's DNA and is subsequently expressed in both the infected cells and their progeny (Hajihosseini et al., 1993; Price and Thurlow, 1988). The retroviral labelling method has proven to be extremely useful for cell lineage analyses within the cerebral cortex. Using these strategies, by time-lapse imaging it was shown that proliferative RGCs directly generate neurons (Miyata et al., 2001; Miyata et al., 2004; Noctor et al., 2001; Noctor et al., 2004). First, with *in utero* intraventricular injections of GFP-expressing retrovirus in the rat cortex of E15 and E16 embryos, single RGCs were labelled and their progeny was followed by clonal analyses and time-lapse imaging (Noctor et al., 2001). In these analysis, after two days of the GFP retroviral vector injection it was possible to access asymmetric divisions of labelled radial glia, with one of them giving rise to one other radial glia and one neuron (Noctor et al., 2004). In parallel other experiments monitored the divisions and fate of DiI-labelled single RGCs in slices from E14 mouse cortex arriving to the same conclusion; RGCs divide asymmetrically to generate one neuron and one progenitor cell (Miyata et al., 2001). Thus, the heterogeneity of these progenitors has been

confirmed by live imaging of dividing RGCs (Miyata et al., 2001; Miyata et al., 2004; Noctor et al., 2001; Noctor et al., 2004).

Based on all these studies it seems that in the developing cortex, most cells are not generated by multipotent progenitors which change their potential during development. It rather appears that the progenitor pool is heterogeneous and consists of cell lineages restricted to either glial or neuronal progeny. This restriction occurs around the onset of neurogenesis when most progenitor cells in the cortex and striatum generate a single cell type, even though some progenitors give rise to large clones containing multiple cell types (Grove et al., 1993; Luskin et al., 1993; Luskin et al., 1988; Price and Thurlow, 1988; Reid and Walsh, 2002; Walsh and Cepko, 1993). The intrinsic lineage of cortical progenitors was confirmed by *in vitro* culture of single cells as most of these generated exclusively a single cell type (Qian et al., 1998). Approximately 15% of the isolated progenitor cells were multipotent stem cells that generate both neurons and glia, while the majority were restricted neuroblasts that generate only neurons (Qian et al., 1998). However, this restricted fate specification of a single progenitor occurs differently in other regions of the CNS. For example, the progeny of a single progenitor in the retina frequently generates neurons and glia (Turner and Cepko, 1987), in contrast to what generally happens in the developing cerebral cortex. In order to understand the molecular mechanisms that specify the neuronal lineage I aimed to isolate the neurogenic progenitors by FACS.

3.1.5 Generation of neurons from two different types of progenitors

During embryonic development it has been shown that neurogenesis precedes gliogenesis. In the developing brain progenitors are arranged in a pseudostratified neuroepithelium lining the ventricular wall in the VZ. Primarily, cortical neurons were thought to be generated from the progenitors in the VZ by asymmetric cell division. The first neurons in the cerebral cortex are indeed generated from NEPs, which are called the preplate cells, the Cajal-Retzius neurons (Frotscher, 1997; Soriano and Del Rio, 2005) (Fig. 1a). Later on, the notion that neurogenesis occurs in two proliferative regions was introduced to the field. Two different types of neuronal progenitors were identified, the VZ progenitors, the NEPs and RGCs described before, and the so called basal or intermediate progenitors located within the developing subventricular zone (SVZ) (Haubensak et al., 2004; Miyata et al., 2004; Noctor et al., 2004) (Fig. 1a-c). The SVZ is a second proliferative region formed at early embryonic stages of neurogenesis localized above the VZ and extending to the intermediate zone (IZ).

Basal progenitors are a distinct population of progenitors mostly present in the telencephalon and defined by the absence of an apical contact to the ventricle as well as by the fact that their nuclei divide at the basal side of the VZ in contrast to NEPs and RGCs. They are generated from NEPs and RGCs in the VZ and then migrate towards the basal surface retracting their apical process during their nuclear migration (Miyata et al., 2004). Generally basal progenitors constitute only a minority of progenitors at early stages in the developing forebrain (approximately 10% at E12) but their proportion increases during further development of the cerebral cortex (25% at E14, 30% at E16) (Fig. 1a-c). At the molecular level, basal progenitors can be distinguished from the RGCs by the expression of the transcription factor Tbr2 (Englund et al., 2005), Cux1 and Cux2 (Nieto et al., 2004; Zimmer et al., 2004), Ngn2 (Miyata et al., 2004) and the non-coding RNA Svet1 (Tarabykin et al., 2001). In contrast to VZ progenitors, they express neither the transcription factor Pax6 nor the pro-proliferative Hes family of transcription factors which are present in VZ progenitors (Cappello et al., 2006; Englund et al., 2005; Ohtsuka et al., 2001). Basal progenitors have been described as being exclusively neurogenic by an additional mode of cell division - symmetric cell division, generating two neurons as daughter cells (Haubensak et al., 2004; Miyata et al., 2004; Noctor et al., 2004; Wu et al., 2005). Therefore, basal progenitors are believed to expand the pool of neurons generated from RGCs, as the latter are thought to largely undergo asymmetric cell division with generating only a single neuron per cell division.

Strikingly, the proportion of basal progenitors and the SVZ becomes very large in the cerebral cortex of primates where it reaches more than 90% of the progenitor pool during mid-neurogenesis (Rakic, 2002; Smart et al., 2002). Moreover, in primates, the SVZ is particularly enlarged during stages when upper layer neurons are generated in the cortex (Lukaszewicz et al., 2005; Smart et al., 2002). This observation gives support to the interpretation that basal progenitors may serve to increase the number of a particular population of neurons during development. Indeed, it has been suggested that symmetric differentiative divisions of the basal progenitors would regulate the size of a given cortex layer (Pontious et al., 2008). Furthermore, the switch from symmetrically dividing NEPs generating two progenitors to asymmetrically dividing RGCs might regulate the size of a given brain or cortex region (Rakic, 1995). The number of subsequent asymmetric neurogenic divisions would then determine the thickness of the respective brain or cortex region (Rakic, 1995). Thus, the regulation of when and how VZ progenitors generate SVZ progenitors should have great impact on the evolution of cortex architecture (Cappello et al.,

2006; Martinez-Cerdeno et al., 2006; Molnar et al., 2006). However, still little is known about the transcriptional regulators of basal progenitor specification in the developing forebrain. Therefore, I set to determine whether basal progenitors may originate from a specific subset of radial glia and study the transcriptome of this particular subset of progenitor cells (Fig. 2).

3.1.6 Neuronal production timing and specification during brain development

When neurons are generated, they need to migrate towards their final laminar position. As described recently by time-lapse imaging of GFP labelled cells, the neuronal migration profile is more complex than previously thought. After their generation not all cortical neurons migrate directly to the cortical plate, as some are arrested in the SVZ, followed by a retrograde movement toward the ventricular surface and only after these three phases migration to the cortical plate occurs (Noctor et al., 2004).

Cortical projection neurons are produced in a precise and programmed timing by progenitor cells. The first generated neurons in the cerebral cortex are the Cajal-Retzius neurons identified by the expression of reelin (D'Arcangelo et al., 1997) followed by the production of neurons of the cortical plate in an inside-out order, where the deep layer cortical neurons, layer VI and V, are born first and the superficial layers IV, III and II later (Bayer et al., 1991). From transplantation experiments there was the indication that the fate potential of neuronal progenitors within the VZ during development becomes gradually more restricted, with later stage progenitors being only able to produce upper layer cortical neurons (Desai and McConnell, 2000). Recently, it was shown that this timing mechanism of neurogenesis is intrinsically programmed and independent of the environment (Shen et al., 2006). Using layer-specific markers and time-lapse lineage analyses they studied the generation of cortical neurons in low-density cortical progenitor cultures at different stages of early mouse cortex development- E10-11 and E11.5-12. The authors showed that the neurons expressing transcription factors indicative of a specific cortical layer neuron fate are born in a proper order over time *in vitro* as *in vivo*, with progenitor cells of pre-neurogenic stage capable of generating Cajal-Retzius and cortical-layer neurons, but later-stage progenitors restricted to generate earlier neuronal types. This restriction in the potential of progenitors for generation of earlier neuronal fates seems to be progressive and intrinsically programmed by the progenitor cells, giving less importance to the environmental cues for the timing of neurogenesis. Moreover, knock down experiments of the transcription factor Foxg1 revealed

that it is required as a cell-intrinsic factor to progress from the production of Cajal-Retzius neurons towards cortical plate neurons (Shen et al., 2006).

Furthermore, the proneural bHLH transcription factors (TFs) Ngn1 and Ngn2 (Schuurmans et al., 2004) and Pax6 (Haubst et al., 2004) play important roles in the specification of cortex layers. Importantly, Ngn2 is only required for early-born deep layer neurons specification (Schuurmans et al., 2004). In addition, these genes are not only important to promote neurogenesis through repression of the other ventral proneural gene Mash1 ((Fode et al., 2000), but also to promote radial migration, to specify a glutamatergic phenotype and dendritic morphology of cortical projection neurons (Hand et al., 2005). The transcription factor Pax6 is required for neurogenesis from radial glia (Götz et al., 1998; Heins et al., 2002) (Fig. 2). In the absence of Pax6, RGCs show defects in their molecular phenotype, proliferation, cell fate and morphology (Götz et al., 1998; Heins et al., 2002) and basal progenitors increase in number but are misspecified (Götz et al., 1998; Haubst et al., 2004), lacking the typical expression of the non-coding RNA *Svet1* (Tarabykin et al., 2001), the transcription factors *Tbr2*, *Cux1* and *Cux2* (Englund et al., 2005; Nieto et al., 2004; Zimmer et al., 2004). Moreover, in the Pax6 mutant, the identity of upper layer neurons is severely disturbed (Schuurmans et al., 2004; Tarabykin et al., 2001). This phenotype has lead to the suggestion that basal progenitors generate upper layer neurons as both are misspecified in the Pax6-mutant cortex (Englund et al., 2005).

Taken together, these studies imply that the cortex is constituted of progenitor subtypes restricted in their potential to generate specific neurons during the different developmental stages mostly based on their cell intrinsic expressing factors. Thus, to study the transcriptome of these distinct progenitor subtypes might bring new insights into the transcription factors regulating the generation of specific types of neurons.

3.1.7 Transcriptional regulators of cell fate in the developing forebrain

Considerable progress has been made in identifying transcriptional regulators of cell fate, such as *Olig1* and *Olig2* in oligodendrocyte specification (Lu et al., 2002; Zhou and Anderson, 2002) or of *Mash1*, *Ngn 1* and *2* (Fode et al., 2000; Nieto et al., 2001; Schuurmans et al., 2004), or the homeobox transcription factor *Pax6* (Götz et al., 1998; Heins et al., 2002) for neuronal fate. Gain- and loss-of-function experiments demonstrated a potent role for these TFs in fate decisions. Deletion of the respective TFs leads to a decrease or even absence of specific cell-types. For example, deletion of *Olig1* and *2* causes the virtual absence of oligodendrocytes in large parts of the CNS and the delay of astrocyte development in the

dorsal neocortex (Lu et al., 2002; Ono et al., 2008; Zhou and Anderson, 2002). Deletion of *Mash1* and *Ngn1* and 2 results in a premature end of neurogenesis in the developing dorsal telencephalon (Nieto et al., 2001; Schuurmans et al., 2004). Gain-of-function experiments confirmed the role of these TFs in promoting the oligodendroglial or neurogenic lineage, respectively (Berninger, 2007; Heins et al., 2002; Mizuguchi et al., 2001; Sugimori et al., 2007), but they also revealed their limitations. Not all cells could be instructed towards a specific fate upon TF overexpression (Heins et al., 2002; Sun et al., 2001), suggesting that other cues may be required to instruct a specific cell-type identity. Moreover, neurogenesis may be governed by different molecular mechanisms not only in different regions of the CNS, but also at different developmental stages. An unbiased approach is therefore needed to identify additional fate determinants that have so far been missed.

3.1.8 Isolation of functionally distinct progenitor subsets by FACS

To identify new fate determinants instructing distinct subsets of progenitors towards the generation of a specific cell-type, I isolated functionally distinct populations of RGCs from the developing cerebral cortex using FACS and analyzed them at the transcriptome level. A number of approaches have already taken advantage of universal progenitor cell markers to isolate, characterize and manipulate neural stem cells by both prospective positive and negative selection strategies. Rao and colleagues have used the absence of expression of neuronal, astrocytic and oligodendroglial markers to enrich samples for stem cells from late fetal stages (Rao, 1999). Using a similar negative selection strategy, Maric et al. used surface ganglioside epitopes appearing on differentiating CNS cells to isolate neural progenitors from E13 rat telencephalon by FACS (Maric et al., 2003). The separation of neuron- or glial-restricted progenitors was achieved by the use of A2B5 to label the glial lineage and cholera toxin B (ChTx) and toxin fragment (TnTx) to isolate the neuronal lineage (Maric et al., 2003). Moreover, Maric et al. used surface labelling against the fibroblast growth factor receptor 1 (FGFR-1), the epidermal growth factor receptor (EGFR) and membrane potential and Ca^{2+} indicator dyes for the selection of immature, neurogenic and gliogenic progenitors (Maric et al., 2003).

Even though it is possible to isolate stem cells prospectively from a mixed population, it is difficult to use an absence of expression of markers to localize them *in vivo*, as multiple markers are required. Thus, parallel strategies have identified positive selection markers that can be used to identify neural progenitor cells. In this context, neuron-restricted progenitor cells were successfully isolated from the developing spinal cord by immunopanning with an

antibody against the embryonic neural cell adhesion molecule (ENCAM) (Mayer-Proschel et al., 1997). However, the same antigens are widely distributed and do not correlated to specific neuronal progenitors in the developing forebrain (Blass-Kampmann et al., 1994; Liepelt et al., 1990). Moreover, more recently, mouse progenitor cells from the developing forebrain were isolated by the LeX surface marker using FACS sorting (Abramova et al., 2005).

Since RGCs have been shown to constitute the majority of progenitors in the developing VZ (Hartfuss et al., 2001; Noctor et al., 2002), the lineage data described above apply to this type of cells. Furthermore, the data described suggest that RGCs are a heterogeneous population of progenitor cells consisting of distinct sublineages, with some specialized to generate neurons and others to generate glial cells. These findings prompted me to attempt to isolate these functionally distinct RGCs subsets from the developing forebrain in order to examine their transcriptomes by the use of Affymetrix microarrays analysis (Pinto et al., 2008). Therefore, I selected RGCs taking advantage of a mouse line in which the promoter elements of human glial fibrillary acidic protein (hGFAP) drives the expression of a strong fluorescent version of the GFP (Nolte et al., 2001). Indeed, hGFAP-eGFP positive RGCs isolated at mid-neurogenesis from the cortex contain three distinct lineages, some that generate only neurons, others generating non-neuronal progeny and a small subset of progenitors that generate neurons and glial cells (Gotz et al., 2002; Heins et al., 2002; Malatesta et al., 2003; Malatesta et al., 2000). I attempted to isolate these distinct lineages of RGCs by selecting for progenitors expressing different levels of the transgene (Pinto et al., 2008). Strikingly, I found that GFP intensity in this mice correlates to the fate of RGCs. Moreover, I aimed to identify molecular fate determinants acting in radial glial subsets that generate neurons and compare them to those acting in non-neurogenic radial glia. The fate determinants acting in RGCs during development may also be of relevance for adult neurogenesis that originates from RGCs (Alvarez-Buylla, 1990).

3.1.9 Adult neurogenesis from astroglia in mammals

A key question arising from the analysis of neurogenesis in the developing brain is why it comes to an end in most adult brain regions but not in others. In the mammalian CNS, neurons and oligodendrocytes become postmitotic during differentiation, however astrocytes seem to retain the potential to proliferate. Most RGCs loose their neurogenic potential at the end of neurogenesis when they transform into astrocytes, while neurogenesis continues in two regions on the adult mammalian forebrain (Alvarez-Buylla et al., 2001), the adult

subependymal zone (SEZ), that lines the lateral wall of the lateral ventricle, (Doetsch et al., 1997; Doetsch et al., 2002) (Fig. 3) and the subgranular layer (SGZ) in the dentate gyrus (DG) (Seri et al., 2004; Seri et al., 2001). These as well as the other astrocytes arise from RGCs, the ubiquitous glial population during development that was recently shown to form the major progenitor cell type in the VZ of the forebrain during embryogenesis (Hartfuss et al., 2001; Malatesta et al., 2000; Merkle et al., 2004). In this regard neurogenic astrocytes of the SEZ were indeed shown to share several characteristics with RGCs such as the expression of similar markers as nestin, vimentin and RC2 (Doetsch et al., 1999a; Doetsch et al., 1999b) and also the maintenance of an apical process contacting the lateral ventricle and the performance of interkinetic nuclear migration (Tramontin et al., 2003).

In the adult mammalian SEZ four classes of cells were identified by distinct antigens expression and named as type A, B, C and E. Type A cells are the neuroblasts expressing PSA-NCAM and β III-tubulin, type B cells are astrocytes expressing GFAP and GLAST (Ninkovic and Götz, 2007), type C cells are the transit amplifying progenitors expressing Dlx2, and type E cells are the ependymal cells (Doetsch et al., 1997; Doetsch et al., 2002). More studies were done to identify specific markers for the different types of cells. The transit amplifying progenitors were more recently shown to express the bHLH transcription factor Olig2 (Hack et al., 2004), Mash1 (Parras et al., 2004) and Gsh2 (Stenman et al., 2003a). Indeed, after this characterization, it was demonstrated that the type B astrocytes are the cells responsible for generating neurons in this adult neurogenic region (Doetsch et al., 1999a; Ninkovic and Götz, 2007) (Fig. 3). The type B astrocytes or at least a subset of these cells, were shown to be slowly dividing and have the capacity to generate the type C transit amplifying progenitors which then generate the neuroblast type A cells that had been labelled by cytosine beta-arabino-furanoside (Ara-C) treatment (Doetsch et al., 1999b). These astrocytes can then be considered as the adult neural stem cells, as they can self-renew and give rise to neurons and oligodendrocytes. *In vitro* experiments further revealed neural stem cell features of these cells, namely to self-renew and generate neurons, astrocytes and oligodendrocytes upon forming neurospheres (Doetsch et al., 2002). These stem cells located within the SEZ and the rostral migratory stream (RMS) generate different types of interneurons that integrate in the granule cell (GCL) or glomerular (GL) layers of the olfactory bulb (OB). Both GABAergic (Kosaka and Kosaka, 2007) and glutamatergic (Nakamura et al., 2005; Pimentel and Margrie, 2008; Rash et al., 2005; Tabor and Friedrich, 2008) transmission has been detected in the OB. However, until now only GABAergic

interneurons have been implicated in adult olfactory neurogenesis (Batista-Brito et al., 2008; Belluzzi et al., 2003; Carleton et al., 2003; Lledo and Saghatelian, 2005).

The problem of neuronal reconstitution arises from the fact that, after development, neurogenesis is permanently stopped in most regions of the CNS. This is the case, however, only in mammals, while neurogenesis continues much more wide-spread in brain regions of other vertebrates. The signals that regulate the end of neurogenesis are unknown. Interestingly, however, neurogenesis is maintained in the two small regions of the adult mammalian forebrain mentioned before, but the signals that allow the continuation of neurogenesis in these, but not other adult brain regions have also not yet been identified.

3.2 The transcription factor AP2 γ

In order to get insights into the mechanisms normally specifying basal progenitors in the developing forebrain, I have previously established a protocol to enrich RGCs generating basal progenitors (Pinto et al., 2008). Amongst the mRNAs enriched in this radial glia subset (Pinto et al., 2008), the transcription factor AP2 γ caught my attention as it was also previously shown to be down-regulated in the Pax6-mutant cerebral cortex (Holm et al., 2007). More interestingly, AP2 γ is expressed in the adult neurogenic regions, suggesting that this fate determinant acting in RGCs during development may also be relevant for adult neurogenesis.

Thus, given the important roles of AP2 transcription factors in various organs during development and especially the important roles of AP2 γ in the trophectoderm lineage (Auman et al., 2002), I decided to examine its role in the developing cerebral cortex by loss- and gain-of-function experiments.

3.2.1 AP2 family of transcription factors

The activating proteins (AP) 2 family of transcription factors consists – in mice and humans – of five members, AP2 α - AP2 ϵ . They have homologs in chicken, *Xenopus* and bony fish and paralogs with very weak similarity in *Drosophila* and *Caenorhabditis*. However, as no AP2 proteins have been found in Yeast so far, they seem to have appeared only late in evolution and considerably emerged in vertebrates.

All members of the AP2 family share common structural as well as functional features. AP2 proteins have a conserved transcriptional activator domain at the amino-terminal end. These transcription factors usually act as homo- or heterodimers and their dimerization is mediated through a Helix-Loop-Helix motif. Moreover, both dimerization as well as the basic domain

are essential for DNA-binding (Fig. 4b).

Generally AP2 proteins are known to play a role in various systems in development and cancer. These proteins regulate a large number of target genes with different biological functions. Among them are cell cycle regulating factors like c-myc (Gaubatz et al., 1995), p21WAF/CIP (Li et al., 2006), molecules involved in cell adhesion like E-cadherin, MMP9 (Schwartz et al., 2007) and MCAM/MUC18 (Jean et al., 1998) and growth factors and their receptors like Her2/neu (Bosher et al., 1995; Perissi et al., 2000), c-kit (Jean et al., 1998), TGF α (Wang et al., 1997) and IGF1. While, most of these interactions have been discovered either in cell lines or in tumor tissue, still nothing is yet known about the role of AP2 proteins in the CNS.

The various functions of AP2 proteins seem to be largely depending on interaction partners in the spatially and locally defined system they act. Many proteins are known to physically interact with these proteins and therefore influence their function. Prominent examples are the adenomatous polyposis coli (APC) gene, which in association with AP2 α - inhibits β -catenin dependent transcription (Li et al., 2004), Pax6 which mediates retinal repair in association with AP2 α (Sivak et al., 2004) and the AP2 coactivators CITED2 (Braganca et al., 2003) and CITED4 (Braganca et al., 2002).

During development different AP2 proteins are often co-expressed and seem to have at least partially redundant functions. However, the phenotype resulting from the deletion of a specific AP2 family member is specific and does not resemble the mutant of another member of this family. For example, selective loss of AP2 α leads to severe craniofacial defects first appearing at E9.5, in both skeletal as well as epidermal tissue, which was supposed to be due to a significant increase in apoptosis of migratory neural crest cells at E9 (Schorle et al., 1996). The Knock-out mice for AP2 β develop evident kidney abnormalities. In these mutant mice, beginning from E16.5 the tubuli and collecting ducts undergo cystic transformation. It was suggested that, due to myc deregulation, loss of AP2 β leads to cell-autonomous apoptosis of renal epithelia (Moser et al., 1997). Both, loss of each AP2 α or AP2 β causes lethal phenotypes.

3.2.2 Expression and functions of AP2 γ in the developing and adult mouse

AP2 γ was shown to be expressed in all trophoblast cells beginning as early as E3.5 and subsequently in all derivatives of the trophoblast lineages (Auman et al., 2002; Sapin et al., 2000; Shi and Kellems, 1998). Many recent studies focused on the role of AP2 transcription factors during early mouse development. In AP2 γ deficient mice, trophoblast giant cells are

significantly reduced, suggesting an important role of AP2 γ in their development (Auman et al., 2002). Interestingly, AP2 γ and the parathyroid hormone-related protein (PTHrP) were shown to have inhibitory effects on c-myc and E-cadherin expression (Cowley and Smith, 1996; Gaubatz et al., 1995). This suggests that both PTHrP and AP2 γ can inhibit apoptosis, possibly at least partly through inhibition of c-myc expression. Several TFs have been similarly identified to progressively regulate trophoblast differentiation (Cross et al., 2003). For example, Eomes (Tbr2) and cdx2 are implicated in FGF4-regulated trophoblast stem (TS) cell maintenance (Russ et al., 2000; Tanaka et al., 1998).

The defects in trophoblast formation with impaired proliferation in the ectoplacental cone and extra-embryonic ectoderm cause the lethality of AP2 γ Knock-outs. Therefore, the embryos are severely growth retarded already at early stages and reabsorbed at E9.5 (Auman et al., 2002). Later during mouse development, AP2 γ is expressed in the forebrain, limb buds and face (Chazaud et al., 1996). In the adult mouse cerebral cortex a small population of cells is immunoreactive for an epitope common for AP2 α , - β and AP2 γ and for Notch1 (Coelho et al., 2005). Together with AP2 α , AP2 γ is also known to be expressed in the peripheral nervous system (PNS), namely in Schwann Cell progenitors, but not in mature Schwann Cells (Stewart et al., 2001).

As other members of the AP2 family, AP2 γ regulates several different proteins in different systems. An important example is the activation of p21 and therefore cell cycle arrest and growth inhibition in human carcinoma cells *in vitro*. In that system, viral overexpression of AP2 γ induces G1-arrest mediated by cyclin D1 repression and decreased Rb-Phosphorylation and a decreased fraction of the cells in S-phase (Li et al., 2006). In the murine mammary gland, forced AP2 γ overexpression leads to an impairment of lactation due to a defect in mammary gland development during pregnancy. Ki-67 staining, which can be detected in G1, G2, M and S-phase of the cell cycle, showed an increased percentage of proliferating cells in AP2 γ transgenic mice (Jager et al., 2003).

Given the potent roles of AP2 transcription factors in various organs and the highly specific expression that I observed for AP2 γ with enriched levels in the subset of radial glia generating the basal progenitors, I decided to perform gain and loss-of function experiments to elucidate its role in the CNS.

4 Abbreviations

Affy	affymetrix
AP2 γ ^{-/-}	AP2 γ conditional knock out
APC-A	Allophycocyanin
BrdU	5-bromo-2-desoxy-uridine
cDNA	complementary DNA
CNS	central nervous system
CP	cortical plate
DAPI	4'-6'-diamidino-2-phenylindole
DNA	desoxyribonucleic acid
DNase	desoxyribonuclease
CTX	cortex
DG	dentate gyrus
Div	days in vitro
E	embryonic day
ES	embryonic stem cells
FACS	fluorescence activated cell sorting
FCS	fetal calf serum
GAPH	glyceraldehydes-3-phosphate dehydrogenase
GCL	granular cell layer
GE	ganglionic eminence
GFP	green fluorescent protein
GL	glomerular layer
H	hour
IRES	internal ribosomal entry side
IZ	intermediate zone
LGE	lateral ganglionic eminence
LI	labelling index
LTR	long terminal repeat
MGE	medial ganglionic eminence
ML	mitral cell layer
MZ	marginal zone
NGS	normal goat serum
OB	olfactory bulb

OSVZ outer subventricular zone

P postnatal day

PBS phosphate buffered saline

PCR polymerase chain reaction

PD paired domain

PD5a paired domain containing exon 5a

PDL poly-D-lysine

PE-A Phycoerythrin

PFA paraformaldehyde

PNS peripheral nervous system

RGCs radial glial cells

RNA ribonucleic acid

RNase ribonuclease

RMS rostral migratory stream

RT room temperature

RT-PCR real time-polymerase chain

SEM standard error of the mean

SEZ subependymal zone

SVZ subventricular zone

TF transcription factor

VZ ventricular zone

WM white matter

WT wild-type

2V second ventricle

V ventricle

5 Materials and Methods

5.1 Animals

Cortices were isolated from time-mated Wistar rats (day of sperm detection was embryonic day (E) 1) and from hGFAP-eGFP transgenic mice (Nolte et al., 2001) that were maintained on a FVB/NCRL background (the day of vaginal plug was considered to be embryonic day (E) 0). Wild-type FVB/NCRL mice were acquired from Charles River Laboratories. Expression analysis e.g. *in situ* hybridization was performed in embryos from C57BL/6J mice.

AP2 γ conditional knock-out mice were maintained on a C57/Bl/6J background and identified by PCR on genomic DNA (Werling and Schorle, 2002a). LoxP sites are flanking the entire Exon 5 and the majority of Exon 6, whose deletion would cause a loss of HSH domain near the protein carboxyterminus (Fig. 4). Antibodies against an aminoterminal epitope did not detect any protein upon combination with Cre-expression. Emx1::Cre knock-in mice (Iwasato et al., 2000) were maintained on C57/Bl/6J background. The day of vaginal plug was considered embryonic day (E) 0, the day of birth as postnatal day (P) 0.

Parasagittal sections of E80 cynomolgus macaque cortex (collaboration with Colette Dehay) and human sections of the occipital pole with 20-22 gestational weeks (midgestation) (collaboration with Nada Zezevic) were used for antibody immunostainings.

5.2 Genotyping of mice

hGFAP-eGFP transgenic mice were genotyped by fluorescence illumination of embryos or neonatal animals under a fluorescence dissecting microscope.

Genotyping of non-fluorescent mice was performed according to a protocol of Larid et al. 1991. Tail biopsies of embryos or adult mice were transferred into 250-500 μ l lysis buffer (consisting of buffer RLT (Quiagen) and β -mercaptoethanol (β -ME)- 10 μ l β -ME per 1ml buffer RLT) and incubated overnight rotating at 55°C. Bones and hairs were removed by centrifugation (10 minutes at 13000 rpm) after tissue lysis was completed. The supernatant was transferred into 250-500 μ l isopropanol, incubated at room temperature (RT) for 10 minutes and then mixed. DNA precipitates were transferred with the help of a pipette tip into 250 μ l H₂O. DNA was dissolved at 55°C for several hours.

AP2 γ conditional mice

To determine the genotype of mice with one or two floxed alleles of the AP2 γ gene, usually 3-5 μ L of DNA (preparation described above) were used as a template for a multiplex PCR with the following primers.

A - AP2 γ In4down: 5' - AAC Agg TTA TCA TTT ggT Tgg gAT T - 3'

B - AP2 γ Ex5up: 5' - CAA TTT TgT CCA ACT TCT CCC TCA A - 3'

C - AP2 γ Ex6up: 5' - AAT AgT CAg CCA CCg CTT TAC TAg g - 3'

The PCR was carried out from a total volume of 25 μ l using (in the final mix) 1x Fermentas PCR buffer without MgCl₂, 200 μ M dNTPs, 200pMol each primer, 2.5mM MgCl₂; 0.2 μ l/25 μ L homemade Taq-Polymerase; under the following cycling conditions: 1 cycle 95°C/180sec; 42 cycles (94°C/45sec; 55°C/30sec; 72°C/60sec); 1 cycle 72°C/180sec. Primers **A** and **B** were used to distinguish the floxed allele (300bp) from the WT allele (343bp) whereas the addition of primer **C** enabled me to detect the null allele (700bp) (Fig. 4a).

Emx1::Cre knock-in mice

To determine the genotype of mice with Cre-recombinase coding sequences in the cortex-specifically expressed in the Emx1 locus, usually 1-3 μ L of DNA (preparation described above) were used as a template for a multiplex PCR with the following primers:

Emx1_fw22: 5' - gTg AgT gCA TgT gCC Agg CTT g - 3'

Emx1_rev22: 5' - Tgg ggT gAg gAT AgT TgA gCg C - 3'

Cre: 5' - gCg gCA TAA CCA gTg AAA CAg C - 3'

The PCR was carried out with a total volume of 25 μ l using (in the final mix): 1x Fermentas PCR buffer without MgCl₂, 200 μ M dNTPs, 200pMol each primer, 2.5mM MgCl₂; 0.2 μ l/25 μ L homemade Taq-Polymerase; under the following cycling conditions: 1 cycle 94°C/120sec; 35 cycles (94°C/30sec; 65°C/60sec; 72°C/30sec); 1 cycle 72°C/600sec. The genotype of the WT gives rise to a PCR product of approximately 200bp length, the Emx1::Cre +/+ PCR product is 500bp long.

5.3 Fixation of mouse brains and cryosections

Prior to cutting cryosections from embryonic and postnatal mouse brains, the tissue was fixed at 4°C in 4% PFA (paraformaldehyde) dissolved in PBS, rinsed with PBS and left in 30% sucrose/PBS at 4°C until the brain or head was embedded in Tissue Tek, frozen and cut into cryosections. Sections were collected on SuperFrost microscope slides and stored at -20°C.

Fixations periods with 4% PFA were the following: E12 whole heads - 2h; E14 whole heads - 3.5h and brains - 2h; E16 brains – 3h; E18 brains - 4h; P2 brains – 6h; P7 brains - 6h after perfusion. Adult mice were deeply anaesthetized with a mixture of fentanyl (0.05mg/kg), from Hexal, midazolam (5mg/kg), from Roche, and metedomidine (0.5mg/kg), from Pfizer,

and were transcardially perfused with cold 4% PFA in 0.1M PBS. Brains were carefully dissected from the skull and post fixed in 4% PFA for 12 hours at 4°C.

5.4 Immunostaining

Live staining of prominin and cell surface markers for FACS analysis was done by incubation of the dissociated cells for 15 min on ice in DMEM/10%FCS/NaN₃ (1:500 from a 10% stock solution 65.01g/mol) using prominin-PE conjugated 1:1000 (Biosciences), p75 1:200 (Chemicon, rabbit), Flrt2 1:100 (kindly provided by Satoru Yamagishi, rabbit) and CD83-PE conjugated 1:1000 (Biosciences) antibodies. Cells were washed twice in DMEM/10%FCS by centrifugation at 1000rpm for 5 minutes at 4°C and re-suspended at a concentration of 1×10^6 cells/ml.

For stainings in cryosections, prior to the staining procedure, cryosections were rehydrated by short pre-incubation in PBS at RT. Eventual pretreatment of the sections is mentioned in the list of used antibodies. Antibodies were dissolved in 0.5% Triton X/10% NGS and applied to the sections. The sections were usually incubated in primary antibody solution overnight at 4°C, washed several times in PBS at RT and incubated with secondary antibody solution for ~2h at RT. The sections were washed in PBS several times. Secondary antibodies or streptavidin-coupled dyes were added dissolved in 0.5% Triton X 100 and incubated for 1h at RT. The sections were mounted with polymount before analysis by fluorescence microscopy. For signal amplification by Tyramid-Kit, secondary antibody was preceded by incubation in 0.3% H₂O₂ in PBS for 30 minutes. The secondary biotinylated antibody was detected with Tyramide detection Kit (Perkin Elmar Life Science).

TUNEL staining was performed using the cell death kit (Roche) following manufacturer's instructions. Sections were incubated for two minutes in 0.1% Triton X-100, 0.1% sodium citrate on ice. The slides were incubated with the TUNEL reaction mixture (Roche) containing the fluorescein labelled nucleotides binding to double stranded low molecular weight DNA fragments occurring during apoptosis for 60 min at 37°C. Apoptotic TUNEL-positive cells were analyzed by fluorescence microscopy and detected in the green (515-565nm) wavelength spectrum.

For stainings *in vitro*, cultures were fixed in 4% paraformaldehyde in phosphate-buffered saline (PFA-PBS) for 15 min at RT and staining was performed as described previously (Götz et al., 1998). Incubation with primary antibodies was performed overnight at 4°C and primary antibodies were detected using subclass specific secondary antibodies labelled with Cy2/FITC, Cy3/TRITC (Jackson ImmunoResearch) or biotin (detected by AMCA-coupled

streptavidines, Cy3-coupled streptavidin, Alexa 488-coupled streptavidin, Vector Laboratories).

5.5 *In situ* hybridization

In situ hybridization was performed on frozen tissue with digoxigenin (DIG)-labelled riboprobes. 5-7µl RNA-antisense probe (corresponding to 0.5-1.0µg RNA) were diluted in 150µl hybridization buffer and denaturated for 5 minutes at 70°C, applied onto the microscope slides carrying the sections of interest and sealed with a clean coverslip. Slides were incubated overnight at 65°C in a sealed box with Whatman paper, soaked with 1x SSC in 50% formamide, in a hybridization oven. Slides were thereafter washed for 10 minutes in pre-warmed (65°C) washing solution at 65°C and the coverslip was removed. Further 2-3 washes at 65°C for 30min were done, followed by 2 washes in MABT for 30min at RT. Sections were blocked in 2% blocking-solution for 1h at RT. Anti-digoxigenin Fab fragments coupled to alkaline phosphatase were diluted 1:2500 in blocking-solution and 150µl of this antibody-solution were applied per slide. Sections were covered with parafilm. The antibody incubation was performed in a humid chamber overnight at RT. Slides were washed 4-5 times in MABT for 20 minutes at RT, and rinsed twice in Alkaline-phosphatase (AP) staining buffer for 10 minutes at RT. 150µl NBT/BCIP-containing staining solution was added per slide and covered with parafilm. Slides were incubated 12 to 24h (occasionally up to 3 days) at RT. When the staining was strong enough, the reaction was stopped by rinsing the slides in AP staining buffer and shortly in water. Slides were dried for several hours at RT and mounted in AquaPoly/Mount.

The plasmids used for *in situ* hybridization are listed in the materials part.

5.6 Cell culture

5.6.1 Cortex dissection and dissociation

Embryos were removed by caesarean section from time-pregnant mice anesthetized by diethylether (Sigma). The meninges were removed, the telencephalic hemispheres separated, the hippocampus and the olfactory bulbs were removed. Cortices were dissected from rat embryos at E15, E19, or from mice hGFAP-eGFP at E14, E18 and AP2γ conditional mouse embryos at E12, E13, E14, E17, as gestational lengths vary between rats and mice and rats 1 day older were considered equivalent to mice 1 day younger. Cortices were dissected in ice cold Hanks balanced salt solution (HBSS, GIBCO) and then incubated in trypsin-EDTA

(GIBCO) for 15 minutes at 37°C. After mechanical trituration and several washes in medium containing 10% fetal calf serum (FCS, GIBCO), 5×10^5 rat and mouse cortex cells were plated on poly-D-lysine-coated glass coverslips in 24 well plates (NUNC) in 500µl DMEM/10%FCS (GIBCO) for 1 day, 3 days or 7 days.

5.6.2 Clonal analysis and overexpression *in vitro*

About 2 hours after plating the rat cortex cells, cells sorted from hGFAP-eGFP mouse cortices were added at a density of 200 cells per well (24 well plate). Cortices from WT and AP2γ conditional mouse embryos at E14 were plated directly on PDL coated glass coverslips. The following day, 500µl of chemically defined medium (SATO) was added and further medium changes were performed as described previously (Götz et al., 1998). Comparison of cell counts after sort and stainings of surviving cells after 2 hours or 7 days revealed an *in vitro* survival of about 80%, further improved in comparison to previous data [(69±15% in (Malatesta et al., 2000)]. Immunostaining for M2M6 labelling of the sorted mouse cells revealed single cells 2 hours after plating, confirming the low proportion of duplets in our sorted population. To label the cells that continue to divide *in vitro*, the DNA base analogue 5-bromo-2'-deoxyuridine (BrdU, Sigma) was added at a final concentration of 10µM. After 3 days or 1 week *in vitro*, all cell-types (neurons, astrocytes, oligodendrocytes) were detected by immunostaining in comparable numbers to those determined in previous retroviral or time-lapse cell lineage experiments (Malatesta et al., 2000; Qian et al., 1998; Williams and Price, 1995).

For overexpression experiments, retroviruses were added 2 hours after plating WT and AP2γ conditional mouse cortices (E14). Further medium changes were performed as described above.

5.6.3 Neurosphere cultures

Embryonic cortical cells were isolated, counted and plated at a density of 5000 cells per well in a 24 well plate without Polylysine or similar coating.

Cells proliferate into spheres that were maintained 7 days in DMEM/F12 media at 37°C with no medium change, counted, redissociated to single cells, counted and plated again at the same density. After seven more days in culture, the number of neurospheres was counted again.

5.6.4 Dual-luciferase reporter assay

Mouse neuroblastoma (Neuro-2A) and Human embryonic kidney (Hek) cells were plated on DMEM/10%FCS/PS media (1×10^5 cells/24 well) and transfected with expression plasmids (3 μ g), firefly (*Photinus pyralis*) luciferase reporter (1.5 μ g) under the Tbr2, Math3 or AP2 γ promoter and the pRL-TK plasmid encoding Renilla (sea pansy-*Renilla reniformis*) luciferase (0.1 μ g, Promega). Total amount of plasmids was kept constant (4.6 μ g). After 24h, medium was changed and on the next day cell extracts were prepared and assayed for luciferase activity. Relative light units were normalized to *Renilla* luciferase activity and results were expressed as the ratio of firefly to *Renilla* luciferase activity (Fluc/Rluc, Fig. 39). Luciferase activity was measured with the Dual-Luciferase Reporter Assay System (Promega) using a luminometer (Berthold Centro LB 960). Values represent the mean \pm SE of three experiments. The level of significance was $p < 0.05$.

5.7 Fluorescence activated cell sorting (FACS) and cell cycle analysis

Dissociated cells from the cortices of E14 or E18 hGFAP-eGFP heterozygous mice were re-suspended in DMEM and GFP- and/or prominin-positive cells were isolated using a FACSaria (BD) set at purity mode and the appropriate sort rate (below 1000 cells per second for high purity and recovery of cells). Gating parameters were determined by side and forward scatter to eliminate debris, dead and aggregated cells and by green (530nm) and red (575nm) fluorescence to separate positive from negative cells (determined by the use of negative control cells from GFP-negative littermates). Dissociated cells were stained using propidium iodide (PI) to reveal dead cells (less than 4%) as PI-positive by analysis with the FACSaria. Less than 1% of non-fluorescent cells were included in the sort gate. Live staining for prominin (anti-prominin PE) was combined with GFP-fluorescent protein to sort the double-labelled cells and compensation was determined using cells with only one staining. Sorted cells were routinely re-sorted to determine their purity (95-98%). After sorting, the cells were centrifuged for 30 minutes at 1000rpm and re-suspended in 100 μ l of lysis buffer (RLT from QIAGEN with β -mercaptoethanol) for RNA isolation. Alternatively, cells were plated on either embryonic rat cortex feeder layer or in some experiments without feeder layer on poly-D-lysine-coated plates (2000 cells plated per well of a 24 well plate and fixed after 2hours). Cells were stained for cell-type specific antibodies and analyzed for their GFP-fluorescence revealing about 5% non-fluorescent cells. These are maybe contaminants of non-fluorescent cells or GFP+ cells that lost the GFP protein due to membrane damage during dissociation and plating.

Cortical cells from WT and AP2 γ ^{-/-}, similarly to hGFAPeGFP cells used for sorting with prominin, were isolated as described before and dissociated by disruption of cation-mediated cell adhesion, to preserve the cell surface molecules. Therefore isolated cortices were placed in dissociation buffer (Ca²⁺/Mg²⁺-free HBSS, 1mM EDTA), washed several times in this buffer and incubated for 15 minutes at 37°C. The cells were dissociated mechanically with a fire-polished Pasteur pipette, and washed twice in DMEM/10% FCS to remove traces of EDTA. For permeabilization, the pelleted cells were resuspended in 200 μ L of DMEM/10%FCS/NaN₃. β -III-tubulin antibody was added and the solution was incubated for 15 minutes on ice in the dark. To remove the primary antibody, the cells were washed twice in permeabilization solution and finally resuspended in a 200 μ L DMEM/10%FCS. For cell cycle analysis, dissociated cells from E14 WT and AP2 γ conditional knock-out embryos were resuspended in 70% (v/v) ethanol overnight at -20°C. The fixative was washed away with PBS and cells were resuspended in PBS containing 1% FCS. The DNA content of cells was stained with propidium iodide (PI, final concentration 1mg/ml) for 5 minutes and used for FACS analysis.

5.8 RNA isolation and microarray analysis

About 2 million of GFP positive (two groups of samples from E14 hGFAP-eGFP cortex, GFP^{high} and GFP^{low}) or GFP/prominin-double positive sorted cells (two groups of samples from E14 cortex, GFP^{high}/prominin positive cells and GFP^{low}/prominin positive cells; one group GFP/prominin positive from E18 cortex) were each split into three groups of biological replicates, re-suspended in lysis buffer and dissociated with a 0.6mm gauge needle for subsequent RNeasy RNA purification (RNeasy kit, QIAGEN). The same procedure was done for microarray analysis of embryonic stem cell derived radial glia (WT and Pax6-deficient (Bibel, 2007; Bibel et al., 2004; Nikolettou et al., 2007)). The resulting RNA concentration was measured by the 260nm/280nm ratio (Nanodrop). RNA quality was examined in the Agilent 2100 Bioanalyser and revealed high purity of all RNA preparations. Agilent has developed software that will assign a specific quality number to the RNA sample based on its electrophoretic profile. The RNA Integrity Number (RIN) ranges from 1 (totally degraded RNA) to 10 (completely intact RNA). Only high quality RNA, with RIN greater than 8 and A_{260/280} greater than 1.8 was considered for microarray analysis.

In a total of seventeen samples, RNA was prepared and used for microarray hybridization. From three replicates of E14 GFP^{low} and three from GFP^{high} sorted cells 1 μ g of RNA was used for each microarray chip. From the three replicates of E14 GFP^{low}/prominin positive,

four of E14 GFP^{high}/prominin positive and four of E18 GFP^{low}/prominin+ sorted cells only 0.5µg was used due to the smaller number of cellular yield. Generation of cDNA, production of labelled cRNA and hybridization to Affymetrix MOE4302.0 GeneChip (46 k probesets) were performed according to standard protocols provided by Affymetrix (www.affymetrix.com). The RNA amplification was performed with MessageAmp II-Biotin Enhanced (Ambion, 1791). The single round aRNA Amplification kit was used similarly for all samples to avoid variations resulting from multiple rounds of amplification. All housekeeping genes were present and the number of present calls was determined as 40% or higher. To process the data we calculated probe set summaries according to the three most popular algorithms – MAS 5.0, dChip, RMA and normalized the data - a nonlinear transformation employing the loess smoother (Cleveland, 1981). To test the quality and reproducibility of the samples, hierarchical clustering was used to find (dis)similarities between the samples, showing that the replicates of each group of cells analyzed were clustering together. Probe-sets (genes) were selected as significantly differentially expressed if they had a p-value <0.05 (i.e. 5% significance level) to reduce the level of false positives. Different false discovery rate controlling algorithms were applied such as the Bonferroni and Benjamini-Hochberg (Benjamini, 1997). We applied statistical tests on the probe set summaries, the Welch's t-test, Bayesian t-test and the Wilcoxon paired rank test on the single probes. Data presented here are the differentially expressed probe-sets that showed a reproducible fold-change above threshold (2-fold in all biological replicates), exhibited a reasonably high expression level (equal or above 50; see Holm et al. 2007 for justification) in both sets of comparisons of cells sorted from E14 (GFP^{low}::GFP^{high} and GFP^{low}/prominin+::GFP^{high}/prominin+) and E18 cortices as the most stringent approach. Confirmation of gene expression differences by real-time RT-PCR supported the reliability of this analysis.

The same microarray data were also analyzed for membrane proteins among the GFP^{low} and GFP^{high} sorted cells. Data were analyzed on chip quality controls, including MAplot, boxplot and density expression values histograms that demonstrated the absence of significant defects. LIMMA package (Bioconductor 2.3) was used to build the “gene by gene” linear model to fit log (2) transformed intensities. The parameters considered to determine differential expression were: two-fold change between gene expression among the two cell lines and an adjusted P-value <0.01. For the GFP^{low} fraction out of the 907 up-regulated nucleotide sequences 285 aminoacid sequences were present in GeneBank, while 387 aminoacid sequences were available in GeneBank, out of 1159 upregulated nucleotide sequences in the GFP^{high} fraction. For each of the 1394 nucleotide sequences with no

aminoacidic translation available, a tblastx query (Gentilini, 2006) has been performed in order to associate the best scoring aminoacidic sequence (e-value<1e-70). The protein databases Non-redundant GenBank CDS translations, PDB, SwissProt, PIR and PRF have been used and protein sub-localization has been performed using the WoLF PSORT (Paul Horton, 2006).

The following link has been created to allow review of all microarray data with the series entry GSE8034:

<http://www.ncbi.nlm.nih.gov/geo/query/acc.cgi?token=tbylhsqmyikogpk&acc=GSE8034>

Total RNA was also isolated from cortical tissue of WT and AP2 γ conditional embryos at E14 using the RNeasy Mini kit (Qiagen) including DNase treatment. RNA quality was examined in the Agilent 2100 Bioanalyzer and Pico Labchip kit. RNA of WT and AP2 γ conditional animals from three different litters was amplified using the MessageAmp II-Biotin Enhanced Single Round aRNA Amplification Kit (Ambion) and hybridized on Affymetrix MOE430 2.0 arrays containing about 46k probe sets according to standard protocols provided by Affymetrix (www.affymetrix.com). Staining and scanning was done according to the Affymetrix expression protocol. For statistical analysis of the expression data the Bioconductor software package implemented in Carma web (Rainer et al., 2006) was employed using RMA preprocessing and the paired moderated limma test. The Benjamini-Hochberg algorithm was used to identify genes with a false discovery rate < 5 %.

5.9 Molecular biology

5.9.1 Plasmids and viral production

The full-length cDNA of mouse AP2 γ (1816 bp; EMBL accession number X94694) (kindly provided by Dr. M. Moser) was cloned into the EcoRI unique restriction site of the retroviral vector pMXIG between the upstream long terminal repeat and the IRES sequence (Mizuguchi et al., 2001) and sequencing confirmed the lack of mutations. The control virus used was the empty retroviral vector pMXIG. Replication-incompetent enhanced GFP-expressing retrovirus was produced from a stably transfected packaging cell line (GPG-293) transiently transfected with the retroviral expression plasmid. Viral titers typically were 10^6 – 10^7 .

The expression plasmids for luciferase reporter assay were constructed using the full-length cDNA of mouse AP2 γ and Pax6 cloned into the pMXIG vector and the full-length cDNA of

Mash1, Ngn1/2/3 cloned into the pcDNA expression vector. For control, empty pMXIG and pcDNA vectors were used, respectively. The pGL3 luciferase reporter vector and *Renilla* luciferase reporter plasmid (pRL) were bought from Promega Company. The promoters of Tbr2, Math3 and AP2 γ were cloned into the pGL3 vector. The Tbr2 promoter was constructed using the GXP_683 from Genomatix and cut of the coding sequence (816bp); the Math3 promoter was constructed using the complete sequence from the Genomatix promoter GXP_216893 (775bp) and the AP2 γ promoter was constructed using the promoter GXP_203628 from Genomatix and cut of the coding region (789bp).

Promoter sequences:

AP2 γ (789bp)

```
TTCCCCTCCCTTCCCTCAGTGGGCAGGTCAGTAAAGTACCCAGGGAGAGGGAAA
GGGGGGGGGGGGGCACTAGGGAACAGTGGGACTTTAGCTATTTCTCAGCCCAATC
CTTAAATGTCTGTCGGAACAGCTGGGGCGAGGTGTCAGGGAACCCCAGGAGTTG
AGACACCCTGGAATGGGGCGTCTTCAACTCTCAAGTGACATCCATTTTTTAGGAG
GATGAAGGACGGTTCTTGAGGTGGGGAAATCCCAGCTGTCAGCTCTGCCAGTCT
AAGGTGTGCAAGGGGGGCTGGCAGGCAAAGGAAGCCACGTTTGGGCACCTCAGCT
TGGCAGGTCTGCGGTTGTCAGAGACCGCCCACTGATGCCCCTGCGAGCCCCTCGC
GACGCCTGGTCCTGCAACACGCTAGGCAGGGTGCGGGGCGGAGCTAGGCAGGGA
CTGGCTGGGGGCTGCCCCGCCCCGGCGCCTGGGCCTCCGCGCGGGCGCCGGCCCC
GGGGAGGAGTTATGATAATTTCTTCCCATTAAGGCGTTCGGGTCCCCCGGCTAT
CGCCGGGACACACTGTGAGGGTGAGGCTTCTCCGGTCCACGGCTGCGGCCTCTAC
ACACCCACGGCGACCACATCTCTGTGCACAGCCACCGATGCGCGTCCAGTGACT
GGGACAGCAAGGCCGGCGCGCGCGGGGGCGGCGGCAGACGCCTGGCCACC
GTGACCCCGATTGTGGATTTACCGCTCGGGGGGTGGGGGGAGCCTGGATTAACT
GGCGACTATTTTGGGGGACGCCGGACGCC
```

Eomes (816bp)

```
CCTGCCAAACTAGACCCGAACCTCAGGAATGATTCCTATGCCGTGGGTAGACCAT
GTTCGCAGACTTCAAACCCGTTTCTCCGGCGCCATAGAGCCACCGGGTACACCAG
GATTGATTCTCAGTGGGATATAGTTCTCCCAAAGACGCTTAAAGAAACACCAAA
CCAGCAATAACAGCCAAATAAGCTAAGAGAAAATGAAACTCGCAGGCGACCCG
ATCCAATTAATAAATACTTAATTGAATTAGTGTCACCTCTAACAGCCAATAGCAA
AGTCCCCTAGCCATGGGGCTGCGAAGCCCCTCCCTGGCCGCACATATATAAGCA
GCCAACCACCGCTCACAAGTTTCCAAGCGGTCAAGTATGCCTAGAGTTTAGCAG
AGCCAGCCGAGAGGAAATGGCTGGTTGCTAAATGGGAACTCAGAGCTAAGTCCT
CTTCTTCCTTAGTGAGTGAGTGTAGGGGTCCTGAGAGGTTAGACAAGGAGGGAAGG
AAGAAAAGAAGGAAGGAAGGAAGGAAGGAAGGAAGGAAGGAAGGAAGGAAGG
AAGGAAGGAAGGAGAGAGACACCTACAACCCGGGGTTTGTCTTCTTGCGGAAGG
AAAGGGGCACCTACAATCCCGAGTTTGTTCCTTGAGGGAAGGACGCTAAATTG
GGCGCGCGCTGAAGCCGCCCCGCAGGTCCGCAGGTGGGTAGCCTAGGCGAGGGA
GGAAGGGGACATTACCTTCCCCTCGGAAGAGGGCGCTGGCTCCCCCAACTGGCC
TTTATAACCAGGCCGCGGGAGGCGAGGAGGCAGCCGGTTGCCGTCTGCGATTCTG
CTAAAGC
```

NeuroD4 (775bp)

```
GCTGGGAATGTAGCTTAGTGGTAAAGTGCTTGTTTAGCATATGCAAGGCTAGGTT
CAAATGTTAGAAATACACACACACACACAAACACACACACACACACACACACAC
ACACACACACACACACACACACACAGCAAAAATAATCTGTCCAAGACACAAAAC
CAAAATCTGAAAAAACAACAACCAACCAATCAAACCAATAATCTCCCCATGTAG
GGTAGTAGAGTCACTAATACTACGTCCTTGCTGTGTAGTTTTCTCAGGTTTTTGATT
CATTTTAAGCATGGGCCACCAATCTCATGTACCTTTTTAGCTTTCTTTCCAAGTGT
GTCTCCAGTTTTCTGACCCCCCTCCTGTTTTGCCTGCTCTACCCTGCCTTGTACCTT
TCTAATCACAAGTCTTTTCAGTTCCTTAGTTTTACCCATCAACTTCAGCAGCCC
ACACCCTCTAGTTCCTTCCTGGTTTAAACAAAAACAAACACGCAGTGGCAAAGCT
GGACCTGGTCAGAGAAGCCTTGTAAGGAGGTGTGTCTTTAGGCTAGGAAGGGG
AGGGGCTACCCTGTGGGCAACATCTCCCGCCCTGGTCAGCAGCCAAAACCAGCA
AAACGGCGGCAAGTCAGAAGCTCCAGTCAGATCACAGGAGCTGCCCAGAGACTG
TGGTACTGAAAGAACTACTCGCGGGAGCTGACCCCGGGAAAGAGGTACTGAAAA
GACATAGAAAACCAGCTGTGGTGGAGGCACTGACATGAAGGCATCCTGGTAGTG
CATCAGAA
```

5.9.2 Transformation into chemically competent *E.coli*

50µL of chemically competent *E.coli DH5α* were incubated with approximately 5µL of vector DNA (~5µg) for 15 minutes on ice. After a 45 seconds heat shock at 42°C the bacteria were chilled on ice for at least 2 minutes, ~500µL LB₀ was added. The cells were incubated for ~1 hour at 37°C on a shaker, subsequently plated on LB_{Amp} plates and placed overnight at 37°C.

5.9.3 DNA-purification

For subsequent sequencing or virus production, plasmids were isolated from *E.coli* using Qiagen Mini, Midi or Maxi-Prep Kits. PCR-Products were purified with the Qiagen PCR Purification Kit, purifications from agarose gels with the Quiagen Gel Extraction Kit. All steps were performed as recommended by the supplier.

For purification of plasmids for purposes other than sequencing or virus production, DNA was separated by phenol-chloroform-extraction. For that, one volume (relative to the sample volume) of phenol/chloroform/isoamylalcohol was added. The mixture was vortexed shortly and centrifuged for 5 minutes at maximum speed in a tabletop microcentrifuge. The upper phase was recovered and 1/10 volume of 3M sodium acetate and 0.7 volumes of 100% ethanol (RNase free) were added to precipitate DNA. The sample was centrifuged (10 minutes at RT, 13000 rpm). The supernatant was removed and the pellet was washed with 70% ethanol. After air drying, the pellet was resuspended in an appropriate amount of RNase free sterile water.

5.9.4 DNA restriction digest

Analytical digests were performed in 50µL total volume with 1-2µg DNA and ~2 units enzyme overnight at 37°C.

5.9.5 Vector dephosphorylation

The dephosphorylation of digested vectors usually decreases religation of the vector. The dephosphorylation procedure was performed with 50µL heat inactivated digested vector. 1µL antarthic phosphatase was added to a total volume of 50µL. After an incubation period of 30 minutes at 37°C another, the mixture was incubated at 65°C for 20 minutes to inactivate enzyme following incubation on ice for 10 minutes.

5.9.6 Ligation

Ligations were usually performed with a 2:1 molar ratio insert/vector. The samples were incubated at 16°C overnight and transformed the next day. Colonies were selected and inoculated in LB medium with Ampicillin at 37°C overnight. To confirm the correct insertion of the insert into the vector, digestion was performed at 37°C overnight and in the next day the resulting products were analyzed on a 1% agarose gel.

5.10 PCR

For cloning of the selected riken genes, these DNA sequences were amplified from E14 WT cortex cDNA of different concentrations. Typically, 40ng of template were used. The PCR was carried out with a total volume of 25µl using (in the final mix) 1x Fermentas PCR buffer without MgCl₂, 400µM dNTPs, 1µM each primer, 2.5mM MgCl₂ (rik15,18,20)/ 3.75µM MgCl₂ (rik4) and 0.2µl/25µL homemade Taq-Polymerase under the following conditions:

	0910001A06RIK	2600009P04RIK/2610017109RIK	2810025M15RIK/ 2300002D11RIK
Preheating	94°C - 4min		
Denaturation	94°C – 45s		
Annealing	54°C - 30s	55°C - 30s	65°C – 30s
Elongation	72°C – 2:30min	72°C – 1min	72°C 1:30min
Final Elongation	72°C – 7min		
Hold	10°C		

For cloning of AP2γ, Tbr2/Eomes and NeuroD4 promoter regions, these DNA sequences were amplified from genomic cDNA. DNA was heated for 5 minutes at 90°C and thereafter placed on ice for 10 minutes. The PCR was carried out with a total volume of 30µl using (in

the final mix) 1x Fermentas PCR buffer with MgCl₂, 400μM dNTPs, 10μM each primer, 6μl Q solution and 2μl Fermentas Taq-Polymerase under the following conditions:

	AP2 GAMMA	EOMES/TBR2	NEUROD4
Preheating	94°C - 10min		
Denaturation	94°C – 30s		
Annealing	62°C - 30s	58°C - 30s	50°C-30s
Elongation	72°C – 1min		
Final Elongation	72°C – 10min		
Hold	10°C		

5.11 cDNA synthesis and real-time PCR analysis

cDNA was synthesized from the RNA samples used for microarray analysis using the SuperScript IITM First-Strand Synthesis System (Invitrogen). Real time PCRs (RT-PCR) were performed according to the manufacturer's recommendations using SYBRGreen master-mixes from Qiagen on a DNA Engine OpticonTM machine (Biorad). Primer dimer melting temperatures were determined in order to exclude primer dimers from the analysis. The housekeeping gene used was GAPDH for normalization of the target gene's expression. The relative expression was calculated as $E = \frac{1}{2}^{-\Delta Ct}$, where Ct is the difference between the threshold of cycle number of GAPDH and the gene analyzed. Primer sequences are described in the materials part.

5.12 *In vivo* injections

5.12.1 *In utero* injections

Timed pregnant mice with embryos at a gestational age of embryonic day 14 (E14) were anaesthetized with a mixture of fentanyl (0.05mg/kg), midazolam (5mg/kg) and metedomidine (0.5mg/kg). Injection needles were made from glass micropipettes pulled to produce a long taper and broken under a dissection microscope at an inner diameter of 10–20 μm. Glass microcapillaries were sharpened with a sharpener (Model EG44, Narishige) to produce a bevel angle between 25° and 35°. After deep anaesthesia was verified by the absence of pain reflexes, the abdomen was wet shaved and the uterine horns were exposed after caesarean incision. The uterine horns were kept wet with sterile saline. Viral vector suspension (0.5±1.0μl) with Fast Green (2.5mg/μl) (Sigma) was injected with a glass micropipette into the cerebral ventricles of the embryos, illuminated with a lamp for better visualization. Successful injections of the virus could be verified by the darkening of the

ventricles by the Fast Green. After injection, the peritoneal cavity was rinsed with warmed 0.9% NaCl, the uterine horns were replaced and the wound was closed. Anaesthesia was terminated by injection of naloxon (1.2mg/kg), flumaceniil (0.5mg/kg) and atipamezol (2.5mg/kg). Painkillers and surveillance were applied several times a day for postoperative care. Animals recovered very well after the operation with no signs of distress. The injected embryos were sacrificed 3 days after injection or 2-5 days after birth. These experiments are under the license number 55.2-1-54-2531-144-07.

5.12.2 Beads injections

Adult WT and AP2 γ ^{-/-} mice were anaesthetized with a mixture of fentanyl (0.05mg/kg), midazolam (5mg/kg) and metedomidine (0.5mg/kg) and placed in a stereotaxic frame. A small portion of the skull overlying the visual cortex was carefully drilled and removed, leaving the dura intact. After exposure of the brain surface, a single injection with red RetroBeads (100nl, LumaFluor) into the midline representation of the visual cortex (stereotaxic coordinates: 2.8 mm lateral to midline, on the AP level of Lambda) was given to WT and AP2 γ ^{-/-} mice starting the injection 600 μ m below the surface and keep injecting very small amounts until 200 μ m below the surface. One week later mice were perfused and the contralateral hemisphere was analyzed (injections performed by Monika Brill).

5.13 BrdU labelling *in vivo*

For interkinetic nuclear migration (INM) analysis during embryonic development, E14 pregnant mice were injected intraperitoneally (5mg BrdU/100g body weight). The pregnant mouse was sacrificed 30 minutes or 6 hours after injection.

For birthdating analysis timed pregnant WT and AP2 γ ^{-/-} mice (E14) were injected intraperitoneally with BrdU and analyzed 3 days later or at postnatal stages P2 or 5.

For labelling of slowly dividing cells in adult mice, BrdU in drinking water (1mg/ml) was given to adult WT and AP2 γ ^{-/-} mice during one week and mice were sacrificed 8 weeks later.

5.14 Data analysis

5.14.1 Quantification of fluorescence intensity at the confocal microscope

GFP-fluorescence intensity was measured in 1047 cells of hGFAP-eGFP mouse cortices sections with Olympus Software FV10-ASW 1.6A in which pixel intensity values range from 0 to 4095.

5.14.2 Clonal analysis

Clones were analyzed at 40x magnification (Zeiss Fluorescent Microscope). The probability of clonal superimposition was calculated as described in (Williams et al., 1991), e.g. for coverslips containing a maximum of 25 clones the probability was calculated to be 0.02. The mean number of clones was obtained from three experimental batches and the mean was determined from the values per coverslip, n indicating the total number of coverslips and \pm indicating the standard error of the mean. The mean number of clones per coverslip obtained in my experiments was 28 ± 4 .

5.14.3 Quantification of PH3-positive cells

The number of PH3-positive was quantified using Neurolucida software 6.0 (MicroBrightField; Inc., Vermont, USA). PH3-positive cells were considered to be located at non-surface positions if they were more than 5 cell diameters distant from the ventricle. Rostral sections were considered as the first cortical slides not containing the hem, intermediate sections contained the hem and caudal sections contained the hippocampus. All other quantifications were done using single confocal optical sections. The number of PH3 immunopositive cells and activated caspase3-positive cells were counted and calculated as the number of cells per μm^2 . For all quantifications at least three different litters of animals were analyzed.

5.14.4 Interkinetic nuclear migration quantifications

INM was measured by quantifying the number of BrdU+ cells in each bin, 6h after a single BrdU injection (a bin was defined as a 20 μm -thick, 100 μm -long stripe parallel to the VZ, with the apical-most bin as bin 1 and the basal-most bin as 10) (Cappello et al., 2006).

5.14.5 Cortical neuronal layers measurements

The number of Cux1+ cells in sagittal sections of WT and AP2 γ ^{-/-} adult brains was calculated per total cells (DAPI) in 100 μm stripes, using ImageJ software. The percentage of control and AP2 γ infected GFP+ cells localized in the cortical layers II-VI was calculated in 500 μm stripes. Values of the AP2 γ infected GFP+ cells were normalized to the control infected GFP+ cells. The thickness of cortical layers II-IV (Cux2+) was measured in sections of the adult WT and AP2 γ ^{-/-} brains at frontal and occipital regions using ImageJ software.

5.14.6 Statistics

Calculations of the arithmetic average - $\bar{x} = \frac{1}{n} \sum_{i=1}^n x_i$, the standard deviation -

$$s = \sqrt{\frac{\sum_{i=1}^n (x_i - \bar{x})^2}{n-1}}$$

and the standard error of the mean (SEM) - $SEM = \frac{s}{\sqrt{n}}$ were

performed with Microsoft Excel. The unpaired Student's t-test was used to examine whether data sets differed significantly. Data were considered as significant with $p < 0.05$ and as highly significant with $p < 0.01$.

5.15 Materials

5.15.1 Kits:

Table 1: Kits used for isolation and extraction of DNA

KITS	COMPANY
RNA extraction Kit	Qiagen
Qiaprep MiniPrep	Qiagen
Qiaprep MidiPrep	Qiagen
Qiaprep MaxiPrep	Qiagen
Qiaquick gel extraction kit	Qiagen
Qiaquick PCR Purification kit	Qiagen
TA cloning kit for Sequencing	Invitrogen

5.15.2 Medium:

Table 2: Composition of medium including manufacturers for cell culture experiments

MEDIUM	COMPOSITION	COMPANY
DMEM	+4500mg/L glucose +Glutamax I -Pyruvate	GIBCO
DMEM/F12		GIBCO
HBSS		GIBCO
B27 supplement		GIBCO
Pen/Strep		GIBCO
HBSS Ca ²⁺ , Mg ²⁺ free		GIBCO

5.15.3 Primers:

Table 3: Primers for PCR reactions (cloning)

NAME	SEQUENCE 5'-3'	AMPLICON	T _M	COMPANY
0910001A0	5' – gAAGgACAAGgACAA	bp 282-1303	55.7°C	MWG

6Rik fwd (cloning)	AAT CAC CAg – 3'			
0910001A0 6Rik rev (cloning)	5' – Cag Tag ggg CTT gCT CCA CAg – 3'		56.2°C	MWG
2600009P0 4Rik fwd (cloning)	5' – AAg CAT TCA gAA gCC AAA CAA – 3'	bp 27-440	54.0°C	MWG
2600009P0 4Rik rev (cloning)	5' – TAT TTT TAg ggA AgA CAC gCA gTT – 3'		53.4°C	MWG
261001709 Rik fwd (cloning)	5' - gAA gCC ACg CgA ggT ATT TgA – 3'	bp 107-624	56.6°C	MWG
261001709 Rik rev (cloning)	5' – gCA CCA TTT CAT CAC ATC AgC ACT – 3'		57.7°C	MWG
2810025M 15Rik fwd (cloning)	5' – Tgg Tgg AAg CAg AgA Cgg TgT T – 3'	bp 430-955	58.2°C	MWG
2810025M 15Rik rev (cloning)	5' – AgA ggA TCC TgA TgT gCT ggT Tg – 3'		56.9°C	MWG

Table 4: Primers used for real-time RT-PCR (synthesized by TibMolBio)

PRIMER NAME	PRIMER SEQUENCES
Ascl1	5'-gcgcgccaacaagaagatgagca-3' 5'-ttgggggagatggtggcgacagg-3'
Arhgap5	5'-gagcctcgacccccatct-3' 5'-ctcggcctccaaagtcaa-3'
Arhgap18	5'-gaaaatcgccaagaaggtcaag-3' 5'-gtccgggtcagtgtagataaaaac-3'
Arhgef7	5'-aagcccgtgtcacccaaatcagg-3' 5'-agtggccgcaggtaggtggacag-3'
Cdc42	5'-gcagggcaagaggattatgac-3' 5'-cccaacaagcaagaaaggagt-3'
Cux2	5'-aggggccaccgaactctcc-3' 5'-tggggctggtactcggcactt-3'
Emx1	5'-ccacggcgtcaactatcctcacc-3' 5'-aacaccagtccggccctccatag-3'
Tbr2	5'-gtgggctcattctggatgtc-3' 5'-attaccctgaccgcaccttc-3'
Fezl	5'-ctgctcgccgctgccctgtatga-3' 5'-cgccgctgcctcctcctccac-3'
GAPDH	5'-attcaacggcacagtcaagg-3' 5'-tggatgcagggatgatgttc-3'
GFP	5'-tggtagcaagggcgaggag-3' 5'-gccggtggtgcagatgaact-3'
Glast	5'-ttggtcgcggtgataatgtgga-3' 5'-cgatgacggcgtgaatgagg-3'

Id3	5'-cgaggccgcggttaagagc-3' 5'-cgaggccgcggttaagagc-3'
Kifap3	5'-gaacgctggcaaatctgacaatc-3' 5'-tctgcggcacctggctttag-3'
Lmo4	5'-cccaaggcaacgtgtatcat-3' 5'-gagggctgtgggtctatcat-3'
Math3	5'-ttgaagggaagggtttgtagaga-3' 5'-gggagccctggagactgatat-3'
Mtap2	5'-agctgtggcaaaagaagg-3' 5'-tggtcttggcctttctggtc-3'
NeuroD1	5'-ctgaacgcggcgtggacaac-3' 5'-gtagggatgcaccgggaaggaagc-3'
Ngn2	5'-accgatgcacaacctaaac-3' 5'-agcggccagatgtaattgtg-3'
Notch1	5'-cgacattccccaccgcagat-3' 5'-gtggccgtcgctaaaatacttc-3'
Par3	5'-cagcgatcagccttctattctct-3' 5'-catcccccttctggcttcagttt-3'
Pax6 PDless	5'-gaggtcaggcttcgctaag-3' 5'-agttttctccacggacgctg-3'
Pax6 paired	5'-gcagaattcgggaaatgtcg-3' 5'-cagcttggtggtgtctttgt-3'
Pax6 homeo	5'-tctaategaaagggccaaatg-3' 5'-aggaggagacaggtgtggtg-3'
Pax6(5a)	5'-gcagatgcaaaagtcaggt-3' 5'-ctcgtaataacctgcccagaa-3'
Pea15	5'-cacaacaagctggacaaagacaa-3' 5'-ggcactgggaatacgggttag-3'
Prkcz	5'-tctaggccccgggtgataacaag-3' 5'-cgcccagccatcatcacaacata-3'
p75	5'-ctcattctgtctattgtcca-3' 5'-ttttgcttcagctgttcc-3'
Rab3d	5'-tcgccgatgatcttggtttgag-3' 5'-ggctgtgggggtgggtatc-3'
Rab6d	5'-acggtggctgtggtggtat-3' 5'-agttctttggcccgtgtt-3'
Rab7	5'-caaggaggtgatggtggacgaca-3' 5'-gggggctggcctggatgag-3'
Rab11a	5'-cccggccgtggaggaggaggagt-3' 5'-ggcggcggtgggggaggttg-3'
Rac1	5'-ggctggccatggcgaaagaga-3' 5'-ttgacaggagggggacagagaacc-3'
Rhoa	5'-ccattgacagccctgatagtttag-3' 5'-gttttaccggctctgcttcatt-3'
Rhob	5'-atcgtttacggccgctctcctate-3' 5'-ctttacctcgggcacccacttctc-3'
Rhoc	5'-gtcccaacgtgcccatcatcc-3' 5'-ctcccgcaccccttcttagtct-3'
Rhog	5'-ggtaagcgcccatcactccac-3' 5'-gacagcctccgcaaacacctctt-3'

Rhoq	5'-ggggcggtgggcaagacg-3' 5'-ccccacggtgacgtgactg-3'
Rhov	5'-acaccgcagggcaggaggacttg-3' 5'-gcggatctcaggcagccattttc-3'
Robo1	5'-ggccccactccccctgtcc-3' 5'-gtcgccgcctcctgtctggt-3'
Satb2	5'-agccccagccagccaagtctcag-3' 5'-gtcggccaccagtcgcatcagg-3'
Socs7	5'-cccggccgtggaggaggaggagt-3' 5'-ggcggcggtgggggagggtg-3'
Sox5	5'-tgccggacagaaaaggaaaaa-3' 5'-ggggctcgttgctaccac-3'
Sox9	5'-atcaagacggagcagctgag-3' 5'-tctgatggtcagtgtagtcg-3'
Sox11	5'-gggcgccggctctactaca-3' 5'-gccgctctgctgccgctggat-3'
Sox21	5'-ccaagacgtgctcaaaaaggaca-3' 5'-cgggggttcgcgagcagagact-3'
Stat3	5'-gctggcggggctcttgc-3' 5'-tcttaattgttggcgggtctgaa-3'
Svet1	5'-gattcctgggcattaagactcacc-3' 5'-cccccaacatcacctacctaac-3'
Syt4	5'-gaagacgtggaccctgttttg-3' 5'-ttggatgtggggataagggaattc-3'
Tcfap2c	5'-atggccacgcggaagagtatgtg-3' 5'-cctggggcgggcctgttgtcc-3'
Tgfbeta2	5'-aggcgagattgcaggtattgatg-3' 5'-cgccggctggactgttgact-3'
Ttyh1	5'-cccggaggaggttcgtcac-3' 5'-tgcctcaccagcctctccac-3'
Zac1	5'-gggcgcaaagaccacctcactcg-3' 5'-caagccaccatcaagcccgttctc-3'
2410005K17Rik	5'-ccacctgcccggaaagaaaa-3' 5'-gaactcatcaaactgctgctgctc-3'
28100025M15Rik	5'-ccgccctggagctggatttat-3' 5'-gctttggcagggtgatgtggact-3'
0910001A06Rik	5'-tttgaaaatgccagcctacag-3' 5'-caccacacgccttctcttg-3'
2600017I09Rik	5'-cgggactgtaaggcggataaga-3' 5'-ccaattggcaggaggagcat-3'

5.15.4 Plasmids and vectors

Table 5: Plasmids and vectors for cloning experiments.

PLASMIDS/ VECTORS	COMPANY/REFERENCE
pSCA cloning vector	Stratagene
pCR4-TOPO	Invitrogen
pCMV-SPORT6	Invitrogen
pMXIG-IRES-GFP	(Nosaka et al., 1999)

pRL-TK	Promega
pGL3-luc	Promega

5.15.5 Primary Antibodies:

Table 6

ANTIGEN (SPECIES)	WORKING DILUTION & PRETREATMENT	COMPANY/SOURCE
active Caspase3 (rabbit)	1:50	Promega
AP2 α (mIgG ₁)	1:50	Santa Cruz
AP2 γ (H-77) (rabbit)	1:50, 5x5min boiling in 0.1M citrate/0.5% Triton X 100/ PBS	Santa Cruz
β -III-tubulin (mIgG2b)	1:100	Sigma
BLBP (rabbit)	1:1500	Kind gift of N. Heintz
BrdU (rat)	1:100, 30min 2N HCL, 2x15min Borate buffer pH8.5	ABCAM
CTIP2 (rat)	1:200	ABCAM
Cux1 (rabbit)	1:100	Santa Cruz
GFAP (mIgG ₁)	1:100	Sigma
GFP (rabbit)	1:500	RDI
GLAST (guinea pig)	1:100	Chemicon
KI67 (rabbit)	1:50, 2x4min boiling in 0.1M citrate/0.5% Triton X 100/ PBS	DAKO
L1 (rabbit)	1:100	kind gift of Thomas Tilling
NeuN (mIgG1)	1:100	Chemicon
Pax6 (rabbit)	1:300, 7min boiling in 0.01M citrate/0.5% Triton X100/ PBS	Chemicon
PH3 (rabbit)	1:200	Upstate
Prominin-PE	1:1000	Biosciences
P75 (rabbit)	1:200	Chemicon
RC2 (mIgM)	1:500	Kind gift of P. Leprince
Satb2 (rabbit)	1:1000	Kind gift of V. Tarabykin
Tbr1 (rabbit)	1:100	ABCAM
Tbr2 (rabbit)	1:2000, 8min boiling in 0.01M citrate/0.5% Triton X100/PBS, 1h 2N HCl	ABCAM

5.15.6 Secondary Antibodies:

Table 7

ANTIGEN (SPECIES)	WORKING DILUTION & PRETREATMENT	COMPANY/SOURCE
mIgG1-FITC	1:200	Jackson ImmunoResearch
rab-Cy3	1:400	Jackson ImmunoResearch
mIgG1-biotin	1:100	Vector Laboratories

rab-Cy2	1:400	Jackson ImmunoResearch
rat-Cy3	1:400	Jackson ImmunoResearch
Streptavidin-AMCA	1:100	Vector Laboratories
Streptavidin-Alexa647	1:1000	Vector Laboratories
Streptavidin-Alexa488	1:1000	Vector Laboratories
rat-Cy2	1:400	Jackson ImmunoResearch
mIgG2b-FITC	1:200	Jackson ImmunoResearch
mIgG2b-biotin	1:100	Vector Laboratories
mIgG2b-TRITC	1:400	Jackson ImmunoResearch

5.15.7 Solutions:

Table 8: Solutions and their compositions

SOLUTIONS	COMPOSITION
BCIP stock	50 mg/ml BCIP in 100% DMF
Embedding solution	4.5 g/l gelatine, 270g/l albumin, 180g/l sucrose in ddH ₂ O
ISH Block buffer	PBT, 2% normal goat serum (NGS), 2 mg/ml bovine serum albumine (BSA)
ISH Hybridization buffer	65% Formamide, 5x SSC, 50 µg/ml Heparin, 0.5 mg/ml yeast tRNA, 0.1% Tween- 20, 9.2 mM citric acid pH 6. 0
LB- medium	20 g/l LB broth base in H ₂ O
LB-Agar	40 g/l LB-Agar in H ₂ O
NBT stock	100 mg/ml NBT in 70% dimethylformamide (DMF)
NBT/BCIP revelation solution	225 µg/ml NBT, 175 µg/ml BCIP, in NTMT
NTMT	0.1% Tween- 20, 50 mM MgCl ₂ , 100 mM NaCl, 100 mM Tris- HCl pH 9.5
NTMT-Fast Red	0.1% Tween- 20, 50 mM MgCl ₂ , 100 mM Tris- HCl pH 8
PBS	1,3 M NaCl, 27 mM KCl, 15 mM KH ₂ PO ₄ , 83 mM Na ₂ HPO ₄
PBT	PBS, 0.1% Tween- 20
PFA 20%	200 g/l PFA, 10 M NaOH, PBS, pH7
SSC 20x	3M NaCl, 0.3 M C ₆ H ₅ Na ₃ O ₇ , pH7
TBE Buffer 5 x	0.45M Tris-Base, 0.45M Boric Acid, 5mM EDTA
TE- Buffer	10mM Tris, 1mM EDTA, pH8
TNE buffer, 10×	100 mM Tris base, 10 mM EDTA, 2.0 M NaCl, pH 7.4
Lysis buffer for genotyping	100mM TrisHCl, 5mM EDTA, 0.2% SDS, 200mM NaCl, 100µg/ml proteinase K (pH= 8.5)

6 Results

6.1 Lineage analysis at the transcriptome level – new insights into functionally distinct radial glial subtypes

6.1.1 Separation of distinct radial glia-derived lineages

In order to separate subsets of radial glia that mostly generate neurons (neurogenic radial glia) from radial glia that generate few neurons (non-neuronal clones and mixed clones in Malatesta et al., 2000, 2003), I examined radial glia from hGFAP-eGFP mice that exhibit differences in their levels of GFP expression (GFP^{low}- and GFP^{high}-expressing cells in Fig. 5a-c). We wanted to examine if the variation in GFP-intensity may be correlate with fate differences. This approach is based on the rationale that radial glia that are neuronal progenitors may down-regulate hGFAP-promoter driven activity and hence have less GFP and be less intense in their green fluorescence.

In order to test this assumption I examined the composition of clones generated by weaker (GFP^{low}) and stronger (GFP^{high}) green fluorescent cells in the cortex of hGFAP-eGFP mice at mid-neurogenesis. Cells isolated from hGFAP-eGFP mouse (Malatesta et al., 2003; Nolte et al., 2001) cortices at E14 were therefore separated into GFP^{low} (Fig. 5d'') and GFP^{high} (Fig. 5d') fractions each of which comprising 30% of all cells from E14 cortex (Fig. 5d). Separation of the GFP-expressing cells was done into two equal proportions with respect to their fluorescence intensity (the range of green fluorescence containing GFP+ cells $10^3 - 5 \times 10^5$ was divided in half, Fig. 5a'). RT-PCR analysis of mRNA isolated from these populations confirmed the correspondence of green fluorescent intensity to mRNA levels of GFP. GFP mRNA in GFP^{high} cells is about 40x higher than in GFP^{low} cells whose GFPmRNA is still much higher than in WT control cells (Histogram in Fig. 5a). Notably, re-analysis of the sorted cells confirmed that contamination by GFP-negative cells was below 5% (see Methods), suggesting that the decrease in fluorescence and GFPmRNA levels are not due to contamination by negative cells.

Next, I analyzed the composition of the sorted cells 2 hours after plating (see Methods) by immunocytochemistry (Fig. 5e, f). A large proportion of the GFP^{high} fraction of sorted cells was radial glia as determined by Nestin, BLBP, GLAST, RC2, Pax6 or LeX immunoreactivity (49%, Fig. 5e). While all RGCs divide *in vivo* (Hartfuss et al., 2001), some of the sorted radial glia seem to stop to proliferate immediately after sorting as they could not be double-stained with the monoclonal antibody directed against Ki67 (Key et al., 1994) (Fig. 5e). Notably, however, there were also quite a few dividing cells that did not double-label

with radial glia markers (23%, Fig. 5e). In order to determine the identity of these cells I used antisera against the transcription factor Tbr2, a protein contained specifically in the SVZ or basal progenitors in the cortex at mid-neurogenesis (Englund et al., 2005). Indeed, Tbr2-positive cells were included amongst the GFP^{high} Ki67-positive progenitors (5.6%, Fig. 5e), while they were absent from the GFP^{low} fraction (Fig. 5f). The presence of a considerable fraction of basal progenitors in the GFP^{high} fraction was confirmed at the transcriptome level as described below. Thus, the GFP^{high} fraction contains many radial glia (~50%), but also other progenitor subsets (~24%) as well as β -III-tubulin-positive (Lee et al., 1990) neurons (~26%, Fig. 5e). In comparison, the GFP^{low} fraction contained many more neurons than the GFP^{high} fraction as well as a large proportion of immuno-negative cells (Fig. 5f). Indeed, marker-negative cells are not dividing (Ki67-negative) and do not contain radial glial markers (Fig. 5f). RGCs comprised only a small subset of the total GFP^{low} fraction (22.5%). However, they still compose the majority of the dividing Ki67-positive cells that are a small population amongst the GFP^{low} sorted cells (Fig. 5f). Thus, eGFP-positive cortical cells from the hGFAP-eGFP mice contain RGCs but also other cell types, such as basal progenitors and young neurons.

To examine the progeny of the progenitors contained within these FAC-sorted populations I performed clonal analysis *in vitro*. As previously described (Malatesta et al., 2000, 2003), I employed the mouse-rat co-culture system to detect the progeny of single cells isolated by FACS. Toward this aim a small number of sorted cells (200 cells) was plated on a rat cortex feeder layer isolated from E15 rat cortex (see Methods and Malatesta et al., 2000, 2003). The cells sorted from mouse cortex can be identified on the basis of their M2M6-immunoreactivity (Lagenaur and Schachner, 1981) 2 hours after sorting, and distinct clusters originating from individual cells that continued to divide *in vitro* can be detected 7 days later. The single or multi-cell clusters were then double-stained for the neuron-specific antigen β -III-tubulin and classified into clusters (clones derived from a single sorted cell) containing exclusively neurons (pure neuronal clones), containing β III-tubulin-positive and -negative cells (mixed clones) and containing exclusively β III-tubulin-negative cells (non-neuronal clones) (Fig. 5g-k). Notably, the proportion of β III-tubulin-positive clones considerably increased from 41% immediately after plating to 78% after 7 days *in vitro* amongst the GFP^{low} sorted cells, supporting the concept that this fraction contains a neurogenic population (Fig. 5h, j). In contrast, the neurogenic fraction was much smaller amongst the GFP^{high} sorted cells, where we observed only an increase from 26% to 41% during the 7 days *in vitro* (Fig.

5g). The GFP^{high} sorted cells also generated more clones immunoreactive for the astroglia marker GFAP (6.3% GFAP+ clones generated by GFP^{high} sorted cells compared to 3.2% generated by GFP^{low} sorted cells, Fig. 5i). In order to discriminate the true progeny of dividing progenitors from cells that had already differentiated into neurons or glia, we added the DNA base analogue BrdU during the entire culture period to identify clones derived from cells continuing to divide *in vitro* (Fig. 5k). Interestingly, these data revealed a large difference between the two lineages with hardly any proliferating cells generating neurons amongst the GFP^{high} sorted progenitors (14.5% - including pure and mixed neuronal clones, n=270), while the few progenitors included in the GFP^{low} fraction generated largely neurons (67.2%, n=210) (Fig. 5k).

In addition, both fractions of sorted cells were able to generate neurospheres *in vitro*, supporting the presence of proliferating progenitor cells with neurosphere forming capacity in both fractions (Fig. 6). However, the GFP^{high} fraction of sorted cells was able to generate a higher percentage of neurospheres with high levels of GFP fluorescence (12.1%, Fig. 6b, c) comparing to the GFP^{low} fraction (4.2%, Fig 6a, c). Only upon high intensity confocal imaging the low GFP expression of the neurospheres formed by the GFP^{low} sorted cells could be visualized, additionally demonstrating varying GFP intensity levels (Fig. 6a). The higher percentage of neurospheres formed by the GFP^{high} fraction of sorted cells is in agreement with the higher percentage of Ki67-positive proliferating progenitor cells present in the GFP^{high} fraction after FACS sorting (Fig. 5e, f).

Thus, separation of GFP-positive cells from the cortices of hGFAP-eGFP mice based on their fluorescence intensity allowed selective enrichment of progenitor subtypes including their immediate progeny. This analysis further suggests that the GFP^{low} fraction is enriched in neurogenic radial glial progenitors, while the GFP^{high} fraction contains a higher fraction of non-neurogenic radial glia.

6.1.2 Prospective isolation of distinct radial glia progenitor subtypes

In order to separate these distinct progenitor fractions (neurogenic versus largely non-neurogenic radial glia) from their progeny, I took advantage of the apical localization of the pentaspan membrane protein prominin (CD133) in neuroepithelial and RGCs in the developing CNS (Weigmann et al., 1997). Prominin allows discriminating cells that have an apical membrane domain, namely all ventricular zone (VZ) cells, from basal/SVZ progenitors and postmitotic neurons (Götz and Huttner, 2005). Prominin-immunostaining labelled about 40% of all cells in E14 cortices, virtually all of which (95%) were also GFP-positive (total

GFP-positive/prominin-positive population: 37.9% - Fig. 7a'). These data are consistent with the notion that the majority of apical VZ progenitors are RGCs in the E14 cortex [(Hartfuss et al., 2003), see however (Gal et al., 2006)]. Conversely, only a third (33%) of all GFP-positive cells were also prominin-positive (Fig. 7a'), consistent with the inclusion of neurons and basal progenitors in the GFP positive fractions and the absence of prominin on these cells. The gating parameters for the FACS analysis were determined by side and forward scatter to eliminate dead and aggregated cells and by green fluorescence for GFP (530nm) and red fluorescence for prominin (575nm) to separate positive from negative cells. I separated GFP/prominin+ cells into two equal proportions with respect to their fluorescence intensity (the range of green fluorescence containing GFP+ cells was divided in half) resulting in the separation of GFP^{low}/prominin+ cells (Fig. 7a', a'', 17% of all cortical cells) and the fraction of GFP^{high}/prominin+ cells (Fig. 7a', a'', 21% of all cortical cells). The percentage of GFP^{low}/prominin positive cells was about 8% of the total GFP^{low} fraction (Fig. 7a'') corresponding closely to the proportion of proliferating Ki67-positive cells in this population (Fig. 5f). Also amongst the GFP^{high} fraction the proportion of Ki67-positive dividing cells (48%, Fig. 5e) resembled the fraction of GFP^{high}/prominin+ cells (41%, Fig. 7a''), with the small difference of 7%. This discrepancy fits well to the fraction of Tbr2-positive basal progenitors (6%) included in the GFP^{high} population (Fig. 5e). Indeed, analysis of the prominin-double-positive GFP^{high} fraction 2 hours after plating, revealed the complete absence of the non-apical, Tbr2-positive progenitors and a high enrichment in RGCs to about 88% of all sorted cells (Blbp in Fig. 7b and d). In addition, the proportion of neurons was strongly decreased in the GFP/prominin-double-positive sortings, even though a small fraction was still present (8-14%, Fig. 7b, c and e), maybe corresponding to newly generated neurons that were still attached to the ventricle and therefore possessed prominin (Cappello et al., 2006; Miyata, 2007). Consistent with the enrichment of RGCs, I also observed an enrichment of cells that continued to divide *in vitro* and were still Ki67-positive 2 hours after plating (65% in the GFP^{high}/prominin positive fraction and 40% in the GFP^{low}/prominin+ population; Fig. 7b,c and e). As the population of RGCs is still higher (88% GFP^{high}/prominin+; 80% GFP^{low}/prominin+), some cells still seem to exit the cell cycle after dissociation and sorting.

Next I determined the progeny of these sets of radial glial progenitors in the clonal co-culture system described above (Fig. 7f, g). Consistent with the above analysis, GFP^{low}/prominin+ cells generated largely neurons (increase from 14% β III-tubulin-containing/M2M6-positive

clones after 2 hours to 87% after 7 days *in vitro*) with a predominance of pure neuronal clones (Fig. 7g), while GFP^{high}/prominin+ cells generated very few neurons (Fig. 7f). Most of the clones derived from GFP^{high}/prominin+ cells were positive for immature progenitor markers such as nestin. Moreover, few clones were positive for GFAP, labelling differentiated mature glial cells (4.3% GFAP+ clones), or O4, labelling oligodendrocyte progenitors (0.9% O4+ clones). Interestingly, when analyzing the progeny of the two subsets of RGCs after only 3 days *in vitro*, the GFP^{high}/prominin+ cells generated a high proportion of Tbr2 positive clones (32.8%), 5x more compared to the GFP^{low}/prominin+ cells (6.1%) (Fig. 8). These Tbr2 positive clones correspond very well to the proportion of clones (32%) containing neurons generated *in vitro* from the GFP^{high}/prominin+ sorted cells (Fig. 7f), suggesting that the neurons generated in these clones are derived via Tbr2+ intermediate progenitors. Thus, this approach allows the prospective separation of distinct radial glial progenitors – the GFP^{low}/prominin-positive fraction with largely neurogenic progenitors, and the GFP^{high}/prominin-positive fraction with progenitors generating largely non-neuronal cells, few of which differentiated fully into mature glia. The small population of neurons generated by the latter seems to be largely generated in an indirect manner via Tbr2-positive basal progenitors. The separation of these populations therefore allows gaining insights into the fate determinants governing neuronal, non-neuronal and basal progenitor fate decisions.

6.1.3 Transcriptome analysis of distinct radial glial lineages

To assess the gene expression differences between these distinct RGCs subsets (GFP^{low}/prominin+; GFP^{high}/prominin+) and to compare them to the GFP^{low} or GFP^{high} populations that contain both progenitors and progeny, we used Affymetrix microarray analysis (microarrays performed in collaboration with Martin Irmeler and bioinformatic analysis performed by Michael Mader, see Pinto et al., 2008). For mRNA isolation used for the Affymetrix microarray analysis, I split each population of sorted cells into three biological replicates and performed RNeasy RNA purification, with subsequent examination of the RNA quality of all samples. Only the samples with high RNA quality were considered for microarray analysis (see Methods).

First we compared the GFP^{low} and the GFP^{high} fractions of sorted cells and detected 2972 differentially expressed genes with a fold change greater than- or equal to a threshold of 2. Statistical tests (see Methods) identified 196 of these as significantly different. In order to test whether the differential expression analysis is sufficiently reliable, I used quantitative real time PCR (RT-PCR) with cDNA synthesized from the same pools of RNA used for the

arrays. I compared the fold change differences of examples of genes that were statistically significant in their expression difference (196, see above) as well as examples that were included in the 2972 genes found to be 2 fold or more differentially expressed in all replicates by RT-PCR (values for genes expressed at higher levels in the GFP^{high} were set to positive and values for genes expressed at higher levels in the GFP^{low} fraction were set to negative, Fig. 9a, b). Virtually all of these samples confirmed the differential expression levels obtained by the fold change analysis of the microarray data and many even showed higher expression differences than predicted by the arrays (e.g. Rhoc, Rab11a, Fezl, Socs7 and Rhov in Fig. 9a, b). This analysis therefore supports the reliability of the gene expression differences predicted by the fold change analysis of the microarray data. I therefore used this analysis and thresholded it by an absolute expression level of 50 (see Methods) to exclude genes of extreme low expression levels.

As expected from the cell type analysis of sorted cells described above, we found a considerable number of neuronal genes enriched in the GFP^{low} fraction, such as Syt4, Tub, Dcx, Mapt and Tbr1. However, we also found genes expressed in the RGCs of the cortex VZ, such as Cdc42, Pax6 and Rac1 (Table 1). Notably, the genes expressed at higher levels in the GFP^{high} fraction were mostly expressed in the VZ, such as Arhgap18, RhoA, Glast, Sox9 or in the SVZ as for example Tbr2, NeuroD4 and Ngn2 (Table 1, Fig. 9c, d). Thus, the observation that GFP^{high} sorted cells contained basal progenitors was confirmed at the transcriptome level.

In agreement with the *in vitro* results described above, the genes expressed in neurons and in the SVZ of the GFP^{low}/GFP^{high} populations were largely lost in the arrays derived from cells labelled for both prominin and GFP (Tables 2 and 3a, b, see below). This was the case for the known neuronal genes Tub, Dcx, Mapt and Tbr1. Moreover, additional mRNAs with previously not described expression in the developing cerebral cortex at mid-neurogenesis, such as Sox5, Sox11 and Rac3 mRNA revealed expression in differentiating neurons in the cortical plate and were also lost in the arrays of the GFP/prominin positive fractions (Fig. 9c, d). This data further supports the cell type analysis with many postmitotic neurons included in the GFP^{low} fraction, thereby also providing transcriptome information for this neuronal population (Table 3a). When we performed a similar comparison of the GFP^{high} and GFP^{high}/prominin+ transcriptome, many mRNAs present in the former but absent in the latter were expressed in SVZ/basal progenitors, such as Satb2 (Fig. 9c, d) or Ngn2 and Eomes/Tbr2 (Fig. 9d, Tables 2 and 3b). Thus, the comparison of the mRNAs expressed in the GFP^{high} but

not GFP^{high}/prominin with those expressed in the GFP^{low} but not in the GFP^{low}/prominin fraction allows determining the transcriptome of basal progenitors (Tables 3a, b and Fig. 10c). Interestingly, there is hardly any overlap between the mRNAs present in the GFP^{high} but no longer present in the GFP^{high}/prominin+ fraction (Table 3b) and those present in the GFP^{low} and absent in the GFP^{low}/prominin+ fraction (Table 3a). This suggests that even the neurons derived from the GFP^{high} and GFP^{low} fractions are rather different in their expression profile. Furthermore, analysis of the total number of genes expressed (13756 genes) in the GFP^{low}/prominin+ and GFP^{high}/prominin+ subsets of sorted cells showed that most were expressed in common (12392), consistent with the isolation of the same cell type, namely radial glia from the E14 cortex (Fig. 10a). However, 652 genes were contained only in the GFP^{low}/prominin+ and 712 were expressed only in the GFP^{high}/prominin+ fraction (Fig. 10a). In addition, the GFP^{low} or GFP^{high} fractions also contain a considerable fraction of RGCs and there is a high degree of overlap in the expression profile of the GFP^{low} and the GFP^{low}/prominin+ fraction (Fig. 10c) as well between the GFP^{high} and GFP^{high}/prominin+ fractions (Fig. 10d) (see also Table 1). However, we also observed genes only expressed in the GFP+/prominin+ but not in the respective GFP+ fractions (Fig. 10c, d). These were found to be expressed at very low levels (below 50 even in the GFP/prominin double positive fraction). Thus, their expression already at very low levels in RGCs became undetectable in the GFP+ fractions that also contain other cell types (Fig. 10c, d). Conversely, this comparison showed a number of genes expressed selectively in the GFP^{low} or GFP^{high} fractions but absent in the respective populations double-labelled with prominin (Fig. 10c, d). Thus, the comparative analysis of RGCs with their immediate progeny allows detection of neurons and progenitors that differ profoundly in their transcriptome.

6.1.4 Transcriptome analysis of distinct radial glia subtypes

When we compared the two sorted subsets of radial glia progenitors, the GFP^{low}/prominin+ and the GFP^{high}/prominin+ cells, at the transcriptome level we obtained 5040 differentially expressed genes (2 fold change difference). As I expected the expression profile of the GFP+(low and high)/prominin+ cells to be a subset of the expression profile of the total GFP+ cell populations, I was surprised to find 3009 genes only expressed in the GFP+/prominin+ but not in the GFP+ fractions. However, these 3009 genes were found to be expressed at very low levels (99% with an absolute expression below 50), indicating that they are expressed at low levels in the sorted RGCs and this expression became undetectable in the GFP+ fractions containing only 10% RGCs. As our previous microarray analysis (Holm

et al., 2007) had shown that genes expressed at levels lower than 50 on the arrays can rarely be detected *in vivo*, we didn't focus on these genes. We therefore chose to focus our analysis on the overlap genes between GFP^{low}/GFP^{high} and the prominin-double-labelled fractions of sorted cells thresholded by an absolute expression level higher than 50 (Table 1). To ensure the reliability of our analysis, I chose 15 genes to confirm their differential expression between the GFP^{low}/prominin+ and the GFP^{high}/prominin+ fraction and thus the reliability of the arrays (Fig. 9e, f). Interestingly, different isoforms of Pax6 (with and without exon 5a) were selectively enriched in the two sorted subsets of RGCs. The total mRNA for Pax6 was detected using primers that recognize all described isoforms and was expressed at higher levels in the GFP^{low}/prominin+ fraction. Conversely, primers that specifically bind to the isoform containing exon 5a in the paired domain of Pax6 (Pax6(5a)), detected higher mRNA levels of this specific isoform in the GFP^{high}/prominin+ fraction (Fig. 9e, f).

To ensure the reliability of our array data and to determine the localization of several differentially expressed mRNAs within the VZ, SVZ or cortical plate of the developing cortex at mid-neurogenesis we performed *in situ* hybridization. Most of the analyzed mRNAs were located in the VZ of the cortex, such as Pax6, Sox9, Sox21 and Cdc42 (Fig. 11a and Table 1), in agreement with previous reports of the localization of these mRNAs (Ohba et al., 2004; Olenik et al., 1999). In addition, I also characterized the expression patterns of mRNAs that were previously not examined within the cortex, such as Rac1 and Rhogef7 that were also expressed in the VZ (Fig. 11a). These mRNAs were expressed at higher levels in the GFP^{low}/prominin+ fraction, i.e. in the neurogenic lineage of RGCs. Additionally, mRNA of Tcfap2c, Rhoq, Rhogap5, expressed at higher levels in the GFP^{high}/prominin+ fraction, was detected in the VZ (Fig. 11a). Notably, a small proportion of the mRNAs detected at higher levels in the GFP^{low}/prominin+ fraction was only weakly expressed in the VZ, but found at higher expression levels in the cortical plate (see e.g. Mef2c in Fig. 11a). These interesting expression patterns suggest that the neurogenic fraction of RGCs starts to up-regulate mRNAs that are further up-regulated during neuronal differentiation. Moreover, we also identified several novel genes with differential expression at higher levels in the GFP^{low}/prominin+ or the GFP^{high}/prominin+ fraction (Fig. 11a and Table 1). For example, 2300002D11Rik was enriched in the GFP^{low}/prominin+ fraction and its mRNA was present at highest levels in the VZ, while two further Riken clones (0910001A06Rik and 2600009P04Rik) enriched in this fraction were expressed at higher levels in the layers containing migrating or differentiating neurons (Fig. 11a). Also novel mRNAs enriched in

the GFP^{high}/prominin⁺ fraction such as 2810025M15Rik and 2610017109Rik were localized in the VZ (Fig. 11a). Furthermore, we examined one of the Riken clones enriched in the neurogenic radial glia fraction and expressed in the VZ (2300002D11Rik) at the protein level. The antibody to recognize the 2300002D11Rik protein was generated in a guinea pig against an epitope with the sequence: AAETPVEGQELQRWRQGAS. To test the specificity of the antibody raised against 2300002D11Rik, HEK cells were transduced and western blot was performed. This showed a protein band of a MW close to 23kDa, the predicted MW of the 2300002D11Rik protein (data not shown, peptide was designed by Robert Blum, peptide generation and immunization was performed by “Peptide Speciality Laboratories GmbH”, Heidelberg and western blot was performed by Ronny Stahl, see Pinto et al., 2008). The immunostaining showed an interesting staining pattern in a subset of neurons and in a subset of VZ radial glia in the E14 cortex (Fig. 11a). As the mRNA expression of the 2300002D11Rik gene was only detected in the VZ, this means that the protein is maintained in neurons. This observation confirms that the differential mRNA levels detected in our arrays translate into differences in protein levels amongst the isolated radial glial subtypes.

To detect where the GFP^{high} and GFP^{low} subpopulations are located *in vivo* I combined GFP *in situ* hybridization with immunolabelling of some of the genes mentioned above (Fig. 11b-d). Because some of the genes highly expressed in the GFP^{low} subpopulation are known to be regionalized in the cerebral cortex, with higher expression levels at rostral compared to caudal regions (e.g Pax6), I expected that the GFP^{low} expressing cells show some regionalization too. Moreover, neurogenesis is further progressed at rostral regions compared to caudal regions, thus, supporting the suggestion that GFP^{low} neurogenic progenitors might be more prominent at rostral regions whereas GFP^{high} cells more prominent at caudal regions. Therefore, GFP mRNA was combined with GFP protein in E14 hGFAP-eGFP cortex sections. GFP mRNA was mostly present in cells expressing high levels of GFP protein (GFP^{high}) and hence showed only partial colocalization with weakly GFP immunoreactive cells lacking an *in situ* hybridization signal (Fig. 11b, lower panels, yellow arrow). Interestingly, this expression analysis of the GFP^{low} and GFP^{high} cells revealed no regionalization between rostral-caudal regions of the cerebral cortex, but appeared with a local salt and pepper expression pattern in the VZ. Indeed, when combining Sox21 immunofluorescence with labelling of GFP mRNA or protein, most cells positive for Sox21 were colocalizing with GFP mRNA and showed high GFP protein (GFP^{high}), confirming the high expression levels of Sox21 in GFP^{high}/prominin⁺ sorted cells observed by microarrays

and RT-PCR analysis (Fig. 11c). Conversely, 2300002D11Rik immunofluorescence combined with labelling of GFP mRNA or protein showed a higher percentage of colocalization with cells with weak GFP-immunoreactivity (GFP^{low}) and were negative for GFP mRNA, thus confirming the higher expression of this gene in GFP^{low}/prominin+ sorted cells (Fig. 11d). Therefore, this analysis allowed the explicit confirmation of our array results, revealing the differential expression of genes in distinct subsets of RGCs in the developing cortex.

6.1.5 Clustering analysis of differential gene expression in subtypes of E14 radial glial cells

After confirmation of the reliability of the microarray data, we performed hierarchical clustering on the genes found to be differentially expressed between GFP^{high}/prominin and GFP^{low}/prominin fractions to characterize the fate determinants expressed by these subsets of RGCs (Fig. 12). This analysis allowed division of the hierarchical tree into 17 clusters. The genes present in each individual cluster were grouped according to their main function based on literature searches and gene ontology (GO) annotation and are represented in pie charts (Fig. 12 and Table 1).

6.1.5.1 GFP^{low}/prominin+ enriched mRNAs

Interestingly, we found a number of genes related to neurogenic fate that were enriched in the GFP^{low}/prominin+ subset of RGCs. This group of genes included the transcription factors Pax6 (canonical isoform excluding exon 5a, see (Haubst et al., 2004)), Nr2f2, Atbf1 and Bhlhb5 that have been previously linked to the neurogenic lineage (Gauchat et al., 2004; Haubst et al., 2004; Heins et al., 2002; Jung et al., 2005) and other genes involved in neuronal differentiation such as Dab1, Vldlr, reelin, Gap43 (Table 1). These are largely included in the clusters 4, 6, 14 and 15 (Fig. 12). Note that the bHLH transcription factor Heyl is also expressed at higher levels in this neurogenic lineage of RGCs. Consistent with their direct neurogenesis, GFP^{low}/prominin+ radial glia expressed already higher levels of genes present in maturing neurons, such as the neuron-specific glutamate transporter EAAT1, Syt1/4, Ntn1, Ica1, or axon guidance involved genes, such as Ablim1, Sema4f and Robo1 (Table 1). Most strikingly, the small RhoGTPase cdc42 was expressed at higher levels in the GFP^{low} compared to GFP^{high} fraction, thus in the neurogenic population. This is very interesting as we recently demonstrated that deletion of cdc42 results in the increase of basal progenitors (Cappello et al., 2006). These data now support the concept that the higher expression level

of *cdc42* in the GFP^{low} fraction is crucial to maintain this lineage distinct from the lineage generating basal progenitors (the GFP^{high} fraction). In this regard, the high number of genes related to small GTPases in the GFP^{low} fraction is also striking, including for example *Rac1* and its GEF *Arhgef7* (Table 1). Moreover, genes involved in cell adhesion or cytoskeleton regulation were expressed at higher levels in the GFP^{low} than the GFP^{high} fraction, including *Protocadherin9*, *Cadherin11* and *13*, the septin *Cdc42ep2*, *Daam1*, *Slim1*, *Ctnna2* (alpha catenin) and *Ccd1* that are mostly contained in clusters 6 and 17 (Fig. 12 and Table 1).

6.1.5.2 GFP^{high}/prominin+ enriched mRNAs

Conversely, most of the genes involved in the maintenance of undifferentiated progenitor cells, as for example *Id1* and *Id4* (Ross et al., 2003), *Nr2e1* (Stenman et al., 2003b) were contained in cluster 13 (*Endostatin*, *Cav2*, *Mina* and *Foxmp1*), 15 and 17 (Fig. 12). Genes related to cell cycle regulation were mostly contained in cluster 5 and expressed at higher levels in the GFP^{high}/prominin+ fraction, such as *Cdc2a/20*, *Check1/2*, *Aurkb*, *Dlg7*, *Bub1b* and *Mcm3* (Fig. 12 and Table 1). This data supports the concept that progenitors generating neurons may slow their cell cycle in comparison to progenitors generating further progenitors [proliferative divisions, see e.g. (Calegari et al., 2005; Lukaszewicz et al., 2005)]. These data are well consistent with the higher fraction of proliferating cells contained in the GFP^{high} fraction and their faster cell cycle (LI=BrdU positive cells/proliferating cells was =0.81 in the GFP^{high} fraction; = 0.26 in the GFP^{low} fraction) (BrdU was injected to E14 pregnant mice 30 minutes before sacrificing them, labelling cells undergoing S-phase). In addition, genes involved in Notch-signalling such as *Jagged3* and *Notch1* and *3*, canonical Wnt and BMP signalling were all expressed at higher levels in the GFP^{high} fraction (Table 1), consistent with their role in maintaining an undifferentiated progenitor cell state.

Taken together, these clustering and GO annotation analyses show an intriguing relation between the cell fate of neurogenic and non-neurogenic RGCs and their gene expression profile. Besides genes of known function we also detected a series of unknown genes (Table 1) that may be useful to better understand fate specification of the neurogenic and undifferentiated lineages.

6.1.6 Cell surface genes identified for distinct radial glial subtypes

Besides intrinsic fate determinants we focused our attention on cell surface molecules as potential signalling candidates or novel markers for prospective radial glia lineages

separation without using transgenic GFP mice (bioinformatics analyses to identify cell surface genes was performed by Alessandro Bulfone and collaborators, see Pinto et al., 2008). Several interesting cell surface proteins were expressed at different levels between the GFP/prominin-double-positive fractions and hence are likely marking subsets of cortical RGCs (Table 4).

Cell surface molecules such as CD83 (mus musculus CD83 antigen), Crb1 (crumbs homolog, in *Drosophila*), p75/Ngfr (nerve growth factor receptor), Flrt2 (fibronectin leucine rich transmembrane protein 2) and Ntrk2 (neurotrophic tyrosine kinase receptor, type 2, TrkB) were expressed at higher levels in the GFP^{low}/prominin⁺ subset (Table 4). Interestingly, p75 and Ntrk2 are involved in neurotrophin signalling. I therefore chose to examine p75 on the surface of cortical progenitors as p75 expression levels also exhibited the highest difference between GFP^{low}/prominin⁺ and GFP^{high}/prominin⁺ fractions (4.4x in log (2) scale = 21 fold change). Strikingly, live staining of E14 cortex cells revealed that the majority of the p75⁺ cells were contained in the GFP^{low} fraction (80%, Fig. 13a) and 83% of p75⁺ cells were prominin⁺ (data not shown), i.e. radial glia. Clonal analysis after sorting revealed the neurogenic fate of the progenitor cells isolated by p75⁺/prominin⁺ staining (Fig. 13b,c,d), demonstrating that p75 is a cell surface protein highly enriched on neurogenic radial glia in the developing mouse cerebral cortex [(see also (Young et al., 2007)]. Strikingly, this enrichment on neurogenic radial glia was to a similar extent as GFP^{low}/prominin⁺ (Fig. 7g). In addition, FACS analysis of CD83 and Flrt2 live staining in hGFAP-eGFP dissociated cortical cells further proved the higher expression of these cell surface markers in the GFP^{low} expressing cells (Fig. 13e, f). Indeed, 89% of the total number of CD83-positive cells and 78% of the total number of Flrt2-positive cells was included in the GFP^{low}/prominin⁺ fraction (Fig. 13e, f). Thus, we identified novel cell surface proteins highly enriched in the neurogenic subset of RGCs which can be used to isolate and identify neurogenic radial glia in the developing mouse cerebral cortex in further studies.

6.1.7 Summary of the transcriptome and lineage of distinct radial glia subsets isolated at mid-neurogenesis

The transcriptome analysis of GFP⁺(high and low) and GFP⁺(high and low)/prominin⁺ sorted cells described in this work showed that the vast majority of mRNAs expressed at different levels in the GFP^{low}/prominin⁺ and GFP^{high}/prominin⁺ sorted cells were localized to

the VZ (Fig 14a), but the GFP+ fractions included other cell types, namely neurons and basal progenitors (Fig. 14b).

The lineage analysis described above further confirm the distinct progeny of the GFP^{low}/prominin+ and GFP^{high}/prominin+ radial glia observed *in vitro* and at the transcriptome level (Fig. 14) and further highlight the importance of the differential transcriptome analysis between these functionally distinct sets of RGCs that co-exist at the same developmental stage. In summary, the separation of the GFP^{low}/prominin+ and GFP^{high}/prominin+ fractions allows the prospective isolation of largely neurogenic radial glia and RGCs that generate largely non-neuronal cells, respectively (Fig. 14c). Furthermore, the few neurons generated by the latter seem to be generated in an indirect manner via Tbr2-positive basal progenitors (Fig. 14c).

6.1.8 Characterization of cortical radial glial cells at the end of neurogenesis

To study how the transcriptome of RGCs may change at the end of neurogenesis, GFP+ and prominin+ cortical cells were also isolated by FACS from E18 hGFAP-eGFP mice (Fig. 15). Surprisingly, the GFP fluorescence intensity had decreased in E18 hGFAP-eGFP cortical cells and became comparable to the GFP intensity of E14 GFP^{low} expressing cells, also confirmed by RT-PCR (Fig. 15a, b). Indeed, in the cortex at E18, neurogenesis is coming to an end and most of the radial glia progenitors become gliogenic, expressing higher levels of GFAP compared to progenitors at mid-neurogenesis. Therefore, I expected an increased GFP fluorescence intensity of E18 hGFAP-eGFP cortical cells, in contrast to what I observed in this analysis. Moreover, FACS sorting analysis showed that double-positive (E18 GFP+/prominin+) cells comprised about 30% of the total GFP positive cells (11.9% of the total number of cells, Fig. 15c), indicating that the proportion of radial glia amongst all GFP-labelled cells had further declined during development (54.7% at E14 versus 30.7% at E18). Indeed, the entire population of GFP-positive cells amongst all cortical cells was highly decreased at E18 (38.8%) compared to 73% at E14 and all cells showed similar intensity. Therefore, it was no longer feasible to divide this fraction into a GFP^{low} and GFP^{high} fractions. When GFP+/prominin+ cells sorted from E18 cortex were examined shortly after plating (2h *in vitro*), the majority of the sorted cells were positive for the radial glial antigens Nestin, RC2, Pax6, LeX, and BLBP (85%) and 45% of them were proliferating (Ki67-positive) (Fig. 15). This data indicated a reduction of proliferating cells in comparison to the RGCs sorted at E14. Clonal analysis of their progeny revealed no increase in the proportion of pure neuronal clusters (Fig. 15e), suggesting that the sorted population no longer comprises RGCs

generating only neurons, consistent with previous observations (Malatesta et al., 2000). However, a small fraction of E18 GFP⁺/prominin⁺ sorted cells was still able to generate neurons and non-neuronal cells in mixed clones (18%, Fig. 15e). Besides this small bi-potent progenitor cell population, all the remaining cells generated non-neuronal clones that were composed of GFAP⁻ (27.9% GFAP⁺ clones, n=213), or nestin⁻ or O4⁺-positive cells (8.3% O4⁺ clones in E18 sorted cells n=146) (61% non-neuronal clones in total, Fig. 15e, f, g). Thus, the clonal analysis of E18 radial glia sorted cells revealed an increase in differentiated glia compared to E14 radial glial sorted cells (27.9% GFAP⁺ clones generated by E18 sorted cells and 4.3% GFAP⁺ clones generated by E14 sorted RGCs).

In order to examine the extent to which E18 radial glia differ in their transcriptome from E14 radial glia, we performed microarrays analysis of those. Next, we examined the transcriptome of the largely non-neurogenic set of late RGCs in comparison with the transcriptome of the distinct subsets of RGCs sorted at mid-neurogenesis (E14 GFP^{low}/prominin⁺ and GFP^{high}/prominin⁺). As E18 RGCs are known to generate less neurons and become more gliogenic, the expected hypothesis would be that E18 RGCs are more similar to the non-neurogenic radial glial subset at E14 (GFP^{high}/prominin⁺ subset of sorted cells) than to the neurogenic radial glial subset (GFP^{low}/prominin⁺ subset of sorted cells). However, the comparison revealed that any of the subsets of E14 radial glia resemble the E18 radial glia. Interestingly, the subsets of E14 radial glia were more similar to each other than to the E18 radial glia, as clustering analysis revealed profound differences between RGCs isolated at E14 and E18 (Fig. 16). In this analysis, two main clusters contained genes expressed at higher levels at E18, while two other main clusters contained genes expressed at lower levels in radial glia at E18 compared with both sets of E14 radial glia. Amongst the genes up-regulated in E18 radial glia were *Olig1*, *Olig2*, *Pdgfra* and *TN-C* that are functionally related to oligodendrogenesis (Table 5; clusters 4 and 6 in Fig. 16). Conversely, transcription factors related to the neurogenic fate were down-regulated in E18 radial glia, including *Pax6* (canonical form), *Ngn1/2*, *Emx1* and *Tbr1* (Table 5, clusters 1 and 2 in Fig. 16) while *Id2*, an inhibitor of the neurogenic bHLH transcription factors was up-regulated (Table 5). In this regard it is of interest that most of the genes involved in BMP and Wnt signalling pathways and differentially expressed in the GFP^{low} and GFP^{high} sets of E14 radial glia, were down-regulated in E18 radial glia. Conversely genes related to Notch-signalling and specific small GTPases were up-regulated in E18 radial glia compared to radial glia subsets at earlier stages (Table 5). A further interesting finding is related to cell cycle regulation. While the

proliferation of parenchymal glial progenitors increases at late embryonic and early postnatal stages, the proliferation of RGCs actually decreases. Consistent with this, the majority of cell cycle promoting genes were down-regulated in E18 radial glia compared to the E14 fractions (clusters 1 and 2 in Fig. 16). To further validate this transcriptome analysis, many genes predicted to be differentially expressed between the E14 subsets of radial glia and the E18 RGCs were examined by *in situ* hybridization and RT-PCR analysis (Fig. 17a, b). Indeed, *Tcfap2c*, *Cdc42* and *Hes5* were confirmed by *in situ* hybridization and RT-PCR to be downregulated in E18 radial glia compared to both subsets of E14 radial glia (Fig. 17a, b). As the VZ of the cerebral cortex during development decreases, it would be expected a decrease of the overall expression of the progenitor mRNAs. However, the mRNAs down-regulated in the E18 radial glia compared to E14 RGCs revealed that amongst all radial glia progenitors, the expression levels of these mRNAs are decreased at E18. Other mRNAs, such as *Sox11* and *Satb2* were confirmed to be up-regulated in the E18 radial glia compared to both subsets of E14 radial glia by *in situ* hybridization and RT-PCR (Fig. 17a, b).

Taken together, RGCs isolated at late stages of embryonic development lose expression of neurogenic and proliferation promoting factors while they up-regulate genes involved in gliogenesis and oligodendroglioneogenesis. Furthermore, these striking differences in mRNA and protein levels revealed candidates for possible cell fate determinants, as for example *Tcfap2c* (also called AP2 γ).

6.1.9 Comparison of primary radial glial subsets with radial glia derived from embryonic stem cells

Recently, homogeneous populations of cells with radial glial properties were derived from embryonic stem (ES) cells using different culturing protocols (Bibel et al., 2004; Conti et al., 2005; Pollard et al., 2006). While exposure of fast proliferating ES cells to retinoic acid in the cell aggregate stage results in a virtually pure population of Pax6-positive RGCs that differentiate into pure glutamatergic neurons (Bibel et al., 2007; Bibel et al., 2004), exposure of ES-derived neural cells to bFGF (basic fibroblast growth factor) and EGF (epidermal growth factor) in an adherent stage results in a pure population of proliferating, expandable RGCs (Conti et al., 2005). As both populations are reminiscent of the neurogenic GFP^{low}/prominin⁺ and the GFP^{high}/prominin⁺ fractions, respectively, we compared the transcriptome of the following 4 populations: E14 GFP^{low}/prominin⁺, GFP^{high}/prominin⁺, Bibel-protocol ES-derived radial glia and Conti-protocol ES-cells (Bibel-protocol ES-derived

radial glia of WT and Sey/Sey ES cells were provided by Vassiliki Nikolettou and microarrays were performed in collaboration with Martin Irmeler; Conti-protocol ES-cells microarrays data was provided by Steven Pollard; bioinformatic analysis of all samples was performed by Michael Mader). Divisive clustering analysis placed the Bibel-protocol ES-derived radial glia (ES J1 RG in Fig. 18a) to the proximity of E14 sorted radial glia, and within these closer to the GFP^{low} (E14 RG GFP^{low} in Fig. 18a) than to the GFP^{high} fraction (E14 RG GFP^{high} in Fig. 18a). Amongst the 2123 genes expressed in common between primary E14 cortex radial glia and the ES-derived radial glia (Bibel protocol), 64% were shared with the GFP^{low} fraction, but only 36% with the GFP^{high} fraction. The higher similarity of ES J1 RG to the neurogenic subset of RGCs from the cortex (GFP^{low}/prominin+) was also apparent from a Venn Diagram analysis (Fig. 18b).

Interestingly, ES-derived radial glia lacking functional Pax6 (ES cells from Sey mutant mice; (Nikolettou et al., 2007) are transcriptionally more similar to the GFP^{high}/prominin+ fraction which comprise the RGCs with little neurogenic capacity (ES Sey RG and E14 RG GFP^{high} in Fig. 18a). This is consistent with the fact that Pax6-mutant RGCs lose the direct mode of neurogenesis (Heins et al., 2002). The divisive clustering analysis also demonstrated the pronounced differences in the transcriptome of expanded cell populations (cor1 and cgr8) to primary radial glia. Notably, the expanded primary cells derived from embryonic cortex (cor1) resemble in their transcriptome the expandable radial glia population derived from ES cells cultured according to the same protocol (Conti et al., 2005), but are pronouncedly different from any of the primary radial glia populations. Finally, the divisive clustering analysis also confirmed the distinct transcriptome of E18 radial glia compared to the two subtypes of radial glia sorted from E14. Taken together, these results demonstrate the feasibility of transcriptome analysis not only for discovery of molecular fate determinants, but also for lineage similarities and differences.

6.2 Expression and function of the transcription factor AP2 γ in a subset of cortical radial glia

6.2.1 AP2 γ expression in the developing and adult mouse cerebral cortex

As described above AP2 γ (also called Tcfap2c) is a transcription factor expressed at higher levels in RGCs generating basal progenitors at mid-neurogenesis in the cerebral cortex and is

down-regulated at later developmental stages when neurogenesis ceases at E18 (Pinto et al., 2008). Moreover, Holm et al also found AP2 γ down-regulated in the Pax6-mutant cerebral cortex at mid-neurogenesis (Holm et al., 2007). To be aware of possible compensatory mechanisms in regard to the functional experiments, I examined the expression of other members of the AP2 family of transcription factors. Interestingly, AP2 γ is the only member of the AP2 transcription factor family expressed in the developing mouse telencephalon (embryonic day (E) 14, Fig. 19a-e). Furthermore, AP2 γ expression is very specific to the developing cerebral cortex as we could not detect expression anywhere else in the nervous system. Within the cerebral cortex, AP2 γ expression started after E10 following the gradient of neurogenesis with higher expression levels laterally and rostrally (Fig. 19f-k). AP2 γ remained restricted to the progenitor layers and mRNA levels increased at mid-neurogenesis (E14) (Fig. 19g). AP2 γ expression decreased at later stages (E18), when neurogenesis ends in the developing cortex (E18) (Fig. 19h and k), in agreement with our transcriptome analysis previously described (Pinto et al., 2008), and no AP2 γ mRNA could be detected in the adult cerebral cortex (Fig. 19i). Thus, AP2 γ expression parallels the appearance and increase in neurogenic basal progenitors in the developing cerebral cortex (Pontious et al., 2008). However, with AP2 γ mRNA is not possible to distinguish if this transcription factor is restricted to the VZ or is expressed in both progenitor layers, the VZ and SVZ. To better discriminate in which type of progenitors AP2 γ is expressed, I examined AP2 γ -immunoreactivity in the known progenitor subtypes of the cortex, the Pax6⁺ radial glia in the VZ and the Tbr2⁺ basal progenitors in the SVZ. Consistent with our previous analysis (Pinto et al, 2008), only a subset of dividing cells in the VZ/SVZ labelled by Ki67 were AP2 γ -immunopositive (Fig. 19o). Co-localization of AP2 γ mRNA and protein with Pax6 revealed many double-positive cells (Fig. 19l-l'' and n). However, not all Pax6⁺ cells expressed AP2 γ (green arrow in Fig. 19n) and not all AP2 γ ⁺ cells expressed Pax6 (red arrow in Fig. 19n). Some AP2 γ -positive cells also contained Tbr2 mRNA or protein (Fig. 19m-m'' and p). Notably, these AP2 γ /Tbr2-double positive cells were still located in the VZ region and hence are likely the most recently generated basal progenitors starting to up-regulate Tbr2 (white arrows in Fig. 19p). Taken together, AP2 γ expression peaks at mid-neurogenesis and localizes mostly to radial glia progenitors in the VZ, some of which start to up-regulate Tbr2.

6.2.2 AP2 γ expression in the adult mouse brain

AP2 γ mRNA is present in several regions of the adult mouse brain, but no expression could be detected in the gray matter of the cerebral cortex in the adult mouse (Fig. 20a). AP2 γ

expression is present in the granular cell layer of the adult cerebellum (Fig. 20c) and in the white matter of the forebrain (Fig. 20d). Neurogenesis persists in two other regions of the adult mammalian forebrain (Alvarez-Buylla et al., 2001; Gage, 2002), the subependymal zone (SEZ) lining the lateral wall of the lateral ventricle (Doetsch et al., 1997; Doetsch et al., 2002) and the subgranular layer (SGZ) in the dentate gyrus (Seri et al., 2004; Seri et al., 2001). In both of these regions astroglial cells have stem cell properties and act as the source of adult progenitor cells (Seri et al., 2004; Seri et al., 2001). In the SEZ, neuroblasts are constantly generated and migrate through the rostral migratory stream (RMS) in a tangential chain-like manner towards the olfactory bulb (OB). Notably, the stem cells hosted within the SEZ and the RMS generate different types of interneurons (Hack et al., 2005; Lledo et al., 2008) that integrate in the granule cell layer (GCL) or glomerular layer (GL) of the olfactory bulb (OB). Interestingly, AP2 γ mRNA is highly expressed in both adult neurogenic regions, namely in the dentate gyrus (DG) and CA1 (CA stands for Cornu Ammonis) region of the hippocampus (Fig. 20e) and in the SEZ (Fig. 20f). AP2 γ mRNA expression was proven to be specific as no signal was detected with a sense RNA probe (Fig. 20b). AP2 γ is also highly expressed in the RMS and in the GCL, GL and mitral cell layer (ML) of the OB (Fig. 20f-h). In the SEZ, AP2 γ is expressed in a subset of BrdU-retaining stem cells, as observed by co-localization of AP2 γ mRNA with immunolabelling for BrdU. To label adult slow dividing stem cells, BrdU was given to adult mice in drinking water for one week, followed by 8 weeks with normal water and sacrificed later (label retaining protocol to detect slow-dividing stem cells in the SEZ, see Material and Methods) (Fig. 21a-c'). Furthermore, in the GCL and GL of the OB, some BrdU labelled cells co-localized with AP2 γ mRNA, suggesting that a proportion of the AP2 γ -positive neurons in the OB are adult generated (Fig. 21d-d'''). In the GL of the OB, AP2 γ mRNA also partially co-localized with Tbr2, which has been shown to be involved in glutamatergic neurogenesis in the embryonic and adult brain (Englund et al., 2005; Hodge et al., 2008) (Fig. 21d-d'''). Thus, our expression data suggest that AP2 γ is involved in adult glutamatergic neurogenesis.

6.2.3 AP2 γ expression in the primate and human cortex

To address if AP2 γ is conserved during phylogeny its expression was analyzed in the brain of higher developed mammalian species, namely in cynomolgus macaque (collaboration with Colette Dehay) and human (collaboration with Nada Zezevic). As it was observed in the mouse brain, AP2 γ was highly expressed in the developing cerebral cortex of monkeys and humans at mid-gestational stages (Figs. 22 and 23). In the E80 monkey cortex, AP2 γ -

immunoreactive cells were detected in the VZ and OSVZ of the occipital cortex (Fig. 22a-h'), while no immunostaining was detectable in more rostral regions (data not shown). Strikingly, there were more AP2 γ -immunoreactive cells in both the VZ and the OSVZ of area 17 compared to area 18 (Fig. 22a-d and i) and no immunopositive cells were detected in the cortical plate of the cortex (Fig. 22c). This observation might implicate the importance of this transcription factor in restricted regions of the monkey cortex, namely in the occipital area 17. Thus, AP2 γ might be important for regionalization of the cortex in higher mammals. Interestingly, upper layer neurons increase in number during phylogeny and reach a high number in the primary visual cortex of cats and monkeys (Batardiere et al., 1998; Smart et al., 2002). There is also a pronounced difference in the size of upper layer neurons between area 17 and 18 in primates (Dehay et al., 1993; Lukaszewicz et al., 2005). Thus, the presented expression data supports a potential function of AP2 γ in progenitors of upper layer neurons in occipital cortex regions of higher mammals. This might also imply AP2 γ in the increase of this specific type of neurons during phylogeny.

Similarly to the expression pattern observed in mouse and monkey, AP2 γ -immunopositive cells were detected in the occipital regions of the human cortex at mid-gestational stages (20-22 gestational weeks) (Fig. 23). AP2 γ -immunopositive cells were highly enriched in the VZ and SVZ (Fig. 23b-d'') with only few scattered cells in the intermediate zone (IZ) (Fig. 23c, c'). No staining for AP2 γ was detected in the cortical plate at this stage (Fig. 23a, a'). Furthermore, AP2 γ highly colocalized with Pax6 and Tbr2 at mid-gestational stages, in line with the expression pattern observed in the mouse cortex (Fig. 23d-d'' and data not shown).

6.2.4 AP2 γ deletion in the developing cortex causes a decrease in the number of neurons and misspecification of basal progenitors at mid-neurogenesis

To properly study the function of AP2 γ in the developing cerebral cortex during the period of neurogenesis, I used AP2 γ conditional knock-out mice. The general AP2 γ knock-out mice could not be used because they are embryonic lethal (death at E8.5-9.5) (Auman et al., 2002). The early death of these mice is caused by impaired proliferation in the ectoplacental cone and extra-embryonic ectoderm (Auman et al., 2002; Werling and Schorle, 2002b). Thus, I inactivated AP2 γ from its onset of expression in the developing forebrain, using the mouse line expressing Cre recombinase in the Emx1 locus with an onset of Cre expression around E9.5 in the developing cerebral cortex (Cappello et al., 2006; Iwasato et al., 2000). These mice were crossed to mice containing exon 5 of the AP2 γ gene flanked by lox P sites (AP2 γ fl/fl) (Werling and Schorle, 2002a). To reveal the efficiency of AP2 γ deletion in the

Emx1^{Cre/AP2γ^{Δex5fl/fl}} (henceforth called AP2γ^{-/-}) telencephalon I performed *in situ* hybridization and immunostaining and could no longer detect AP2γ mRNA and protein by E12 (Fig. 24). However, examination of these E12 AP2γ^{-/-} forebrains revealed no difference compared to their WT littermates in the overall cortical architecture (Fig. 25). Immunostaining or *in situ* hybridization for progenitor markers, such as Ki67, Pax6 and Hes5 also showed no obvious difference between E12 cortices of WT and AP2γ^{-/-} littermates (Fig. 25a-b' and c-c''). The number of neurons, basal progenitors and mitotic cells was not affected in the AP2γ^{-/-} cortex as detected by immunostaining or *in situ* hybridization for βIII-tubulin, NeuroD1 and PH3, respectively (Fig. 25c, c' and e-e''). This qualitative analysis was confirmed by quantification of βIII-tubulin-positive cells by FACS analysis (Fig. 25f). Quantification of cells in G2/M phase in the SVZ, labelled by PH3, i.e. the proportion of basally dividing progenitors, revealed no difference between E12 WT and AP2γ^{-/-} cortices (Fig. 25g).

At mid-neurogenesis (E14), the time when AP2γ expression peaks, the AP2γ^{-/-} cortex appeared slightly thinner at intermediate-caudal but not at rostral regions of the cortex (see Materials and Methods, intermediate defined as the first coronal sections containing the hem and caudal defined as the sections containing the hippocampus). The decreased cortex width in the intermediate-caudal regions of the AP2γ^{-/-} compared to WT cortices was confirmed by quantification (Fig. 26g). The overall number of progenitor cells at E14, labelled by Ki67 (Fig. 26d, d'), and the number and morphology of RGCs were not affected by the absence of AP2γ as observed by immunostaining for Blbp and GLAST at intermediate-caudal regions of the cortex (Fig. 26a-b'). Interestingly, by immunostaining for Pax6 and RT-PCR analysis, using primers that recognize all described isoforms for Pax6, I observed a slight decrease of the total protein and mRNA in the AP2γ deficient mice at intermediate-caudal regions of the cortex (Fig. 26c, c' and f). I also examined the regulation of distinct DNA-binding domains of Pax6, the homeodomain (HD), the paired domain (PD) and its splice variant (5a), in the AP2γ^{-/-} cortices, as each of these domains have distinct functions in the developing cortex regarding to proliferation and neurogenesis (Haubst et al., 2004). In the AP2γ^{-/-} cortices only the isoform containing the canonical paired domain was down-regulated (Fig. 26f), suggesting the regulation of one specific DNA-binding domain of Pax6 by AP2γ. The decrease of Pax6 upon loss of AP2γ in the cortex suggests that apical progenitors were decreased. However, the total number of apical progenitors was not changed in the AP2γ^{-/-} compared to the WT cortex as observed by quantification of prominin-positive cells by FACS (Fig. 26h). Moreover, I also used Rhodamine labelled Phalloidin to visualize the F-actin

filaments (Chenn et al., 1998) in order to examine the nature of adherens junctions and thus the integrity of the ventricular surface after the loss of AP2 γ (Fig. 26e, e'). F-actin was localized properly in the honeycomb pattern characteristic for adherens junctions at the ventricular surface in the AP2 γ ^{-/-} cortices similar to the WT cortices (Fig. 26e, e'). Therefore, these data suggest that Pax6 expression is decreased in the apical progenitors upon loss of AP2 γ in the intermediate-caudal regions of the cortex, but the total number of apical progenitors and the integrity of the ventricular surface is not affected.

Quantification of neuron numbers by FACS at E14 (see Materials and Methods) and immunostaining for several neuron markers, such as β III-tubulin, Cux1 and Ctip2 revealed a significant, though small (20%) decrease in mutant compared to WT littermate cortices (Fig. 27a-g). Similar to the cortex width, the reduction on the number of neurons was only significant at intermediate-caudal regions as I could observe by immunostaining for β III-tubulin at rostral, intermediate and caudal levels of the AP2 γ ^{-/-} compared to WT cortices (Fig. 27a-c'). As AP2 γ is expressed higher in the lineage of RGCs that generate basal progenitors (Pinto et al, 2008) and each of these generates two postmitotic neurons, I examined whether a reduction in basally dividing progenitors may be the cause for this decrease in the number of neurons. I found an aberrant increase in the number of basally mitotic cells (defined as the PH3⁺ mitotic cells located at non-surface positions more than 5 cell diameters from the ventricle) in the AP2 γ ^{-/-} compared to WT cortices (Fig. 28a, a' and f). In contrast, immunostaining for Tbr2⁺ basal progenitors revealed a significant decrease in their numbers in the AP2 γ ^{-/-} cortices at intermediate-caudal regions (Fig. 28b, c and h). Furthermore, in WT cortices about 90% of all basally dividing cells labelled for PH3 were also Tbr2⁺, while in the mutant cortex only half (55%) of all basally dividing cells were Tbr2⁺ (Fig. 28a-c'''' and i), suggesting an aberrant phenotype of basally dividing progenitors in the absence of AP2 γ . Surprisingly, the total number of mitotic cells was similar in the WT and AP2 γ ^{-/-} cortices (Fig. 28g), thus suggesting a specific defect in the location of mitotic cells at basal positions in the AP2 γ ^{-/-} cortex. Indeed, some of these basally located mitotic cells in the AP2 γ ^{-/-} cortex expressed improperly the radial glia marker GLAST, which was never observed in WT cortices (Fig. 28d-e''). In the WT cortex, GLAST only co-localizes with PH3 in the ventricular surface, where normally apical progenitors (RGCs) undergo cell division. Thus, in the AP2 γ ^{-/-} cortex, RGCs undergo cell division improperly at basal positions. Notably, this phenotype predominated at intermediate to caudal levels (Fig. 28f).

The abnormal increase in basally dividing cells in the AP2 γ deficient cortex could be caused by defects in interkinetic nuclear migration (INM) - the movement of progenitor nuclei to a

basal position during S-phase and subsequent relocation to the apical surface during M-phase (Sauer, 1935a). To further examine if there were INM defects in the AP2 γ ^{-/-} cortices, cells in S-phase were labelled with a short pulse of the DNA base analog BrdU for 30 minutes. Most of the BrdU-labelled nuclei that underwent S phase at this time of labelling were located at non-surface positions more than 5 cell diameters from the ventricle in WT and AP2 γ ^{-/-} cortices (Fig. 29a, a'). Similarly, I examined the location of BrdU-labelled nuclei 6 hours after injection when most cells had progressed towards M-phase. In this case, most of the BrdU-labelled cells in both WT and AP2 γ ^{-/-} cortices had moved to the apical part of the VZ (Fig. 29b, b'). This analysis was performed at intermediate-caudal levels, where the proportion of cells dividing at basal positions was increased from 25% in WT cortices to 40% in AP2 γ ^{-/-} cortices. Therefore, I expected that about 15% of all cells will not move down to the apical surface in the mutant compared to WT. In order to detect this small change in the overall progenitor pool, I quantified the location of BrdU⁺ cells 6 hours after labelling and found a significant increase in the percentage of mitotic cells that did not move down to the apical surface (Bin 2 and 6 in Fig. 29c, see Materials and Methods). Indeed, Bin 6 corresponds to the position of the SVZ, where normally apical progenitors undergoing cell division are not located. Thus, the increase in the basally located mitotic cells in the AP2 γ ^{-/-} compared to WT cortices is accompanied by a slightly higher proportion of progenitor cells remaining at more basal positions during M phase.

6.2.5 Transcriptome analysis of AP2 γ ^{-/-} cortices at mid-neurogenesis

The decrease in neuron numbers and the misspecification of basal progenitors observed in the intermediate-caudal regions of AP2 γ ^{-/-} cortices prompted us to study the specific molecular changes in the different rostral and intermediate-caudal regions of the cortex of these mutants. To get further insights into the general changes in gene expression in the AP2 γ ^{-/-} cortices, we performed microarrays of E14 cortices dividing them in 2 parts - rostral and intermediate-caudal regions. Based on my previous experience with microarray data from the embryonic cortex (Pinto et al., 2008) the genes considered significant in this analysis had to be significant at least in two of the statistical tests performed (see Materials and Methods). I further selected the genes based on a threshold of fold change between WT and AP2 γ ^{-/-} (fold change equal or higher than 1.5) and absolute expression (higher than 50). This analysis revealed few significant changes in gene expression at rostral regions between WT and AP2 γ ^{-/-} cortices, while more (51) mRNAs were significantly changed in their expression in the intermediate-caudal levels comparing WT and mutant cortices (Fig 30 and Table 6a, b).

In rostral regions, only 18 mRNAs were significant in two of the statistical tests performed (Table 6b). Amongst them, most were up-regulated in the AP2 γ ^{-/-} cortices (10, Table 6b). This result at rostral levels may be due to indirect changes in expression as AP2 γ has been so far observed as a transcriptional activator, thus predicting reduced gene expression levels in the AP2 γ ^{-/-} cortices. On the contrary, in the intermediate-caudal levels most of the genes changed, were expressed at lower levels in the AP2 γ ^{-/-} cortices (44) and AP2 γ itself was amongst them expressed at 2.5x lower levels (Fig.30 and Table 6a). Therefore, at caudal levels the changes in gene expression observed might be rather direct effects resulting from the loss of AP2 γ . Interestingly, these results also show that AP2 γ can regulate itself, as the probesets used in the microarrays are designed against the 3'UTR region and do not detect the exon 5 that is deleted in the AP2 γ conditional knock-out mice.

Next, I tested the reliability of the transcriptome analysis by performing RT-PCR, *in situ* hybridization and immunostaining of some of the significant genes (Fig. 31). Most of the genes analyzed by RT-PCR showed similar fold change differences between WT and AP2 γ mutant cortices comparing to the array data, thus confirming the reliability of the microarray results (Fig. 31a, b and Table 6). The most interesting result was the prominent down-regulation of transcription factors expressed in basal progenitors, as NeuroD4/Math3 and Tbr2 in the AP2 γ ^{-/-} cortices at intermediate-caudal regions (Fig. 31a and Table 6). Math3 expression, as well as AP2 γ itself, were the only genes reduced in expression at rostral as well as intermediate-caudal regions. This was confirmed by RT-PCR and *in situ* hybridization, showing almost no signal in the AP2 γ ^{-/-} cortex compared to the strong expression in the SVZ of WT cortices (Table 6 and Fig. 31a, b, f, f'). Consistent with our immunohistochemical analysis, Tbr2 was also down-regulated at the mRNA level, however, only at intermediate-caudal regions (Fig. 31a, i, i'). Several other markers of basal progenitors shown to be differentially regulated in the microarrays, but not significant according to the statistical tests performed, could be confirmed to be downregulated in the AP2 γ ^{-/-} cortices by RT-PCR and *in situ* hybridization (Svet1, NeuroD1, and Cux2, Fig. 31a, c-e'). This discrepancy can be due to our very stringent microarray analysis potentially excluding false positives, but maybe also including false negatives. This analysis thus revealed a striking decrease on virtually all genes known to be expressed in basal progenitors after loss of AP2 γ in the cortex.

Notably, transcriptome analysis of the AP2 γ ^{-/-} cortex also revealed downregulation of some mRNAs encoding for proteins acting as pro-survival factors and protecting from cell death, such as the signalling molecule Stat3 (Table 6 and Fig. 31b, g, g'). Moreover, the

transcription cofactor Lmo4 is a positive mediator of IL-6/Stat3 signalling (Chen et al., 2007). Lmo4 also turned out to be expressed in the SVZ of the E14 WT cortex, but was virtually absent in the AP2 γ ^{-/-} cortices as confirmed by RT-PCR and *in situ* hybridization (Table 6 and Fig. 31b, h, h'). Lmo4 was previously shown to be expressed in the telencephalon over mid and late embryonic stages, stronger expressed in the SVZ and marginal zones than in the VZ (Hermanson et al., 1999). This transcription factor is also essential for survival of neural progenitor cells (Lee et al., 2005b; Tse et al., 2004). Other genes as the axonal guidance gene Slit2, the metallothionein 1 and 2 (MT1/2) and the inhibitor of differentiation/DNA binding (Id3) were also down-regulated in the AP2 γ ^{-/-} cortices, possibly due to the reduction of neurons in the mutant cortex (Table 6 and Fig. 31b). Interestingly, these genes confer a protective effect within the mammalian CNS (Carrasco et al., 2000; Hidalgo et al., 2001; Kee and Bronner-Fraser, 2001). Therefore, this analysis suggests that basal progenitors lose the expression of their characteristic fate determinants as well as factors involved in the regulation of their survival after AP2 γ deletion, bringing new insights on the molecular regulation downstream of AP2 γ . The loss of AP2 γ might affect the fate specification and the cell survival of cortical progenitor cells and neurons, the latter likely mediated by Lmo4, Stat3 and MT1/2 signalling down-regulation.

Besides these, Emx1 was similarly down-regulated in the AP2 γ ^{-/-} cortices (Table 6 and Fig. 31b). This gene appeared to be involved in regionalization of the cortical primordium promoting medial fates and is expressed in a caudal high to rostral low gradient (Muzio and Mallamaci, 2003). Given the restriction of our phenotype to intermediate-caudal levels, it was interesting to see a decrease in Emx1 mRNA in the AP2 γ ^{-/-} cortices, that might be one of the downstream targets of AP2 γ restricting the phenotype to caudal regions. In this context, further genes down-regulated in the AP2 γ ^{-/-} cortices, such as Tcf3, are involved in regionalization. Interestingly, the neural cell recognition molecule Close Homolog of L1 (Chl1) was also changed in its expression in the AP2 γ ^{-/-} cortices. Chl1 displays a graded pattern of expression with highest levels caudally in the visual cortex, moderate levels in the somatosensory region, and low levels rostrally in the motor region (Liu et al., 2000). This factor is expressed at highest levels in the caudal cortex at E14.5 during migration of neuronal progenitors from the VZ to the cortical plate (Demyanenko et al., 2004). Thus, several molecular changes observed in the AP2 γ ^{-/-} cortices are also related to regionalization and are caudalizing factors, possibly contributing to the restriction of the phenotype mostly to caudal regions.

6.2.6 Cell death of basal progenitors in the AP2 γ ^{-/-} cortex at mid-neurogenesis

The misspecification of progenitors in the AP2 γ ^{-/-} cortex, namely the increase in RGCs undergoing mitosis at basal positions might be caused by alterations in cell cycle. Moreover, the microarray results were hinting to alterations in cell survival and AP2 γ indeed regulates cell survival in the trophoctoderm lineage (Auman et al., 2002; Hilger-Eversheim et al., 2000). Therefore, I examined the cell cycle and cell death of E14 WT and AP2 γ ^{-/-} cortical cells by FACS analysis, using propidium iodide labelling (PI) (Fig. 32a-c). The AP2 γ ^{-/-} cortices showed a slight increase in the percentage of cells in G1 phase and a decrease in S/G2/M phase (M2=G1 phase; M3=S phase; M4=G2/M phase in Fig. 32a-c). An increase in cells in G1 phase may reflect an arrest of the RGCs in this cell cycle phase and consequently result in these cells remaining at the place of S phase at the basal positions in the AP2 γ ^{-/-} cortices. Moreover, at E14, the AP2 γ ^{-/-} cortices showed double the proportion of cells in subG1, observed by FACS (subG1 bars in Fig. 32c). Events contained in the subG1 fraction correspond to subdiploid nuclei, thus corresponding to death cells. Indeed, double the number of apoptotic cells was confirmed by TUNEL that labels DNA strand breaks (red arrows in Fig. 32d, d') and by activated-caspase3 staining (Fig. 32e-f'''). Interestingly, most of the activated caspase 3-positive cells were located in the VZ/SVZ of the AP2 γ ^{-/-} cortex and many co-localized with mRNA of basal progenitor markers (Neurod1, Cux2 and Svet1), but only few apoptotic cells were observed in the differentiating neurons (Fig. 32d-g). In the WT cortex, about 25% of all dying cells express these SVZ markers (Fig. 32g). In contrast, more than half of all activated-caspase3⁺ cells contained SVZ markers in the AP2 γ ^{-/-} cortices (Fig. 32g). This result suggests that basal progenitor cells are particularly prone to die in the absence of AP2 γ . Thus, a high increase in cell death of basal progenitors occurs after deletion of AP2 γ , in agreement with the molecular changes observed in the transcriptome analysis.

6.2.7 Defects in neuron generation and basal progenitor specification in the AP2 γ ^{-/-} cortex at the end of neurogenesis

Consistent with the high increase in cell death of basal progenitors around mid-neurogenesis in the AP2 γ ^{-/-} cortex, the total number of mitotic cells is significantly decreased in the E17 mutant cortex at intermediate-caudal regions (Fig. 33a). This demonstrates that basal progenitors are depleted due to apoptosis during the second half of neurogenesis in the absence of AP2 γ , explaining the reduction in neurons generated during this period. Furthermore, there was a striking decrease in the percentage of basally located mitotic cells, confirming the specific depletion of basal progenitors in the AP2 γ ^{-/-} cortices at later

developmental stages (Fig. 33b). Indeed, the apical progenitors are properly maintained in the AP2 γ ^{-/-} cortex as observed by *in situ* hybridization for Hes5 or immunostaining for Pax6 and Ki67 (Fig. 33c, c', e-f'). However, *in situ* hybridization for basal progenitor markers, such as Svet1 or immunostaining for Tbr2 revealed a decrease in these basal progenitor markers in the E17 mutant compared to WT cortices at intermediate-caudal regions (Fig. 33d, d', f, f'). This decrease in Tbr2-positive basal progenitors was much more pronounced at E17 compared to the E14 AP2 γ mutant cortex, consistent with the increased cell death of basal progenitors observed at mid-neurogenesis.

At E17 in the cortex, some mRNAs expressed in basal progenitors, such as Satb2 and Cux2, are also expressed in cortical plate neurons (Fig. 33g, h). Interestingly, in the E17 AP2 γ ^{-/-} cortex, I noted a high decrease of Satb2 and Cux2 mRNA in the neurons of the cortical plate compared to the WT cortex (Fig. 33g-h'). This observation suggested a respective decrease of neurons that might result from defects in their generation, as basal progenitors are severely misspecified already at mid-neurogenesis. However, a reduction of neuronal mRNAs in the cortical plate could also result from a delay in neuronal maturation or from neuronal migration defects in the AP2 γ ^{-/-} cortex. Indeed, I observed a slight increase in the Cux2 and Satb2 mRNA in the SVZ of the AP2 γ ^{-/-} compared to WT cortices (Fig. 33g-h'), thus suggesting that these neuronal cells have problems to migrate to their proper positions in the cortical plate. The high decrease of neurons in the cortical plate of the E17 AP2 γ ^{-/-} cortices at intermediate-caudal regions was confirmed by immunostaining for the neuronal marker β III-tubulin (Fig. 33 i, i'). Immunostaining for the neuronal antigens Cux1, Tbr1 and Ctip2 also revealed a strong decrease in the neuronal band in the cortical plate of the AP2 γ deficient cortex (Fig. 33 j-l'). It is important to note that these neuronal markers are transiently expressed in most neurons of the cortex during embryonic stages and become restricted to specific neuronal cortical layers only in the postnatal and adult cortex.

Taken together, the depletion of basally located mitotic cells and neurons in E17 AP2 γ ^{-/-} cortices compared to WT littermates likely result from the misspecification and the cell death of basal progenitors at mid-neurogenesis.

6.2.8 AP2 γ deletion reduces upper layer neuron generation

The mature cerebral cortex shows a layered structure that is formed during development. The neuronal layers of the cortex are created in an inside-out order, with deep layers (V/VI) being generated first, followed by the generation of upper layers (II-IV). Previous reports suggest that basal progenitors in the E14 cortex are specified to the generation of upper layer neurons

(Pontious et al., 2008; Tarabykin et al., 2001; Zimmer et al., 2004). The partial misspecification and increased cell death of basal progenitors in the AP2 γ ^{-/-} cortex therefore suggest possible aberrations in upper layer neuron generation. In order to examine the neuronal fate of cells generated at E14, the stage when defects start to occur in the AP2 γ ^{-/-} cortex, I performed BrdU-birthdating analyses (Fig. 34). BrdU is permanently integrated into the DNA of dividing cells during DNA synthesis in S phase, allowing the identification of cells that were dividing in the period of BrdU exposure. BrdU has been used to identify the birthdate of cells during development and to examine their fate at later stages as BrdU is kept in the postmitotic cells. Thus, BrdU was given to E14-timed pregnant mice and brains of the offspring were analyzed at postnatal day 7 (P7). Immunostaining for BrdU was combined with several neuronal markers, namely Cux2 mRNA for layers II/III, Ror β mRNA for layer IV, Sorla and vGlut2 mRNAs for layers II-IV, Er81 mRNA and Ctip2 for layer V and partial layer VI and Tbr1 protein for layers V/VI (Fig. 34; (Molyneaux et al., 2007)). These antigens or mRNAs are expressed in specific neuronal layers at postnatal stages, thus allowing me to identify the generation of distinct subtypes of neurons in the WT and AP2 γ ^{-/-} cortex. As at postnatal stages the neurons generated during development are still migrating to their final layer position in the cortical plate, I used these neuronal layer markers to identify their subtype. In both WT and AP2 γ ^{-/-} cortices, cells labelled with BrdU at E14 were detected in all neuronal layers with increased number in the upper cortical layers (Fig. 34a-h'). Therefore, neurons residing in all cortical layers could be generated, however, in the AP2 γ ^{-/-} cortex we observed a decrease in the number of BrdU positive cells colocalizing with upper neuronal layer (II-IV) markers (Cux1/2, Satb2, VGlut2, SorLa, Ror β), from 65% in WT to 50% in the mutant (Fig. 34a-f' and m). Conversely, the proportion of BrdU positive cells colocalizing with deep neuronal layer (IV-V) markers (Er81, Tbr1) was increased to 42% in the AP2 γ ^{-/-} compared to 30% in WT cortices (Fig. 34g-h' and m). In addition, the total number of BrdU positive cells was significantly decreased, suggesting that this phenotype is due to specific deficits in the generation of upper neuronal layers caused by an increased cell death of progenitors at mid-neurogenesis as demonstrated above (Fig. 34n). Instead, the total number of BrdU positive cells in deep neuronal layers (IV-V) was similar between AP2 γ ^{-/-} and WT cortices (Fig. 34n). These observations are in agreement with data revealed from Cux1, Satb2 and Tbr1 stainings of P7 AP2 γ ^{-/-} and WT cortices that demonstrate a decrease in the thickness of the upper layer neuron band labelled by Cux1, but not of the band of Tbr1-positive deep layer neurons, in the mutant cortex (Fig. 34i-l). These results support a specific reduction of upper layer neuron progenitors while lower layer neuron progenitors are not

affected in the AP2 γ deficient mouse cortex. This BrdU-birthdating experiment also allowed me to exclude the possibility of defects in neuronal migration in the AP2 γ ^{-/-} cortex, as the distribution of BrdU⁺ cells and neuronal layer markers was similar to the WT. Moreover, as most BrdU-positive cells were positive for neuronal markers and a similar number of BrdU-marker negative cells was observed in the P7 WT and AP2 γ ^{-/-} cortices, it suggests that neurons generated in the AP2 γ mutant cortex were at a similar level of maturation as neurons in the WT cortex. Therefore, neither a delay in neuronal maturation nor defects in neuronal migration seem to participate in the phenotype of the AP2 γ ^{-/-} cortex, but rather problems in cell survival.

6.2.9 Defects in layers II/III callosal projection neurons in the adult AP2 γ ^{-/-} occipital cortex

As demonstrated above, AP2 γ is important for the generation/survival of basal progenitors in the cortex. The decrease of these progenitors in the AP2 γ ^{-/-} cortex has effects on the production of upper layer neurons progressing into postnatal stages. I next examined whether this decrease in upper layer neurons was only transient or persisted into adult stages. A specific decrease in the thickness of upper neuronal layers in the AP2 γ ^{-/-} cortex compared to WT could be observed in the adult cortices of 2 months old mice by immunohistochemistry for Cux1 and mRNA expression of Cux2 and Ror β (Fig. 35a-b', d, e-f). However, the thickness of lower neuronal layers (V-VI) was not changed as revealed by mRNA of Er81 and immunostaining for Tbr1 (Fig. 35c, c', g, g'). To note, this phenotypic alteration of upper neuronal layers was only significant at occipital regions of the cortex, as apparent in sagittal sections of the adult AP2 γ ^{-/-} cortices. This phenotype was also seen in AP2 γ conditional knock-out mice crossed with Sox2::Cre (Sox2^{Cre/AP2 γ Δ ex5fl/fl}), in which the Cre mediated recombination starts earlier in development (E6.5; Fig. 35h-i'). In both adult mutants the thickness of the layers II/III-containing Cux2-positive neurons was strikingly reduced, especially at occipital regions, whereas the thickness of lower layers was normal (Fig. 35d, h,h').

It is known that upper layer neurons consist of distinct types of projection neurons, namely neurons projecting to the contralateral hemisphere - callosal projection neurons - and neurons that project within the cerebral cortex - cortico-cortical projection neurons. To discriminate which type of neurons was affected in the adult AP2 γ ^{-/-} cortex I looked at callosal projection neurons. Indeed, the size of the corpus callosum was strongly decreased in the AP2 γ deficient cortices. Fewer callosal fibers were also detected in the AP2 γ ^{-/-} adult brain by L1 protein

immunostaining (Fig. 36a, a'). Interestingly, mRNA for *Lmo4*, described to be expressed only in layers II/III callosal projection neurons (Arlotta et al., 2005) and layer V neurons, revealed a strong decrease in its expression in the layers II/III of the *AP2γ*^{-/-} occipital cortex (Fig. 36b, b'), thus suggesting a high decrease in callosal projection neurons in this mutant. To test this directly, we retrogradely traced callosal projection neurons by injecting fluorescent beads into the visual cortex of one hemisphere (Fig. 37a; see Materials and Methods) and analyzing the retrograde labelled cells in the contralateral hemisphere of the visual cortex 1 week later (Fig. 37b-d'). Interestingly, quantification of the proportion of retrograde labelled neurons in the upper layers of the cortex revealed a significant decrease in the *AP2γ*^{-/-} cortices to half the proportion observed in WT adult mice (Fig. 37b-f). Notably, the number of callosal projection neurons in layers V/VI was comparable between WT and mutant cortices (Fig. 37g). Thus, as the total number of neurons is reduced in the *AP2γ*^{-/-} cortex, this can be explained by the reduced callosal projection neurons in upper layers. Although, we can't exclude that cortico-cortico projections were reduced as well in these mutant mice. Therefore, the defects in basal progenitors in the embryonic *AP2γ*^{-/-} cortex clearly manifest at adult stages in a reduction of layers II/III callosal projection neurons in the visual cortex.

6.2.10 Functional defects in visual acuity in the *AP2γ*^{-/-} mice

Given the specific reduction of upper layer neurons only in the occipital cortex of the *AP2γ*^{-/-} adult cortex, we examined the effect of this phenotype on the visual performance of these mice. Towards this, a collaborator of ours, Matteo Caleo, used visual evoked potentials (VEPs) recorded from regions of the visual cortex in response to visual grated patterns. He measured the visual and behavioral capabilities (visual acuity, contrast threshold, response latency, temporal resolution) using VEPs as described previously (Porciatti et al., 1999). Interestingly, visual acuity (cortical spatial resolution evaluated by VEPs) of the *AP2γ*^{-/-} adult mice was abnormally low and reached only half of the normal value of the control mice (0.57 ± 0.07 c/deg; t-test, $p = 0.002$; Fig. 38a-c and Table 7). Visual acuity is indeed an important parameter that predicts performance in visual behavior. Notably, this parameter was suggested to be affected by callosal projections during development (Caleo et al., 2007). In this study, blocking of callosal connections caused a reduction in visual acuity (Caleo et al., 2007). Moreover, the ratio between the contralateral and ipsilateral VEPs was significantly reduced (t-test, $p = 0.027$ in Fig. 38d, e and Table 7), showing alterations in cortical binocularity in *AP2γ*^{-/-} mice. Moreover, the latency of the visual response in the

AP2 γ ^{-/-} mice was tendentially increased (t-test, $p = 0.05$; Fig. 38f). These data thus show significant defects in visual function of the AP2 γ ^{-/-} cortices, demonstrating the relevance of upper layer neuron numbers and the regulation of callosal projection neurons for cortex function.

6.2.11 AP2 γ overexpression increases the generation of basal progenitors

So far, the consequences of the loss of AP2 γ protein in the mouse cerebral cortex were described. To analyze if AP2 γ is also sufficient to induce basal progenitor fate, we performed *in vitro* or *in vivo* overexpression with MLV-based retrovirus containing either only GFP or AP2 γ GFP (Fig. 39a, a'). *In vitro* experiments were done in E14 primary cortical cultures and *in vivo* experiments were performed by *in utero* injections into the telencephalic ventricles of E14 embryos in timed pregnant mice (Fig. 39 and 40). Three days after infection of E14 cultures, the GFP infected cells derived from a single infected progenitor (=clone) were analyzed in regard to Tbr2-, β III-tubulin- or Pax6-immunoreactivity (Fig. 39a-d). Overexpression of AP2 γ caused a significant increase in the number of GFP/Tbr2-positive clones to about 60% compared to 45% observed in control infected clones (green bars in Fig. 39d). As Tbr2-positive basal progenitors are known to be committed to the generation of neurons, I also analyzed E14 cultures infected with AP2 γ virus after seven days *in vitro* and analyzed the proportion of pure neuronal clones generated (Fig. 39e). Indeed, upon AP2 γ overexpression, I observed a decrease in the percentage of mixed clones, containing neurons and progenitor cells, and an increase in the percentage of pure neuronal clones, immunostained with β III-tubulin (55% in Fig. 39f) compared to control GFP virus infected cultures (48% in Fig. 39f). In addition, the clone size after AP2 γ virus and control virus infections was not strikingly different, but there was a significant increase in clones with 3 to 8 cells upon AP2 γ overexpression (Fig. 39g), suggesting that AP2 γ may promote proliferation of progenitors *in vitro*. These results also suggest that radial glia progenitors upon AP2 γ overexpression instead of giving rise directly to neurons, first give rise to basal progenitors which then generate two neurons each, thus amplifying the number of neurons generated at the end. Therefore, overexpression of AP2 γ may induce indirect neurogenesis from apical progenitors, via the generation of basal progenitors, increasing the number of pure neuronal clones and the size of the clones generated *in vitro*. This observation is consistent with the higher expression of AP2 γ in the apical progenitors generating basal progenitors *in vivo* as described above (Pinto et al., 2008), and further shows that AP2 γ

overexpression is sufficient to drive apical progenitors to the generation of basal progenitors, at least *in vitro*.

Furthermore, three days after infection with AP2 γ into the lateral ventricle of E14 mouse embryos *in utero*, I analyzed the GFP positive cells in regard to Tbr2-, β III-tubulin- or Pax6-immunoreactivity (Fig. 40a-d). As observed *in vitro*, overexpression of AP2 γ *in vivo* also caused a significant increase in the number of Tbr2-positive cells amongst all GFP-positive cells. Cells infected with control GFP virus expressed Tbr2 in about 18%, and this proportion was almost doubled upon overexpression of AP2 γ (Fig. 40a-d). The number of GFP/Pax6-double positive cells was similar in both control and AP2 γ virus infections (Fig. 40d). Thus, AP2 γ overexpression induced Tbr2-positive basal progenitor generation but did not affect the proportion of apical progenitors. The increase in GFP/Tbr2-double positive cells after infection with AP2 γ virus occurred mostly at the expense of β III-tubulin+ cells (Fig. 40d). Interestingly, a higher number of GFP-positive cells after overexpression of AP2 γ was located in the VZ/SVZ regions, with some cells showing a leading process towards the cortical plate still expressing Tbr2. This was very rarely observed in control injected mice (Fig. 40c-c''). Thus, AP2 γ overexpression delays the down-regulation of Tbr2 with a consequent delay in the up-regulation of neuronal differentiation genes.

To examine if AP2 γ may interfere with neuronal differentiation in the long term or rather increase upper layer neuron fate, I analyzed the E14 injected mice at postnatal day 2 (Fig. 40e-i). Analysis of P2 cortices after AP2 γ overexpression revealed an increase in the percentage of infected cells adopting an upper layer II/III neuron fate compared to control virus infections, as monitored by Cux1 and Satb2 immunostaining and by the position of the neurons within the cortical plate of the cortex (Fig. 40e-f', h and i). The percentage of layer IV neurons was not changed as monitored by Ror β (not shown) and Ctip2 immunostaining (Fig. 40h and i), but a decrease in the percentage of Tbr1-positive neurons in lower layers V/VI was detected (Fig. 40g-i). This suggests that the increase in upper layer neuron generation occurred at the expense of neurons of lower layers V/VI. These observations also support the importance of AP2 γ in the generation of upper neuronal layers in the cortex and suggest that AP2 γ is sufficient to convert deep layer progenitors to an upper layer neuron fate. It is still possible that the total number of deep layer neurons may not be affected but only more upper layer neurons may be added.

Strikingly, the effects of AP2 γ overexpression on basal progenitor generation and upper layer neurons fate in the cortex were stronger at intermediate-caudal regions compared to rostral regions, suggesting that some region-specific cues restrict AP2 γ function to occipital regions.

6.2.12 Molecular mechanisms regulating AP2 γ in the cortex

Given the increase in Tbr2⁺ progenitors after AP2 γ overexpression, we examined whether AP2 γ directly regulates Tbr2 and Math3, the other basal progenitor transcript highly affected by the loss of AP2 γ . Direct regulation of basal progenitor transcripts by AP2 γ was examined using luciferase assays. Mouse neuroblastoma (Neuro-2A) cells were transfected with the pGL3 luciferase vector containing all 775bp of the Math3 promoter or 816bp of the Tbr2 promoter (see Material and Methods). The latter sequence was selected on the basis of AP2 binding sites in the Tbr2 promoter. I observed a significant activation of the Tbr2 promoter upon co-transfection with AP2 γ cDNA containing plasmids (3.1 fold, Fig. 41a) and a smaller but significant regulation of the Math3 promoter (1.5 fold, Fig 41a). As Math3 and Tbr2 are also highly down-regulated in the Pax6-mutant, I examined the effect of Pax6 on these promoters (Fig. 41a). Indeed, the Tbr2 and the Math3 promoter were activated upon transfection with the canonical form of Pax6 (Fig. 41a). However, co-transduction with Pax6 and AP2 γ did not show a cooperative effect (Fig. 41a). Thus, the Math3 and Tbr2 promoters are common downstream targets of Pax6 and AP2 γ , probably mediating the function of AP2 γ on basal progenitors and upper layer neurons generation in the developing cortex. The fact that both AP2 γ and Pax6 can regulate Tbr2 and Math3 promoters may explain the restriction of the AP2 γ ^{-/-} phenotype in basal progenitors to the occipital regions of the cortex where Pax6 expression is very low and can not compensate the absence of AP2 γ .

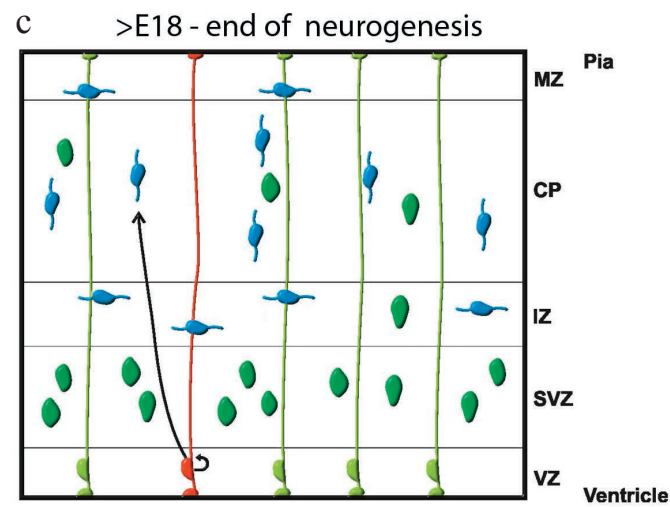
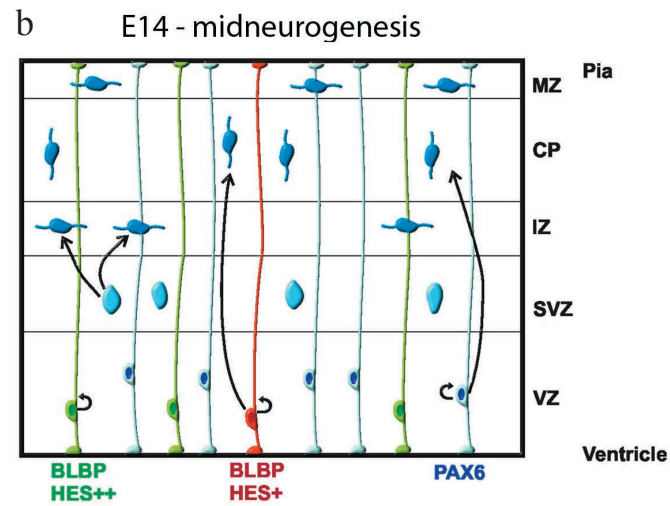
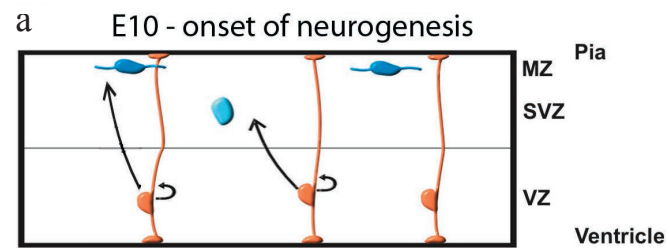
I next examined potential up-stream regulators of AP2 γ , focusing on the candidate genes Pax6, Ngn1/2/3 and Mash1, all of which have binding sites in the AP2 γ promoter, as predicted by bioinformatics analysis (Fig. 41b). These candidates were tested in the luciferase assay using 789bp of the AP2 γ promoter (Fig. 41b, see also Material and Methods). Pax6 transduction lead to strong activation of expression from the AP2 γ promoter, however, Ngn1 and 2, but not 3, as well as Mash1 actually repressed expression (Fig. 41b). The repression of AP2 γ by Mash1 observed in the luciferase assay could be confirmed *in vivo* by the virtual absence of AP2 γ expression in E14 cortices of mice expressing Mash1 in the Neurogenin 2 locus (Ngn2KiMash1) (Fig. 42c, c'). Interestingly, AP2 γ can activate itself, consistently with the data from microarray analysis of the AP2 γ ^{-/-} cortices, where AP2 γ was significantly down-regulated (Fig. 41b and Table 6).

Taken together, AP2 γ possibly mediates some Pax6 functions positively in the developing cortex. These data, therefore, reveal a partially redundant network of transcriptional regulation for basal progenitor fate determinants (Summary in Fig. 43). This transcriptional

regulation of basal progenitors is crucial to ensure the reliable specification of the progenitor set of upper layer neurons, the set of cortical neurons highly expanded during phylogeny.

7 Figures and Tables

Figure 1



- neuroepithelial cells
- neurons
- basal progenitors
- neurogenic radial glia
- bi/multipotent radial glia
- gliogenic radial glia
- glial progenitors

Figure 1. Subtypes of progenitors present in the embryonic mammalian cortex during development.

The panels depict different stages of development ranging from the onset of neurogenesis (**a**) to mid-neurogenesis (**b**) and gliogenesis (**c**). (**a**) At early neurogenesis, E10-11 in the mouse, the VZ progenitors are neuroepithelial progenitor cells (NEPs) with radial processes contacting the pia (top of the panels) and the ventricle (bottom of the panels as indicated). NEPs can self-renew (indicated by the semi-circular arrow) and generate two NEPs, or they can divide asymmetrically generating a neuron (left hand cell in panel **a**) and a neuroepithelial cell or a basal progenitor and a neuroepithelial cell (cell in the middle of panel **a**). (**b**) At mid-neurogenesis, at E14 in the cerebral cortex, VZ progenitor cells are radial glial cells (RGCs) derived from the earlier NEPs. Distinct subtypes of RGCs can be identified based on their molecular, cellular and lineage characteristics. BLBP and high levels of Hes-expression characterize RGCs that only generate other RGCs dividing symmetrically (green radial glia to the left in panel **b**). Other RGCs are neurogenic, express Pax6 and divide asymmetrically self-renewing and generating a postmitotic neuron (radial glia to the right in panel **b**), or a basal progenitor. These RGCs will divide symmetrically at the end of neurogenesis ending with the generation of 2 postmitotic neurons. Other RGCs are BLBP-positive and supposedly have lower levels of Hes-expression. They may be bi-potent progenitors giving rise to neurons and glial cells. (**c**) At late neurogenesis, around E18, only two subtypes of RGCs remain. Gliogenic RGCs (green) that divide symmetrically and generate further RGCs that then transform into astrocyte progenitors (glial progenitors) and a small proportion of bi/multipotent RGCs that have previously produced neurons and now give rise to glial progenitors (red).

Figure 2

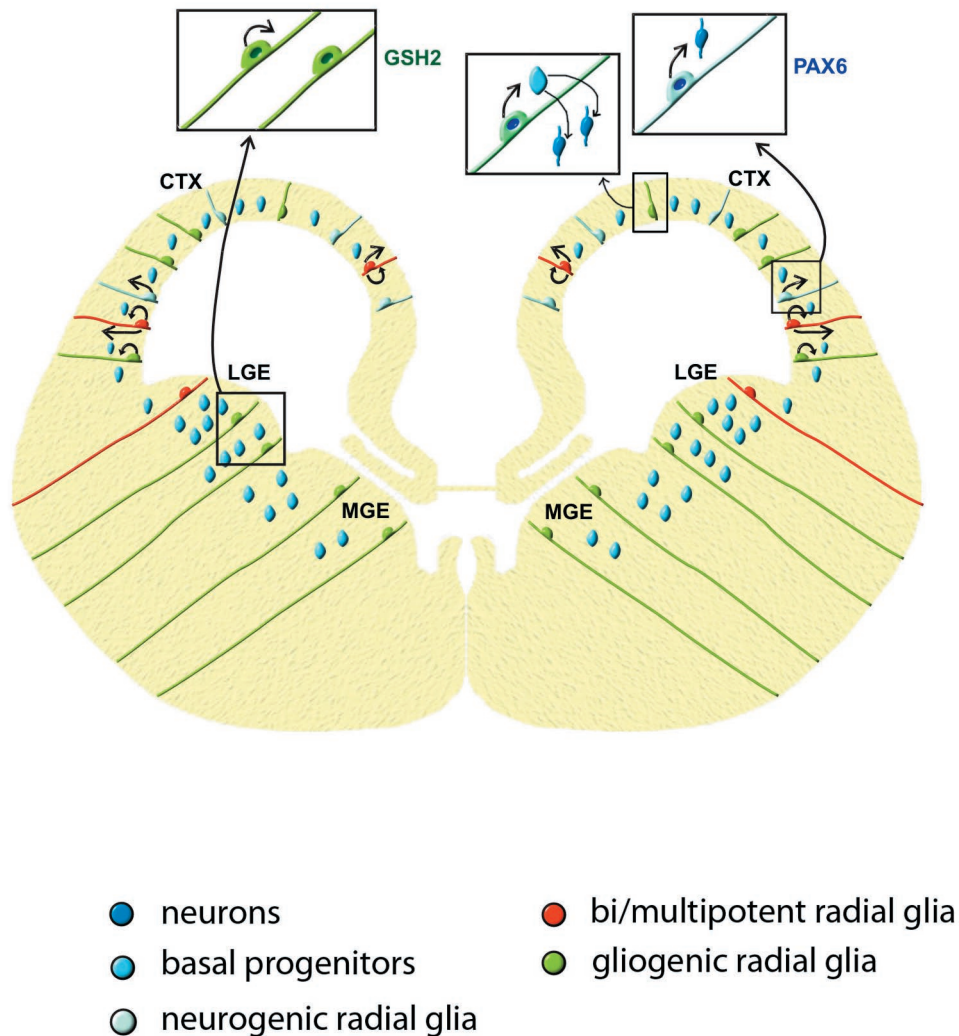


Figure 2. Distinct subsets of radial glial cells in the dorsal and ventral telencephalon

Radial glial cells (RGCs) differ in the dorsal and ventral telencephalon during neurogenesis (around E10-E17). RGCs in the ventral telencephalon (LGE and MGE - lateral and medial ganglionic eminence, respectively) express Gsh2 (see insert to the left) and are mostly gliogenic with the capacity of self-renewing thus giving rise to two other RGCs. Bi/multipotent RGCs are also present in the ventral part of the forebrain. Basal progenitors are the majority of the progenitor pool in the LGE and MGE, generating the majority of neurons. In the dorsal forebrain (CTX - cortex) several subsets of RGCs are present, defined as the neurogenic RGCs expressing Pax6 (see insert to the right) and generating only neurons, gliogenic RGCs only self-renewing and generating other RGCs or basal progenitors (see insert in the middle) and bipotent RGCs that generate neurons and glial cells. Basal progenitors constitute a minority in the dorsal telencephalon. In my work I studied the transcriptome of the distinct subsets of RGCs existent in the dorsal telencephalon.

Figure 3

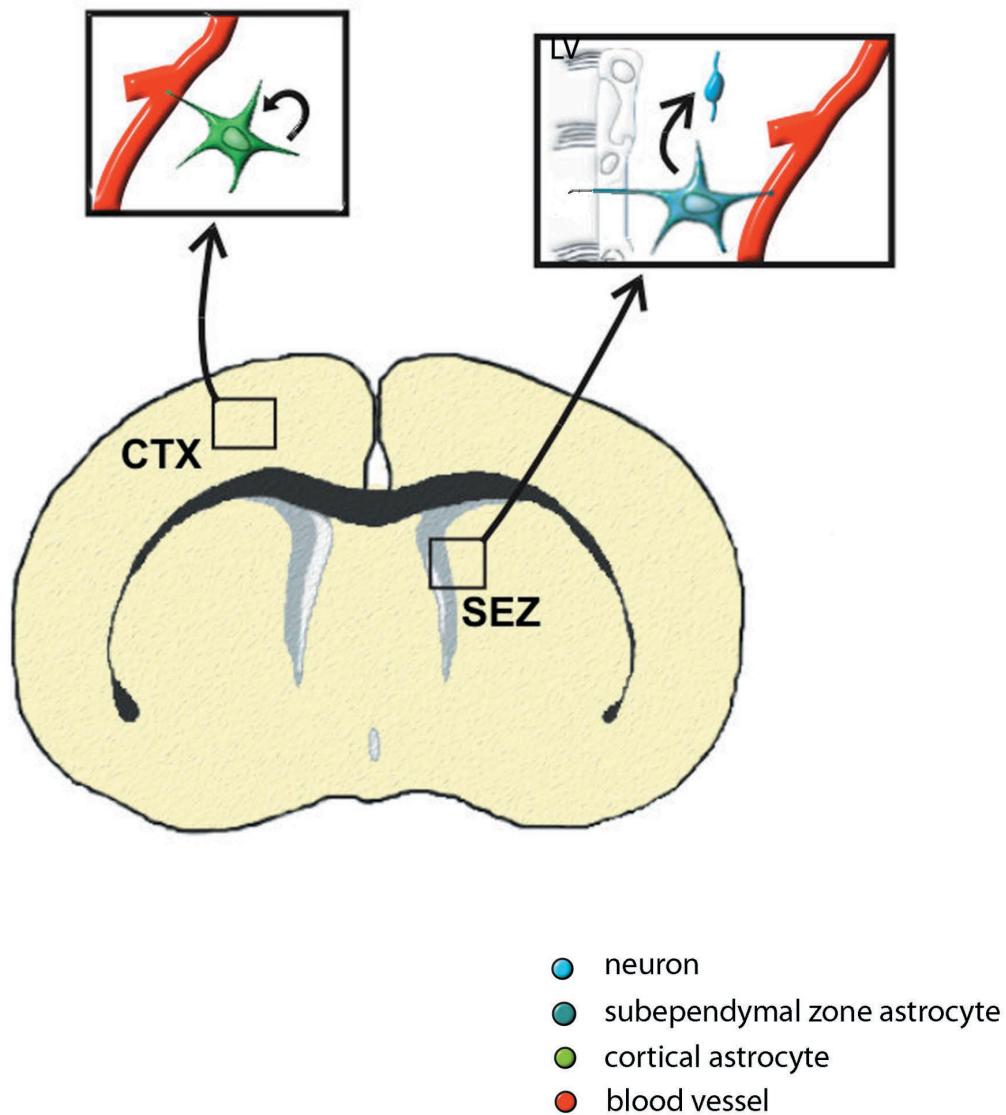


Figure 3. Astrocyte heterogeneity in the adult mammalian brain

Adult astrocytes are generated by radial glial cells (RGCs). A subpopulation of astrocytes acts as adult neural stem cells in specific neurogenic niches of the adult brain such as the SEZ. These astrocytes share with other astrocytes the characteristic that they contact the basal lamina but differ from other astrocytes in maintaining an apical contact to the lateral ventricle. Abbreviations: LV=lateral ventricle

Figure 4

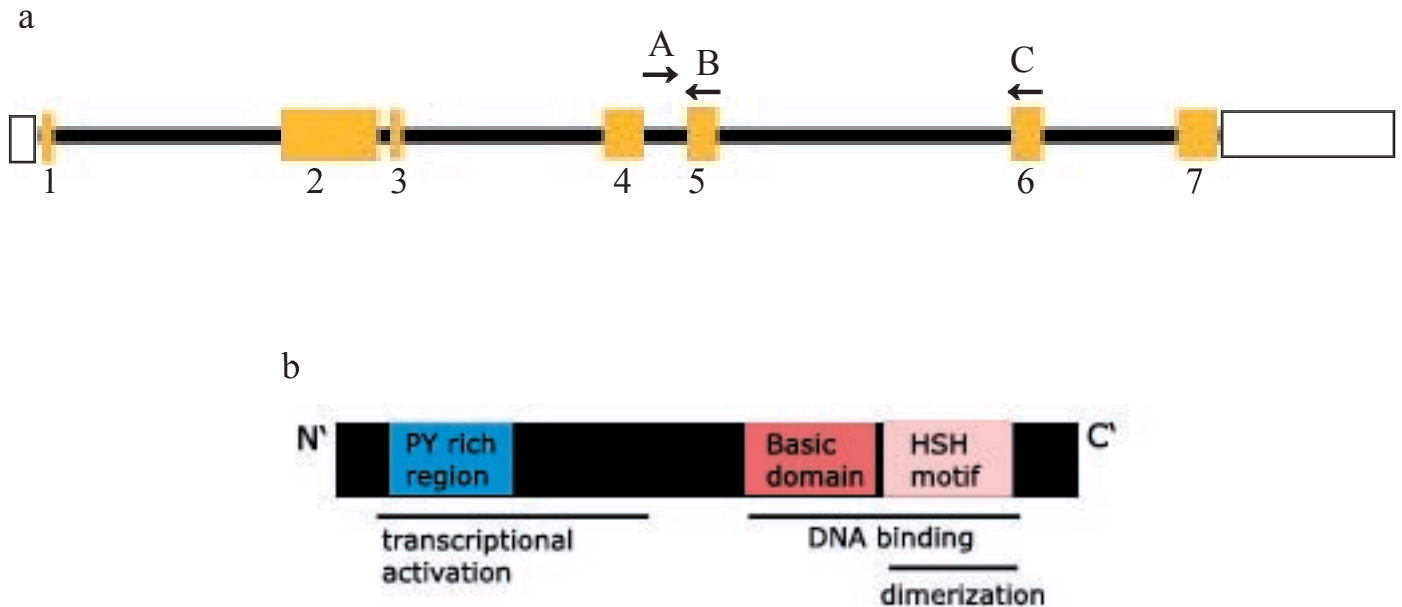


Figure 4. Schematic representation of the genomic fragment and protein structure of the transcription factor *AP2γ*

(a) Schematic representation of the 6-kb genomic fragment of *AP2γ* spanning exons 2 to 7. The exons are designated by numbers and colored in yellow. The letters A-C represent the primers used for *AP2γ* conditional knock-out mice genotyping. A and B were used to distinguish the floxed allele (300bp) from the WT allele (343bp) whereas the addition of primer C was used to detect the null allele (700bp). (b) All members of the *AP2* family, including *AP2γ*, share a characteristic protein structure containing a unique C-terminal helix-span-helix (HSH) motif that mediates protein dimerization; together with a basic domain they are involved in DNA binding with varying affinity to GC-rich elements. An N-terminal proline- and glutamine-rich (PY rich) region mediates transcriptional activation. In the *AP2γ* conditional knock-out mice the LoxP sites are flanking the entire Exon 5 and the majority of Exon 6, whose deletion cause a loss of the HSH domain near the protein carboxyterminus

Figure 5

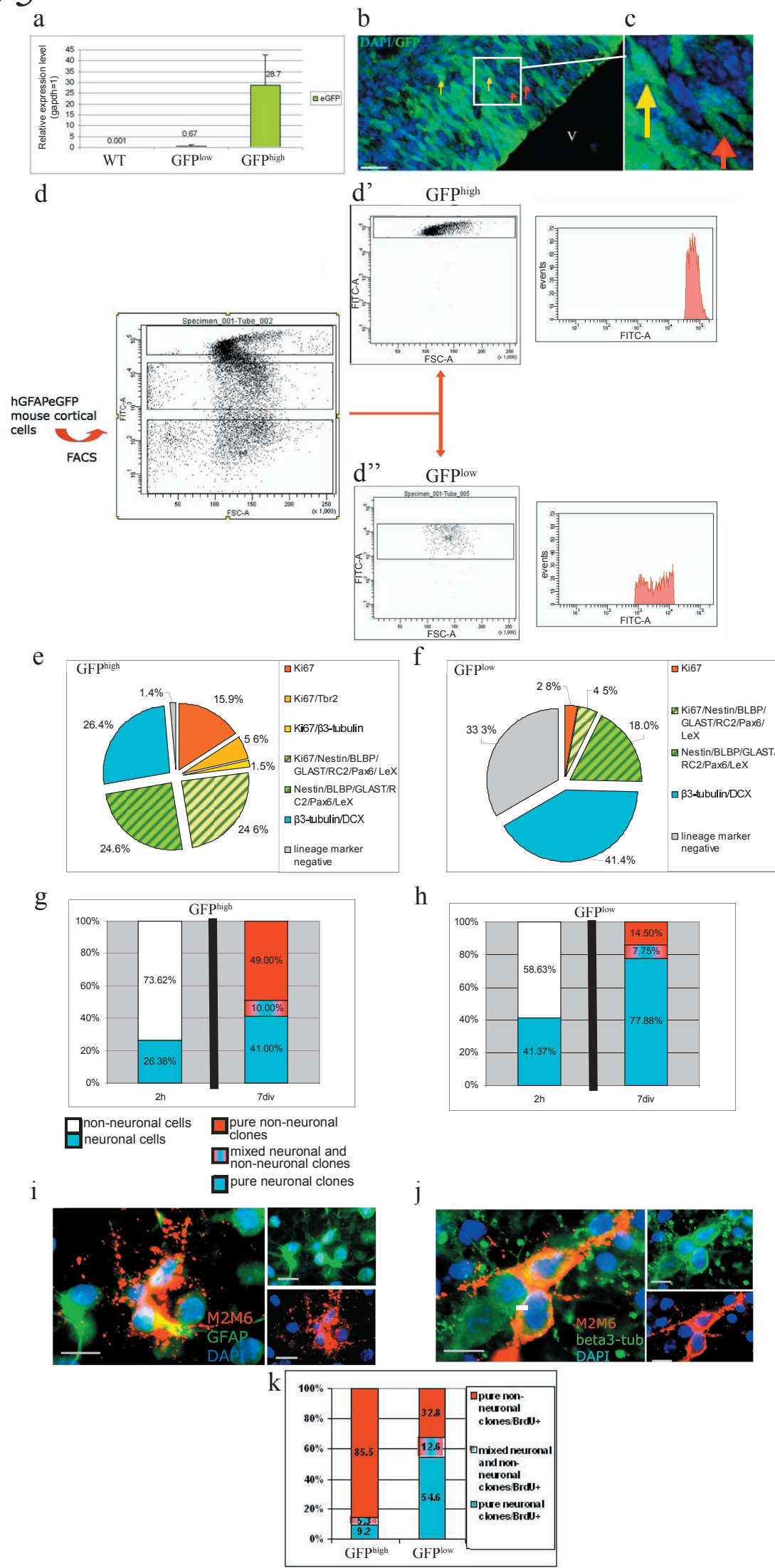


Figure 5. FACS isolation and clonal analysis of distinct radial glia-derived lineages

(a) Histogram depicts the GFPmRNA levels as determined by real time RT-PCR in GFP^{high} or GFP^{low} fractions compared to cortical cells dissociated from WT mice. (b, c) Confocal image of a DAPI stained cortical section from an E14 hGFAP-eGFP brain (not immunostained for GFP) displaying cells with distinct GFP intensity levels – GFP^{high} and GFP^{low}. Red and yellow arrows depict GFP^{low} and GFP^{high} cells, respectively. (d) FACS analysis of E14 dissociated cortices of hGFAPeGFP. Dot blots depict forward scatter on the X- and green fluorescence on the Y-axis. The frequency of events is depicted in the histograms with red area for cells after sorting. From a total of 73% of GFP positive cells, two groups were identified based on their fluorescence intensity – 30% GFP^{high} (d') and 30% GFP^{low} (d'') fractions. (e-f) GFP^{high} (e) and GFP^{low} (f) sorted cells were directly plated *in vitro* for 2 hours and characterized based on markers for radial glial cells (BLBP and GLAST, green strips), proliferating cells (Ki67, orange and yellows), basal/SVZ progenitors (Tbr2, light orange) and for postmitotic neurons (β -III-tubulin, blue). Histograms in g and h depict the clonal analysis for GFP^{high} (g) and GFP^{low} (h) sorted cells after 7 days *in vitro* (div). (i, j) Depict fluorescence micrographs of examples of a non-neuronal clone generated in cultures of GFP^{high} sorted cells (i) and a neuronal clone positive for β -III-tubulin generated by the GFP^{low} sorted cells (j) after 7 days *in vitro* stained for the antigens depicted in the panels. (k) Histogram depicts the quantification of neurogenic, mixed and non-neurogenic clones proliferating (BrdU positive) after 3 days *in vitro* for GFP^{high} and GFP^{low} fractions. Scale bars: 20 μ m.

Figure 6

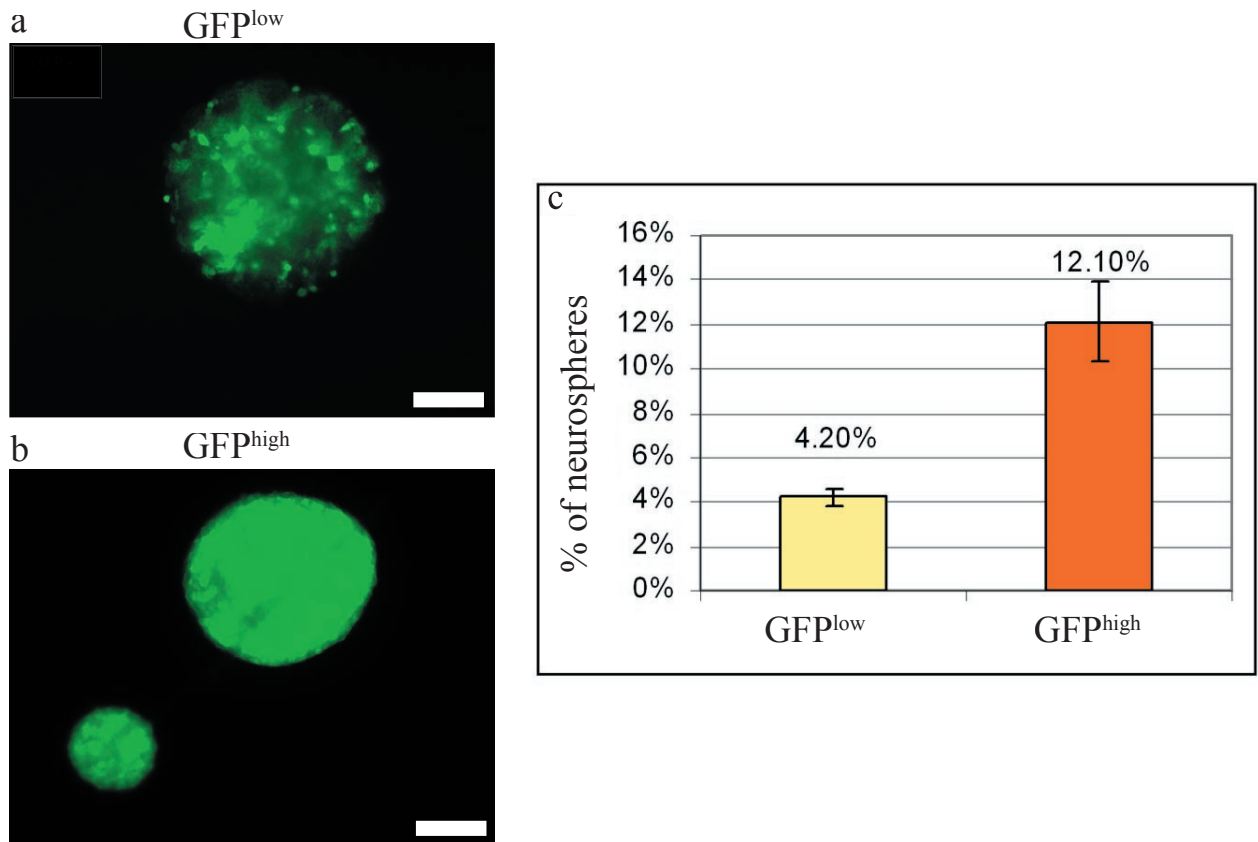


Figure 6. Neurospheres forming capacity of distinct radial glia-derived lineages

(a and b) Fluorescent micrographs depict neurospheres formed by GFP^{low} (a) and GFP^{high} (b) fractions of sorted cells after 7 days *in vitro*. Note the different GFP fluorescence intensity between the neurospheres generated by GFP^{low} and GFP^{high} fractions. (c) Histogram depicts the quantification of the percentage of neurospheres generated by the GFP^{low} (yellow bar) and GFP^{high} (orange bar) fractions of sorted cells. For this neurosphere assay, 2000 events of GFP^{high} and GFP^{low} sorted cells counted by the FACS machine were plated per well (24 well plate). Note the higher number of neurospheres formed by the GFP^{high} fraction. Bars in the histogram represent mean \pm S.E.M. Scale bars: 20 μ m

Figure 7

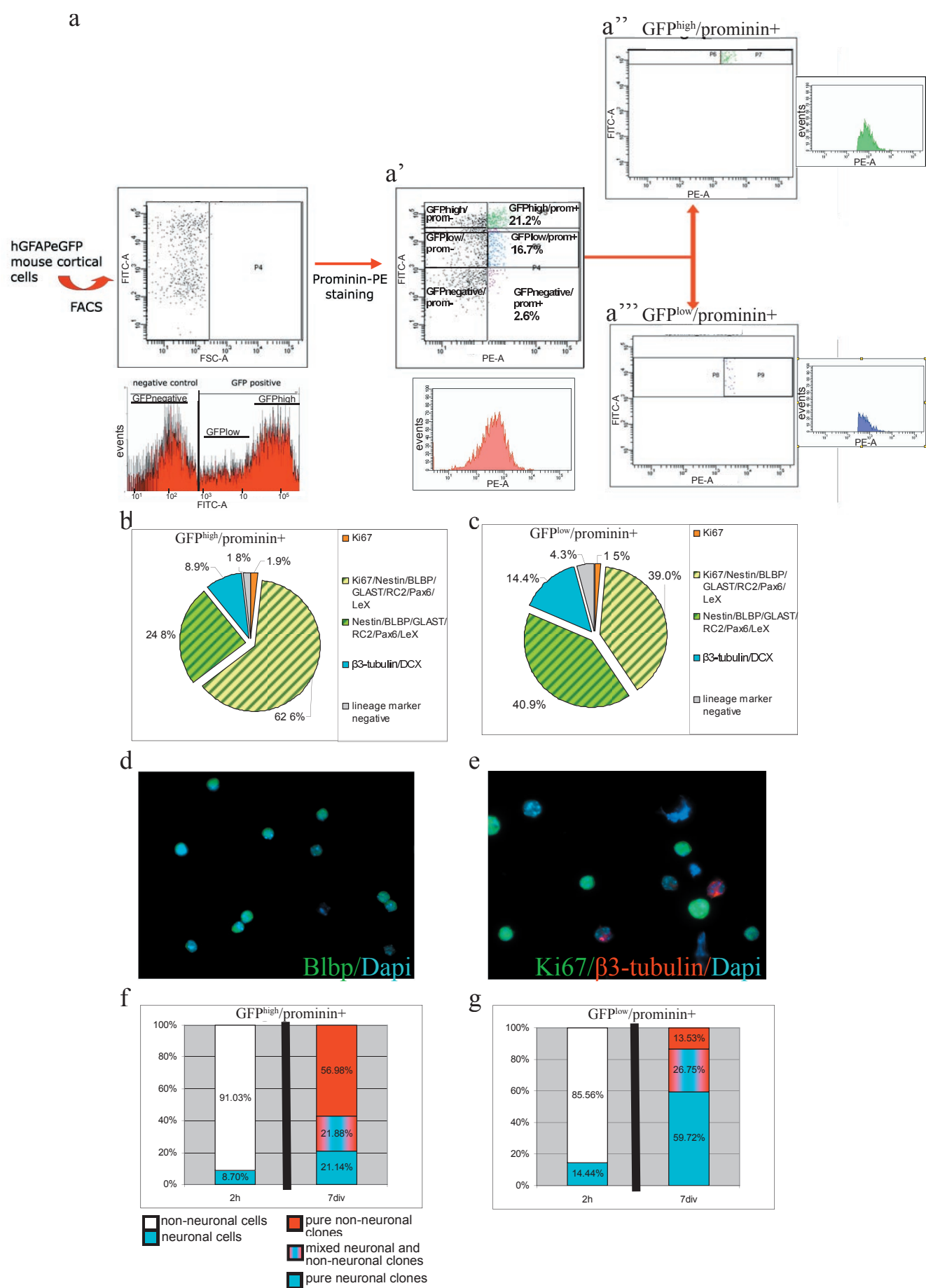


Figure 7. Isolation and characterization of distinct radial glial subsets

(a) Prominin staining (Prominin-PE) was combined with GFP expression of cortical cells isolated from hGFAPeGFP mice and analyzed by FACS as depicted in the dot blots (prominin-PE in X-axis, GFP in Y-axis). Prominin immunostaining revealed an average of 40% positive cells in E14 cortex and almost all of them were GFP positive (37.9%) (panel a'), (first panel = no prominin staining). The frequency of events is depicted in the histograms with red area for cells prior to sorting and with green and blue area for cells after sorting. Pie diagrams in **b** and **c** depict the cell type compositions of sorted cells GFP^{high}/prominin+ (**b**) and GFP^{low}/prominin+ (**c**) after 2 hours *in vitro*. (**d** and **e**) Fluorescence micrographs depict examples of GFP^{high} sorted cells kept in culture for 2 hours stained for the antigens depicted in the panels. The bar histograms in **f** and **g** depict the clonal analysis performed with the GFP^{high}/prominin+ (**d**) and GFP^{low}/prominin+ (**e**) sorted cells.

Figure 8

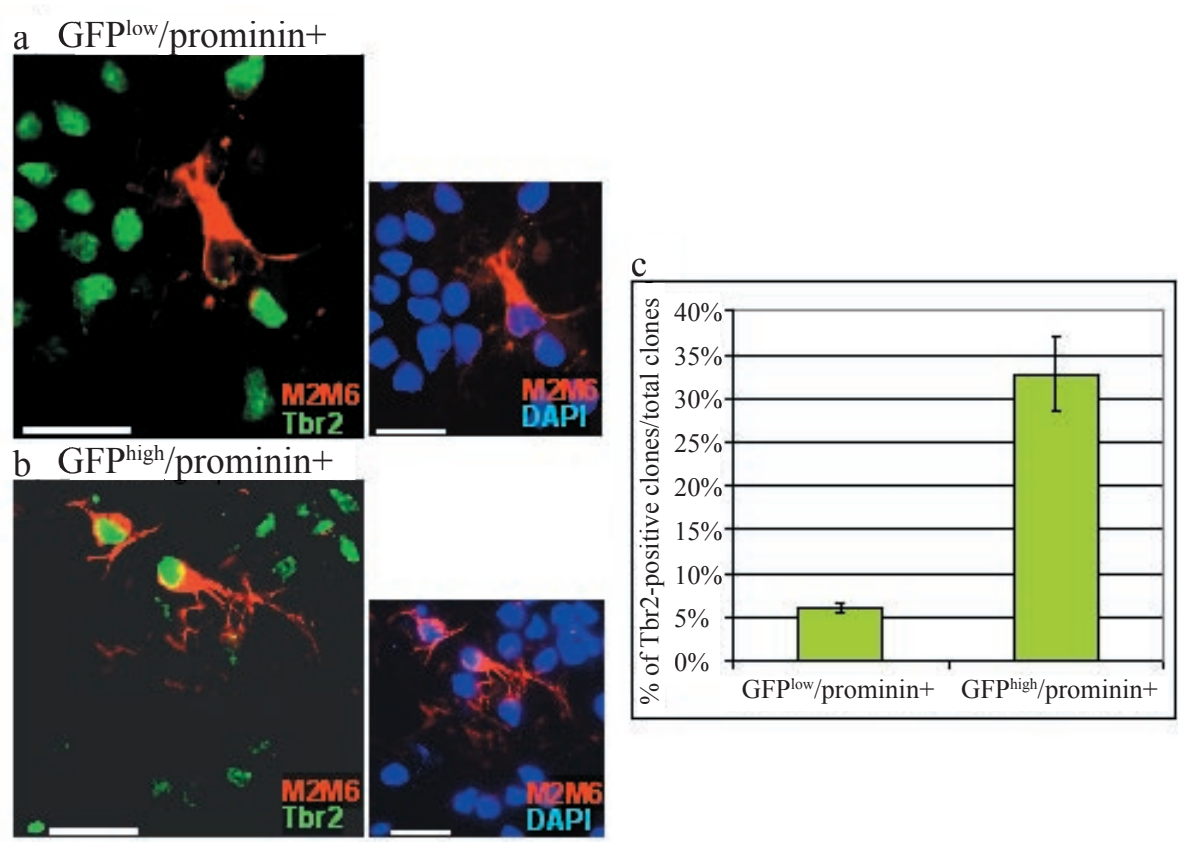


Figure 8. Generation of Tbr2-positive clones by distinct subsets of radial glial cells

(a, b) Examples of a pure Tbr2-negative clone (a) and a pure Tbr2-positive clone (b) generated by the GFP^{low}/prominin+ and GFP^{high}/prominin+ subsets, respectively, after 3 days *in vitro* on a rat co-culture system. (c) Histogram depicts the proportion of Tbr2-positive clones amongst all clones generated by the GFP^{low}/prominin+ (left bar) and the GFP^{high}/prominin+ population (right bar) after 3 days *in vitro*. Bars in the histogram represent mean ± S.E.M. Scale bar: 20μm

Figure 9

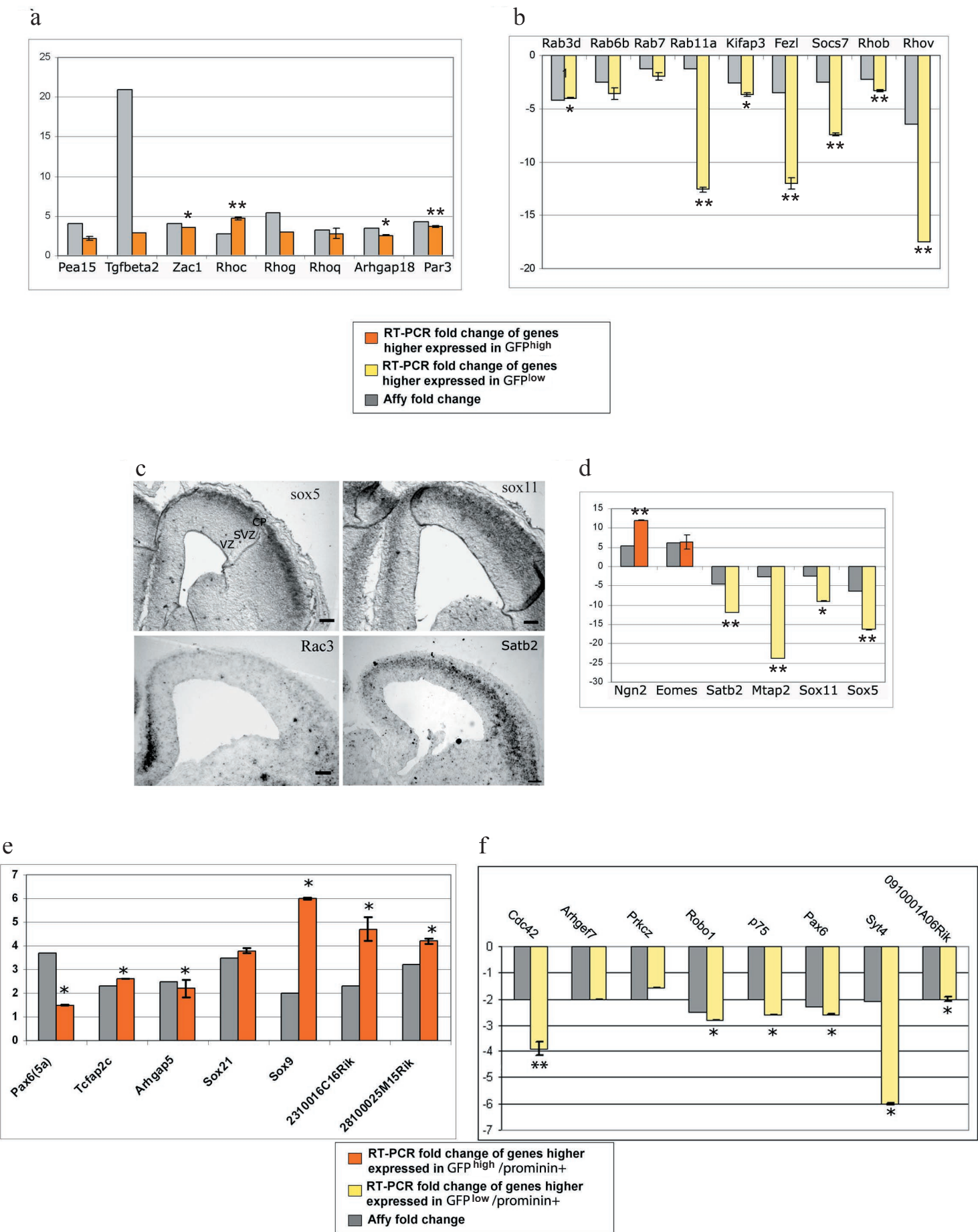


Figure 9. RT-PCR analysis of differentially expressed genes between distinct subsets of radial glia

(a and b) RT-PCR was performed for 17 mRNAs predicted to be differentially expressed by microarray analysis in the GFP^{high} versus GFP^{low} fractions of cells sorted from E14 cortex. Coloured bars represent RT-PCR of the different fractions with the respective standard deviations between all the replicates and grey bars represent the equivalent microarray result. Values of the Y-axis represent linear ratios, between GFP^{high}/GFP^{low} expression and values for genes expressed at higher levels in the GFP^{low} fraction were set to negative. (c) In situ hybridization analysis of 4 mRNAs absent in the microarrays of GFP^{high}/prominin⁺ and GFP^{low}/prominin⁺ but present in the GFP^{low} (Sox5 and Sox11) and GFP^{high} (Rac3 and Satb2) fractions. Note the expression in the cortical plate and in the subventricular zone (SVZ) in the E14 cortex. (d) RT-PCR analysis of mRNAs expressed in neurons and in basal progenitors differentially expressed between the GFP^{high}/GFP^{low} fractions and absent in the GFP^{high}/prominin⁺ and GFP^{low}/prominin⁺ fractions. (e and f) 12 mRNAs from GFP^{low}/prominin⁺ and GFP^{high}/prominin⁺ radial glial cells predicted to be differentially expressed by Affymetrix analysis (grey bars) were examined by real time RT-PCR (orange and yellow bars in e and f, respectively, depict the linear fold change of mRNA levels between the respective populations after normalization to GAPDH mRNA levels. Values for genes expressed at higher levels in the GFP^{low}/prominin⁺ fraction were set negative). Grey bars represent the equivalent ratios according to the microarray results. T-test was performed for all genes analyzed (*= p≤0.05; **=p≤0.01). Scale bar: 100 μm. Abbreviations: VZ=ventricular zone; SVZ=subventricular zone; CP= cortical plate.

Figure 10

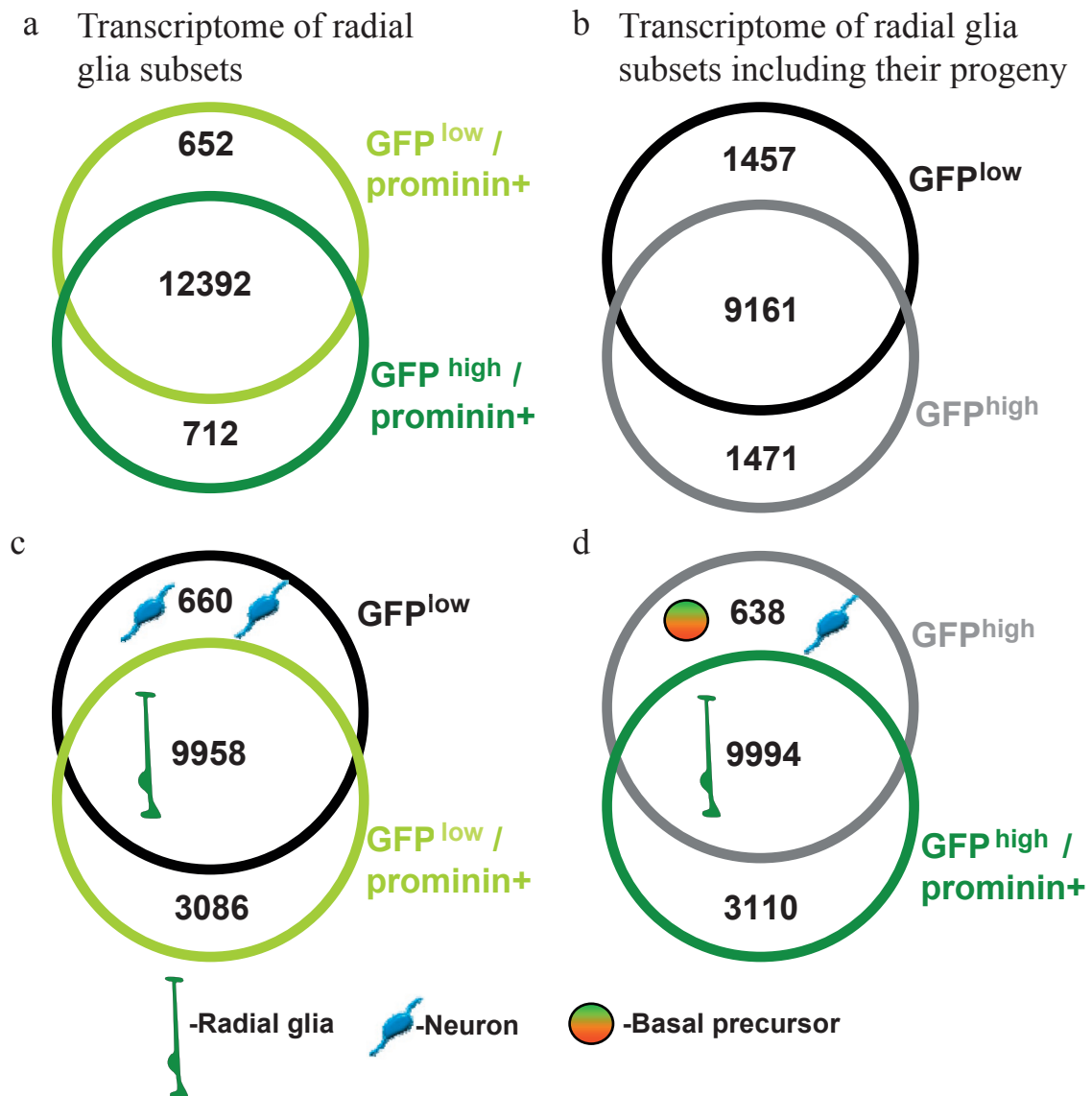


Figure 10. Summary of the transcriptome of GFP+(high and low) and GFP+(high and low)/prominin⁺ sorted cells

(a-d) Venn diagrams depict the total number of expressed genes that are common between the two subsets indicated in a-d as the number in the overlap between the circles and that are distinct between the subsets as the numbers depicted outside the area of overlap. The populations sorted are indicated in the panels. Genes expressed in all populations were obtained using the mean of the triplicates for each fraction of RGCs and Mas 5.0 linear scale.

Figure 11

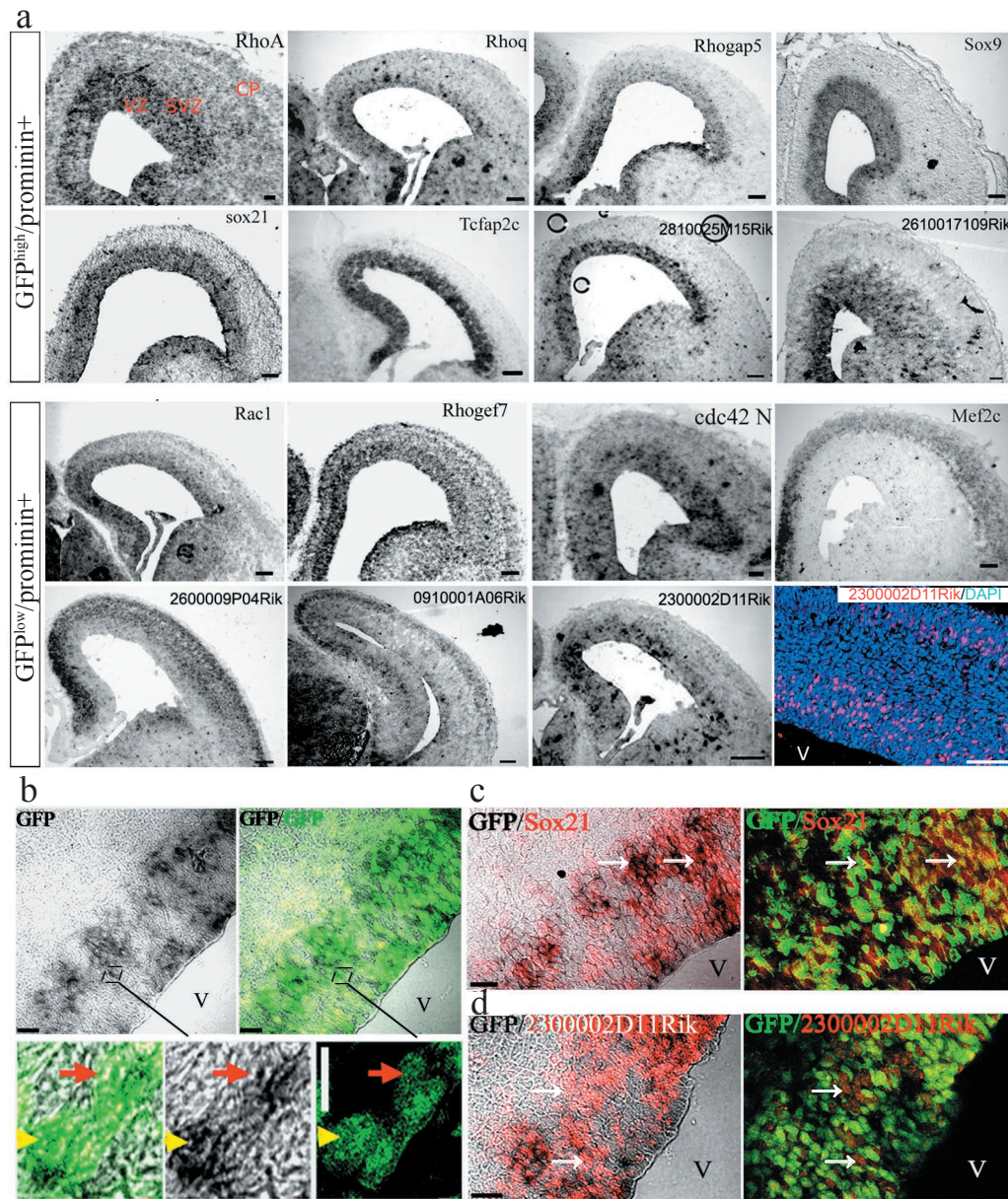


Figure 11. *In situ* hybridization of mRNAs with differential expression levels in the GFP^{high}/GFP^{low} and GFP/prominin double positive radial glia subsets

(a) *In situ* hybridization on E14 WT cortex sections of 12 selected mRNAs with differential expression levels between the GFP^{high}/prominin⁺ and GFP^{low}/prominin⁺ fractions. Most of the genes expressed at higher levels in the GFP^{low}/prominin⁺ sorted cells on the two lower columns show strong expression in the ventricular zone of the cortex (Rac1, Rhogef7, cdc42, 2300002D11Rik) with few of them showing expression in the neurons of the cortical plate (Mef2c, 0910001A06Rik, 2600009P04Rik). Cortical section of E14 WT brain was immunolabelled with DAPI (blue) and antibody against 2300002D11Rik (red) (lower right corner)- Scale bar: 20µm. Each mRNA with higher expression level in the GFP^{high}/prominin⁺ fraction (two upper columns) show strong expression in the ventricular zone of the cortex (e.g. Tcfap2c, Sox21, Rhogap5). Scale bars: 100µm (b) *In situ* hybridization on E14 hGFAP-eGFP cortex sections to detect GFP mRNA (grey) was combined with GFP immunolabelling (green). Yellow arrow indicates colocalization of GFP mRNA with GFP^{high} positive cells. Red arrow indicates GFP^{low} positive cells (light green) showing no signal for GFP mRNA. Scale bars: 20µm (upper panels) and 5µm (lower panels). (c, d) Cortical sections from an E14 hGFAP-eGFP brain were immunolabelled with antibodies against Sox21 (red in c) and 2300002D11Rik (red in d) and combined with GFP *in situ* hybridization (black) and GFP immunolabelling (green). Most of the Sox21 positive cells were colocalized with GFP mRNA and with GFP^{high} positive cells (indicated by the white arrows). 2300002D11Rik positive cells were highly colocalized with GFP^{low} positive cells and a lower number of cells showed colocalization with GFP mRNA (indicated by the white arrows). Scale bars: 20µm. Abbreviations; VZ=ventricular zone; SVZ=subventricular zone; CP=cortical plate; V=ventricle.

Figure 12

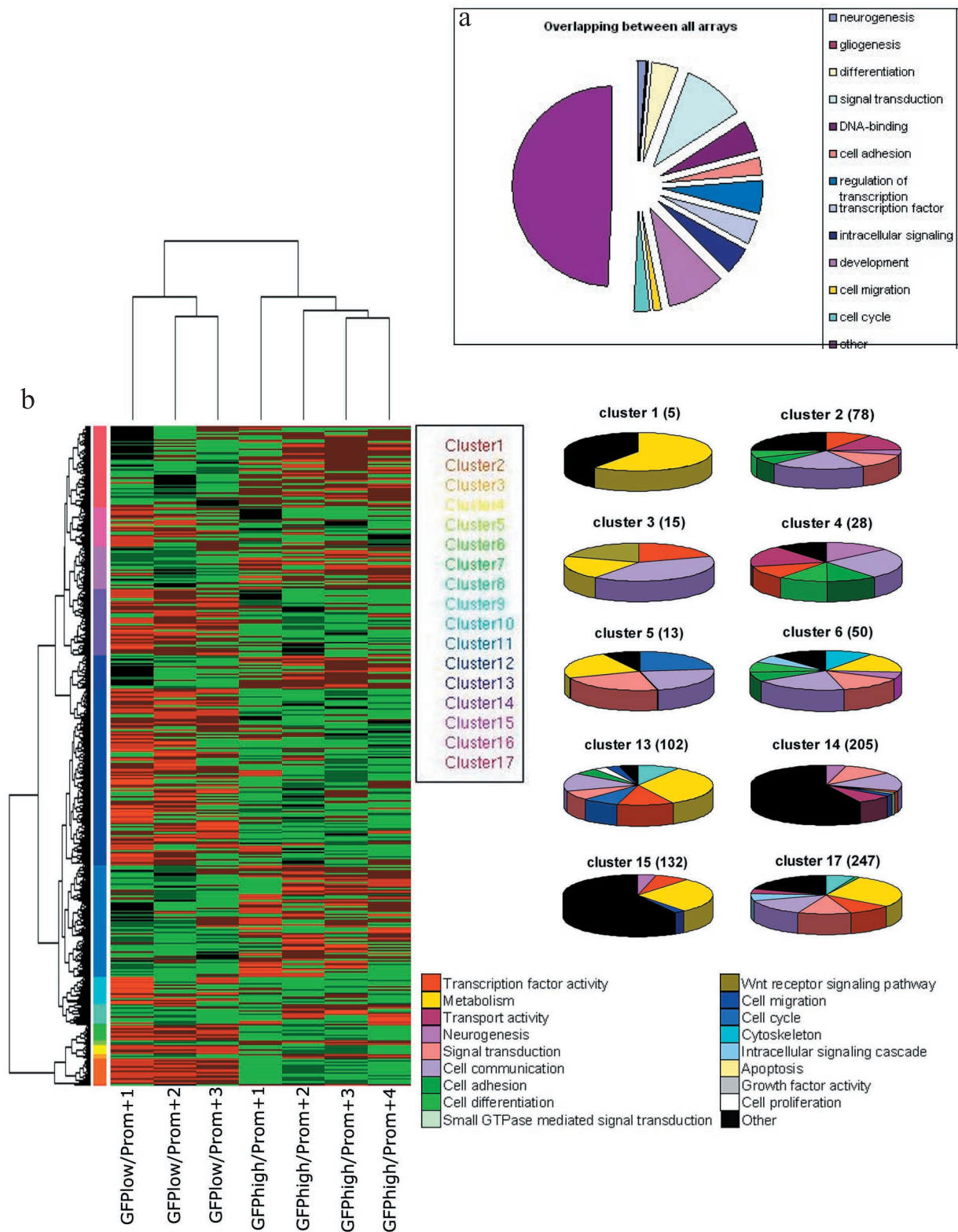


Figure 12. Hierarchical clustering of overlapping genes differentially expressed between GFP^{high}/GFP^{low} fractions and GFP/prominin double positive fractions isolated from E14 cortex
(a) Pie chart represents all genes differentially expressed between GFP^{high}/prominin+ versus GFP^{low}/prominin+ fractions of sorted cells grouped according to their main function. (b) Gene clustering represents the 2031 genes found to be differentially expressed displaying at least a 2 fold (linear) average expression change for each of the replicates of GFP^{high}/GFP^{low} fractions and GFP^{high}/prominin+ versus GFP^{low}/prominin+ fractions of sorted cells. Red indicates increased and green decreased expression levels. The hierarchal tree was divided into 17 clusters represented by different colors. Pie charts: Each cluster was subdivided according to the main function of the genes according to gene ontology analysis. The main function of each gene was established by literature searches and according to DAVID Bioinformatics Functional annotation resources. The number of genes included in each cluster is depicted next to the cluster number on the top of the pie.

Figure 13

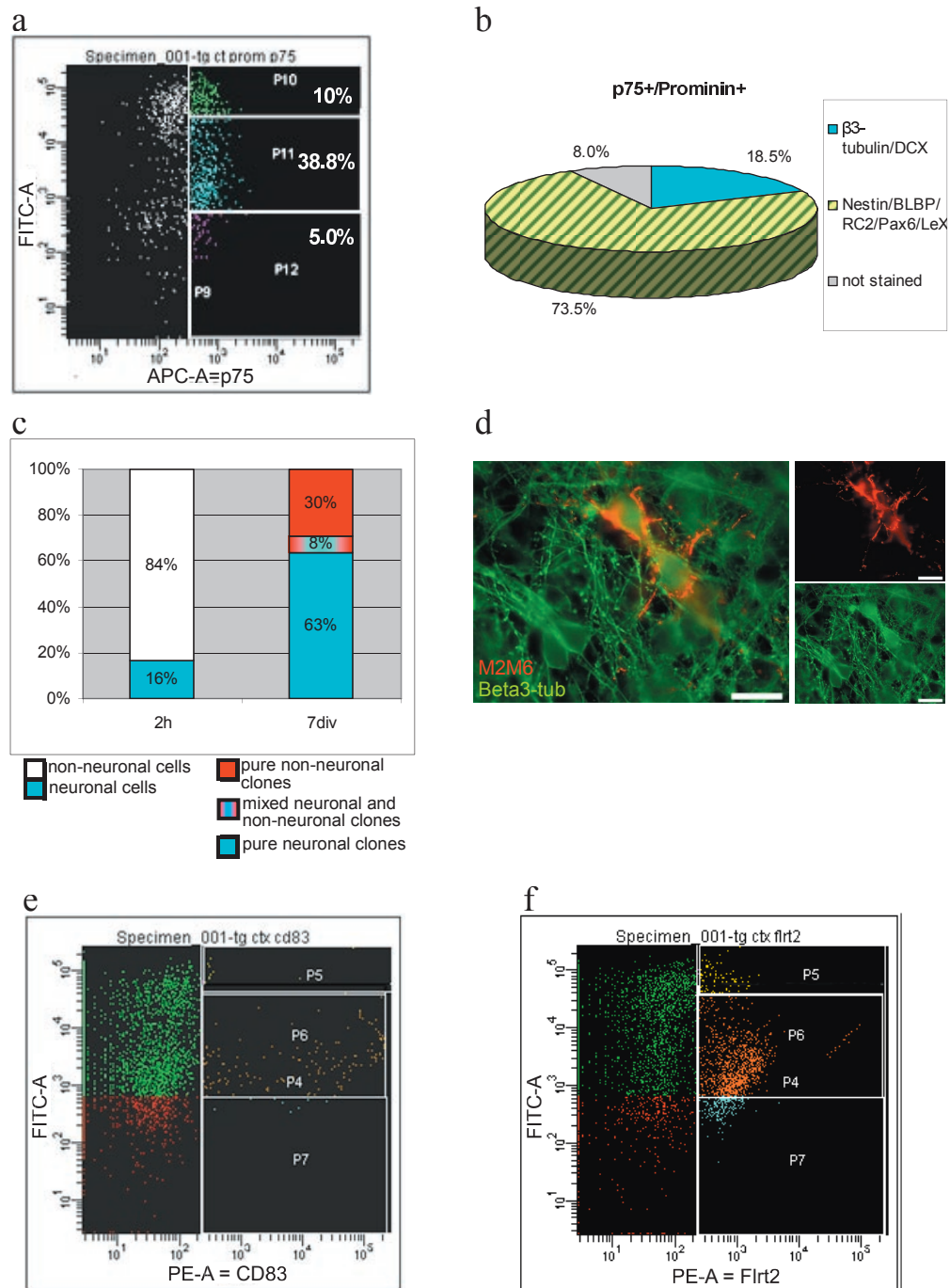


Figure 13. Prospective isolation of neurogenic radial glia from E14 cortex by staining of p75, CD83 and Flrt2 cell surface markers

(a) Dot plot of p75 immunostained cells from E14 cortices of hGFAPeGFP mice (GFP on Y-axis, p75 on X-axis). Note that the majority of p75+ cells were also GFP positive (total p75+ cells: 54%- gates P10-P12; 39% have low GFP (P11); 10% have high GFP (P10)). (b) Pie chart of the composition of cells double positive for p75 and prominin 2 hours after FACS isolation. (c) Bar histogram depicting the clones generated from p75+/prominin+ cells sorted from E14 cortex after 7 days *in vitro*. (d) Micrographs depicting an example of one clone immunostained for M2M6 and β III-tubulin derived from p75+/prominin+ cells sorted from E14 cortex after 7 days *in vitro*. (e, f) Dot plot of CD83 (e) and Flrt2 (f) immunostained cells from E14 cortices of hGFAPeGFP mice (GFP on Y-axis, CD83 and Flrt2 on X-axis, respectively). Note that the majority of CD83 and Flrt2 positive cells were also GFP positive and were enriched in the GFP^{low} fraction. Scale bars: 20 μ m.

Figure 14

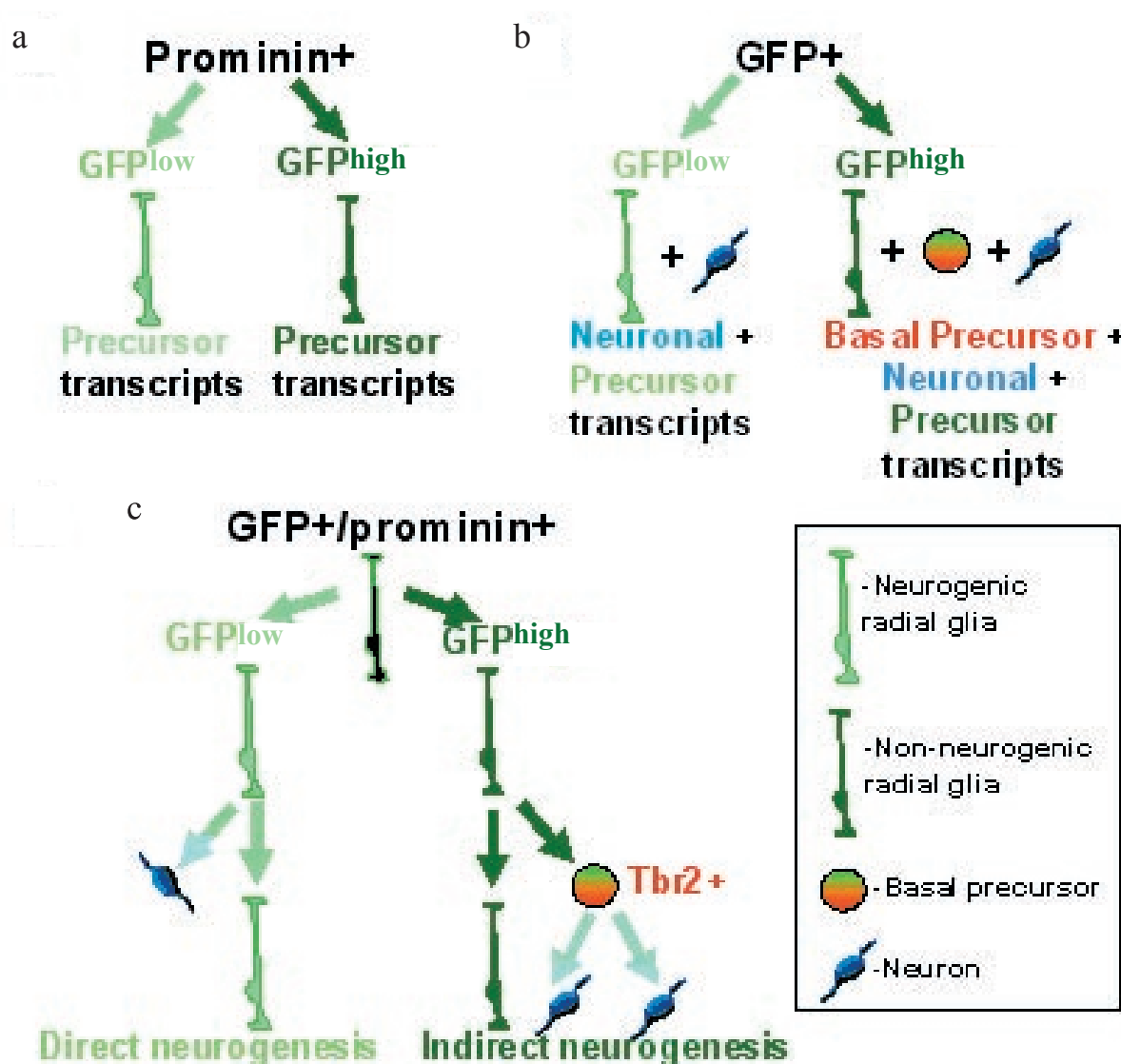


Figure 14. Summary of the lineage analysis of GFP+(high and low) and GFP+(high and low)/prominin+ sorted cells

(a-d) Schematic drawing depicts the transcripts obtained with Affymetrix microarrays for GFP+(high and low)/prominin+ and GFP+(high and low) fractions, respectively. (e-g) Schematic drawing illustrating the progeny of the two distinct subsets of radial glial cells GFP^{low}/prominin+ (light green) and GFP^{high}/prominin+ (dark green).

Figure 15

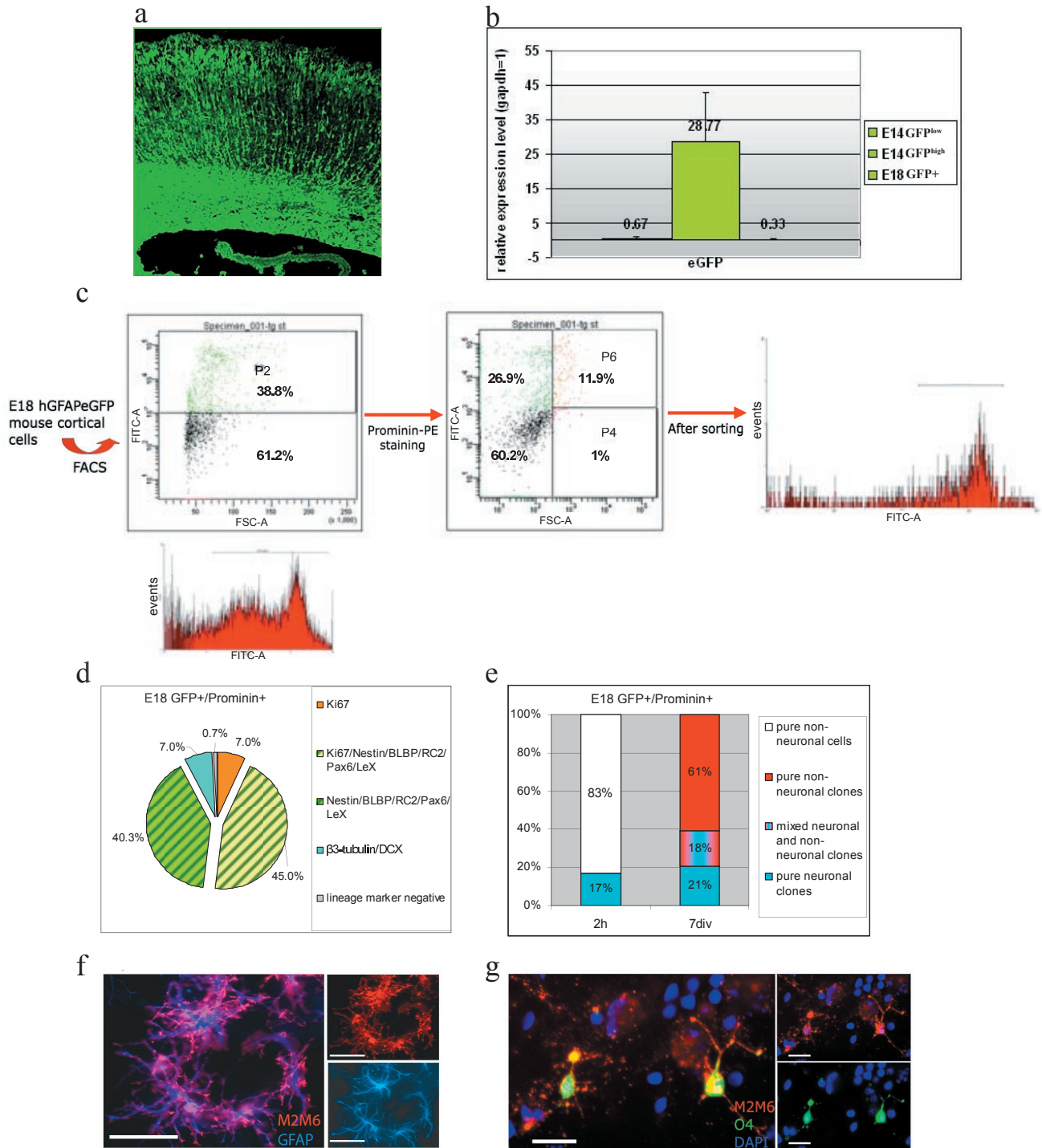


Figure 15. Characterization of cortical radial glial cells at the end of neurogenesis (E18)

(a) Fluorescent micrograph of a hGFAP-eGFP mouse cortex section at E14. (b) Histogram depicts the GFP mRNA levels as determined by real time RT-PCR in E18 GFP⁺ and E14 GFP⁺ fractions compared to cortical cells dissociated from WT mice. (c) FACS analysis and sorting of GFP⁺ cells (dot plot to the left) double stained for prominin (dot plot in the center) isolated from E18 cortices of hGFAPeGFP mice were dissociated and analyzed by FACS. The total percentage of GFP-positive cells observed was about 35% (P2 gate in green in the left panel). From these GFP-positive cells about 20% of the cells were also positive for prominin (P6 gate in orange, middle panel) and only 1% of the total number of cells was shown to be prominin positive and GFP negative (P4 gate in red). GFP⁺/prominin⁺ cells were sorted with high purity (histogram on the right). (d) Pie diagrams depict the composition of E18 GFP⁺/prominin⁺ sorted cells after 2 hours *in vitro*. (e) Bar histogram depicts the composition of clones generated from GFP⁺/prominin⁺ sorted cells after 7 days *in vitro*. (f and g) Fluorescent micrographs depict examples of a GFAP⁺ (clone f) and an O4 oligodendrocyte clone (clone g) after 7 days *in vitro* immunostained as indicated in the panels. Scale bars: 20 μ m.

Figure 16

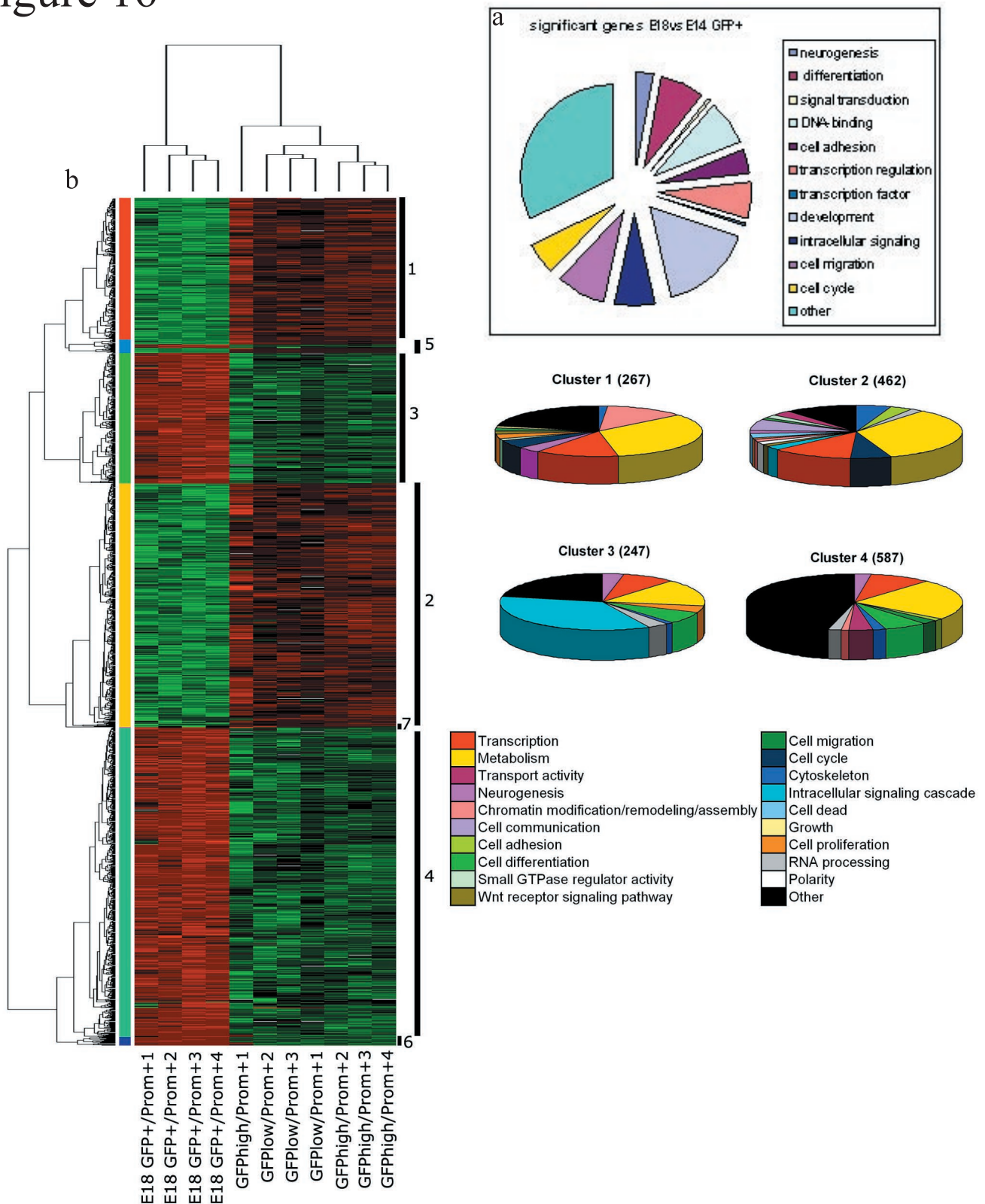


Figure 16. Hierarchical clustering of genes differentially expressed between E18 GFP+/prominin+ and E14 GFP/prominin radial glia subsets

(a) Pie chart represent all genes differentially expressed between E18 GFP and E14 GFP fractions of sorted cells grouped according to their main function. (b) Gene clustering of the 1606 genes found to be differentially expressed with at least a 2 fold (linear) change and a mean average expression of 50 for each of the replicates of E18 GFP+/prominin+ sorted cells comparing to E14 GFP^{high}/prominin+ and GFP^{low}/prominin+ radial glia subsets. Red and green depicts at least 2 fold increased and decreased expression, respectively. The hierarchal tree could be divided into 7 major big clusters. Only clusters 1 to 4 showed significant functional enrichments (criteria for “enrichment” are: minimum three probe-sets in the cluster annotated to the gene ontology (GO) term, p-value of the hypergeometric distribution against whole chip background smaller than 5%). Clusters 1 and 2 represent genes down-regulated from E14 to E18 and clusters 3 and 4 represent genes up-regulated in this fraction. Pie charts: Each cluster was subdivided according to the main function of the genes belonging to them (GO analysis). The number of genes included in each cluster is mentioned after the cluster number.

Figure 17

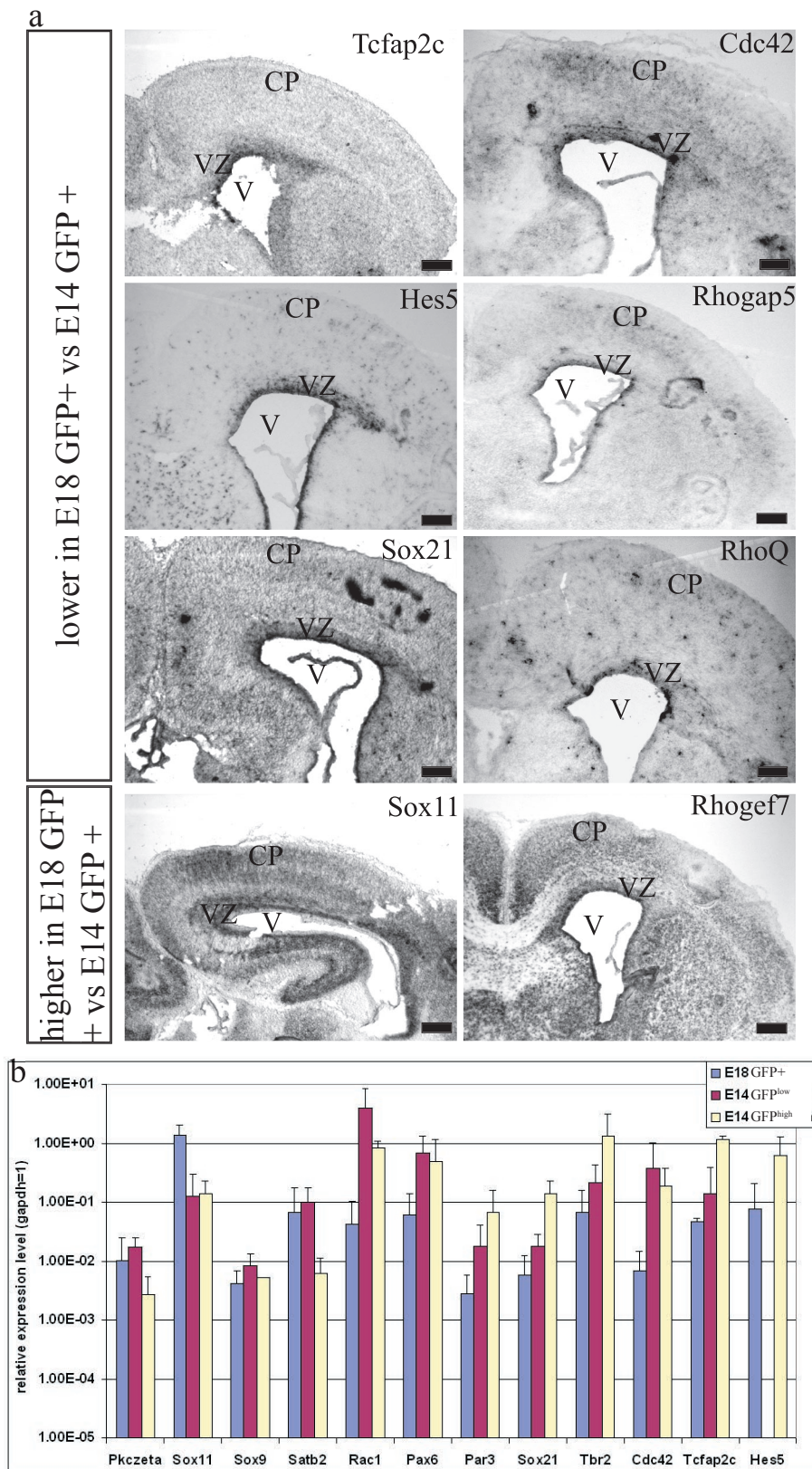


Figure 17. *In situ* hybridization of mRNAs with differential expression levels in the E18 GFP+ and E14 GFP+ fractions of sorted cells

(a) *In situ* hybridization on E18 WT cortex sections of 8 selected mRNAs with differential expression levels between the E18 GFP+ and E14 GFP+ fractions of sorted cells. Most of the genes expressed at lower levels in the E18 GFP+ fraction show strong expression in the ventricular zone of the cortex (Tcfap2c, Cdc42, Hes5, Rhogap5, Sox21 and RhoQ). The genes expressed at higher levels in the E18 GFP+ fraction show expression in the ventricular zone and in neurons of the cortical plate (Sox11 and Rhogef7). (b) 12 mRNAs predicted by Affymetrix analysis to be differentially expressed between E18 GFP+ and E14 GFP+ fractions of sorted cells were examined by real time RT-PCR. Bars in the histogram represent mean \pm S.E.M. Asterisks depict the significance levels (* = $p \leq 0.05$; ** = $p \leq 0.01$) obtained by T-test. Scale bar: 50 μ m. Abbreviations; VZ=ventricular zone; CP=cortical plate; V=ventricle.

Figure 18

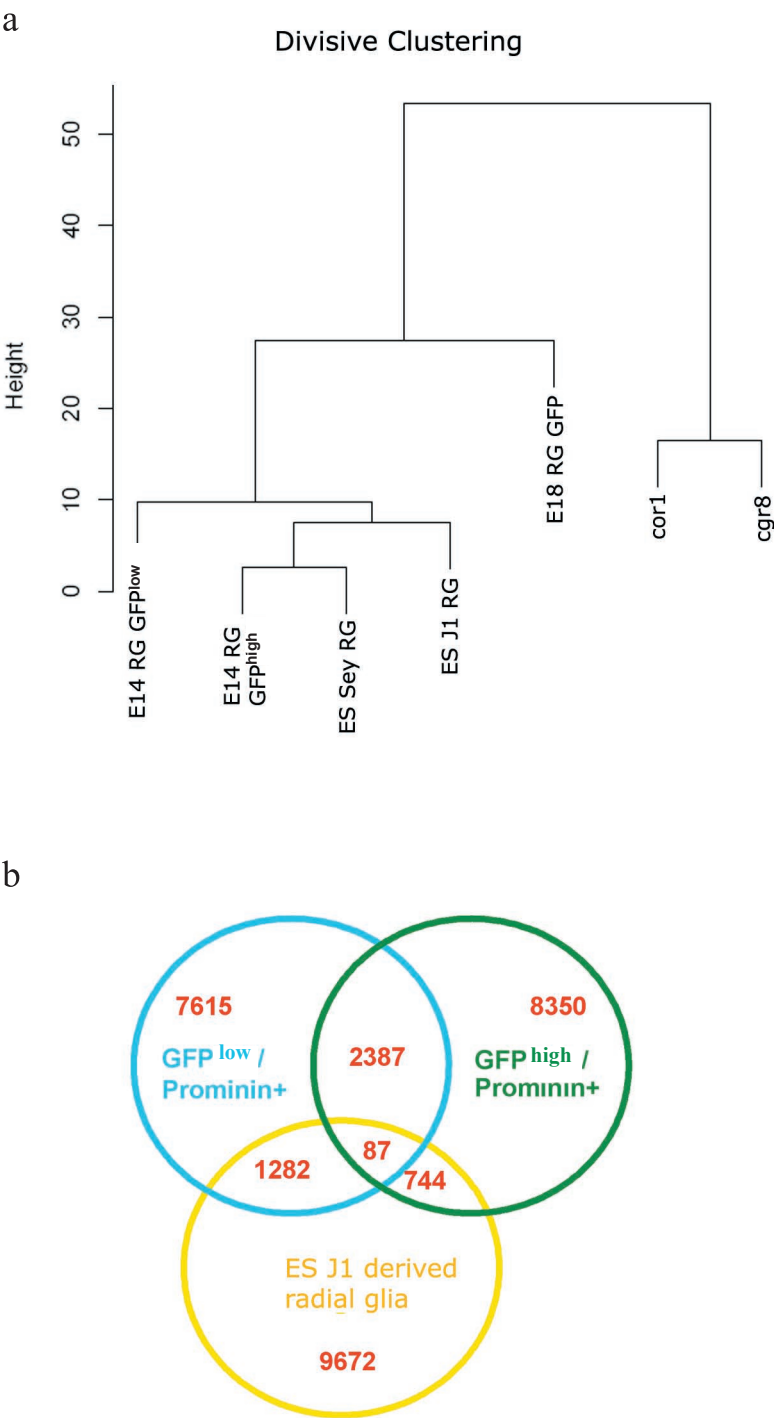


Figure 18. Comparison of the expression profile of ES cell-derived radial glia and subsets of radial glia sorted at different developmental stages

(a) Divisive clustering analysis of E14 GFP^{high}/prominin+ (E14 RG GFP^{high}) and GFP^{low}/prominin+ (E14 RG GFP^{low}), E18 GFP/prominin+ fractions (E18 RG GFP), WT (ES J1 RG) and Sey/Sey (as ES sey RG) ES cell-derived radial glia (Bibel et al, 2004) and ES-derived radial glia according to Conti et al, 2005 (cgr8), or expanded neurosphere cells (cor1). (b) Venn diagram of genes expressed (absolute expression higher than 50) in the GFP^{high}/prominin+, GFP^{low}/prominin+ fractions sorted from E14 cortex and in WT ES cells-derived radial glia (ES J1 derived radial glia, Bibel et al, 2004)). Numbers of genes are indicated in red.

Figure 19

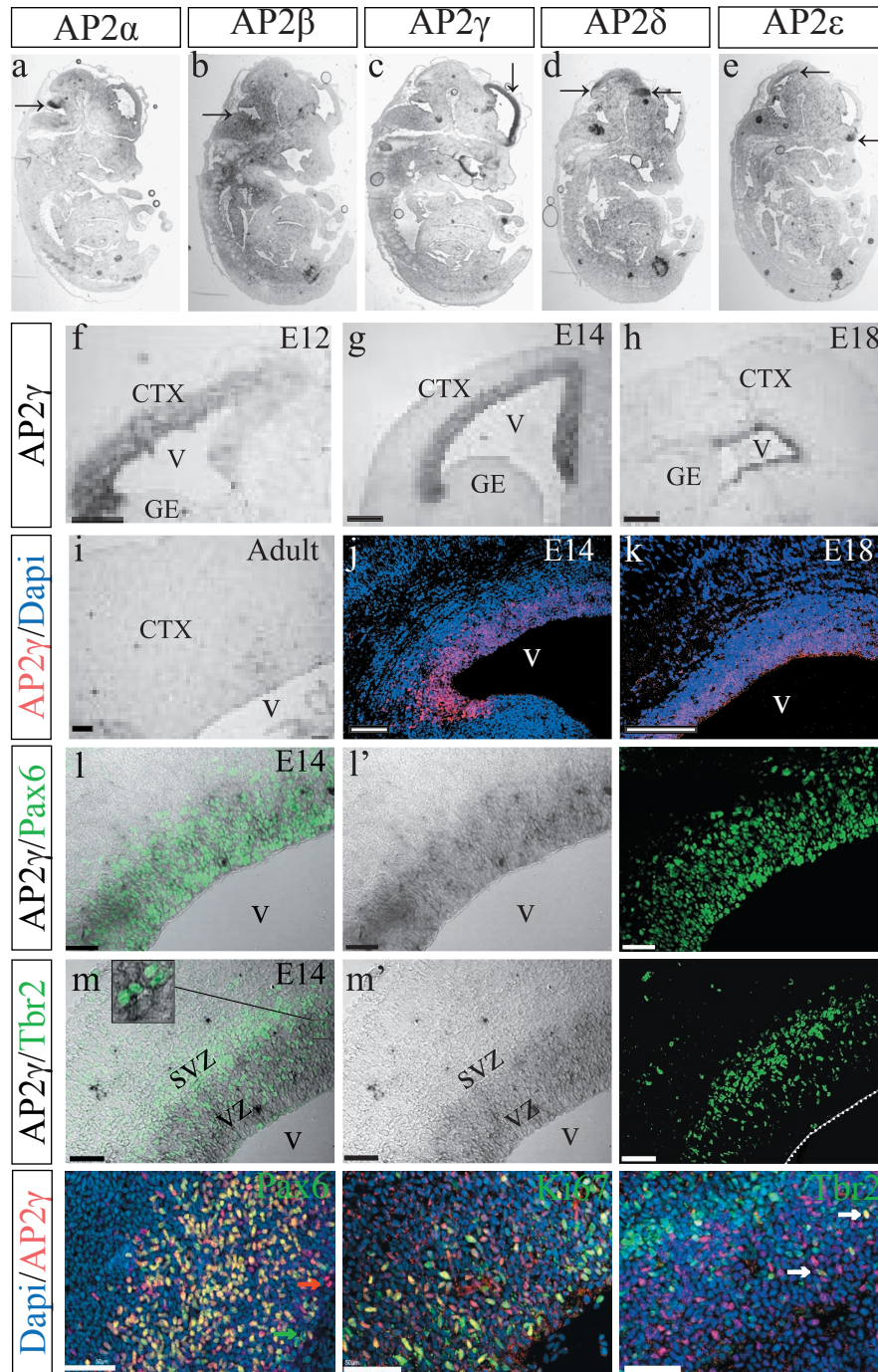


Figure 19. AP2 γ expression in the mouse brain

(a-e) ISH of all genes of the AP2 family of transcription factors-AP2 α - ϵ , respectively, on sagittal sections of the all embryo at E14. Note that AP2 γ is restrictedly localized to the cerebral cortex (black arrow in c). (f-i) ISH of AP2 γ on coronal sections of the cerebral cortex at developmental stages E12 (f), E14 (g) and E18 (h) and at adult stages - 2 months (i). (j,k) Coronal sections of the cerebral cortex at E14 (j) and E18 (k), immunolabelled with AP2 γ . Note the gradient of AP2 γ protein - lateral high to medial low. Panels l-m' depict co-localization of AP2 γ mRNA with Pax6 (l-l') and Tbr2 (m-m') protein. Panels n-p depict sagittal sections of the cerebral cortex at E14, immunolabelled with AP2 γ and Pax6 (n), Ki67 (o) or Tbr2 (p). Note that AP2 γ only co-localizes with a subset of Ki67+ cells (o). AP2 γ and Pax6 show high co-localization, but not all Pax6+ cells express AP2 γ (green arrow in n) and not all AP2 γ + cells express Pax6 (red arrow in n). Scale bars: f-i 100 μ m; j-p 50 μ m. Abbreviations; V=ventricle; CTX=cortex; GE=ganglionic eminence, SVZ=subventricular zone; VZ=ventricular zone

Figure 20

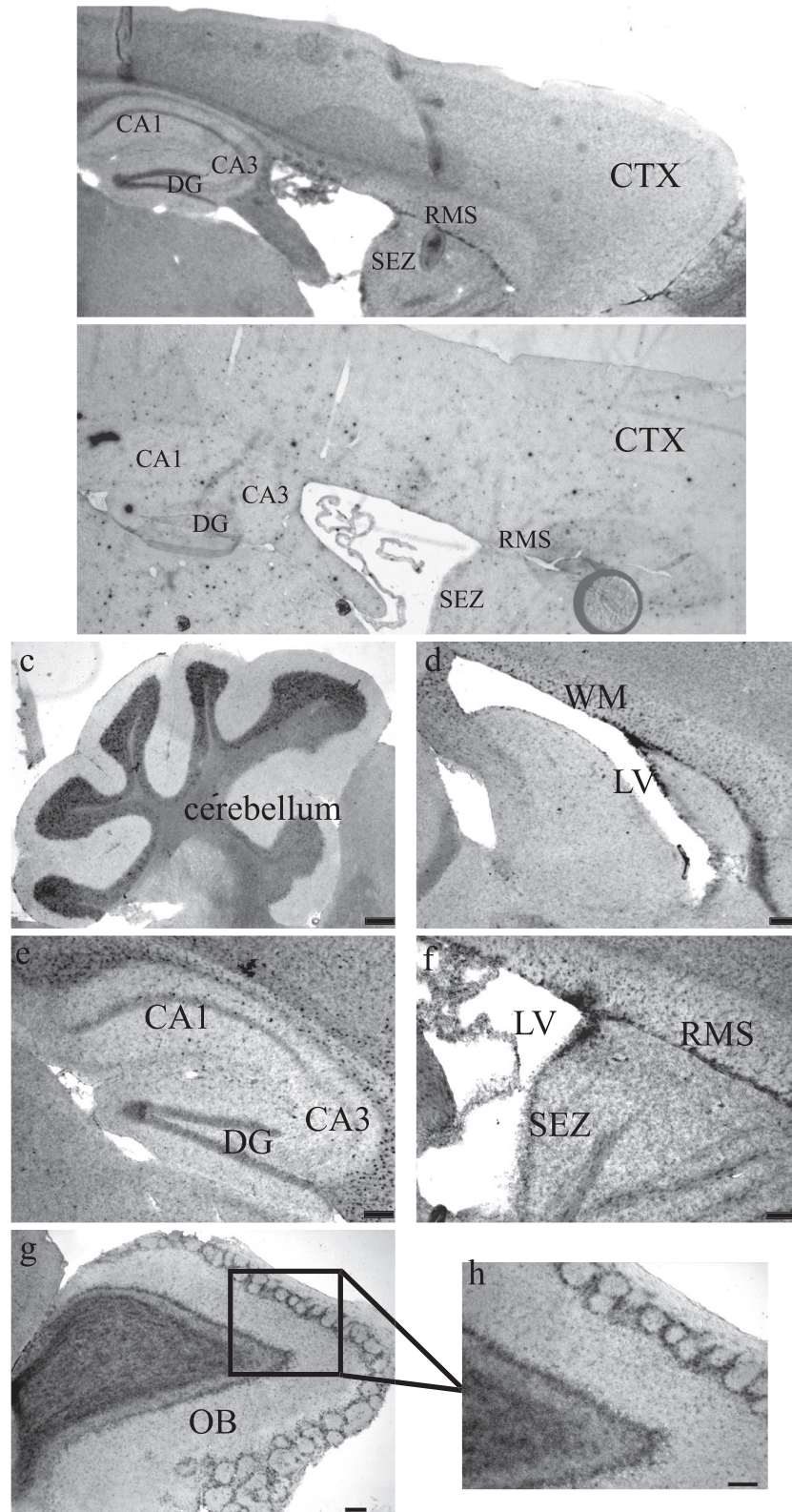


Figure 20. AP2 γ expression in the adult mouse brain

(a-h) ISH of AP2 γ on sagittal sections of a 2 months old WT mouse brain. (a) Micrograph depicts an overview of the cerebral cortex, hippocampus and subependymal zone (SEZ) of the adult mouse brain. Note the absence of AP2 γ mRNA expression in the cortex-CTX (a) and the absence of signal using the AP2 γ sense control (b). (c-h) Micrographs depict AP2 γ mRNA expression in the granular cell layer of the cerebellum (c), white matter-WM of the forebrain and lateral ventricle -LV (d), dentate gyrus-DG, CA1, CA3 regions (e), subependymal zone-SEZ and rostral migratory stream-RMS (f) and olfactory bulb-OB (g, h). Scale bars: 100 μ m. Abbreviations: GCL=granular cell layer; ML=mitral cell layer; GL=glomerular layer; OB=olfactory bulb; SEZ=subependymal zone; RMS=rostral migratory stream; DG=dentate gyrus; CA=Cornu Ammonis; LV=lateral ventricle; WM=white matter

Figure 21

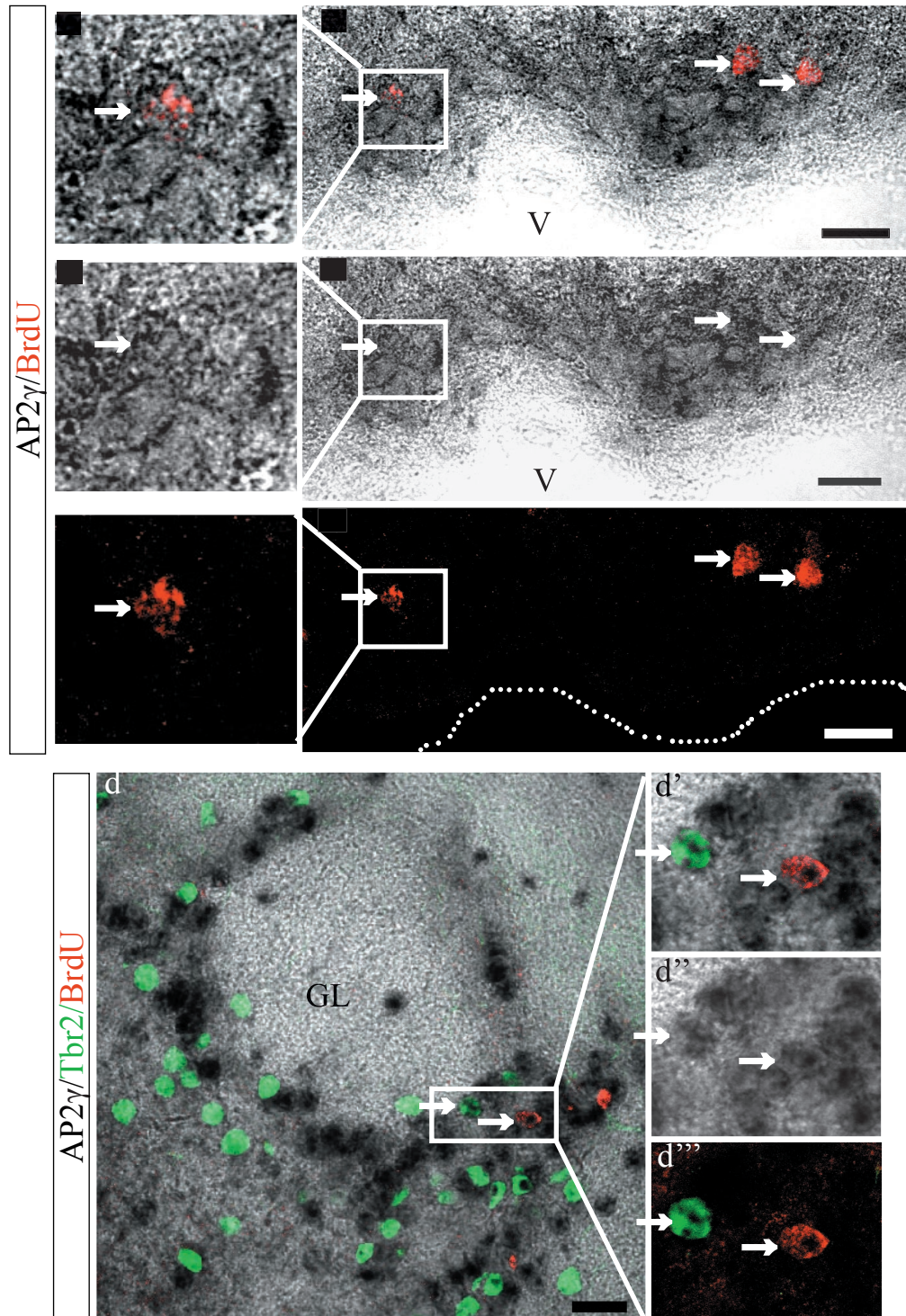


Figure 21. AP2 γ expression in the adult neural stem cells in the SEZ and their progeny in the olfactory bulb (OB)

(a-c') Micrographs depict ISH of AP2 γ in the SEZ on sagittal sections of a adult WT mouse brain treated with BrdU in drinking water for 1 week and sacrificed 8 weeks later to label slow dividing and label-retaining stem cells in the adult proliferative regions (a', b' and c') as well as their neuronal progeny in the OB (d-d'''). Note the co-localization of AP2 γ mRNA with BrdU positive cells (red) in the SEZ. (d-d''') Micrographs depict the glomerular layer of the olfactory bulb of an adult mouse brain sagittal section immunolabelled with Tbr2 and BrdU combined with ISH for AP2 γ . Note the colocalization of AP2 γ mRNA with Tbr2 and BrdU (d'-d'''). Scale bars: 20 μ m. Abbreviations: SEZ=subependymal zone; V=ventricle; GL=glomerular layer

Figure 22

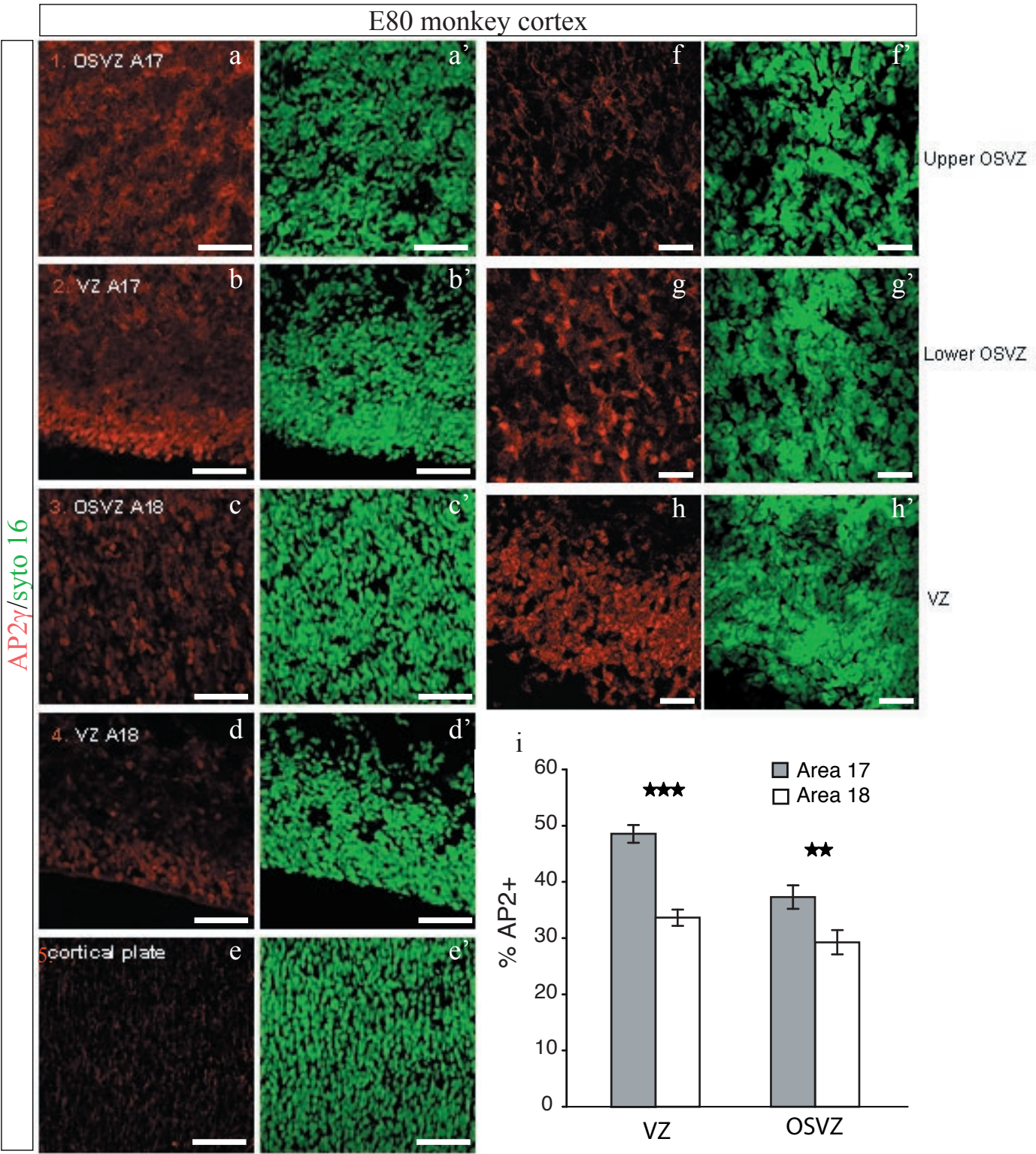


Figure 22. AP2γ expression in the E80 primate cortex
(a-h') Micrographs of sagittal sections of E80 monkey cortices immunolabelled with AP2γ (red) and syto16 to label all nuclei (green). Panels a-a' and f-f' depict the outer SVZ (OSVZ) of the area 17 (A17) of the cortex, panels b,b' depict the VZ of area 17, panels c,c' depict the OSVZ of area 18 (A18), panels d,d' and h,h' depict the VZ of area 18 and panels e,e' depict the cortical plate of the cortex. Panels f-g' depict the upper OSVZ (f,f') and lower OSVZ (g,g') of area 17. Histogram i depicts the quantification of the number of AP2γ+ cells in the VZ and OSVZ of areas 17 and 18. Note the higher expression of AP2γ in area 17 comparing to area 18 of the cortex and the absence of immunolabelling in the cortical plate. (Collaboration with Dr. Colette Dehay). Bars in the histogram represent mean ± S.E.M. Asterisks depict the significance levels (** =p≤ 0.01; ***=p≤ 0.001) obtained by T-test. Scale bars: 50μm

Figure 23

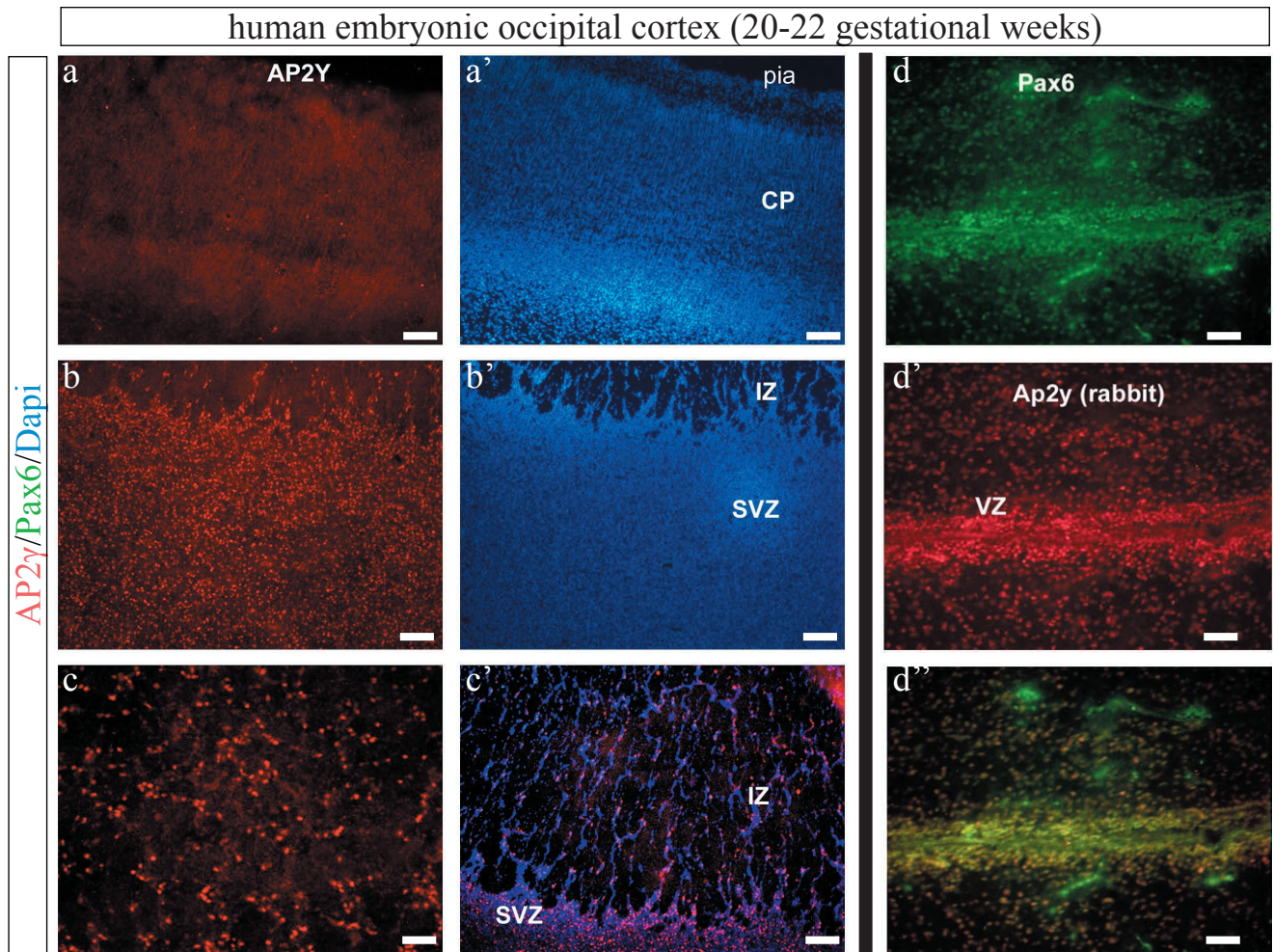


Figure 23. AP2 γ expression in the human occipital cortex at 20-22 gestational weeks

(a-c') Micrographs of coronal sections of the human occipital cortex at 20-22 gestational weeks (mid-gestation), immunolabelled with AP2 γ (red) and DAPI (blue). Panels a,a' depict the cortical plate (CP) of the cortex, panels b,b' depict the SVZ and panels c-c' depict the intermediate zone (IZ). Note the high expression of AP2 γ in the SVZ and scattered positive cells in the IZ, with no immunolabelling in the CP. (d,d'') Micrographs depict the VZ of the human occipital cortex at 20-22 gestational weeks (mid-gestation), immunolabelled with AP2 γ (red) and Pax6 (green). Note the high co-localization of both antigens. (Collaboration with Dr. Nada Zezevic). Scale bars: 50 μ m

Figure 24

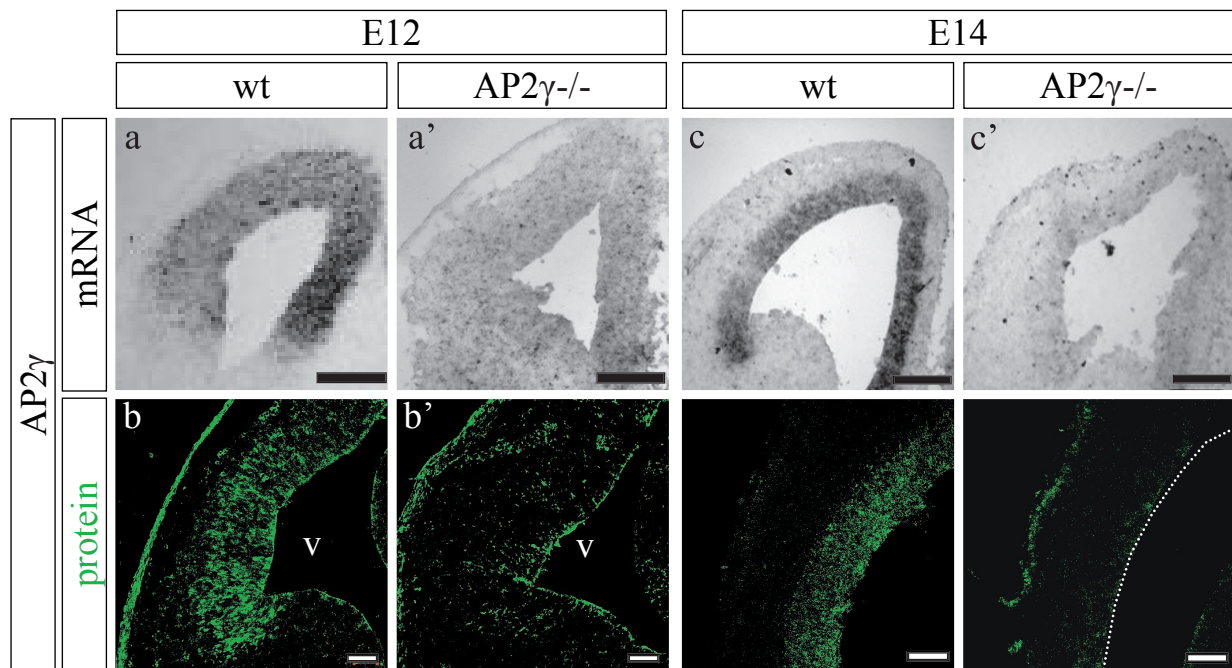


Figure 24. AP2 γ deletion by Emx1::Cre in the mouse cerebral cortex

(a-d') Histograms depict cortex coronal sections of E12 (a-b') and E14 (c-d') WT and AP2 γ ^{-/-} embryos, labeled for AP2 γ mRNA (a-a', c-c') and protein (b-b', d-d'). Note the disappearance of the AP2 γ mRNA and protein already at E12. Scale bars: 100 μ m. Abbreviations; V=ventricle

Figure 25

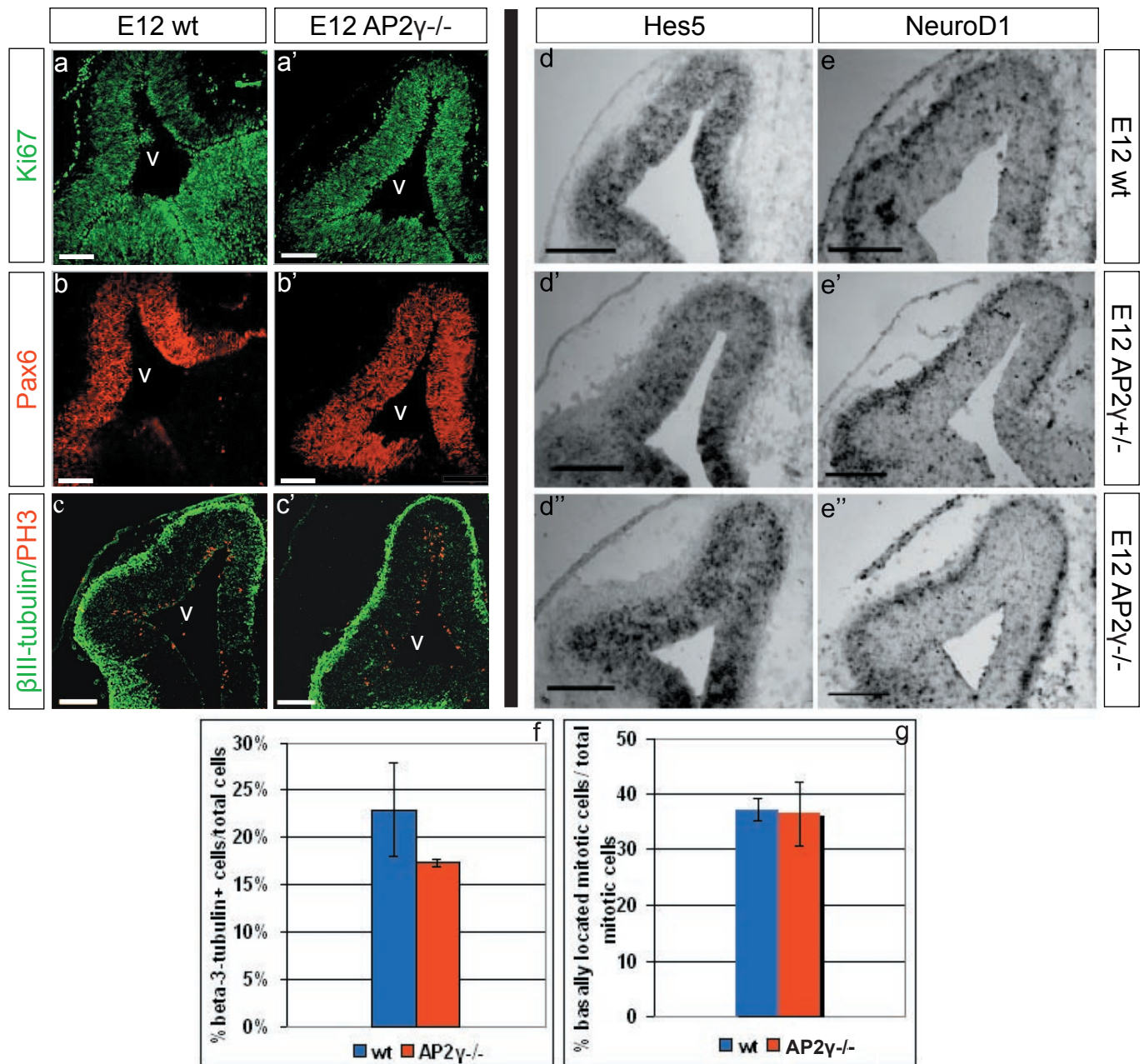


Figure 25. Neuron and progenitor identity in the AP2 γ ^{-/-} cortex at E12

(a-c') Coronal sections of the WT and AP2 γ ^{-/-} cerebral cortex at E12, immunolabelled with Ki67 (a,a'), Pax6 (b, b'), β III-tubulin and PH3 (c, c'). Panels d-e'' depict ISH of Hes5 (d-d'') and NeuroD1 (e-e'') in coronal sections of WT (d, e), AP2 γ heterozygous mutant mice (d', e') and AP2 γ ^{-/-} mice (d'', e''). Histograms f and g depict the quantification of the percentage of β III-tubulin⁺ cells by FACS (f) and the percentage of basally located mitotic cells (g) in the WT and AP2 γ ^{-/-} cortex at E12. Bars in all histograms represent mean \pm S.E.M. Scale bars: 100 μ m. Abbreviations; V=ventricle

Figure 26

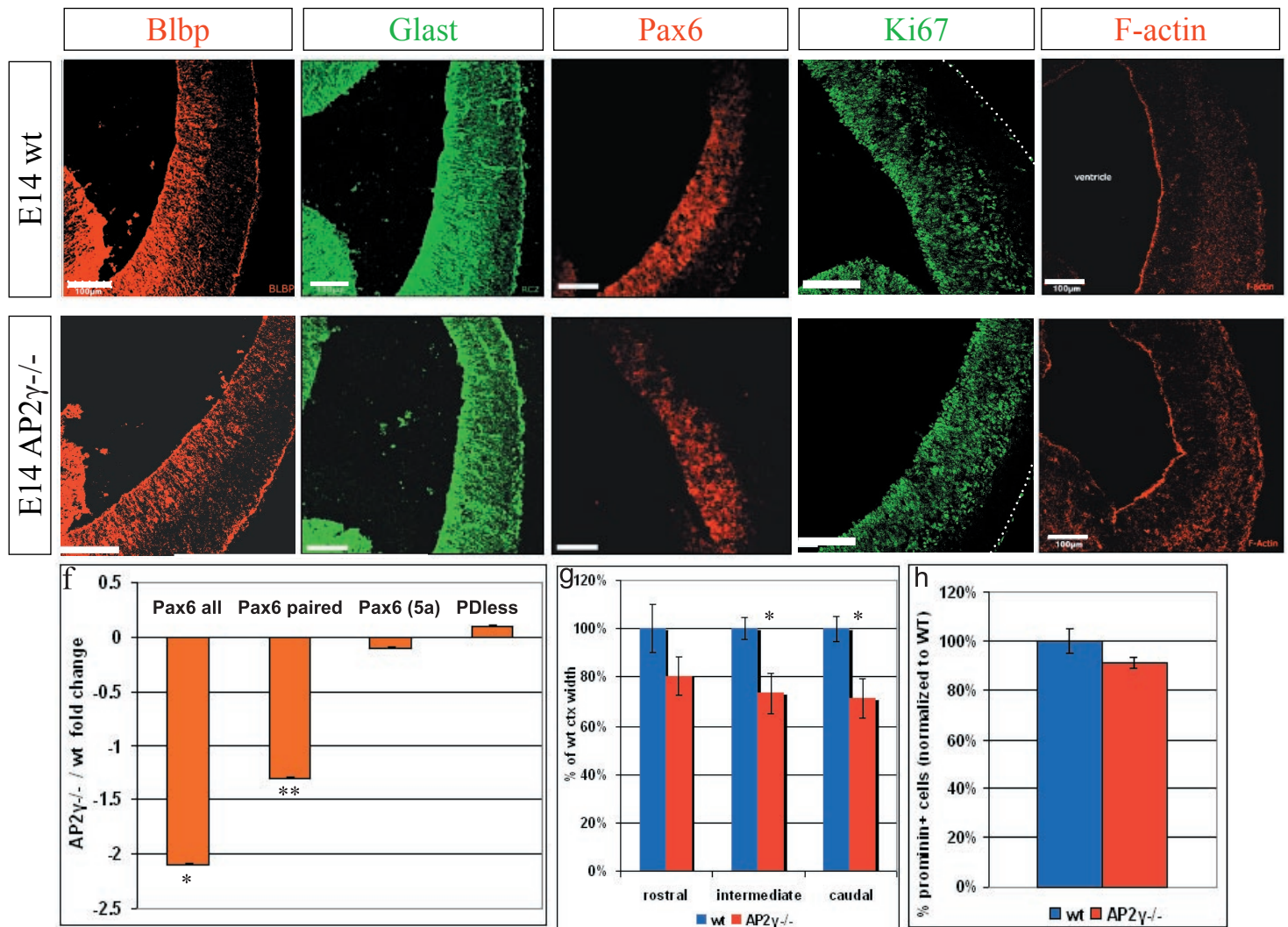


Figure 26. Apical progenitor identity in the cerebral cortex of AP2 γ ^{-/-} mice at mid-neurogenesis (E14)

(a-e') Coronal sections of the E14 WT and AP2 γ ^{-/-} cerebral cortex at intermediate-caudal regions, immunolabelled with Blbp (a, a'), Glast (b, b'), Pax6 (c, c'), Ki67 (d, d') and F-actin (e, e'). No change in Ki67 and Blbp⁺ apical progenitors was observed, but a small decrease in Pax6 protein was detected. Histogram f depicts RT-PCR of all Pax6 isoforms in the AP2 γ ^{-/-} cortex compared to WT. Note the significant decrease of Pax6 canonical and the Pax6 paired isoform exclusively. Histogram g depicts the quantification of the E14 WT (blue bars) and AP2 γ ^{-/-} (red bars) cortex width (normalized to WT) at rostral, intermediate and caudal regions. Histogram h depicts the quantification of prominin-positive cells in the E14 AP2 γ ^{-/-} compared to WT cortices performed by FACS analysis (values are normalized to WT). Bars in all histograms represent mean \pm S.E.M. Asterisks depict the significance levels (* = $p \leq 0.05$; ** = $p \leq 0.01$) obtained by T-test. Scale bars: 100 μ m. Abbreviations; V=ventricle

Figure 27

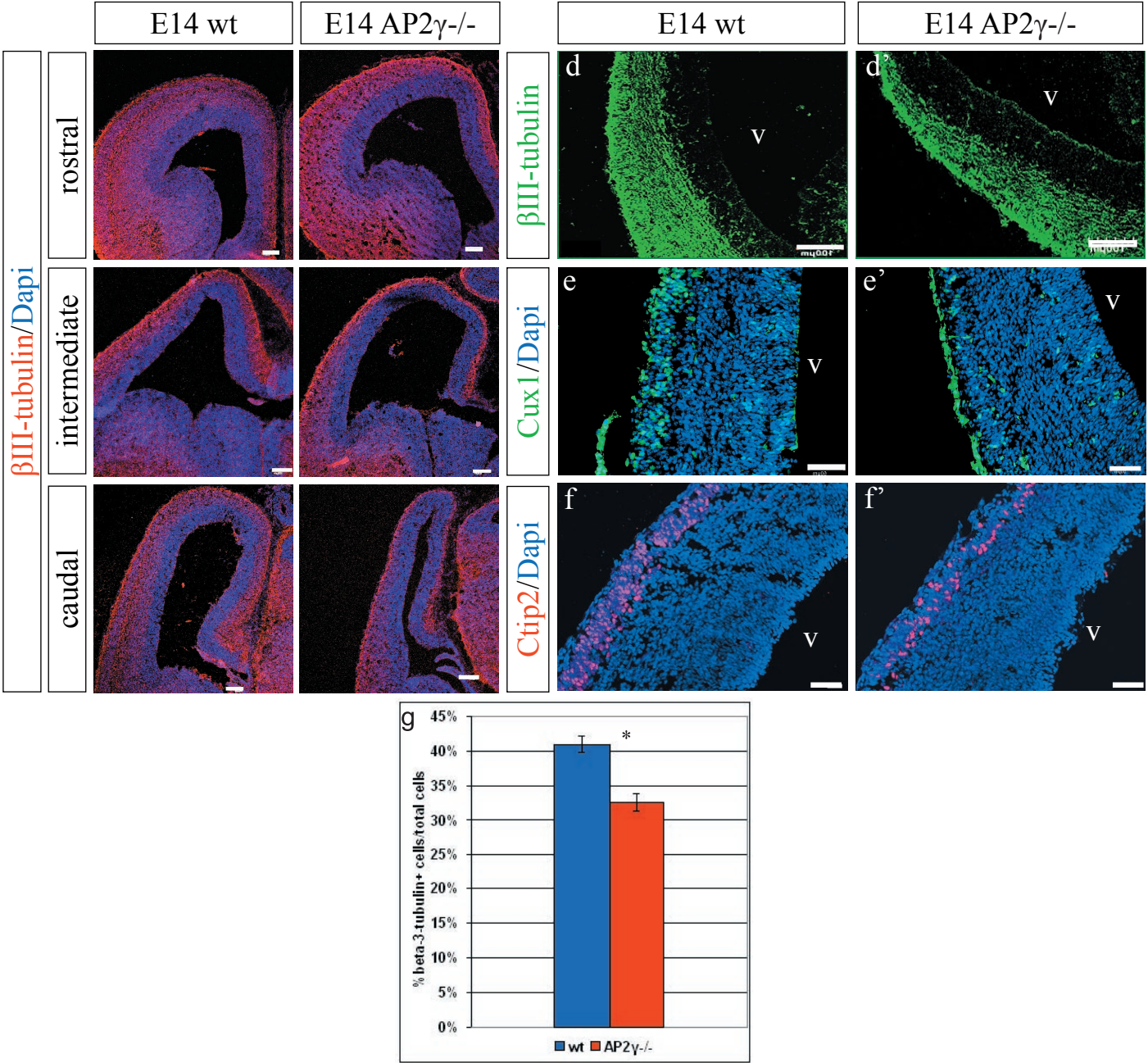


Figure 27. Neuron defects in the cerebral cortex of AP2γ^{-/-} mice at E14

(a-c') Coronal sections of E14 WT and AP2γ^{-/-} cortices immunolabelled for βIII-tubulin and Dapi at rostral, intermediate and caudal regions. (d-f') Coronal sections of the WT and AP2γ^{-/-} cerebral cortex at E14, immunolabelled with βIII-tubulin (d, d'), Cux1 (e, e') and Ctip2 (f, f') neuronal markers. Histogram g depicts FACS analysis of the number of βIII-tubulin positive neurons in the WT and AP2γ^{-/-} cortices at E14. Note the high decrease in the number of neurons in the AP2γ^{-/-} cortex detected by FACS analysis and the smaller band of βIII-tubulin⁺ cells in the AP2γ^{-/-} compared to WT cortex only at intermediate-caudal regions. Bars in the histogram represent mean ± S.E.M. Asterisks depict the significance levels (* = p ≤ 0.05) obtained by T-test. Scale bars: 100μm. Abbreviations; V=ventricle

Figure 28

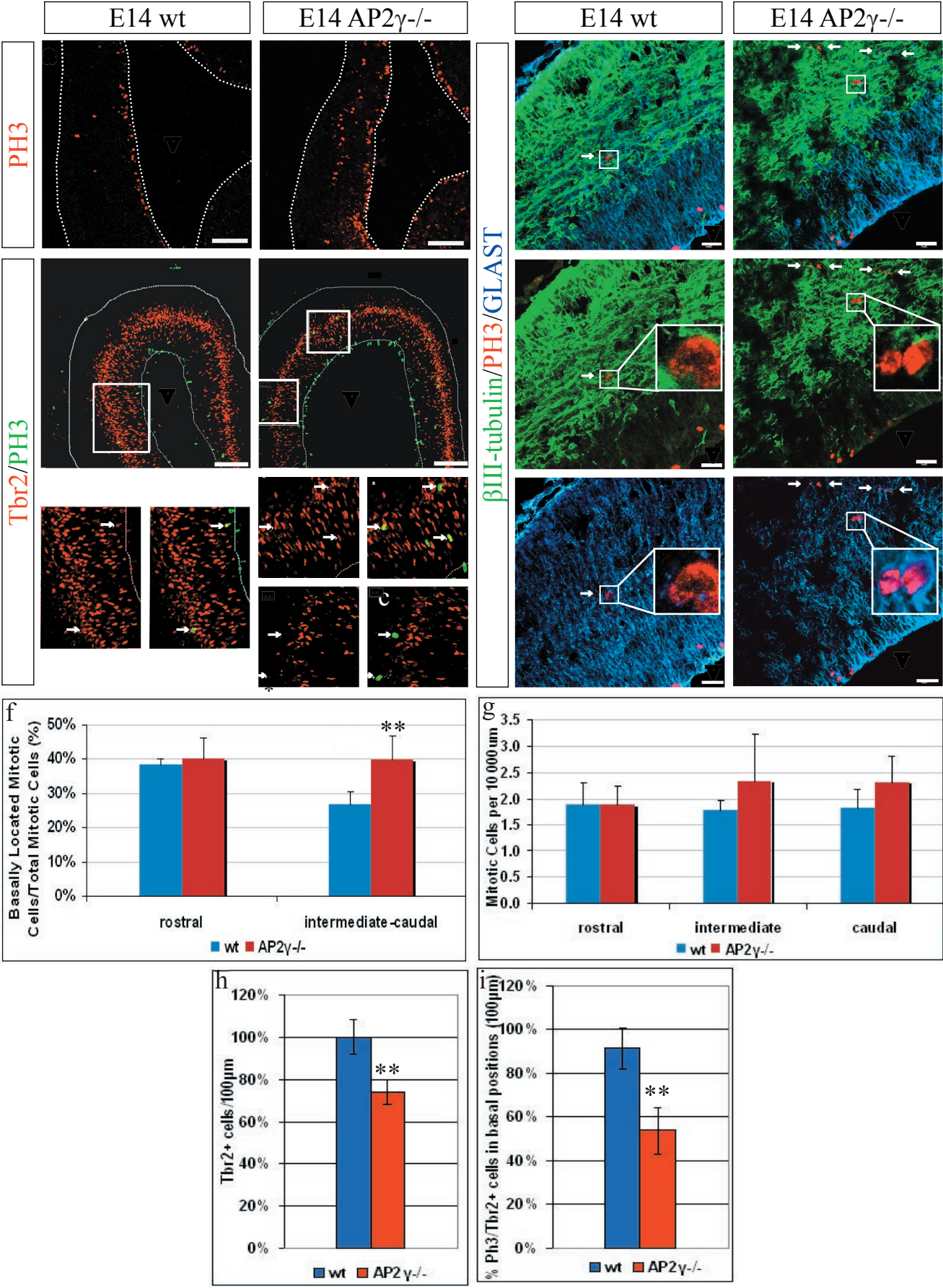


Figure 28. Cell division defects and misspecification of basal progenitors in the AP2γ^{-/-} cortex at E14

(**a-a'**) Coronal sections of the cortex at E14 immunolabelled with PH3, showing a higher number of PH3-positive cells in G2/M phase located at non-surface positions more than 5 cell diameters from the ventricle in the AP2γ^{-/-} compared to WT cortex. Panels **b-c'** depict immunolabelling with Tbr2 and PH3 in coronal sections of the cortex at E14. Panels **b',b''** and **c',c''** depict high power pictures of Tbr2-PH3 double-positive cells at basal positions of the WT and AP2γ^{-/-} cortices, respectively (white arrows). Panels **c''',c''''** depict high power pictures of PH3⁺ cells at basal positions that are immuno-negative for Tbr2 in the AP2γ^{-/-} cortex (white arrows). Panels **d-e''** depict coronal sections of the WT and AP2γ^{-/-} cortex at E14 immunolabelled with βIII-tubulin, PH3 and GLAST. Note the presence of GLAST/PH3 double-positive cells located basally in the AP2γ^{-/-} cortex (**e''**). Histogram **f** depicts the percentage of basally located mitotic cells in the AP2γ^{-/-} compared to WT cortex. Note the increase of basally located mitotic cells only at intermediate-caudal regions of the AP2γ^{-/-} cortices. Histogram **g** depicts the total number of mitotic cells in the cortex of WT and AP2γ^{-/-} at rostral, intermediate and caudal regions. Histograms **h** and **i** depict the number of Tbr2⁺ cells (**h**) and the percentage of Tbr2-PH3 double positive cells (**i**) in the AP2γ^{-/-} and WT cortex at E14. Note the significant decrease in the number of Tbr2⁺ and Tbr2-PH3 double-positive cells in the AP2γ^{-/-} compared to WT cortex. Bars in all histograms represent mean ± S.E.M. Asterisks depict the significance levels (* = $p \leq 0.05$; ** = $p \leq 0.01$) obtained by T-test. Scale bars: **a-c** 100μm; **d-e''** 20μm; Abbreviations; V=ventricle; CTX=cortex; GE=ganglionic eminences

Figure 29

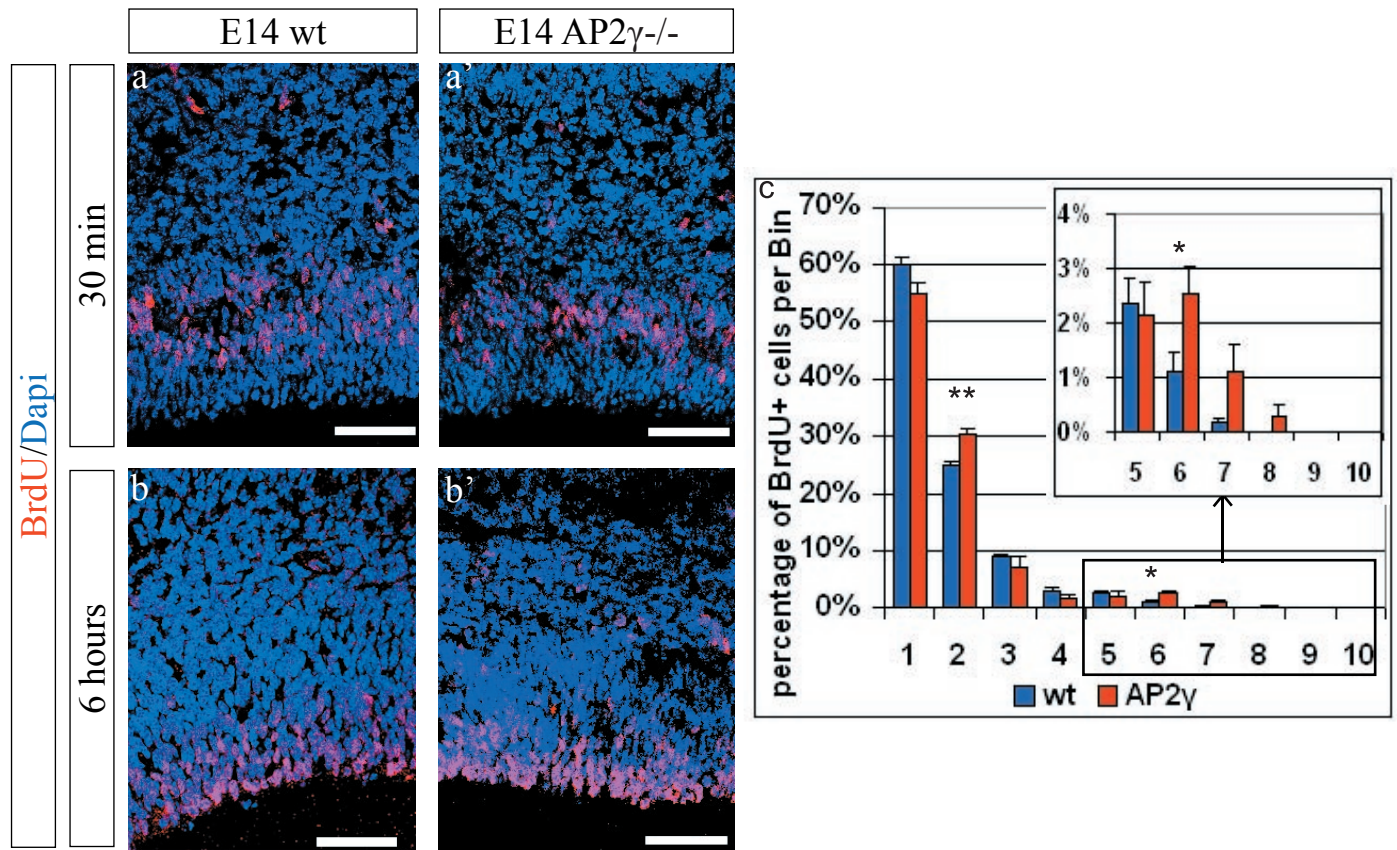


Figure 29. Interkinetic nuclear migration in the WT and AP2 γ ^{-/-} cortex at E14

(a-b') Fluorescent micrographs of coronal sections of E14 WT and AP2 γ ^{-/-} cortex 30 minutes (a,a') or 6 hours (b,b') after BrdU (red) injection. (c) Distribution of the BrdU-positive nuclei as percentage of all BrdU-positive nuclei per bin (one bin: 20- μ m high and 100- μ m wide). Note the significant increase in the number of BrdU-positive cells in bins 2 and 6, 6 hours after BrdU injection in the AP2 γ ^{-/-}-cortex. Bars in the histogram represent mean \pm S.E.M. Asterisks depict the significance levels (* = $p \leq 0.05$; ** = $p \leq 0.01$) obtained by T-test. Scale bars: 100 μ m

Figure 30

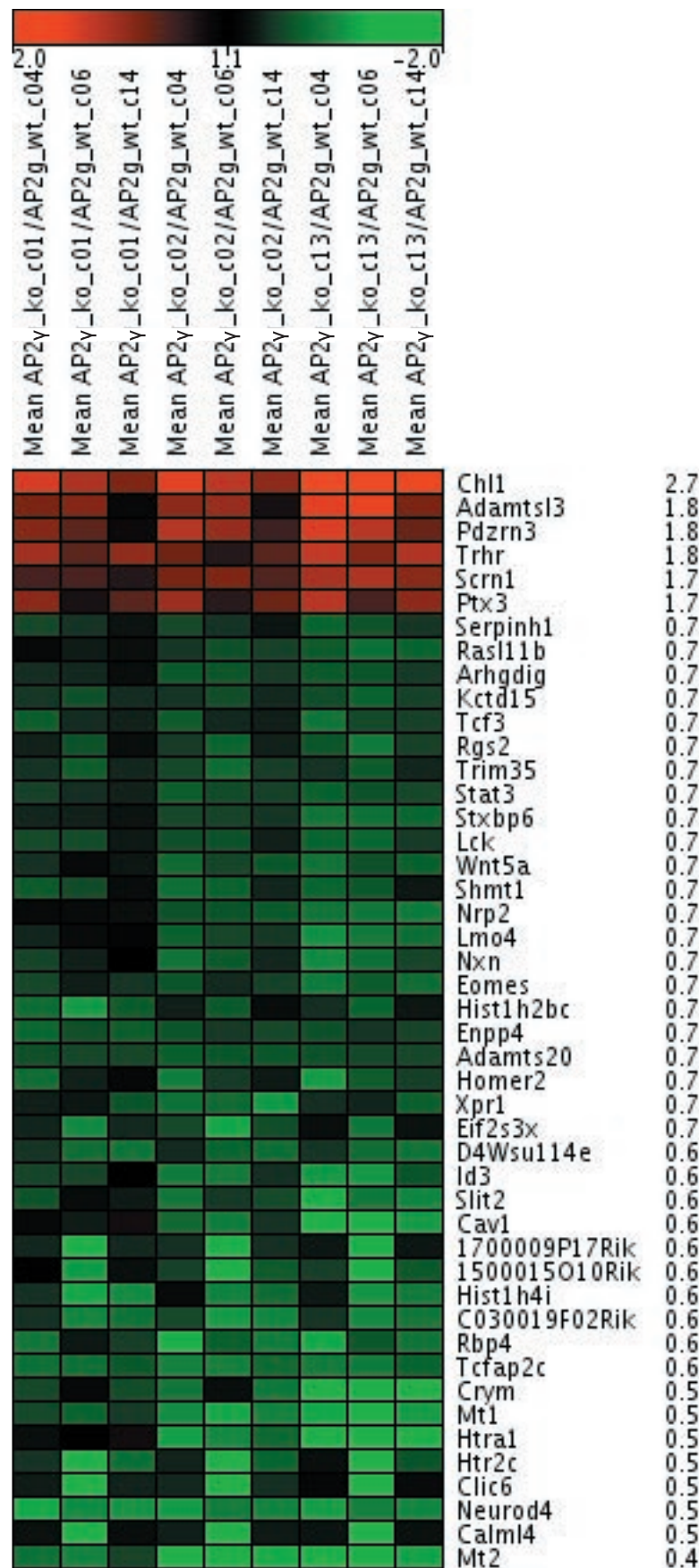


Figure 30. Heat map representing the genes significantly regulated between E14 WT and AP2 γ ^{-/-} cortices at intermediate-caudal regions

Heat map representing the genes found to be statistical significant differentially expressed between E14 WT and AP2 γ ^{-/-} cortices at intermediate-caudal regions, by microarray analysis. These genes displayed at least a 1.5 fold (linear) average expression change and an absolute expression equal or higher than 50 for each of the biological replicates of WT versus AP2 γ ^{-/-} comparison (unpaired test). Red indicates increased and green decreased expression levels in AP2 γ ^{-/-} compared to WT cortices. Note that most significant genes are down-regulated in the AP2 γ ^{-/-} compared to WT cortices.

Figure 31

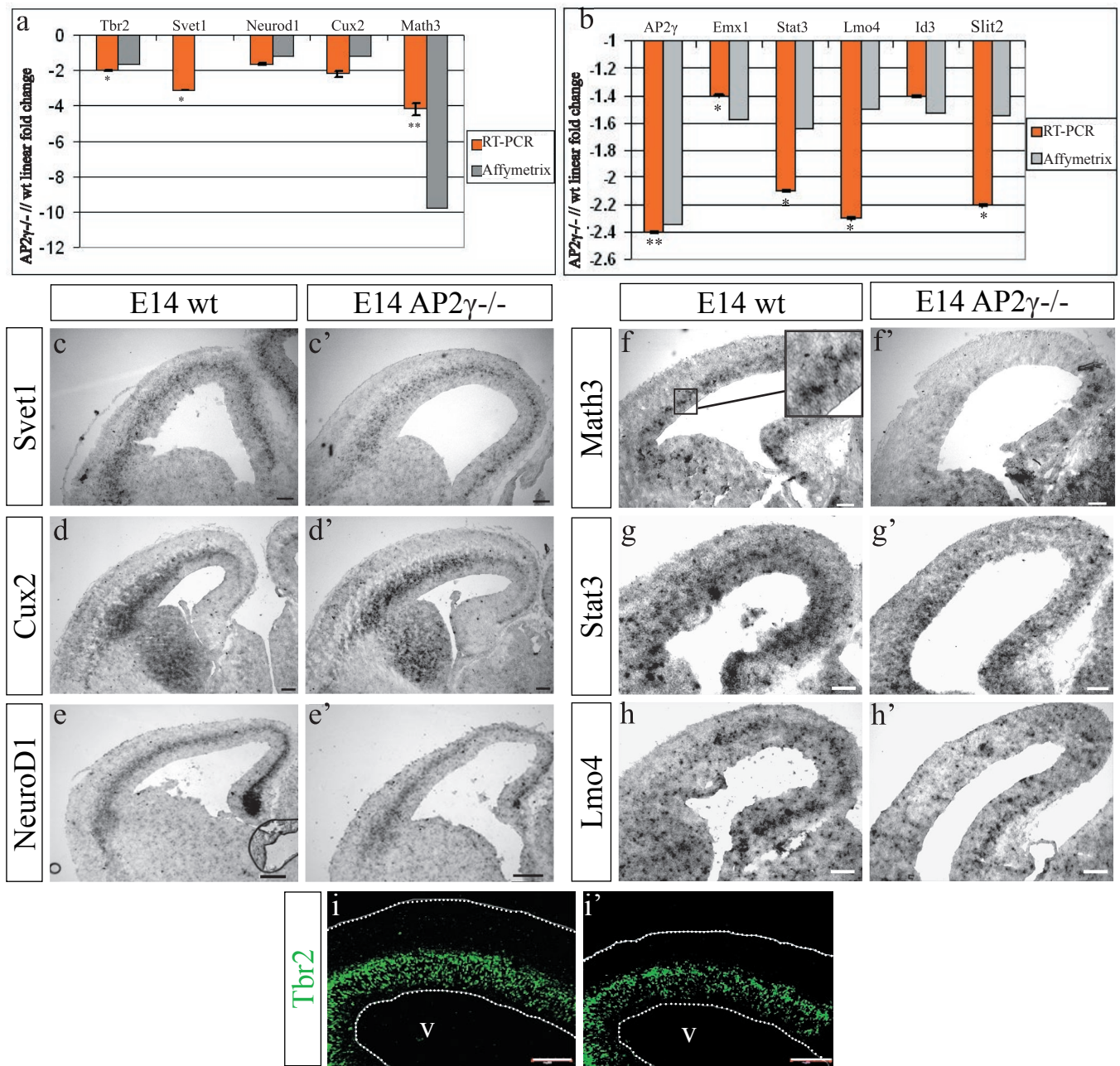


Figure 31. Transcriptome analysis and basal progenitor defects in the AP2γ^{-/-} cortex at E14

(a,b) mRNAs predicted to be significantly changed in their expressed in the intermediate-caudal levels comparing WT and AP2γ^{-/-} cortices by Affymetrix analysis (grey bars) were examined by real-time RT-PCR (orange bars in panels a and b depict the linear fold change of mRNA levels between WT and AP2γ^{-/-} cortices after normalization to GAPDH mRNA levels. Values for genes expressed at lower levels in the AP2γ^{-/-} cortices were set negative. Grey bars represent the equivalent ratios according to the microarray results. T-test was performed for all genes analyzed (* = $p \leq 0.05$; ** = $p \leq 0.01$). (c-h') ISH on E14 WT and AP2γ^{-/-} cortex sections of 6 selected mRNAs with differential expression levels between WT and AP2γ^{-/-} cortex in the microarrays analysis. Note that all genes were confirmed to be expressed at lower levels in the AP2γ^{-/-} cortex as predicted by the microarrays results. (i, i') Coronal sections of the WT and AP2γ^{-/-} cerebral cortex at E14, immunolabelled with Tbr2. Note the decrease in Tbr2⁺ basal progenitors in the AP2γ^{-/-} compared to WT cortex. Bars in all histograms represent mean \pm S.E.M. Asterisks depict the significance levels (* = $p \leq 0.05$; ** = $p \leq 0.01$) obtained by T-test. Scale bars: c-h' 50μm; i, i' 100μm. Abbreviations; V=ventricle.

Figure 32

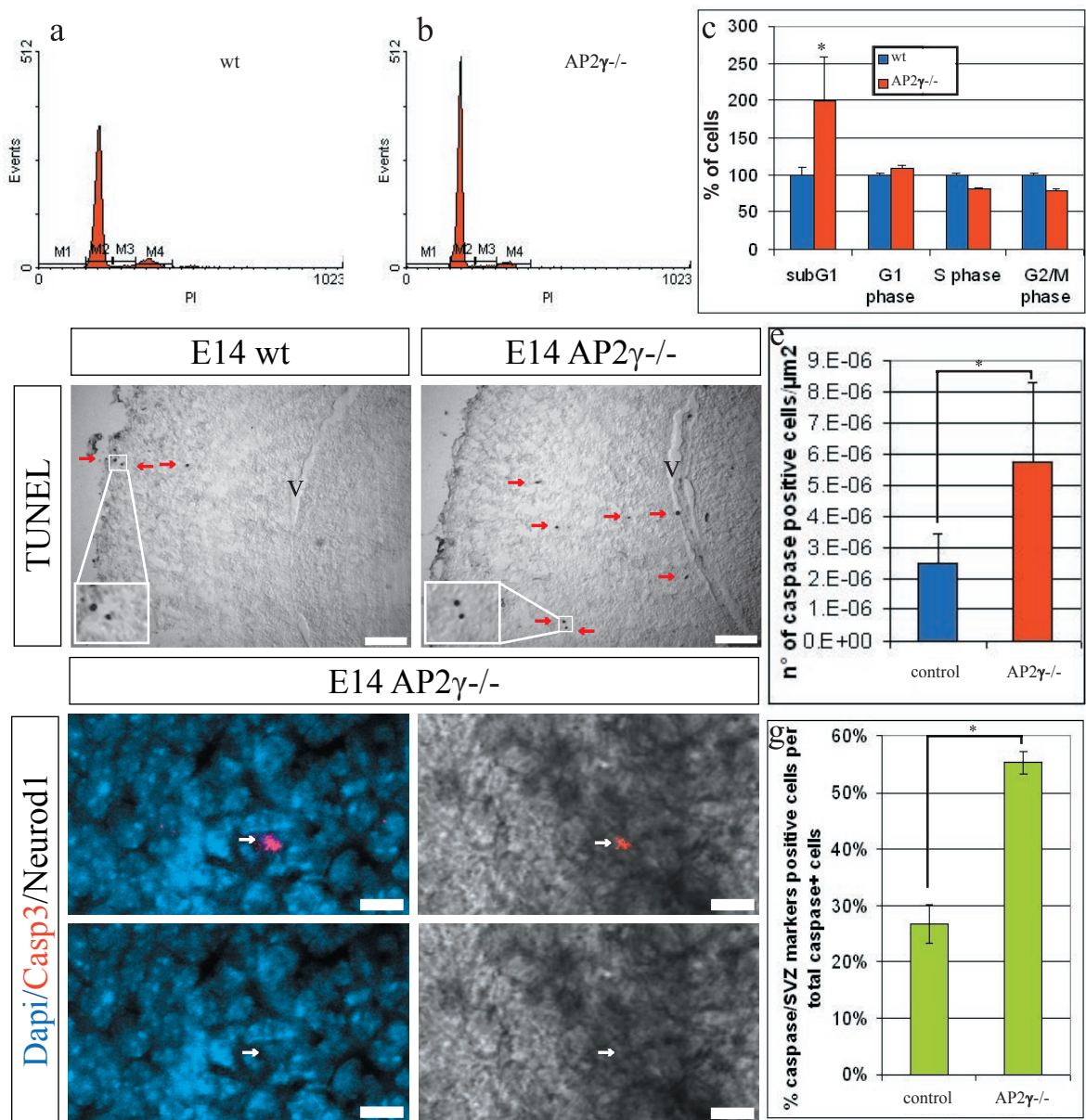


Figure 32. Cell death of basal progenitors in the AP2γ^{-/-} cortex at E14

Histograms **a-c** depict cell cycle analysis of WT (**a**) and AP2γ^{-/-} (**b**) cortices by FACS using propidium iodide labelling (M1=SubG1; M2=G1 phase; M3=S phase; M4=G2/M phase). Histogram **c** depicts the percentage of cells in all phases of the cell cycle in the WT (blue bars) and AP2γ^{-/-} (red bars) cortices examined by FACS. Note the high increase in the number of events in subG1 (cell death), a minor increase in the percentage of cells in G1 phase and decrease of cells in S/G2/M phase for mutant compared to AP2γ^{-/-} cells. (**d-d'**) Panels depict E14 WT and AP2γ^{-/-} cortex coronal sections labelled with TUNEL. Note the increase in the number of TUNEL+ cells in the VZ/SVZ of the AP2γ^{-/-} cortices. Histogram **e** depicts the number of activated caspase3+ cells in WT and AP2γ^{-/-} cortices. Note the significant increase on caspase3+ cells in the AP2γ^{-/-} cortices. Panels **f-f'''** and histogram **g** depict the colocalization of caspase3+ cells with SVZ markers (NeuroD1 in panels **f,f'**). Note that 25% of all caspase3+ cells express SVZ markers (**g**). Bars in all histograms represent mean ± S.E.M. Asterisks depict the significance levels (* = p ≤ 0.05) obtained by T-test. Scale bars: **d,d'** 100μm; **f-f'''** 20μm. Abbreviations; V=ventricle

Figure 33

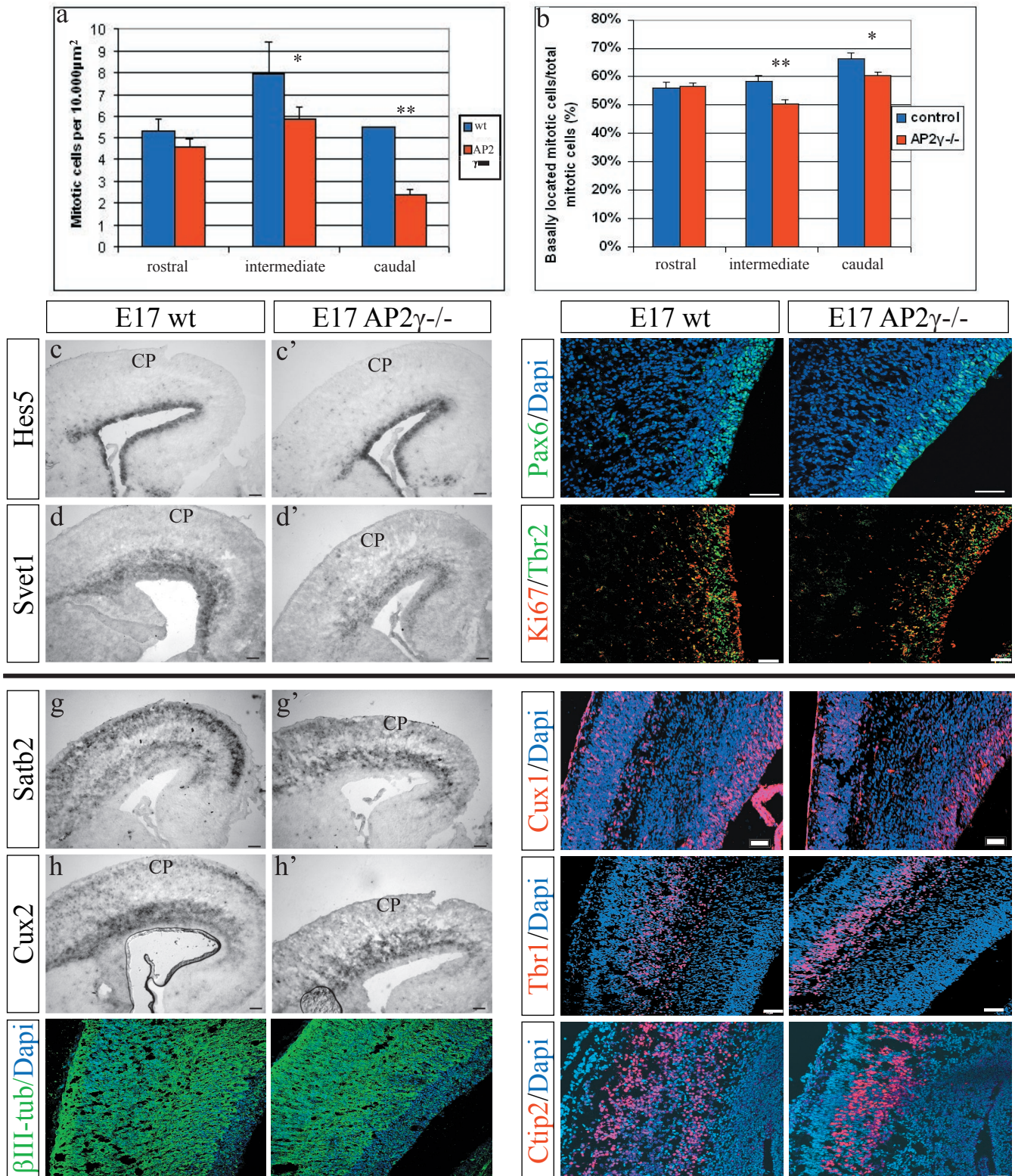


Figure 33. Neuron and progenitor identity in the AP2γ^{-/-} cortex at the end of neurogenesis (E17)
 Histogram **a** depicts the total number of mitotic cells in the cortex of E17 WT and AP2γ^{-/-} at rostral, intermediate and caudal regions. Note the decrease in the number of total mitotic cells at intermediate and caudal regions in the AP2γ^{-/-}. Histogram **b** depicts the percentage of basally located mitotic cells in the E17 AP2γ^{-/-} compared to WT cortex. Note the decrease of basally located mitotic cells only at intermediate and caudal regions of the AP2γ^{-/-} cortices. (**c-d'**) ISH on E17 WT and AP2γ^{-/-} cortex sections of the progenitor marker Hes5 (**c, c'**) and the basal progenitor marker Svet1 (**d, d'**). (**e-f'**) Coronal sections of the E17 WT and AP2γ^{-/-} cerebral cortex immunolabelled with Pax6 (**e, e'**), Ki67 and Tbr2 (**f, f'**). (**g-h'**) ISH on E17 WT and AP2γ^{-/-} cortex sections of Satb2 (**g, g'**) and Cux2 (**h, h'**). Note the absence of Satb2 and Cux2 mRNA in the cortical plate of the AP2γ^{-/-} cortex. (**i-l'**) Coronal sections of the E17 WT and AP2γ^{-/-} cerebral cortex immunolabelled with βIII-tubulin (**i, i'**), Cux1 (**j, j'**), Tbr1 (**k, k'**) and Ctip2 (**l, l'**). Note the decrease in the width of β3-tubulin/Cux1/Tbr1/Ctip2 band of neurons in the AP2γ^{-/-} cortex at E17. Asterisks depict the significance levels (* = p ≤ 0.05; ** = p ≤ 0.01) obtained by T-test. Scale bars: **a, d'** 50 μm; **g-k'** 100 μm. Abbreviations; V=ventricle; CP=cortical plate

Figure 34

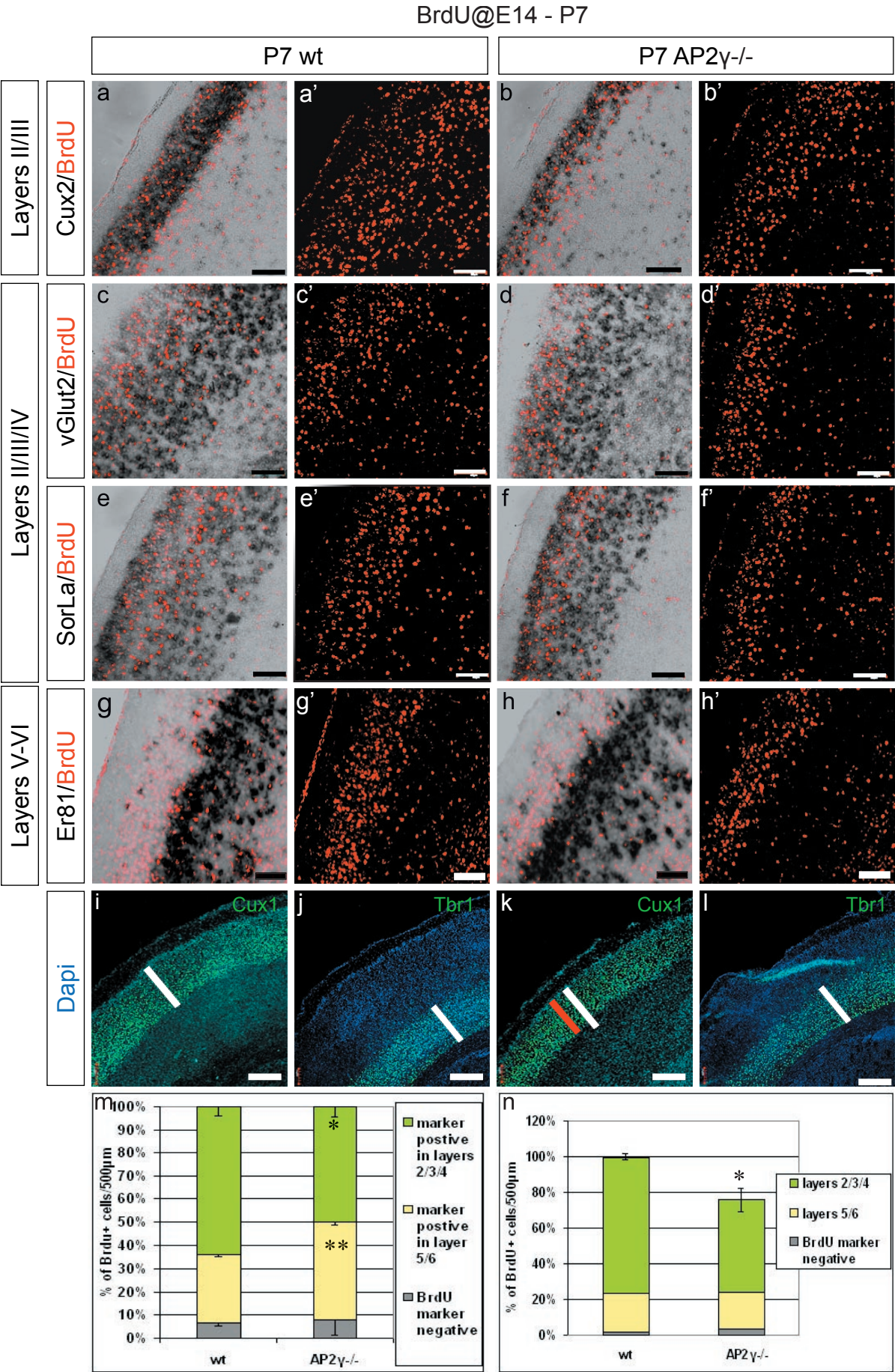


Figure 34. Neurogenesis in the cerebral cortex of AP2 γ ^{-/-} mice

(**a-h'**) Micrographs depict sagittal sections of the WT and AP2 γ ^{-/-} cortex at P7, in which mice BrdU was given at E14. Cortical sections were immunolabelled with BrdU and co-localized with layer neuron markers as Cux2 mRNA for layers II/III (**a-b'**), vGlut2 (**c-d'**) and SorLa mRNA (**e-f'**) for layers II/III/IV and Er81 mRNA for layers V/VI (**g-h'**). Note the decrease of BrdU positive cells in upper cortical layers II/III/IV (**a-f'**). (**i-l**) Micrographs depict sagittal sections of the WT and AP2 γ ^{-/-} cortex at P7, immunolabelled with Cux1 (**i, k**) and Tbr1 (**j, l**). Note the thinner band of Cux1+ cells in the AP2 γ ^{-/-} (red bar in **k**) compared to the WT cortex (white bar in **i**). Histogram **m** depicts the percentage of BrdU+ cells co-localized with markers for cortical layers II-VI. Note the decrease of the percentage of BrdU+ cells in upper layers II-IV and the increase in deep layers V/VI in the AP2 γ ^{-/-} compared to the WT cortex. Histogram **n** depicts the percentage of total BrdU+ cells at P7 (injection at E14), showing a 22% decrease in the AP2 γ ^{-/-} compared to the WT cortex. Bars in all histograms represent mean \pm S.E.M. Asterisks depict the significance levels (* = $p \leq 0.05$; ** = $p \leq 0.01$) obtained by T-test. Scale bars: 100 μ m.

Figure 35

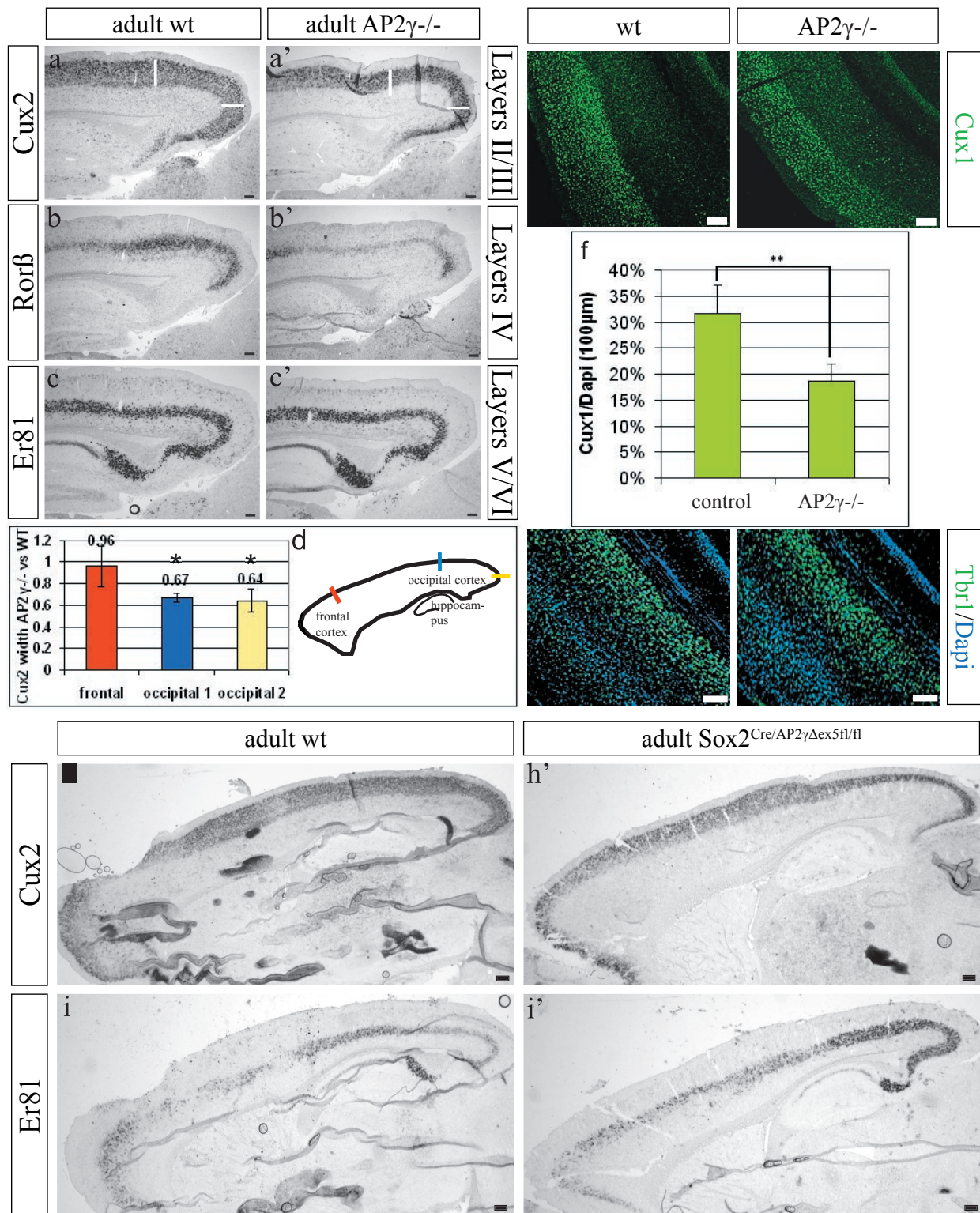


Figure 35. Upper layer neuron defects in the adult AP2 γ ^{-/-} mice

(a-c') Micrographs of sagittal sections of 2 months old WT and AP2 γ ^{-/-} mice cortices labeled with Cux2 mRNA for layers II/III (a-a'), Ror β for layer IV (b, b') and Er81 for layer V (c, c'). Histogram d depicts the measurement of the width of Cux2⁺ band of neurons in rostral-occipital levels of WT and AP2 γ ^{-/-} adult cortices, shown as ratio between mutant vs control. Note the decrease of the thickness of Cux2⁺ upper layers II/III in the AP2 γ ^{-/-} compared to the WT cortex at occipital regions. (e, e', g, g') Micrographs of sagittal sections of the cortex of WT and AP2 γ ^{-/-} at adult stages immunolabelled with Cux1 (e, e') and Tbr1 (g, g'). Histogram f depicts the number of total Cux1⁺ cells in the cortex of WT and AP2 γ ^{-/-} at adult stages, showing a decrease of 15% in the AP2 γ ^{-/-} cortex. (h-i') Micrographs of sagittal sections of 2 months old WT and AP2 γ ^{-/-} mice cortices labeled with Cux2 mRNA for layers II/III (h, h') and Er81 for layer V (i, i'). In panels h-i' AP2 γ was deleted by Sox2::Cre, inducing recombination in all epiblast cells by embryonic day E6.5. Note the decrease of the thickness of Cux2⁺ upper layers II/III in the Sox2^{Cre}/AP2 γ ^{Δex5fl/fl} mutant compared to the WT cortex. Bars in all histograms represent mean \pm S.E.M. Asterisks depict the significance levels (* = $p \leq 0.05$; ** = $p \leq 0.01$) obtained by T-test. Scale bars: 100 μ m. Abbreviations; V=ventricle

Figure 36

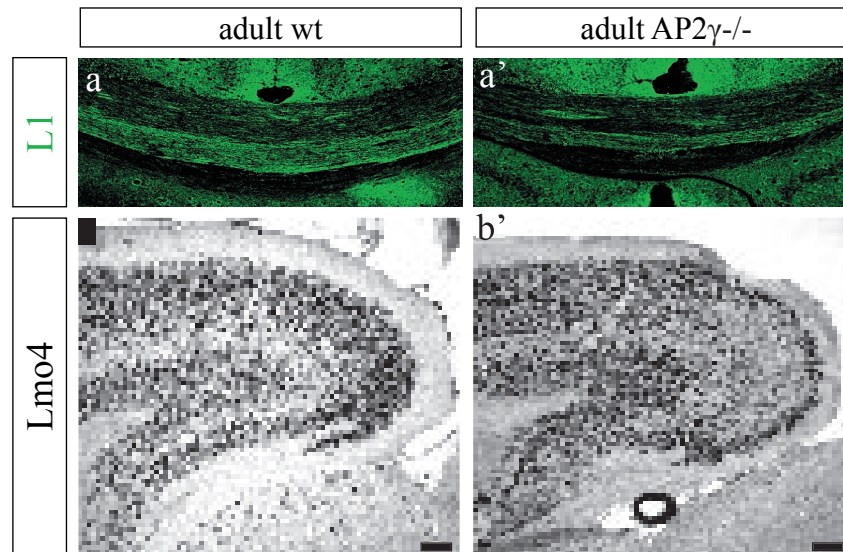


Figure 36. Defects in layers II/III callosal projection neurons in the adult AP2 γ ^{-/-} cortex

Panels **a**, **a'** depict coronal occipital sections of WT and AP2 γ ^{-/-} adult mice cortices, immunolabelled with L1 for the callosal projection neurons, showing a decrease in the AP2 γ ^{-/-} mice. (**b**, **b'**) Micrographs of sagittal sections of 2 months old WT and AP2 γ ^{-/-} mice cortices labeled with Lmo4 mRNA for layers II/III and IV. Note the decrease of the Lmo4 mRNA in the layers II/III of the AP2 γ ^{-/-} occipital cortex. Scale bars: 100 μ m.

Figure 37

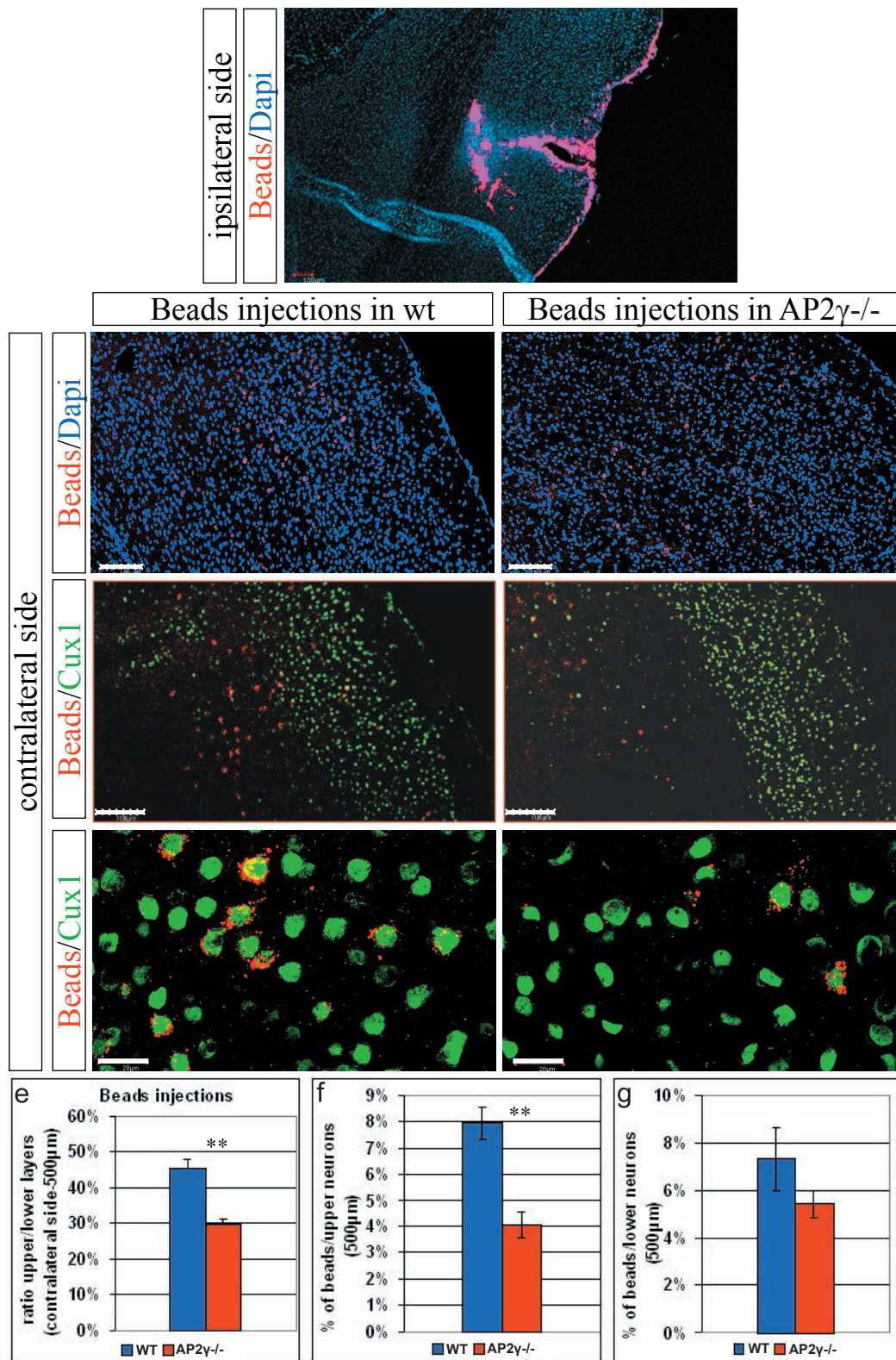


Figure 37. Bead injections in the occipital cortex of adult AP2γ^{-/-} mice

Pannel **a** depicts one example of the site of bead injection (red) in the cortex of adult WT mice. (**b-d'**) Fluorescent micrographs of coronal sections of E14 WT and AP2γ^{-/-} 2 months old cortex injected with fluorescent beads (red) and analyzed the contralateral side 1 week after by immunolabelling with Dapi (**b, b'**) and Cux1 (**c-d'**). Histograms in **e-g** depict the ratio of beads-containing cells in upper neuronal layers divided by those located in lower neuronal layers expressed as percentage (**e**) and the proportion of beads-containing cells amongst all Cux1+ neurons (= upper layer neurons) (**f**) and Tbr1+ neurons (=lower layer neurons) (**g**) of WT and AP2γ^{-/-} cortices. Note the decrease to half of the proportion of beads in upper layers in the AP2γ^{-/-} compared to the WT cortex. Bars in all histograms represent mean ± S.E.M. Asterisks depict the significance levels (* = p ≤ 0.05; ** = p ≤ 0.01) obtained by T-test. Scale bars: **a-c'** 100μm; **d, d'** 20μm

Figure 38

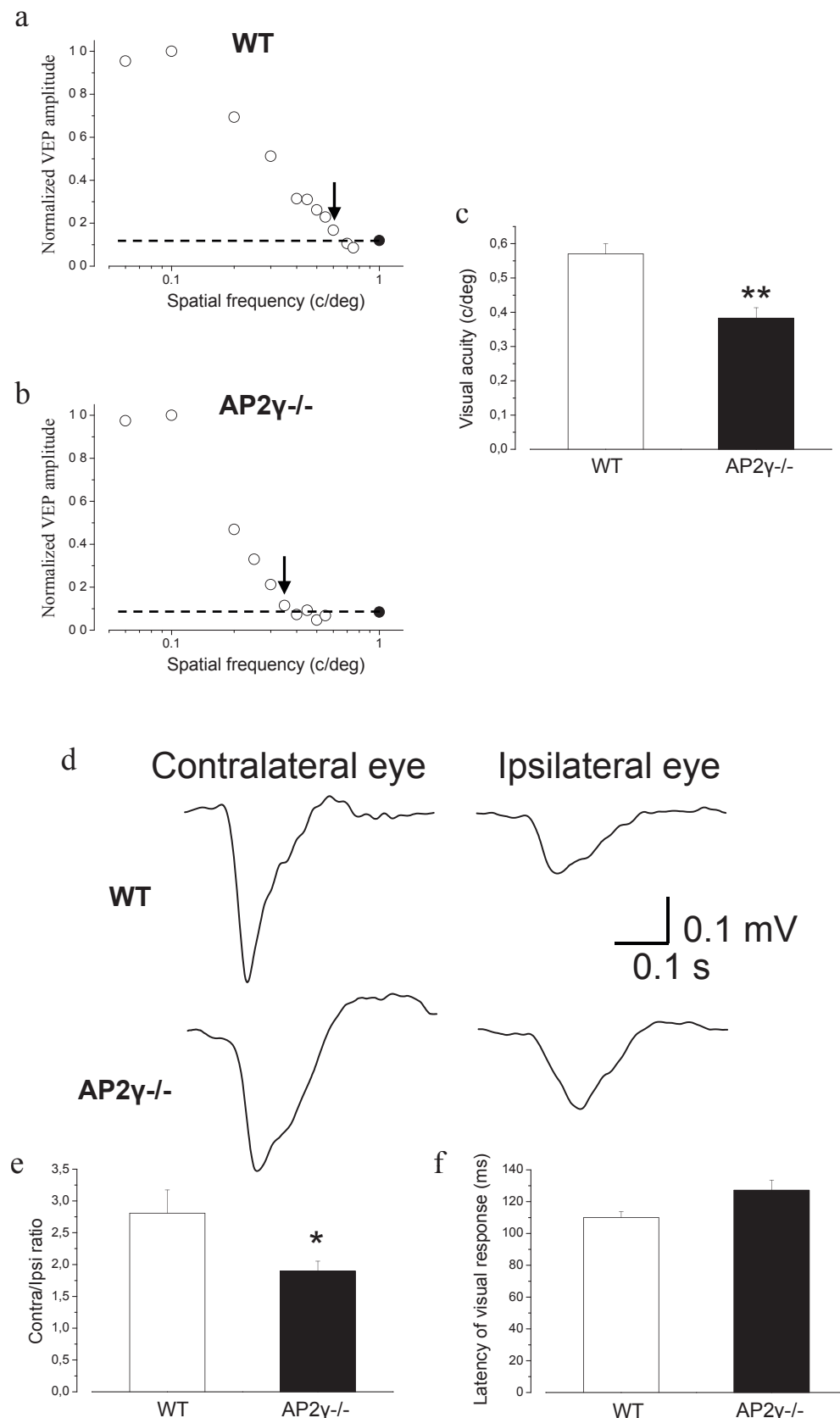


Figure 38. Visual performance of WT and AP2 γ ^{-/-} adult mice

(a, b) Representative visual acuity curves in a WT (top) and a AP2 γ ^{-/-} mouse (bottom). VEP amplitudes decrease with increasing spatial frequency of stimulus. In each graph, an arrow indicates the last point above noise level (marked by a dotted line) that was taken as the threshold in that animal. (c) Spatial resolution in the visual cortex of WT and AP2 γ ^{-/-} mice. Visual acuity is significantly reduced in the mutant animals (t-test, $p = 0.002$). (d) Representative examples of VEPs evoked by patterned visual stimulation of the contralateral and ipsilateral eye, in WT (top) and AP2 γ ^{-/-} mice (bottom). (e) Ratio of contralateral eye VEP amplitude to ipsilateral eye VEP amplitude (Contra/Ipsi ratio) in WT and AP2 γ ^{-/-} mice. The ratio is significantly lower in the mutant animals (t-test, $p = 0.027$). Bars represent mean \pm S.E. (f) Latency of the major VEP negative component in WT and AP2 γ ^{-/-} mice. Bars represent mean \pm S.E. (Collaboration with Dr. Matteo Caleo)

Figure 39

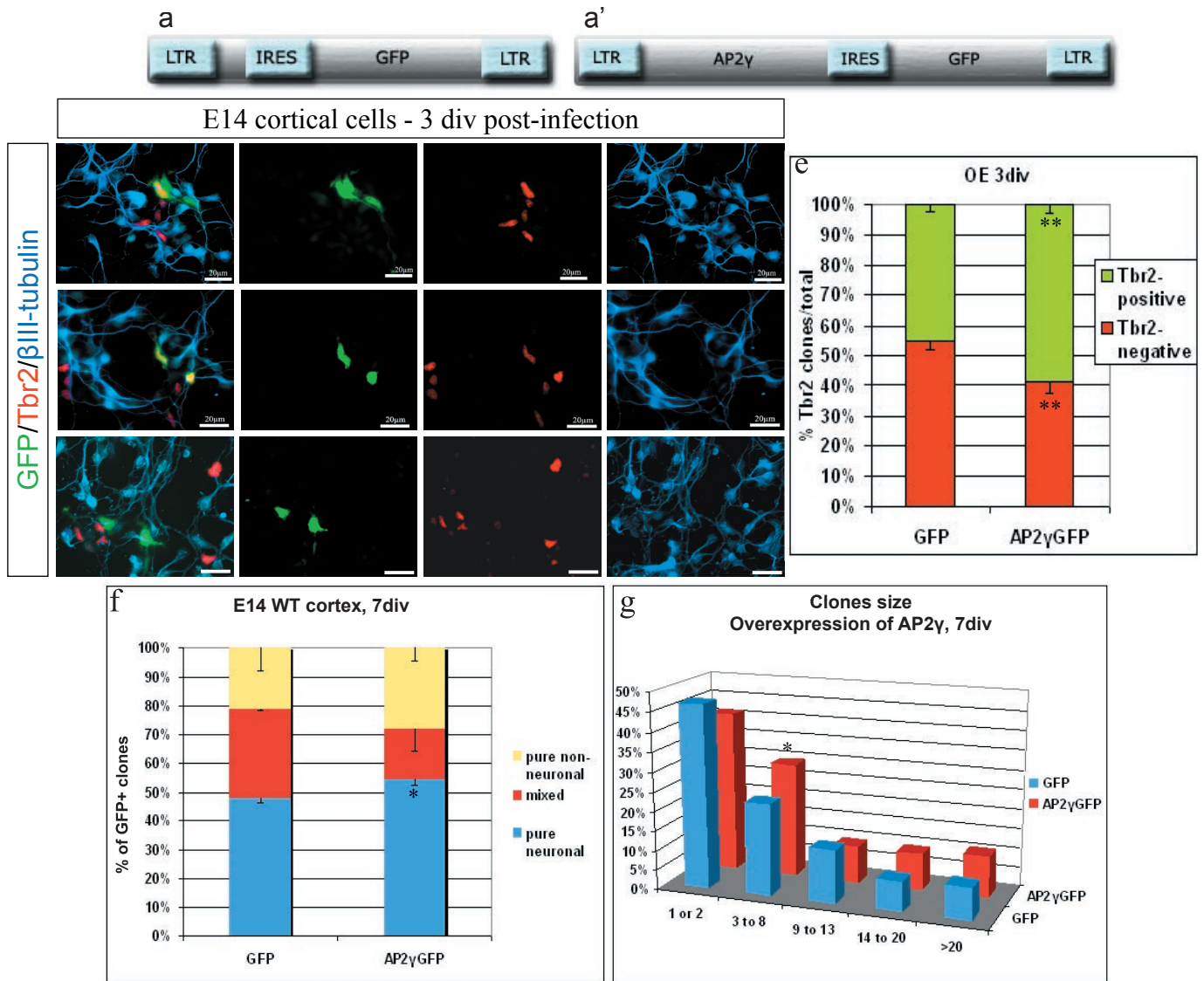


Figure 39. AP2γ overexpression of E14 cortical cells *in vitro*

(**a, a'**) Schematic drawing of the retroviral constructs used for control (GFP in **a**) and overexpression of AP2γ (AP2γGFP in **a'**). (**b-d'''**) Micrographs depict infection of E14 WT cortical cells with retroviral constructs used for control GFP and overexpression of AP2γ and analyzed 3 days post-infection, immunolabelled with GFP, Tbr2 and βIII-tubulin. Panels **b-b'''** depict one infected mixed clone GFP+/Tbr2+/βIII-tubulin+, panels **c-c'''** depict one infected GFP+/Tbr2-negative clone and panels **d-d'''** depict one GFP/Tbr2 double-positive clone. Histogram **e** depicts the quantification of the percentage of GFP/Tbr2 double-positive clones after control GFP and AP2γGFP overexpression in cortical cultures 3 days post-infection. Note the increase in the percentage of GFP/Tbr2 double-positive clones in AP2γGFP compared to GFP overexpression in cortical cultures (green in **e**). Histograms **f** depicts the quantification of the percentage of pure-, mixed- or non-neuronal clones after control GFP and AP2γGFP overexpression in cortical cultures 7 days post-infection. Note the increase in the number of pure neuronal clones after AP2γ-GFP overexpression. Histogram **g** depicts the quantification of the clone size after overexpression of E14 WT cortical cells with control GFP and AP2γGFP virus, after 7 days *in vitro*. Note the increase in the clones with 3-8 cells in the AP2γ^{-/-} cortical cultures. Bars in all histograms represent mean ± S.E.M. Asterisks depict the significance levels (* = $p \leq 0.05$) obtained by T-test. Scale bars: 20 μm.

Figure 40

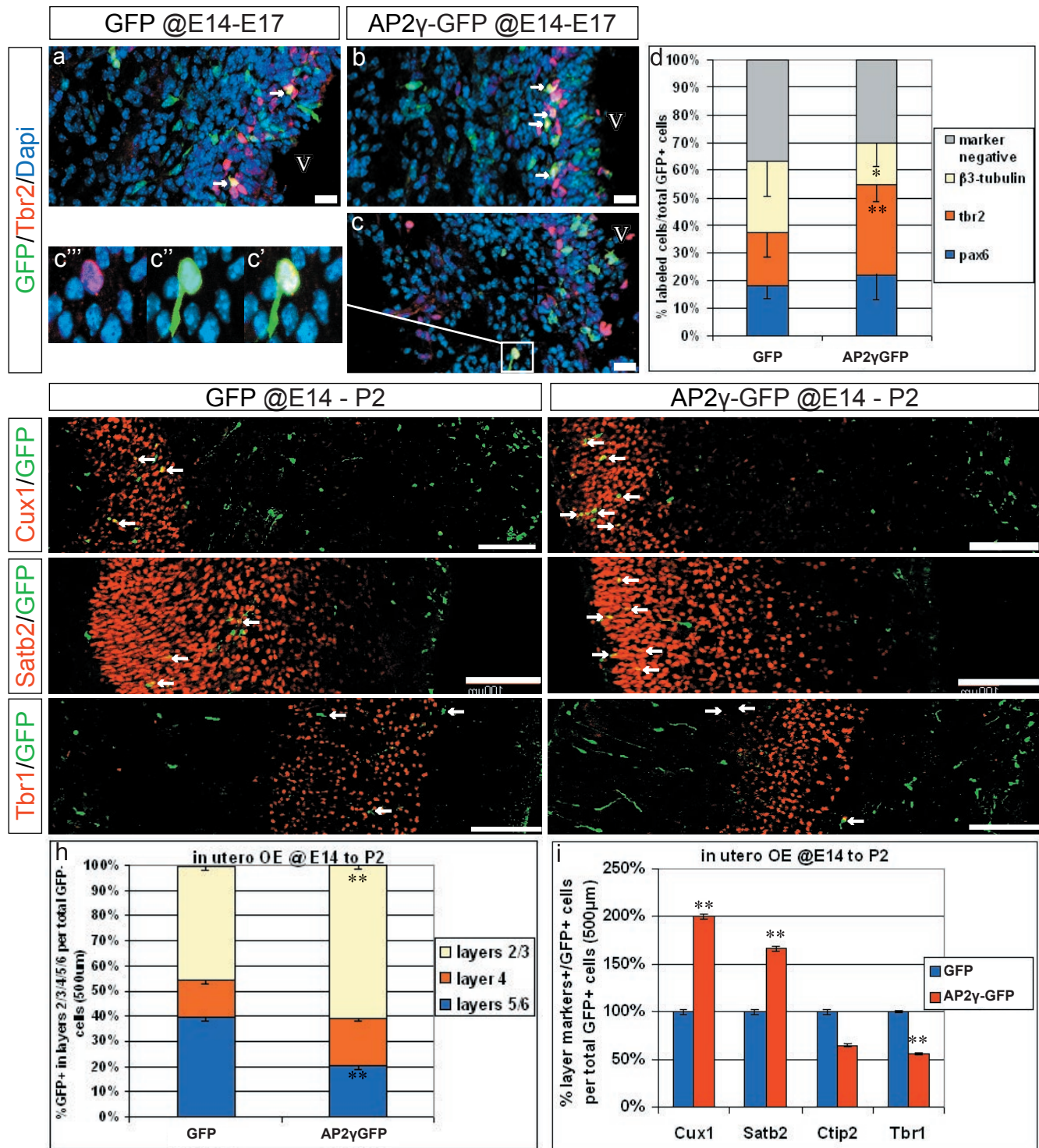


Figure 40. AP2γ overexpression *in vivo* in the developing cortex

(a-i) Injections of the constructs presented in Fig. 39a, a' into the ventricle of E14 WT embryos and analysis done at E17 (a-d) or at postnatal day 2 (P2 in e-i) post-injection. Panels a-c''' depict coronal sections of the cortex at E17 post-injection immunolabelled with GFP, Tbr2 and Dapi. Histogram d depicts the quantification of the percentage of control GFP and AP2γ infected GFP+ cells co-localized with Pax6, Tbr2 or βIII-tubulin in the cortex at E17 post-injection. Note the increase in the percentage of GFP+ cells co-localized with Tbr2 (orange bars in d and white arrows in a, b) upon AP2γGFP overexpression. Panels e-g' depict sagittal sections of the cortex at P2 post-injection immunolabelled with GFP, Cux1 (e, e'), Satb2 (f, f') and Tbr1 (g, g'). Histograms h, i depict quantification of the percentage of control GFP and AP2γ infected GFP+ cells localized in the cortical layers II-VI (h) and the percentage of control GFP and AP2γ infected GFP+ cells co-localized with neuronal layer markers II-VI (i). Bars in all histograms represent mean ± S.E.M. Asterisks depict the significance levels (* = $p \leq 0.05$; ** = $p \leq 0.01$) obtained by T-test. Scale bars: a-c 50μm; e-g' 100μm. Abbreviations; V=ventricle

Figure 41

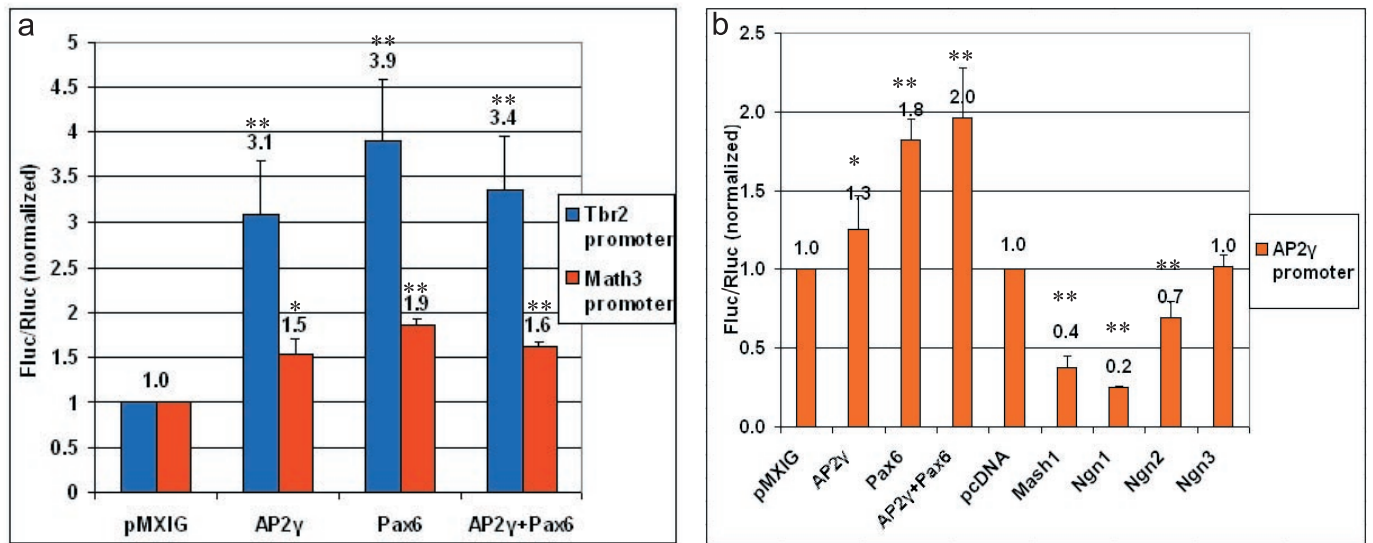


Figure 41. Upstream regulators and downstream targets of AP2γ in the developing cortex

(a, b) Histograms depict luciferase assay in mouse neuroblastoma (Neuro-2A) cells for the Tbr2 and Math3 promoters (a) and for the AP2γ promoter (b) activation by AP2γ, Pax6 or both. Note the significant activation of the Tbr2 and Math3 promoters by AP2γ (a) and the strong activation of the AP2γ promoter by Pax6, while Mash1 and Ngn1/2 repress it (b). Bars in all histograms represent mean \pm S.E.M. Asterisks depict the significance levels (* = $p \leq 0.05$; ** = $p \leq 0.01$) obtained by T-test.

Figure 42

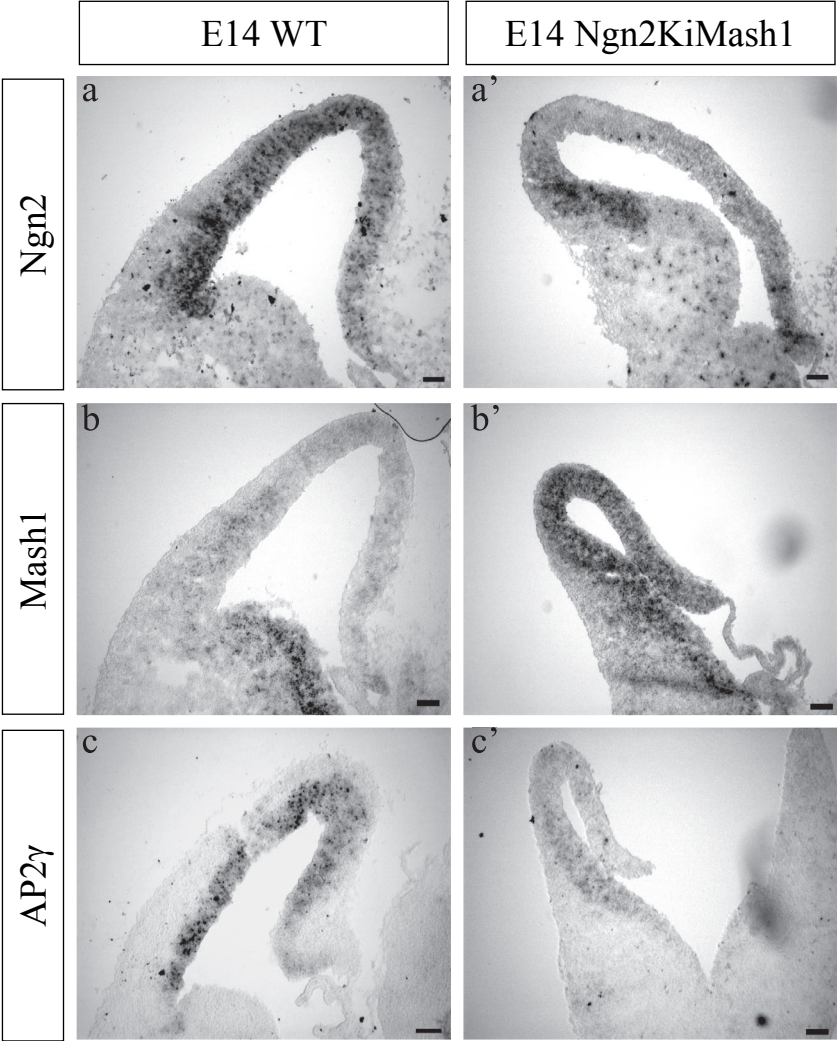


Figure 42. Regulation of AP2γ by Mash1 and Ngn2 in the developing cortex
(a-c') ISH for Ngn2 (a, a'), Mash1 (b, b') and AP2γ (c, c') on coronal sections of the cortex of E14 WT and mice expressing Mash1 in the Neurogenin 2 locus (Ngn2KiMash1). Note the virtual absence of AP2γ mRNA in the cortex of Ngn2KiMash1 mice. Scale bars: 50μm.

Figure 43

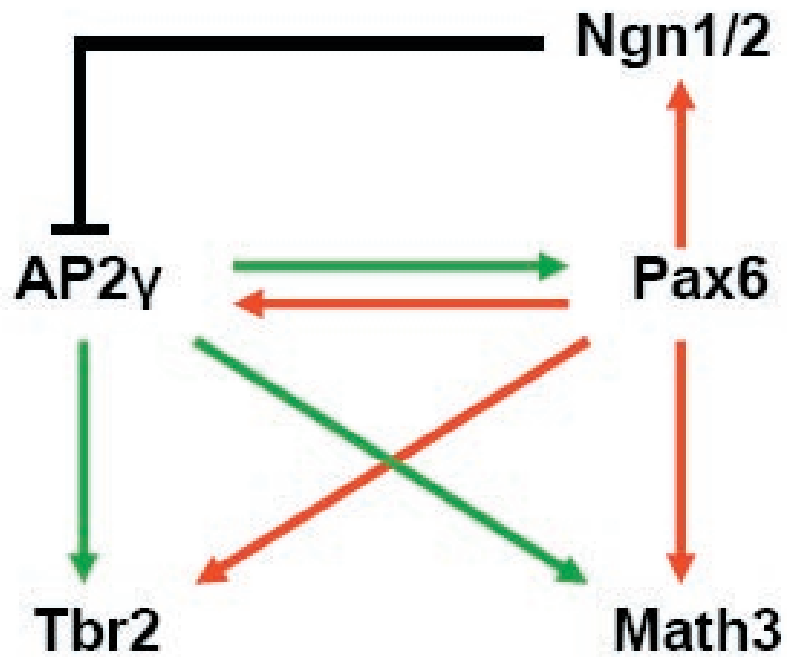


Figure 43. Molecular mechanisms regulating AP2 γ in the cortex

Scheme of the transcriptional regulation for basal progenitor fate determinants by AP2 γ and Pax6. Note that AP2 γ directly regulates Tbr2 and Math3, similarly to Pax6. AP2 γ is negatively regulated by Ngn1 and 2 and positively regulated by Pax6.

Table 1: Differentially expressed genes between subsets of radial glia excluding and including their progeny

Function (GO annotation)	Probe set	Gene	Fold change (FC)	
			FC E14 GFP ^{high} /prom+ vs GFP ^{low} /prom+	FC E14 GFP ^{high} vs GFP ^{low}
<i>Transcription factor activity</i>				
	1455080_at	Ppp1r16b	-1.2	-3.6
	1458802_at	Hivep3	-1.2	-3.3
	1427640_a_at,	Cbfa2t1h/Runx1t1	-1.1	-5.8
	1422018_at,	Hivep2	-1.6	-4.0
	1416160_at	Nr2f2	-1.1	-1.2
	1428377_at, at	Btbd11	-1.7	-5.1
	1459838_s_			
	1434298_at,	Zfxh1b	-1.1	-3.5
	1456389_at			
	1420346_at	Asb12	-1.0	-1.3
	1424852_at	Mef2c	-1.2	-4.8
	1456342_at	Pax6	-0.2	-2.5
	1434904_at	Nr2e1	1.1	3.3
	1450194_a_at	Myb	1.1	3.5
	1452526_a_at	Pax6(5a)	1.9	3.2
	1421193_a_at	Pbx3	1.1	2.4
	1451538_at	Sox9	1.0	2.5
	1451835_at	Sox21	0.8	2.5
	1427764_a_at	Tcf2a/E2A	1.2	1.6
	1448977_at	Tcf2c/AP2γ	0.7	2.5
	1448519_at	Tead2	1.1	2.5
	1451776_s_at	MGI:1916782/Hod	1.6	2.1
	1416487_a_at	Yap1	1.6	2.6
<i>Basic helix-loop-helix</i>				
	1419303_at	Heyl/Hesr3	-1.2	-1.6
	1418271_at	Bhlhb5	-1.0	-2.5
	1423260_at	Id4	1.2	3.2
	1425895_a_at	Id1	1.4	2.1
	1450164_at	ascl1	1.3	1.5
	1449967_at	Sim1	1.3	0.9
<i>Gliogenesis</i>				
	1423260_at	Id4	1.2	3.2
	1434921_at	Nr2e1	1.0	3.3
<i>Neurogenesis/Neuronal differentiation</i>				
	1456342_at	Pax6	-0.2	-2.5
	1419473_a_at	Cck	-1.3	-4.7
	1416160_at	Nr2f2	-1.1	-1.2
	1446453_at	Atbf1	-2.1	-2.4
	1438258_at	Vldlr	-1.3	-1.7
	1449465_at	reln	-2.8	-2.3
	1423537_at	Gap43	-1.1	-2.5
	1450863_a_at	Dcamk1	-1.4	-3.3
	1438551_at	ngn1	1.6	3.2
<i>Neurotransmitter secretion</i>				
	1433884_at	Syt1	-1.4	-4.7
	1415844_at	Syt4	-1.1	-2.4
	1454691_at	Nrxn1	-1.7	-2.7
	1417901_a_at	Ica1	-1.1	-4.7

	1418493_a_at	Snca	-1.9	-2.5
	1436602_x_at	Cacna1b	-1.2	-3.8
	1435021_at	Gabrb3	-1.4	-3.4
Axon guidance				
	1453103_at	Ablim1	-1.7	-2.6
	1419328_at	Sema4f	-1.3	-2.5
	1454903_at	Ngfr/p75	-1.3	-4.4
	1427231_at	Robo1	-1.4	-4.6
Cell adhesion				
	1435807_at	Cdc42	-1.1	-2.8
	1423551_at	Cdh13/T-cadherin	-1.5	-4.6
	1450757_at	Cdh11	-1.2	-3.0
	1426283_at	MGI:2446259/Hnt	-1.5	-3.3
	1427256_at	Cspg2/Vcan	-1.1	-2.2
	1433474_at	Edil3/Del1	-1.2	-2.7
	1429861_at	Pcdh9	-1.3	-3.6
	1448895_a_at	Ctnna2	-1.0	-2.8
	1438133_a_at	Cyr61/Igfbp10	1.1	3.1
	1421344_a_at	Jub	1.2	3.3
	1424010_at	Mfap4	1.0	4.1
	1420911_a_at	Mfge8	1.0	2.4
Cytoskeleton				
	1421090_at	Epb4.1l1	-1.1	-3.4
	1424523_at	Elmo1	-1.2	-2.4
	1434582_at	D14Ert171e/Cast	-1.3	-2.9
	1428750_at	Cdc42ep2	-1.1	-2.8
	1422117_s_at	Khdrbs2/Slim1	-1.0	-2.1
	1429651_at	Phactr3	-1.1	-3.3
	1458662_at	Daam1	-1.4	-4.3
	1435207_at	Dixdc1/Ccd1	-1.0	-2.6
	1458768_at	Epb4.1l5	1.0	2.1
	1425654_a_at	D15Ert366e/Lima1	1.1	1.6
	1450767_at	Nedd9	1.4	2.8
	1423196_at	Nedd1	1.5	2.4
Transporter activity				
	1448299_at	Slc1a1/EAAC1 glutamate transporter	-1.7	-4.4
	1426376_at	Dp1/Reep5	-1.3	-2.0
	1422158_at	Clstn2	-1.5	-3.8
	1437675_at	Slc8a1/Ncx1 Na ⁺ /Ca ²⁺ exchanger	-1.0	-3.2
	1426340_at	Slc1a3/GLAST	1.0	1.7
	1416637_at	Slc4a2/Ae2 anion exchanger	1.1	1.7
Cell Cycle				
	1427005_at	Plk2	-1.1	-5.3
	1450677_at	Chek1	1.2	2.6
	1456280_at	Clspn	1.2	2.5
	1455980_a_at	Gas2l3	1.0	2.9
	1424128_x_at	Aurkb	1.2	3.1
	1448314_at	Cdc2a	1.0	3.1
	1439394_x_at	Cdc20	1.5	3.8
	1455730_at	Dlg7	1.3	3.6
	1422747_at	Chek2	1.0	2.1
	1448494_at	Gas1	1.2	2.6
	1447363_s_at	Bub1b	1.1	3.2
	1426653_at	Mcm3	2.2	4.3
	1426955_at	Col18a1/endostatin	1.2	2.9
	1417327_at	Cav2	1.4	2.5

	1451042_a_at	Mina	1.1	2.1
	1453107_s_at	Foxm1/Pbp	1.4	2.6
Signal transduction				
	1424896_at	Gpr85	-1.0	-3.5
Small GTPase related genes				
	1455840_at	Rapgef5	-1.1	-3.2
	1450931_at	Dock9	-1.2	-2.8
	1447669_s_at	Gng4	-1.2	-3.1
	1428268_at	Psd2	-1.1	-3.0
	1453093_at	Rasgef1c	-1.3	-1.8
	1424482_at	Arhgef7	-1.0	-2.6
	1437674_at	Rac1	-0.2	-1.1
	1450896_at,			
	1450897_at	Arhgap5	1.3	2.3
	1438543_at	Spata13	1.0	1.7
	1437628_s_at	RhoA	1.1	2.3
	1427918_a_at	Rhoq	1.7	1.2
Notch signaling				
	1421105_at	Jag1	1.7	0.6
	1421964_at	notch3	1.8	2.7
	1418634_at	notch1	1.0	3.1
Wnt signaling				
	1417937_at	Dact1/Frodo	-1.8	-3.6
	1427529_at	Fzd9	1.0	2.3
	1423348_at	Fzd8	1.3	2.6
	1450117_at	tcf3	1.1	2.8
BMP signaling				
	1429273_at	Bmper/Cv2	1.2	2.6
Chemokine				
	1417625_s_at	Cmkor1/Cxcr7	-1.0	-2.2
Growth factor activity				
	1449545_at	Fgf18	-1.2	-2.6
	1415855_at	Kitl	-1.5	-2.6
	1418498_at	Fgf13	2.0	1.3
	1449041_a_at	Trip6	1.0	2.8
	1438303_at	Tgfb2	1.2	1.4
	1424932_at	Egfr	1.4	0.9
Protein metabolism				
	1455733_at	A130052D22/Taok3	-1.1	-2.6
	1456606_a_at	Chst11 /// Phactr1	-1.2	-3.2
	1433596_at	Dnajc6	-1.3	-3.3
	1418085_at	Prkcz	-1.1	-2.7
	1445767_at	Ptprd	-1.8	-3.6
	1437195_x_at	Mapk10	-2.0	-3.6
	1456527_at	Hecw1	-1.2	-3.4
	1434325_x_at	Prkar1b	-1.1	-3.5
	1455401_at	Camkk2	-1.1	-2.0
	1455346_at	Masp1	-1.0	-2.3
	1417676_a_at	Ptpro	-1.4	-4.9
	1433826_at	AW212607/Tsyp13	-1.1	-2.4
	1439843_at	Camk4	-1.8	-4.2
	1415834_at	Dusp6	-1.5	-4.3
	1418046_at	Nap1l2c	-1.1	-2.8
	1434017_at,	Znrf2	-1.1	-2.9
	1455378_at	BC057371	-1.3	-2.6
	1435793_at	Aph1b	-1.0	-2.1

1429298_at	Ddah1	1.0	2.5
1434891_at	Ptgfrn	1.1	2.8
1418649_at	Egln3	1.2	3.1
1450843_a_at	Serpinh1	1.4	2.7
1423596_at	Nek6	1.0	2.6

Riken genes

1436088_at	0910001A06Rik	-0.9	-1.8
1455484_at	2600009P04Rik	-0.3	-1.7
1441693_at	6330442E02Rik	-1.6	-3.5
1425616_a_at	2410005K17Rik	-0.5	-1.4
1448251_at	9030425E11Rik	-1.2	-3.6
1456609_at	1810006K23Rik	-0.9	-3.0
1453008_at	2300002D11Rik	-0.8	-3.1
1424099_at	2310016C16Rik	1.2	3.4
1435678_at	2610017I09Rik	0.4	1.9
1428452_at	2810025M15Rik	0.7	2.2

The table includes mean fold change of 158 differentially expressed genes (with 2 fold or higher difference and absolute expression higher than 50) between the GFP^{high}/GFP^{low} fractions and GFP/prominin double conjugated fractions, organized according to their gene ontology function. Fold change is represented in log (2) with positive values representing higher expression in the GFP^{high} and negative values higher in the GFP^{low} lineages.

Table 2: Genes differentially expressed in the GFP^{low}/^{high} but absent in the GFP/Prominin sorted cells

	<i>Probe set</i>	<i>Gene</i>	<i>Fold change GFP^{high}/GFP^{low}</i>
a)	1423500_a_at	Sox5	-2.6
	1420925_at	Tub	-3.0
	1420892_at	Wnt7b	-2.3
	1427017_at	Satb2	-2.2
	1417885_at	Mapt	-4.9
	1451990_at	Mapre2	-1.6
	1421017_at	Nrg3	-2.5
	1416711_at	Tbr1	-2.4
	1427347_s_at	Tub2b	-2.4
	1420530_at	Neud4	-3.1
	1434194_at	Mtap2	-1.4
b)	1436694_s_at	Neurod4	3.1
	1426001_at	Eomes/Tbr2	2.6
	1422839_at	Neurog2	2.4

The table includes example of genes expressed in the GFP^{low}/GFP^{high} subsets but not present in the GFP/prominin sorted cells differentially expressed list of genes, with negative **a)** and positive **b)** values representing higher expression in the GFP^{low} and in the GFP^{high} subsets. Values are shown in log (2) scale.

Table 3a: mRNAs differentially expressed in the GFP^{low} but absent in the GFP^{low}/Prominin sorted cells

ProbesetID	GeneSymbol	ProbesetID	GeneSymbol	ProbesetID	GeneSymbol
1425863_a_at	Ptpro	1436013_at	C230098I05Rik	1428118_at	Lrrn6a
1420818_at	Sla	1456500_at	Aph1b	1419517_at	Cnih3
1421922_at	Sh3bp5	1417747_at	Cplx1	1426785_s_at	Mgll
1416754_at	Prkar1b	1437472_at	Unc13a	1435780_at	Psd
1420901_a_at	Hk1	1434270_at	Nptxr	1452249_at	Prickle1
1422779_at	Smpd3	1416114_at	Sparcl1	1423630_at	Cygb
1427481_a_at	Atp1a3	1458268_s_at	Igfbp3	1430686_at	4833418N02Rik
1431045_at	D12Ert553e	1443997_at	C130040D06Rik	1436250_at	5430405G05Rik
1450486_a_at	Oprl1	1457936_at	Mapk8	1454902_at	Prkcz
1431137_at	Rusc1	1434728_at	Gria3	1419489_at	AW049604
1420891_at	Wnt7b	1426959_at	Bdh	1434194_at	Mtap2
1420146_at	Tiam2	1421192_a_at	Itsn1	1448676_at	Camk2b
1451250_at	Gprin1	1430307_a_at	Mod1	1437386_at	Lrrn6a
1420885_a_at	Sez6	1444956_at	---	1435038_s_at	Aak1
1418452_at	Gng2	1438017_at	Rusc1	1437214_at	Lrrtm4
1457066_at	Abcc8	1420938_at	Hs6st2	1451601_a_at	BC011467
1452806_at	1500016O10Rik	1434429_at	Syt16	1448487_at	Lrrfip1
1416936_at	Aatk	1457446_at	Opcml	1436602_x_at	Cacna1b
1426791_at	Rusc2	1439021_at	Centb5	1422531_at	Syt5
1421606_a_at	Sult4a1	1417520_at	Nfe2l3	1437366_at	AI608492
1449228_at	Sh3gl2	1423544_at	Ptpn5	1426972_at	Sec24d
1442019_at	B230343A10Rik	1419237_at	Usp29	1448019_at	2900006A08Rik
1421190_at	Gabrb3	1424379_at	Car11	1424942_a_at	Myc
1423557_at	Ifngr2	1452202_at	Pde2a	1439743_at	AW048948
1455526_at	Diras1	1416711_at	Tbr1	1420799_at	Ntsr1
1432189_a_at	Sox5	1418161_at	Jph3	1419745_at	Arhgap23
1442175_at	C030027H14Rik	1424726_at	BC014685	1443306_at	---
1418655_at	Galgt1	1457270_at	B230343A10Rik	1425202_a_at	Ank3
1451484_a_at	Syn1	1437787_at	---	1432182_at	4922502B01Rik
1418247_s_at	Rbm9	1435261_at	4732416N19Rik	1435968_at	---
1451094_at	Ggtl3	1427017_at	Satb2	1427347_s_at	Tubb2 /// 2410129E14Rik /// LOC544939
1438780_at	---	1421017_at	Nrg3	1418177_at	Gabrg2
1426517_at	Gnaz	1416305_at	Sh3bp4	1420529_at	Neud4
1439333_at	Kcnv1	1420925_at	Tub	1455344_at	AW494418
1451331_at	Ppp1r1b	1435310_at	A230052G17Rik	1418500_at	Nap1l3
1416786_at	Acvr1	1449956_at	Prkce	1423288_s_at	Cbln1
1433815_at	MGI:1923321	1421255_a_at	Cabp1	1423062_at	Igfbp3
1452663_at	1110030H18Rik	1435026_at	Spock2	1434467_at	Atcay
1425180_at	Sgip1	1455443_at	---	1437574_at	Adamts18
1436961_at	Hspa12a	1455406_at	---	1460223_a_at	Epb4.9
1454972_at	Atcay	1418360_at	Zfp179		
1435239_at	Gria1	1434221_at	BC030863		
1429274_at	2310010M24Rik	1425656_a_at	Baiap2		
1426792_s_at	Rusc2	1421090_at	Epb4.1l1		
1450977_s_at	Ndr1 /// Ndr1	1456944_at	C230009H10Rik		
1451990_at	Mapre2	1452728_at	Kirrel3		
1433526_at	Klhl8	1449563_at	Cntn1		
1421124_at	Cdk5r1	1426991_at	1810048J11Rik		
1417885_at	Mapt	1429131_at	Ube2v2		

Complete list of differentially expressed mRNAs, with respective probe-set ID, highly expressed in the GFP^{low} subset but absent in the GFP^{low}/prominin+ radial glia subset.

Table 3b: mRNAs differentially expressed in the GFP^{high} but absent in the GFP^{high}/Prominin sorted cells

ProbesetID	GeneSymbol	ProbesetID	GeneSymbol	ProbesetID	GeneSymbol
1450379_at	Msn	1429734_at	4632434I11Rik	1429809_at	8430438D04Rik
1448127_at	Rrm1	1443694_at	Rgs20	1452715_at	2310022K01Rik
1426341_at	Slc1a3	1417926_at	Luzp5	1435246_at	Paqr8
1416043_at	Nasp	1418102_at	Hes1	1424107_at	Kif18a
1426653_at	Mcm3	1416774_at	Wee1	1422839_at	Neurog2
1415811_at	Uhrf1	1452924_at	2310007D09Rik	1418026_at	Exo1
1421102_a_at	Vamp3	1423613_at	---	1455544_at	Zranb3
1427797_s_at	Ctse	1433892_at	Spag5	1432361_a_at	1700022C02Rik
1449293_a_at	Skp2	1417862_at	A830059I20Rik	1448638_at	Mtbp
1427579_at	Rhbdl4	1448369_at	Pola2	1455271_at	1810020C19Rik
1448834_at	Foxm1	1452458_s_at	Ppil5	1436694_s_at	Neurod4
1420847_a_at	Fgfr2	1450496_a_at	2810433K01Rik	1437872_at	AB112350
1450113_at	---	1417019_a_at	Cdc6	1436738_at	Al449441
1422544_at	Myo10	1434666_at	Pcgf5	1418481_at	Pkmyt1
1454221_a_at	Kif2c	1433807_at	6720463M24Rik	1435054_at	Eme1
1419361_at	Ss18	1424971_at	2600001J17Rik	1436332_at	Hspb6
1428304_at	Esco2	1436931_at	Rfx4	1457157_at	Plcl3
1454011_a_at	Rpa2	1436186_at	4432406C08Rik	1425178_s_at	Shmt1
1431430_s_at	Trim59	1434911_s_at	Arhgap19	1422535_at	Ccne2
1452315_at	Kif11	1423718_at	Ak3	1452386_at	Sall3
1417986_at	Nrarp	1427100_at	Metrn		
1417401_at	Rai14	1420897_at	Snap23		
1424950_at	Sox9	1425476_at	Col4a5		
1426001_at	Eomes	1452714_at	1200003E16Rik		
1426110_a_at	Edg2	1417445_at	Kntc2		
1421262_at	Lipg	1422598_at	Casq1		
1449060_at	Kif2c	1450156_a_at	Hmmr		
1422879_at	Sypl	1451287_s_at	2810003C17Rik		
1449699_s_at	C330027C09Rik	1428774_at	Gpc6		
1426314_at	Ednrb	1436723_at	Fshprh1		
1415989_at	Vcam1	1423311_s_at	Tpbg		
1425416_s_at	5430413I02Rik	1435292_at	Tbc1d4		
1426340_at	Slc1a3	1433623_at	Zfp367		
1429299_at	Ddah1	1444761_at	---		
1450489_at	Sall1	1452881_at	4833427B12Rik		
1419382_a_at	Dhrs4	1452912_at	2600005O03Rik		
1434279_at	---	1455262_at	0610010D24Rik		
1417748_x_at	Foxm1	1436913_at	Cdc14a		
1425796_a_at	Fgfr3	1434286_at	Trps1		
1436665_a_at	Ltbp4	1428227_at	Rest		
1451246_s_at	Aurkb	1423049_a_at	Tpm1		
1422146_at	Sema5b	1427062_at	Rbbp8		
1423813_at	Kif22	1425177_at	Shmt1		
1456652_at	Dtl	1425597_a_at	Qk		
1426231_at	Vit	1425179_at	Shmt1		
1423586_at	Axl	1424766_at	Ercc6l		
1422528_a_at	Zfp36l1	1454350_at	Pdzk6		
1422513_at	Ccnf	1421317_x_at	Myb		
1420643_at	Lfng	1427568_a_at	Wdr56		

Complete list of differentially expressed mRNAs, with respective probe-set ID, highly expressed in the GFP^{high} subset but absent in the GFP^{high}/prominin+ radial glia subset.

Table 4: Cell surface genes significantly expressed in the distinct subsets of radial glial cells

<i>Gb-ID</i>	<i>Gene</i>	<i>Fold change GFP^{high}/prominin+/ GFP^{low}/prominin+</i>
NM_033217	Ngfr/p75	-4.4
BB817332	Flrt2	-4.1
NM_009856	CD83	-2.3
NM_133239	Crb1	-1.4
AK018789	Ntrk2	-1.0
NM_021324	Ttyh1/Ly6h	4.4
BB209710	CD163c-alpha	3.4
BB801134	Sema5b	2.3

List of cell surface genes significantly expressed in the GFP^{low}/prominin+ (negative values) and in the GFP^{high}/prominin+ (positive values) subsets with respective fold change in log (2) scale.

Table 5: Differentially expressed genes between subsets of radial glia at mid-neurogenesis and radial glia at the end of neurogenesis

Function (GO annotation)	Probe set	Gene	Fold change (FC)	
			FC E18 prom+ vs E14 GFP ^{low} /prom+	FC E18 prom+ vs E14 GFP ^{high} /prom+
<i>Transcription factor activity</i>				
	1460700_at	Stat3	-----	-1.4
	1448519_at	Tead2	-1.2	-2.2
	1448977_at	Tcfap2c	-2.4	-2.9
	1457289_at	Nr2e1/Tlx	-2.7	-3.5
	1448835_at	E2f6	-1.7	-1.7
	1437187_at	E2f7	-1.3	-1.7
	1432189_a_at	Sox5	-2.3	-1.8
	1447655_x_at	Sox6	-1.5	-2.0
	1451538_at	Sox9	----	-1.7
	1437059_at	Sox21	-----	-1.6
	1441777_at	Emx1	-1.9	-2.4
	1419271_at	Pax6	-----	-1.7
	1422839_at	Neurog2	-1.8	-2.4
	1438551_at	Neurog1	-5.1	-6.7
	1416711_at	Tbr1	-1.2	-----
	1416149_at	Olig1	6.7	5.7
	1432007_s_at	Ap2a2	1.6	1.6
	1421027_a_at	Mef2c	1.4	2.4
	1453478_at	Pou3f2/Brn2	2.2	1.9
	1460038_at	Pou3f1/Brn1	1.1	1.1
	1440954_at	Pbx1	2.3	2.3
<i>Basic helix-loop-helix</i>				
	1415999_at	Hey1	-1.9	-2.0
	1456010_x_at	Hes5	-----	-1.7
	1423260_at	Id4	----	-1.7
	1422537_a_at	Id2	----	1.2
<i>Distal less homeobox</i>				
	1449470_at	Dlx1	3.5	4.4
	1448877_at	Dlx2	2.6	2.7
	1449863_a_at	Dlx5	2.1	2.7
<i>LIM homeobox</i>				
	1417627_a_at	Limk1	-2.2	-1.8
	1425094_a_at	Lhx6	1.9	2.5
<i>Gliogenesis</i>				
	1419700_a_at	Prominin1	-1.3	-2.1
	1450641_at	Vim	----	-1.7
	1451461_a_at	AldoC	-----	-1.3
	1447043_at	ErbB4	3.7	3.9
	1450779_at	Fabp7	1.7	1.3
	1416342_at	TNC	3.4	3.3
<i>Oligodendrogenesis</i>				
	1416149_at	Olig1	6.7	5.7
	1416232_at	Olig2	----	4.1
	1449187_at	Pdgfra	----	1.2

Neurogenesis/Neuronal differentiation

1422839_at	Neurog2	-1.8	-2.4
1438551_at	Neurog1	-5.1	-6.7
1418024_at	Narg1	-1.3	-1.3
1416711_at	Tbr1	-1.2	----
1449465_at	Reln	-1.8	1.0
1434465_x_at	Vldl3	----	1.0
1424271_at	Dcamk1	----	1.1
1421100_a_at	Dab1	----	1.3
1418178_at	Ina	----	1.2
1448296_x_at	Tuba3 /// Tuba7	----	1.2

Neurotransmitter secretion/receptor

1415845_at	Syt4	2.0	3.0
1433884_at	Syt1	---	1.9
1428240_at	Nrxn1	----	1.6
1435908_at	Nrxn2	---	1.1
1456137_at	Nrxn3	2.4	2.8
1455444_at	Gabra2	3.3	3.8
1423187_at	Gabarapl2	1.3	1.2
1416418_at	Gabarapl1	1.1	----
1435021_at	Gabrb3	---	2.3

Axon guidance

1459453_at	Robo1	2.6	3.0
1458229_at	Robo2	1.3	1.4
1454022_at	Ephb2	1.8	---
1424659_at	Slit2	1.0	----
1454708_at	Ablim1	----	1.4

Cell adhesion

1421344_a_at	Jub	-2.1	-3.3
1423503_at	Jam3	-1.1	-1.1
1437807_x_at	Ctnna1	-1.1	-1.6
1426865_a_at	Ncam	1.2	1.6
1441995_at	Ncam1	1.9	1.8
1430533_a_at	Ctnnb1	1.1	1.5
1435807_at	Cdc42	----	1.6
1448895_a_at	Ctnna2	---	1.4
1418815_at	Cadh2	1.2	1.4

Cytoskeleton

1434748_at	Ckap2	-1.2	-1.8
1431035_at	Daam1	-1.1	----
1428132_at	Cdc42se1	----	-1.1
1416511_a_at	Cdc42ep4	----	-1.0
1457374_at	Nedd4l	1.5	1.4
1455244_at	Daam1	1.4	1.8
1435847_at	Cdc42bpa	----	1.3

Chromatin remodeling

1452333_at	Smarca2	-1.9	-1.4
1423417_at	Smarcc1	-1.6	-1.8
1424207_at	Smarca5	-1.4	-1.5
1426805_at	Smarca4	-1.2	-1.3
1435856_x_at	Smarcb1	-1.1	----
1459859_x_at	Chrac1	-1.0	-1.2
1420813_at	Hdac7a	1.2	----

Symmetric/asymmetric cell division

1418925_at	Celsr1	-1.8	-2.6
------------	--------	------	------

	1422073_at	Celsr2	-1.2	-1.5
	1436764_at	Pard3	-1.2	-1.5
	1420851_at	Pard6g	----	-1.1
Transporter activity				
	1417416_at	Kcna1	-2.3	-1.3
	1443749_x_at	Slc1a3/glast	1.4	----
	1448299_at	Slc1a1	----	2.6
	1437675_at	Slc8a1	1.3	2.3
	1457528_at	Slc4a7	1.5	1.2
	1448676_at	Camk2b	1.4	2.3
Cell cycle				
	1448494_at	Gas1	-2.2	-3.4
	1437244_at	Gas2l3	-1.5	-2.3
	1416961_at	Bub1b	-1.7	-2.5
	1420028_s_at	Mcm3	-1.6	-2.4
	1448777_at	Mcm2	-1.4	-2.4
	1419943_s_at	Ccnb1	-1.5	-2.3
	1417419_at	Ccnd1	-1.1	-1.7
	1450920_at	Ccnb2	-1.3	-2.2
	1439377_x_at	Cdc20	-1.5	-2.4
	1416802_a_at	Cdca5	-1.4	-2.2
	1455983_at	Cdca2	-1.2	-2.0
	1422747_at	Chek2	-1.0	-2.1
	1422440_at	Cdk4	-1.0	-1.2
	1416816_at	Nek7	-1.2	-1.7
	1418947_at	Nek3	-1.3	----
	1424511_at	Aurka	----	-1.2
	1448191_at	Plk1	----	-1.5
	1427005_at	Plk2	----	1.6
	1424843_a_at	Gas5	1.1	----
Signal transduction				
	1426782_at	Gpr125	-1.1	-1.3
	1421118_a_at	Gpr65	-1.0	-1.4
	1443535_at	Gpr21	1.8	1.5
	1424896_at	Gpr85	----	1.8
Small GTPase related genes				
	1423194_at	Arhgap5	-1.4	-1.7
	1421546_a_at	Racgap1	----	-1.5
	1451159_at	Arhgef12	1.2	1.3
	1447206_at	Arhgap21	2.1	1.5
	1424482_at	Arhgef7	----	1.6
	1444028_s_at	Dock9	2.1	3.3
	1423445_at	Rock1	1.1	1.4
Notch signaling				
	1421965_s_at	Notch3	-1.4	-2.3
	1418634_at	Notch1	-1.1	-2.1
	1455556_at	Notch2	0.9	----
	1456379_x_at	Dner/ delta/notch-like EGF-related receptor	----	1.4
Wnt signaling				
	1436207_at	Tcf3	-3.6	-4.5
	1418534_at	Fzd2	-1.7	-2.3
	1423348_at	Fzd8	-1.5	-2.8
	1449730_s_at	Fzd3	-1.4	-1.7
	1427529_at	Fzd9	-1.1	-2.1
	1420892_at	Wnt7b	-1.4	-1.0
	1428136_at	Sfrp1	-1.2	-1.8

	1423809_at	Tcf19	-----	-1.1
	1439949_at	Gsk3b	1.1	1.1
	1434149_at	Tcf4	1.8	1.3
	1421910_at	Tcf20	1.2	1.4
<i>BMP signaling</i>				
	1419616_at	Bmpr2	-1.6	-2.0
	1416081_at	Smad1	-1.5	-1.4
	1454960_at	Smad3	-1.2	-1.9
<i>Shh signaling</i>				
	1446086_s_at	Gli2	-1.9	-2.5
	1455154_at	Gli3	-1.6	-2.2
	1428853_at	Ptch1	-----	1.2
<i>Chemokine</i>				
	1448823_at	Cxcl12	-1.5	-1.9
	1448710_at	Cxcr4	1.1	2.5
<i>Growth factor activity</i>				
	1447878_s_at	Fgfr1	-1.0	-1.4
	1449041_a_at	Trip6	-1.7	-2.7
	1417694_at	Gab1	-1.3	-----
	1439959_at	Fgf11	-----	-1.1
	1421841_at	Fgfr3	-----	-1.5
	1435305_at	Ntrk2	1.0	2.5
	1455917_at	Ntrk3	1.7	1.7
<i>Apoptosis regulation</i>				
	1437537_at	Caspase9	-1.1	-----
<i>Riken genes</i>				
	1424099_at	2310016C16Rik	----	-1.7
	1428452_at	2810025M15Rik	----	-1.3
	1436088_at	0910001A06Rik	----	1.4
	1441693_at	6330442E02Rik	----	1.4
	1448250_at	9030425E11Rik	----	1.4
	1456609_at	1810006K23Rik	----	1.6

The table includes mean fold change of 156 differentially expressed genes (with 2 fold or higher difference and absolute expression higher than 50) between E18 GFP/prominin+ radial glia and GFP/prominin double conjugated fractions from E14 cortices, organized according to their gene ontology function. Fold change is shown in log (2) with positive values representing higher expression in E18 sorted cells and negative values higher in the E14 lineages.

Table 6 - Transcriptome analysis of E14 WT and AP2γ^{-/-} cortices

a - Caudal cortex

Probe Set ID	Gene Title	GeneSymbol	Entrez Gene	Chromosomal Location	Mas Av_c_ko	Mas Av_c_wt	Mas Ratio
1435513_at	5-hydroxytryptamine (serotonin) receptor 2C	Htr2c	15560	chrX D-F4 X 66.15 cM	6	63	0.09
1436694_s_at	neurogenic differentiation 4	Neurod4/Math3	11923	chr10 D3 10 72.0 cM	17	86	0.20
1424713_at	calmodulin-like 4	Calm4	75600	chr9 B	14	63	0.23
1428942_at	metallothionein 2	Mt2	17750	chr8 C5 8 45.0 cM	129	430	0.30
1457797_at	expressed sequence AI605517	AI605517	106622		19	57	0.34
1426225_at	retinol binding protein 4, plasma	Rbp4	19662	chr19 D1 19 38.0 cM	31	88	0.35
1423261_at	RIKEN cDNA 1500015O10 gene	1500015O10Rik	78896	chr1 C1	31	87	0.35
1429181_at	RIKEN cDNA 1700009P17 gene	1700009P17Rik	75472	chr1 H3	32	71	0.45
1416776_at	crystallin, mu	Crym	12971	chr7 F2 7 55.0 cM	133	285	0.47
1448977_at	transcription factor AP-2, gamma	Tcfap2c	21420	chr2 H3-H4	127	267	0.48
1422596_at	RIKEN cDNA C030019F02 gene	C030019F02Rik	58237	chr2 H4	74	153	0.48
1416749_at	HtrA serine peptidase 1	Htra1	56213	chr7 F3	157	309	0.51
1425749_at	syntrophin binding protein 6 (amisyn)	Stxbp6	217517	chr12 B3	113	219	0.51
1428077_at	transmembrane protein 163	Tmem163	72160	chr1 E3	99	187	0.53
1424367_a_at	homer homolog 2 (Drosophila)	Homer2	26557	chr7 D3	171	315	0.54
1425396_a_at	lymphocyte protein tyrosine kinase	Lck	16818	chr4 D2.2 4 59.0 cM	53	96	0.55
1422557_s_at	metallothionein 1	Mt1	17748	chr8 C5 8 45.0 cM	162	293	0.55
1417120_at	DNA segment, Chr 4, Wayne State University 114, expressed	D4Wsu114e	28010	chr4 E2 4 76.4 cM	98	174	0.56
1424854_at	histone cluster 1, H4i	Hist1h4i	319158		42	74	0.57
1434165_at	chloride intracellular channel 6	Clic6	209195	chr16 C4	56	94	0.59
1449145_a_at	caveolin, caveolae protein 1	Cav1	12389	chr6 A2	265	439	0.60
1426587_a_at	signal transducer and activator of transcription 3	Stat3	20848	chr11 D 11 60.5 cM	99	162	0.61
1421895_at	eukaryotic translation initiation factor 2, subunit 3, structural	Eif2s3x	26905	chrX C-D X 32.0 cM	248	400	0.62
1436791_at	wingless-related MMTV integration site 5A	Wnt5a	22418	chr14 A3 14 7.8 cM	40	63	0.65
1424659_at	slit homolog 2 (Drosophila)	Slit2	20563	chr5 B3	230	355	0.65
1426001_at	eomesodermin homolog (Xenopus laevis)	Eomes	13813	chr9 F3 9 67.0 cM	918	1417	0.65
1444216_at	empty spiracles homolog 1 (Drosophila)	Emx1	13796	chr6 C3 6 35.5 cM	104	165	0.6
1418072_at	histone cluster 1, H2bc	Hist1h2bc	68024	chr13 A3.1	193	294	0.65
1416630_at	inhibitor of DNA binding 3	Id3	15903	chr4 D3 4 66.0 cM	92	141	0.65
1436207_at	transcription factor 3	Tcf3	21415	chr6 C1 6 30.4 cM	187	286	0.66
1425621_at	tripartite motif-containing 35	Trin35	66854	chr14 D1	138	208	0.66
1420981_a_at	LIM domain only 4	Lmo4	16911	chr3 H2 3 73.1 cM	560	842	0.66
1426528_at	neuropilin 2	Nrp2	18187	chr1 C2	80	117	0.68
1450843_a_at	serine (or cysteine) peptidase inhibitor, clade H, member 1	Serpinh1	12406	chr7 E1	368	542	0.68
1456901_at	a disintegrin-like and metalloprotease (reprolysin type) with	Adams20	223838	chr15 E3 15 44.4 cM	164	239	0.69
1422465_a_at	nucleoredoxin	Nxn	18230	chr11 B5 11 45.2 cM	256	367	0.70
1423854_a_at	RAS-like, family 11, member B	Rasl11b	68939	chr5 D	288	408	0.71
1448660_at	Rho GDP dissociation inhibitor (GDI) gamma	Arhgdig	14570	chr17 A3.3	84	118	0.72
1434580_at	ectonucleotide pyrophosphatase/phosphodiesterase 4	Enpp4	224794	chr17 B3	141	193	0.73
1435339_at	potassium channel tetramerisation domain containing 15	Kctd15	233107	chr7 B1	818	1116	0.73
1426053_a_at	xenotropic and polytropic retrovirus receptor 1	Xpr1	19775	chr1 G3 1 81.6 cM	57	77	0.73
1422196_a_at	serine hydroxymethyltransferase 1 (soluble)	Shmt1	20425	chr11 B2	41	56	0.74
1423824_at	G protein-coupled receptor 177	Gpr177	68151	chr3 H4	55	74	0.74
1419247_at	regulator of G-protein signaling 2	Rgs2	19735	chr1 F 1 78.0 cM	166	222	0.75
1428717_at	secernin 1	Scrn1	69938	chr6 B3	439	300	1.5
1418666_at	pentraxin related gene	Ptx3	19288	chr3 E1 3 33.8 cM	861	559	1.5
1440668_at	ADAMTS-like 3	Adamts3	269959	chr7 D3	124	78	1.6
1435204_at	protein arginine N-methyltransferase 8	Prmt8	381813	chr6 F3	423	239	1.8
1416846_a_at	PDZ domain containing RING finger 3	Pdzrn3	55983	chr6 D3	627	322	1.9
1449571_at	thyrotropin releasing hormone receptor	Trhr	22045	chr15 B3.2 15 24.7 cM	97	42	2.3
1417795_at	cell adhesion molecule with homology to L1CAM	Chl1	12661		194	60	3.3

b - Rostral cortex

Probe Set ID	Gene Title	GeneSymbol	Entrez Gene	Chromosomal Location	Mas Av_r_ko	Mas Av_r_wt	Mas Ratio
1436694_s_at	neurogenic differentiation 4	Neurod4	11923	chr10 D3 10 72.0 cM	33	143	0.2
1455056_at	LIM domain only 7	Lmo7	380928	chr14 E2.3	76	200	0.4
1429833_at	lymphocyte antigen 6 complex, locus G6E	Ly6g6e	70274		39	84	0.5
1425952_a_at	glucagon	Gcg	14526	chr2 C1.3 2 36.0 cM	27	58	0.5
1425396_a_at	lymphocyte protein tyrosine kinase	Lck	16818	chr4 D2.2 4 59.0 cM	58	97	0.6
1431422_a_at	dual specificity phosphatase 14	Dusp14	56405	chr11 C 11 48.0 cM	266	415	0.6
1452714_at	tetratricopeptide repeat, ankyrin repeat and coiled-coil containing 1	Tanc1	66860	chr2 C1.1	99	151	0.7
1436392_s_at	transcription factor AP-2, gamma	Tcfap2c	21420	chr2 H3-H4	315	473	0.7
1452067_at	N-acylsphingosine amidohydrolase (acid ceramidase)-like	Asah1	67111	chr5 E3	78	55	1.4
1455141_at	trinucleotide repeat containing 6a	Tnrc6a	233833	chr7 F3	593	403	1.5
1455696_a_at	PRP4 pre-mRNA processing factor 4 homolog B (yeast)	Prpf4b	19134	chr13 A5	693	466	1.5
1440108_at	forkhead box P2	Foxp2	114142	chr6 A2	347	224	1.6
1454793_x_at	DEAD (Asp-Glu-Ala-Asp) box polypeptide 5	Ddx5	13207	chr11 E2 11 63.0 cM	1537	967	1.6
1435297_at	gap junction membrane channel protein alpha 9	Gja9	14617	chr2 F3	119	70	1.7
1428607_at	v-raf murine sarcoma 3611 viral oncogene homolog	Araf	11836	chrX A2-A3.1 X 6.2 cM	229	120	1.9
1435204_at	protein arginine N-methyltransferase 8	Prmt8	381813	chr6 F3	384	206	1.9
1449571_at	thyrotropin releasing hormone receptor	Trhr	22045	chr15 B3.2 15 24.7 cM	108	51	2.1
1437262_x_at	breast carcinoma amplified sequence 2	Bcas2	68183	chr3 F2.2	160	59	2.7

Table 6. Transcriptome analysis of E14 WT and AP2γ^{-/-} cortices

The table includes the average absolute expression (Mas Av_ko=average for AP2γ^{-/-} and Mas_Av_WT=average for WT) and mean fold change of the significant genes (Mas ratio (ko/wt) – 1.5 fold or higher difference, absolute expression higher than 50 and significant in at least 2 statistical tests – see Materials and Methods) differentially expressed between E14 WT and AP2γ^{-/-} (ko) cortices at intermediate to caudal (**a**) and rostral (**b**) regions. Abbreviations; Av=average; c= intermediate-caudal regions; r=rostral regions.

Table 7 - Visual performance of adult WT and AP2 γ ^{-/-} mice

	Visual acuity (c/deg)	VEP inversion (μ m from dura)	Vertical meridian (mm from λ)	Contrast threshold	Temporal resolution (Hz)	Contra/Ipsi ratio	Response latency (ms)	Cortical magnification ($^{\circ}$ /0.1 mm)
control (Mean)	0.57 (N=6)	250 (N=4)	3.31 (N=6)	0.054 (N=6)	10.67 (N=3)	2.81 (N=6)	109.95 (N=6)	5.92 (N=4)
AP2γ^{-/-} (Mean)	0.38 (N=7)	200 (N=5)	3.25 (N=8)	0.046 (N=7)	9.4 (N=5)	1.9 (N=8)	127.19 (N=7)	5.8 (N=5)
control (SEM)	0.03	12.5	0.0461	0,00678	1,333	0,365	3,815	0,458
AP2γ^{-/-} (SEM)	0.0306	46.3249	0.0549	0,00429	0,765	0,157	6,447	0,555
t-test (P-value)	0.002	0.556	0.387	0.302	0.404	0.027	0.05	0.873
	**	N.S	N.S	N.S	N.S	*	N.S	N.S

Table 7. Visual performance of adult WT and AP2 γ ^{-/-} mice

The table includes visual performance examination by recording visual evoked potentials (VEPs) from the visual cortex in response to grated patterns. VEPs were analyzed in regard to visual acuity, VEP inversion, vertical meridian, contrast threshold, temporal resolution, contra/ipsilateral ratio, response latency and cortical magnification. Note the significant decrease in visual acuity and contra/ipsilateral ratio in the AP2 γ ^{-/-} 6-7 months old mice.

8 Discussion

8.1 Lineage analysis at the transcriptome level – new insights into functionally distinct radial glial subtypes

Here I showed for the first time the prospective isolation of distinct radial glia subtypes that differ in their progeny. We devised a strategy to examine not only the RGCs themselves, but also their immediate progeny by clonal analysis *in vitro* and expression profiling. Using a strong version of the GFP, the enhanced GFP, driven by the promoter element hGFAP (hGFAP-eGFP, (Nolte et al., 2001)), the GFP labelled cells revealed a high fraction of non-radial glia, supposedly due to persistence of GFP into the progeny of RGCs. By *in vitro* and *in vivo* experiments we could exclude the possibility that GFP was ectopically expressed in non-RGCs, but persisted into the progeny of RGCs. This allowed us to follow RGCs and their immediate lineage by using this GFP line and isolating all GFP-positive cells. These could then be compared with isolation of the GFP-positive cells that are in contact with the ventricle by double-staining for the apical membrane protein prominin (Götz and Huttner, 2005), i.e. the RGCs only. We have shown that the fraction of RGCs (prominin+) isolated from mid-neurogenesis mouse cerebral cortex that has weaker levels of GFP expressed under control of the hGFAP promoter was largely restricted to the generation of neurons only (pure neuronal clones) *in vitro*. Conversely, the fraction of RGCs (prominin+) with higher levels of hGFAP-eGFP largely generated non-neuronal progeny. The few neurons that these RGCs generated seem to be produced via the generation of Tbr2+ basal progenitors *in vitro*. This lineage analysis *in vitro* was confirmed by the isolation of RGCs and their progeny from the cortex *in vivo*, taking advantage of the stability of GFP. Sorting of cells with lower GFP levels resulted in the isolation of mostly neurons and only few RGCs. However, virtually no basal progenitors were contained in this fraction. Thus, the composition of the GFP^{low} fraction isolated from the cortex *in vivo* was fully consistent with the progeny generated from the RGCs contained in this fraction (GFP^{low}/prominin+) *in vitro* (many neurons but few Tbr2+ basal progenitors). The same consistency was found when GFP^{high} cells were isolated by FACS. They contained a higher proportion of dividing RGCs, consistent with the generation of many (radial) glial cells from the RGCs contained in this fraction (GFP^{high}/prominin+) *in vitro*. Moreover, GFP^{high} cells isolated from the E14 cortex contained many basal progenitors as identified by immunostaining of the sorted cells for Tbr2, as well as at the transcriptome level.

Our transcriptome analysis further supported the lineage differences of GFP^{low} and GFP^{high} radial glial (prominin+) cells. Isolation of RGCs only (labelled by prominin) and their separation into GFP^{low} and GFP^{high} resulted in the strong reduction of mRNAs expressed in neurons or basal progenitor cells – consistent with the selective isolation of RGCs. When the progeny of these RGCs was included in the sort, by collecting respectively all GFP^{low} or all GFP^{high} cells, only the later contained transcripts detected in basal progenitors. Therefore, these data demonstrated that distinct lineages of RGCs exist that generate many neurons or generate few neurons and some basal progenitors. Previous molecular data already suggest distinct molecular pathways for direct neurogenesis from RGCs and indirect neurogenesis via basal progenitors (Heins et al., 2002 and below), but until now the prospective isolation of these distinct lineages was not successful. Moreover, our data demonstrated the feasibility to gain insights into lineage and progeny differences by transcriptome analysis of the progenitor population in comparison with the progenitor population and its progeny by taking advantage of the GFP stability as a short term lineage marker. Indeed, previous studies already took advantage of the GFP lineage marker to follow the progeny of progenitor populations. For example, Zhou and colleagues used the Olig2 knockin marker GFP as a short-term lineage tracer to analyze the progeny of Olig2-derived progenitors in heterozygous versus homozygous Olig1/2 double-mutant embryos (Zhou and Anderson, 2002).

Taken together, the present study revealed not only the transcriptome of distinct RGC subsets, but also novel insights into their lineages. Therefore, this is the first study that characterizes distinct RGC subsets co-existing in the mouse developing cortex.

8.1.1 Novel insights into radial glial lineages in the developing cortex – direct versus indirect neurogenesis

Our results obtained by FACS analysis can be reconciled with data from live and time lapse video microscopy of radial glia and their progeny. Consistent with their mainly neurogenic fate, RGCs have been observed to divide asymmetrically, generating for example a postmitotic neuron and a RGC (Miyata et al., 2001; Noctor et al., 2001). RGCs also divide asymmetrically to generate a progenitor cell that then continues to proliferate basally - basal progenitor - and other RGC (Miyata et al., 2004). These basally dividing progenitors differ in their mode of division from the apically dividing neuroepithelial or RGCs in that they largely generate two postmitotic neurons, as shown by live video microscopy only four years ago (Haubensak et al., 2004; Miyata et al., 2004; Noctor et al., 2004). Only a minor proportion of these progenitors seems to divide more than once (Wu et al., 2005). These studies also show

that basal progenitors arise from RGCs (Miyata et al., 2004). Thus, these studies raise the question when and how RGCs generate basal progenitors. Indeed, live imaging of cortical slices show the existence of RGCs generating directly postmitotic neurons (Miyata et al., 2001; Miyata et al., 2004; Noctor et al., 2001; Noctor et al., 2004). However, the direct generation of neurons by RGCs was observed with less frequency (16%, E13 mouse cortex) compared to the generation of other RGCs (23%) or the generation of one radial glia and a basal progenitor (63%) (Miyata, 2007; Miyata et al., 2004).

All these time lapse studies are consistent with our RGCs population analysis. With our FACS sorting experiments we enriched the population of direct neurogenic radial glia or the radial glia generating basal progenitors. The quantitative FACS data show that the RGCs directly generating neurons are the minority and the RGCs generating basal progenitors are the majority, at mid-neurogenesis stage of cortical development (E14). Indeed, GFP^{low} RGCs were less frequent (40% of all RGCs) than the GFP^{high} radial glia (60% of all RGCs). The GFP^{high} radial glia fraction strikingly correlated with the 63% of RGCs generating one radial glia and a basal progenitor observed by Miyata and colleagues (Miyata, 2007; Miyata et al., 2004). The fraction of GFP^{low} RGCs possibly comprised the RGCs directly generating neurons (16%) and generating other RGCs (23%) visualized by Miyata and colleagues (total of 39%) (Miyata, 2007; Miyata et al., 2004). Furthermore, live imaging studies also suggest that the RGCs that have been generated by a division generating a RGC and a basal progenitor, then often generate a postmitotic neuron and a RGC (Miyata, 2007). Thus, GFP^{high} radial glia may then generate GFP^{low} radial glia – being consistent with a down-regulation of activity of the human GFAP promoter in this process.

8.1.2 Molecular mechanisms regulating direct versus indirect neurogenesis in the developing cortex

Notably, our transcriptome analysis now allows the identification of the molecular differences between these two lineages of RGCs. For example, we discovered very interesting differences in the expression levels of Pax6 isoforms between both subsets of RGCs. The direct neurogenic radial glia lineage, the GFP^{low}/prominin+ fraction, expressed higher levels of canonical Pax6 and the GFP^{high}/prominin+ fraction showed higher expression of the Pax6 (5a) isoform that contains a 14AA insert in the N-terminal part of the paired domain. As it was previously shown, the loss of Pax6 affects the direct neurogenic lineage from RGCs (Heins et al., 2002), consistent with our results on the transcriptome of these RGCs. Indeed, RGCs sorted from the Pax6-mutant mice (Sey/Sey mice, using the weaker

GFP expressed under the GFAP promoter selecting largely for RGCs, Malatesta et al., 2000 and Heins et al., 2002) generate only few neurons compared to their WT littermates (Heins et al., 2002). Moreover, neurons are highly reduced in the cerebral cortex of Pax6-mutant mice (Heins et al., 2002). All these data suggest that Pax6 is indeed important for direct neurogenesis from RGCs in the cerebral cortex, consistent with our results. Furthermore, the higher expression level of the canonical Pax6 form in the neurogenic subset of radial glia fits well with previous analysis of canonical Pax6 overexpression and mutant analysis revealing a potent neurogenic role of this isoform (Berninger et al., 2007; Buffo et al., 2005; Hack et al., 2005; Haubst et al., 2004; Heins et al., 2002).

However, basal progenitors are also affected in the Pax6-mutant cortex. Basal progenitor numbers are increased (Haubst et al., 2004) but their identity is abnormal, as they fail to express the proper markers - Tbr2, Svet1 and Cux2 (Englund et al., 2005; Nieto et al., 2004; Tarabykin et al., 2001; Zimmer et al., 2004). Furthermore, other studies suggest that Pax6 does not interfere with neurogenesis from the basal progenitors, but with the proper specification of upper layer neurons (Schuermans et al., 2004; Tarabykin et al., 2001; Zimmer et al., 2004). However, we found the isoform Pax6 (5a) being higher expressed in the RGCs generating neurons indirectly via basal progenitors. Consistently, it was previously shown that Pax6 (5a) has no neurogenic role, even after overexpression (Haubst et al., 2004). Therefore, Pax6 (5a) might be involved in the specification of basal progenitors, possibly upregulating Tbr2, Svet1, Cux2 and Satb2. Consistent with this suggestion, the Tbr2 promoter was activated by Pax6 (5a) using luciferase assays (data not shown). Taken together, our prospective isolation and characterization of subsets of radial glia generating neurons directly or indirectly suggests that the canonical (neurogenic, Haubst et al., 2004; Heins et al., 2002) form of Pax6 is required for direct neurogenesis from RGCs, while the higher levels of the Pax6 (5a) isoform does not allow direct neurogenesis from these cells, but may be important for the specification of basal progenitors.

Strikingly, there is a correlation between expression of certain genes in basal progenitors (Svet1, Cux1/2, Satb2) and upper layer neurons that maintain the expression of these genes (Britanova et al., 2005; Tarabykin et al., 2001; Zimmer et al., 2004). This data is also consistent with the failure of these genes to be expressed in the Pax6-mutant basal progenitors and the identity of upper layer neurons being severely disturbed in the Pax6-mutant cortices (Schuermans et al., 2004; Tarabykin et al., 2001). Therefore, these data implicate the basal progenitors specifically in the generation of upper layer neurons. Consistent with this suggestion, I found the transcription factor AP2 γ (Tcfap2c) to be

enriched in the lineage of RGCs generating the basal progenitors and indeed, this gene plays an important role in the generation of basal progenitors and is involved in the specification of upper layer neurons in the cerebral cortex. Thus, AP2 γ is a functional prove for this lineage. The function of this transcription factor in the cerebral cortex was further studied and it is described in the second part of this work.

Taken together, the separation of radial glial subpopulations involved either in the generation of basal progenitors (GFP^{high}/prominin+) or involved in direct neurogenesis (GFP^{low}/prominin+) may have profound relevance for our understanding of the molecular mechanisms regulating the specification of lower versus upper layer neurons in the cerebral cortex (McConnell, 1995).

8.1.3 Radial glial subsets are comparable to ES cell derived radial glia

The distinct nature of the different lineages of RGCs isolated in this study was further supported by their comparison to embryonic stem (ES) cell derived RGCs. Homogeneous populations of cells with radial glial properties were derived from ES cells using distinct culturing protocols (Bibel et al., 2004; Conti et al., 2005; Pollard et al., 2006), either exposing ES cells to retinoic acid in the cell aggregate stage resulting in a virtually pure population of Pax6-positive RGCs (Bibel et al., 2007; Bibel et al., 2004), or exposing ES-derived neural cells to bFGF and EGF in an adherent stage resulting in a quite pure population of expandable RGCs (Conti et al., 2005). Indeed, the RGCs derived from ES cells following the Bibel protocol closely resembled the GFP^{low} RGCs. However, the absence of Pax6 (Pax6-mutant ES cells) moved the transcriptome similarity towards the other subset of primary RGCs, the GFP^{high} population. This was even more striking taking into consideration the data described above with the absence of Pax6 in the cerebral cortex resulting in a shift from the direct neurogenesis from radial glial to the indirect neurogenesis via basal progenitors (Heins et al., 2002). Thus, the molecular cues regulating neurogenesis from different sets of progenitors are different. These data suggested that these ES-derived RGCs closely resemble the *in vivo* lineages of RGCs in the developing cerebral cortex. Indeed, both of these populations are fate-restricted and generate only specific neuronal subtypes (Nikoletopoulou et al., 2007; Plachta et al., 2004). Thus, ES cells via the Bibel protocol represent normally direct neurogenesis, supposedly not generating Tbr2+ basal progenitors. These ES cells would then be committed to the generation of deep layer neuron subtypes only.

Conversely, the neurons generated by expanded RGCs – either in neurosphere cultures or by the protocol described by Conti and colleagues (Conti et al., 2005; Pollard et al., 2006) –

seem to be rather different from primary progenitors. I showed here that the transcriptome of expanded primary cells from the cortex or ES-derived expanded cells differs from the transcriptome of primary radial glia sorted directly from the cortex. Indeed, RGCs usually undergo a limited number of cell divisions (Takahashi et al., 1995) and their unlimited expansion requires obvious changes in gene expression (Gabay et al., 2003; Hack et al., 2004). While these cells may not exist as such *in vivo*, their expansion and broadening of potential *in vitro* may prove to be extremely useful for repair of the nervous system (Conti and Cattaneo, 2008; Conti et al., 2006). Taken together, our lineage analysis of defined isolated radial glial subtypes identified distinct lineages of RGCs that are also resembled by differentiation of ES cells into neurons. The possibility to isolate these functional radial glial subtypes prospectively now also allows understanding the molecular fate cues regulating these lineage differences.

8.1.4 Novel insights into the transcriptome of distinct radial glial lineages at mid-neurogenesis

8.1.4.1 Transcripts enriched in the subset of radial glia directly generating neurons

Interesting molecular pathways were found to be differently regulated between distinct lineages of RGCs populations, the direct neurogenic and the largely non-neurogenic set of radial glia isolated at mid-neurogenesis (E14) in the cortex. Our transcriptome analysis of defined subsets of functionally RGCs was one of the first examining defined progenitor subtypes [(see however (Abramova et al., 2005)]. Most transcriptome analyses have so far been performed either with tissue samples or cell cultures *in vitro* (Easterday et al., 2003; Geschwind et al., 2001; Ramalho-Santos et al., 2002). There are important advantages of examining defined progenitor populations in comparison to the previous analyses. For example, most of the genes expressed at higher levels in the neurogenic radial glial subset (GFP^{low}/prominin+) were not picked up in previous gene expression profiles of neural stem (progenitor) cells (Abramova et al., 2005; Easterday et al., 2003; Geschwind et al., 2001; Ramalho-Santos et al., 2002). This includes genes encoding for small GTPases (e.g. cdc42, Rac1 and Arhgef7), genes involved in chemokine signalling pathway, cell adhesion and cytoskeleton regulation. The neurogenic set of RGCs were also characterized by higher expression levels of the transcription factors Pax6, Mef2c, Bhlhb5, Nr2f2 and Atbf1 that were previously linked to a neurogenic fate (Gauchat et al., 2004; Heins et al., 2002; Jung et al., 2005; Lu et al., 1994; Mattar et al., 2004). The expression of Pax6 and cdc42 in this

population is interesting as deletion of either of these genes in the cortex results in an increase in basal progenitors (Cappello et al., 2006; Haubst et al., 2004; Heins et al., 2002; Holm et al., 2007). Therefore, these genes might be important to maintain the direct neurogenic lineage of RGCs and inhibit the generation of basal progenitors via the other subset of RGCs as briefly mentioned above (GFP^{high}/prominin+). Moreover, it becomes interesting to look at the role of Arhgef7 and other small RhoGTPases in the maintenance of the direct neurogenic lineage of RGCs and inhibition of the generation of basal progenitors, as so far their functional role has not yet been studied. The molecular function of Mef2c, Bhlhb5, Nr2f2 and Atbf1 in neurogenesis also remains to be unraveled. So far, no direct function of these transcription factors as neurogenic fate determinants *in vivo* has been described. For example, Mef2c has been only implicated in development of the cortical architecture and in neuronal differentiation and maturation in the CNS (Lin et al., 1996; Lyons et al., 1995), and Nr2f2 has been directly implicated in tangential migration in the developing forebrain (Tripodi et al., 2004).

Interestingly, we identified cell surface molecules contained specifically on the neurogenic radial glia fraction, as Crb1, CD83, Flrt2 and p75, and further proved that p75 is indeed selective for neurogenic radial glia. Strikingly, p75 expression persists on neurogenic progenitors in newborn and adult animals (Young et al., 2007). Crb1 is also expressed in the VZ of the cortex during development and maintained in the adult neurogenic regions (hippocampal dentate gyrus and subependymal zone) (den Hollander et al., 2002). Therefore, we identified new cell surface molecules that define neurogenic progenitor populations during development and possibly at adult stages. These new cell surface markers will be very useful to directly identify neurogenic progenitors *in vivo* and monitor their possible alterations in mutant analyses.

8.1.4.2 Transcripts enriched in the largely self-renewing radial glial subset

The isolated subset of radial glia that generated few neurons and comprised largely self-renewing RGCs (GFP^{high}/prominin+) showed striking differences in their transcriptome in comparison to the direct neurogenic set of RGCs (GFP^{low}/prominin+). In the largely non-neurogenic radial glia subset, we observed an enrichment of molecules involved in Notch signalling such as Notch1/3 and Jag1, canonical Wnt and BMP signalling. For example, Notch1 is expressed predominantly in proliferating neural progenitor cells in the VZ of the embryonic brain (Lindsell et al., 1996). Furthermore, activated Notch1 is expressed in a large subset of RGCs in the developing cerebral cortex (Tokunaga et al., 2004) and constitutive

activation of Notch signalling was shown to cause maintenance of RGCs and abolish neurogenesis in the embryonic cortex (Gaiano et al., 2000). Thus, these studies are consistent with the expression of Notch1 at higher levels in the largely non-neurogenic set of RGCs and the roles of Notch signalling in the maintenance of progenitor cells (Mason et al., 2006; Mizutani et al., 2007; Yoon and Gaiano, 2005). Moreover, this fraction of RGCs also showed a high expression of cell cycle regulatory genes. Several of these genes were found to be up-regulated in previous gene expression analysis of the Pax6-mutant cortex at mid-neurogenesis, including *Aurkb*, *Bub1* and *Chek1* (Holm et al., 2007), confirming the switch from the neurogenic progenitor set to the largely self-renewing progenitor set in this mutant. Interestingly, the fraction of largely self-renewing RGCs shared genes previously identified in gene expression profiling of mouse embryonic, neural and hematopoietic stem cells (Ramalho-Santos et al., 2002). For example, genes considered to be important for stemness were related to Notch, JAK/STAT (Janus kinase/signal transducers and activators of transcription), TGF- β (transforming growth factor) and Yes (Yamaguchi sarcoma) signalling in this study (Ramalho-Santos et al., 2002). In our transcriptome analysis of the largely non-neurogenic radial glia subset we found a high overlap with this expression profile in regard to some transcription factors, such as AP2 γ , Yap1, Tead2, mRNAs related to growth factor activity as *Egfr*, *Tgfb2*, *Trip6* or to cell cycle regulation (e.g. *Cdca2*, *Gas1*). In addition, we observed some overlap between the largely non-neurogenic subset of radial glia (but less with the direct neurogenic subset of radial glia) and the expression profile of mouse progenitor cells isolated by the surface marker LeX (Abramova et al., 2005). Some genes found in both analysis were Notch1, *Ttyh1*, *Nedd9* and Sox genes (Abramova et al., 2005). Notably, some known stem cells markers absent in Abramova et al and Ramalho-Santos et al studies (e.g. *Bnr-1*, *Sox1* and *Musashi*) were also absent in our transcriptome analysis, confirming some similarity with previous reports. However, we detected few genes in common with the transcriptome profile of heterogeneous neural progenitor cultures (Easterday et al., 2003; Geschwind et al., 2001). Thus, the use of homogenous materials like FACS sorted cells may be important to study gene expression profiles of a specific cell type, avoiding the dilution of relevant genes or gene expression differences that may result from the contamination with other cell types.

In our gene expression profiling, several genes highly expressed in the largely non-neurogenic set of RGCs were not picked in other studies and are considered “novel”. Cell surface markers as *Sema5b* and *Cdc163c-alpha* and small GTPases related genes as *Arhgap5*, *RhoA* and *Rhoq* were found to be up-regulated in the non-neurogenic set of RGCs. Some of

these genes (Arhgap5 and RhoA) were indeed confirmed to be expressed in the progenitors of the cortical VZ at mid-neurogenesis but the possible function of these genes in radial glia still remains to be elucidated.

8.1.4.3 Novel transcripts expressed in both radial glial lineages during development and maintained in the progenitors of the adult brain

Importantly, further novel genes were identified in the present transcriptome analysis of distinct subsets of RGCs, such as mRNAs with only a Riken code which have not even been classified so far. The expression of some of these unknown genes was also confirmed to be confined to the VZ of the cortex during development. Thus, these genes might have novel and important functions in maintaining RGCs in an undifferentiated state or inducing direct neurogenesis in the cortex during development. For example, the gene 2300002D11Rik was shown in this study to be localized in the nucleus of only a subset of RGCs *in vivo* and additionally in neurons at mid-neurogenesis in the mouse cortex. This interesting expression pattern was thus consistent with the higher expression of this mRNA in only one subset of RGCs - the neurogenic set of radial glia, observed in our transcriptome analyses. Strikingly, the mRNA and protein of the 2300002D11Rik was present specifically in stem and progenitor cells in the adult SEZ and OB - one of the adult neurogenic regions. Moreover, I found the transcription factor AP2 γ higher expressed in the other lineage of RGCs – the radial glia subset largely self-renewing and giving rise to basal progenitors, as mentioned above. Interestingly, AP2 γ was also expressed in the adult neurogenic regions, namely in the SEZ and DG. Thus, the expression of 2300002D11Rik and AP2 γ in the progenitors of the embryonic and adult brain suggests that both lineages found in the developing cortex are maintained in the adult brain. However, these lineages are only maintained in the neurogenic regions of the adult brain but severe changes seem to happen in non-neurogenic regions, as for example the cortex.

Several other genes were found in this transcriptome analysis, whose function is still not known. Future functional analysis of these novel genes may give new insights into the molecular mechanisms regulating both progenitor lineages in the embryonic and adult mouse brain.

8.1.5 Novel insights into transcriptional changes in radial glial cells at the end of neurogenesis

At late developmental stages (E18 in the mouse) cells are switching from neurogenesis to gliogenesis (Qian et al., 2000; Temple and Qian, 1995). To elucidate the transcriptome of RGCs at the end of the neurogenic period we looked at genes differently regulated compared with isolated E14 subsets of RGCs. Consistent with the decreased neurogenesis at this developmental stage, transcription factors related to a neurogenic fate (e.g. Pax6, Neurog1/2, Emx1) were down-regulated similar to genes involved in Wnt and BMP signalling pathways [(see e.g. (Chenn and Walsh, 2002)]. These data suggest that Wnts and BMPs may promote self-renewal or maintenance of undifferentiated radial glia. Indeed, Wnt signalling appears to regulate proliferation and differentiation of neuronal lineages in a stage-specific and cellular context-dependent manner (Chenn and Walsh, 2002; Hirabayashi et al., 2004). BMPs promote astroglia differentiation during embryogenesis and in dorsal regions of the telencephalon they not only promote astrocyte fate, but also inhibit neurogenesis and oligodendrocytogenesis (Mabie et al., 1997; Mehler et al., 2000; Nakashima et al., 2001). Some members of the BMP family, such as BMP2 and BMP4, have been shown to have anti-neurogenic effects in several systems, where they inhibit proliferation and/or induce apoptosis of neural progenitor cells during development (Furuta et al., 1997; Mabie et al., 1999; Shou et al., 1999). In some systems, however, BMP2 and BMP4 have been reported to have positive effects on neurogenesis, for example by promoting neuronal differentiation (Li et al., 1998). BMP6 and BMP7, members of a separate BMP subfamily, have been reported to have both positive (Arkell and Beddington, 1997; Furuta et al., 1997) and negative (Li et al., 1998; Shou et al., 1999) effects on neurogenesis. Interestingly, Wnt signalling indirectly regulates gliogenesis by inducing BMPs in neuronal cells (Kasai et al., 2005). Thus, cooperation between Wnt and BMP signalling seems to play an important role in determining the sequence of neurogenesis and gliogenesis during development and their tight regulation may be important to terminate neurogenesis in the cortex.

mRNAs encoding for proteins positively regulating cell cycle progression also decreased in E18 radial glia, consistent with a decreased proliferation rate and a slower cell-cycle of RGCs at late developmental stages (Caviness et al., 2003). This finding is in agreement with the gene expression profiling of isolated progenitors Lex⁺ cells at E17 where genes maintaining proliferation were reduced (e.g. eif3s7, cdk9 and sin3a also found in our arrays) (Abramova et al., 2005).

Interesting pathways that were up-regulated at this stage included Notch signalling (e.g. Notch2 and Dner), genes involved in gliogenesis (FABP7, TN-C and Erbb4), oligodendrogenesis (Olig1/2 and Pdgfra) and in the oligodendrocyte lineage (Brn-1 and Brn-2) (Schreiber et al., 1997). Indeed, a third wave of Emx1-derived oligodendrocytes progenitors was described in the cortex around birth, demonstrating that these oligodendrocytes were generated from endogenous cortical progenitors (Kessaris et al., 2006). As our data showed that oligodendrocytes related genes start to be up-regulated in RGCs at late developmental stages, this suggests that these RGCs might generate the oligodendrocytes in the early postnatal cortex. In addition, other reports show that VZ cells in the motoneuron progenitor domain of the ventral spinal cord also express oligodendrocyte markers (Olig2) (Mukouyama et al., 2006). The isolation of these Olig2+ progenitors show that they lose their neurogenic potential in the gliogenic period and therefore they are not multipotent stem cells (Mukouyama et al., 2006). Early Olig2 positive cells (from murine E9.5) generate neurons and oligodendrocytes, while late Olig2 positive cells generate only oligodendrocytes upon transplantation (Mukouyama et al., 2006). Thus, throughout the CNS, oligodendrocytes appear to be the late progeny of radial glia, accordingly with our transcriptome analysis.

Another interesting finding related to the transcriptome analysis of radial glia at the end of neurogenesis is related to the down-regulation of chromatin remodeling genes, such as Chrac1 and Smarca2/a4/a5/b1/c1. These novel results may indicate that the down-regulation of these factors is important to inactivate certain genes involved in self-renewal of RGCs and for closing their neurogenic potential. Indeed, nucleosome remodeling factors were previously shown to be important to increase the accessibility of chromatin and thus activating gene expression (Baker et al., 2003; Sif et al., 1998; Simone, 2006). Furthermore, recent reports show the important role of Smarca4 in the maintenance of proliferating neural progenitors (Matsumoto et al., 2006).

We compared the transcriptome of pure RGCs isolated at the end of neurogenesis with the subsets of RGCs at E14 and the ES cells-derived radial glia using different culturing conditions (Bibel et al., 2004; Conti et al., 2005) by divisive clustering analysis. Interestingly, E18 isolated RGCs had a very distinct transcriptome comparing to ES-derived RGCs and were also very distinct from both subtypes of radial glia sorted from E14. Thus, E18 RGCs showed very pronounced changes at the transcriptome level.

In summary, our results evidence the fact that we were able to isolate two different lineages of RGCs in the cortex at mid-neurogenesis and we further identified the molecular

differences between these distinct sets of radial glia. One set consisted of radial glia that expressed canonical Pax6 and directly generated neurons, whereas the other set of radial glia expressed endogenous low levels of canonical Pax6 and had less neurogenic capacity. This second population generated only few neurons indirectly through the generation of basal progenitors which were enriched in this fraction. Importantly, both subsets of RGCs were very distinct from non-neurogenic RGCs isolated at the end of neurogenesis at the transcriptome level. Thus, our transcriptome analysis gave new insights into the potential fate determinants of distinct lineages of RGCs in the developing mouse cerebral cortex. The functional relevance of the two lineages isolated at mid-neurogenesis was confirmed by our functional analysis of the AP2 γ transcription factor.

8.2 Expression and function of the transcription factor AP2 γ in a subset of cortical radial glia

8.2.1 The role of AP2 γ in the specification and cell survival of basal progenitors

Here I showed a specific role of the transcription factor AP2 γ in the regulation of basal progenitor fate as observed in gain and loss of function analysis. One of the most striking findings of this work was indeed the effect of AP2 γ on many basal progenitor transcripts, such as Tbr2, Math3, Lmo4, Cux2 and Svet1. The reduced expression of all of these transcripts upon AP2 γ deletion in a concerted fashion – either directly or indirectly, caused a severe misspecification of basal progenitors. These changes had no consequences on proliferation as I did not observe any significant increase in cells in S or G2/M-phase or any other alterations in cell proliferation upon conditional AP2 γ deletion. Consistently, the microarray analysis did not reveal any changes in expression of cell cycle regulators, such as p21 or c-myc that are affected by AP2 γ in other contexts (El-Hashash et al., 2005; Li et al., 2006). Therefore, AP2 γ acted as a fate determinant for basal progenitors rather than regulating their proliferation. The severe misspecification of basal progenitors upon loss of AP2 γ was not only demonstrated by reduced expression of key transcription factors, but also by the ectopic expression of radial glia features, such as GLAST-immunoreactivity, in half of all basally dividing AP2 γ ^{-/-} progenitors. As the number of proliferating cells was not increased, the AP2 γ ^{-/-} cortex at mid-neurogenesis contained a proportion of cells that neither proliferate nor differentiate. Indeed, I showed that the number of apoptotic cells was doubled in the AP2 γ mutant cortex, suggesting that cells failing to proliferate or differentiate upon

loss of AP2 γ were subject to cell death. Strikingly, most of the misspecified basal progenitors or their immediate progeny in the absence of AP2 γ were the cells that underwent cell death. Conversely, overexpression of AP2 γ in cortical progenitor cells induced Tbr2 expression and delayed its down-regulation in progenitor cells. Moreover, I showed that AP2 γ directly regulated the basal transcripts Tbr2 and Math3. Therefore, from these observations, I conclude that AP2 γ largely affects the fate specification of basal progenitors – reflected by its effect on virtually all transcription factors known to be expressed in these progenitors and hence may rather indirectly affect cell survival by dysregulation of fate determinants of basal progenitors.

The transcriptome analysis of AP2 γ -mutant cortices indeed revealed downregulation of some mRNAs that have been directly linked to regulating cell survival, as the signalling molecule Stat3, Lmo4, Id3, Slit2, Homer2 and MT1/2. For example, Stat3 often acts as a pro-survival factor in glioblastoma cells (Rahaman et al., 2002) or neurons (Yadav et al., 2005). Notably, activation of the IL-6 receptor and phosphorylation of Stat3 promotes neuron survival positively mediated by the Lim-only factor Lmo4 (Chen et al., 2007). Lmo4 is also essential for normal patterns of proliferation and for survival of neural progenitor cells (Lee et al., 2005b; Tse et al., 2004). As Lmo4 expression was virtually absent in the SVZ of AP2 γ mutant cortices, a possible prosurvival role of this signalling pathway may be compromised. Moreover, the axonal guidance genes Slit were previously proposed to play an important role during development of the nervous system mediating cellular survival (Piper et al., 2002). Similarly, MT2 as well as Homer mRNAs were down-regulated in the occipital cortex of AP2 γ ^{-/-} mice and have been implicated in protecting cells from cell death in the mammalian CNS (Carrasco et al., 2000; Hidalgo et al., 2001; Sakamoto et al., 2007). Interestingly, mice in which the MT1 and MT2 genes are knocked-out are susceptible to physical, chemical and ischemic brain injury (Carrasco et al., 2000). In this context, the inhibitor of differentiation/DNA binding 3 (Id3) was similarly down-regulated in the AP2 γ ^{-/-} cortices and was shown to be involved in proliferation, differentiation, apoptosis, and carcinogenesis (Kee and Bronner-Fraser, 2005). Furthermore, misexpression of Id in cortical progenitors inhibits neuron-specific gene expression (Cai et al., 2000). Homer proteins are integral to the assembly of proteins regulating glutamate signalling and synaptic plasticity and were shown to protect striatal neurons from apoptosis (Brakeman et al., 1997; Sakamoto et al., 2007). Thus, AP2 γ seems to regulate in a concerted manner various transcription factors specifying the fate of basal progenitors cells, as well as their survival, consistent with previous studies in the trophoctoderm lineage showing the importance of AP2 γ in the regulation of cell survival

(El-Hashash et al., 2005; Hilger-Eversheim et al., 2000). Taken together, the role of AP2 γ in cortical development reiterates the key functions of AP2 transcription factors in regulating the specification and survival of specific lineages during early development. Importantly, the regulation of basal progenitor fate by AP2 γ in the developing cortex is consistent with its high expression in the lineage of RGCs generating basal progenitors discussed above (Pinto et al, 2008), therefore confirming the functional relevance of this lineage of RGCs.

Our work further revealed an intricate cross regulation of different transcription factors regulating basal progenitor transcripts. I showed by luciferase assays that Pax6 directly regulates the basal progenitor markers Tbr2 and Math3 in the absence of AP2 γ , consistent with previous data on the loss of Tbr2 expression in the Pax6-mutant cortex. Notably, AP2 γ is regulated by Pax6 in a positive manner and by the Pax6 target Ngn2 and Mash1 in a negative manner. This negative regulation could be confirmed *in vivo*, as AP2 γ expression is virtually absent in the cortex of mice that express Mash1 in the locus on Ngn2. In the WT cortex, however, Ngn1 and 2 are expressed at higher levels than Mash1. Notably, Ngn proteins mostly increase in basal progenitor cells (Miyata et al., 2004) and thus may be implicated in the down-regulation of AP2 γ in these set of progenitors. This is consistent with the observation that AP2 γ and Tbr2 were only co-expressed in cells within the VZ but rarely in the SVZ. As Mash1 expression levels are normally much lower than Ngn2 expression in the cortex, but up-regulated in the Pax6-mutant cortex (Heins et al., 2002; Stoykova et al., 2000), this up-regulation may in part be responsible for the down-regulation of AP2 γ observed in the Pax6 mutants (Holm et al., 2007). Taken together, the regulation of basal progenitor transcripts by AP2 γ is achieved through an intricate network of transcription factors.

8.2.2 Maintenance of the embryonic lineage of progenitors expressing AP2 γ in the adult brain

The function of AP2 γ in the regulation of basal progenitor fate shows the functional relevance of the lineage of RGCs generating basal progenitors existent during embryonic development. One remarkable observation of this work was the maintenance of this lineage of AP2 γ -expressing progenitors in the adult neurogenic regions, namely the DG and SEZ and in the RMS and OB. Our data further suggest that AP2 γ may be involved in adult glutamatergic neurogenesis not only in the embryonic but also in the adult brain, as recently shown for Tbr2 (Englund et al., 2005).

Interestingly, some genes shown to be regulated by AP2 γ at the transcriptome level showed similar expression patterns to AP2 γ in the adult brain. For example, the protein arginine *N*-methyltransferase PRMT8 is strongly expressed in neurons of the mitral cell layer (ML), granular cell layer (GCL), and periglomerular cells (GL). PRMT8 is also highly expressed in the hippocampus, in all the pyramidal cells of Ammon's horn CA1 to 3 and all the granule cells in the dentate gyrus (DG) (Lee et al., 2005a), similarly to AP2 γ . Emx1, shown here to be regulated by AP2 γ , is expressed in the hippocampus and interestingly Emx1 mutant mice show reduced hippocampal neurogenesis (Hong et al., 2007). The metallothioneins MT1 and 2 are highly expressed in the olfactory bulb and cerebellum (Aschner et al., 1997) similarly to AP2 γ . Moreover, Homer2 or Cupidin is expressed in the granular, external plexiform and glomerular layers of the olfactory bulb and in the granular cell layer of the cerebellum. Homer 2a/b immunoreactivity is also intense in the CA1-CA2 sub areas of the hippocampus, and is detectable at low levels in the CA3 region and DG (Shiraishi et al., 2004). Thus, the similar expression of AP2 γ and the genes discussed above suggest that some of them might possibly regulate the functions of AP2 γ in these specific regions of the adult mouse brain.

8.2.3 AP2 γ -/- phenotype reveals specific molecular program for upper layer neuron generation

Basal progenitors have been recently suggested to contribute to the generation of all cortical neuronal layers (Pontious et al., 2008), while previous work had suggested that basal progenitors are mostly involved in the generation of upper layer neurons only (Nieto et al., 2004; Pontious et al., 2008; Tarabykin et al., 2001; Zimmer et al., 2004). As mentioned above, the suggestion that basal progenitors generate only upper layer neurons is based on the expression of a series of transcription factors and other mRNAs in basal progenitors and upper layer neurons in common. However, it is important to note that the expression of these transcription factors only starts at mid-neurogenesis, such as Cux2, Lmo4 and Svet1. Our results now brought new insights into the contribution of basal progenitors to the generation of cortex neuronal layers. I demonstrated that AP2 γ is a key regulator of the later basal progenitor program, starting at mid-neurogenesis, but has no effect on the specification of earlier sets of basal progenitors. This is supported by loss-of-function experiments conditionally deleting AP2 γ and gain-of-function experiments overexpressing AP2 γ at early stages (E12) (data not shown) as both did not affect basal progenitor specification before mid-neurogenesis. These data therefore demonstrated different molecular programs

regulating basal fate and survival at early and later developmental stages with AP2 γ being involved only in the specification of mid-neurogenesis basal progenitors.

Indeed, the partial misspecification of basal progenitors after AP2 γ deletion and their subsequent cell death at mid-neurogenesis lead to defects in the generation of upper layer neurons only. Already at the developmental stage E17, there was a clear decrease in the band of Cux2- and Satb2-expressing neurons in the AP2 γ deficient mice. I showed here that the reduction of neurons in the cortical plate of the cortex was not due to neuronal migration defects, but rather due to increased cell death during cortex development. At postnatal and adult stages, a specific reduction in the number and thickness of Cux1/2-, Satb2-, SorLa- or vGlut2-expressing upper layer neurons (II-IV) was observed in the AP2 γ mutant cortex, while the thickness of deep layer neurons was not affected. This suggests a specific reduction of upper layer neuron progenitors already at mid-neurogenesis, where the first abnormalities in basal progenitors were observed in the AP2 γ mutant cortex. In addition, overexpression of AP2 γ at E14 resulted in a prominent increase in upper layer neurons at the expense of deep layer neurons (V/VI), suggesting that AP2 γ overexpression is sufficient to convert deep layer progenitors to an upper layer neuron identity. Thus, our studies suggest a role of basal progenitors in the generation of upper layer neurons only at mid-neurogenesis in the mouse cerebral cortex, as previously suggested (Nieto et al., 2004; Pontious et al., 2008; Tarabykin et al., 2001; Zimmer et al., 2004).

8.2.4 AP2 γ acts in a region-specific manner in the cortex

One of the most remarkable results in this work was the specific role of the transcription factor AP2 γ in the developing cortex at occipital regions. Indeed, the phenotypic defects in basal progenitors and upper layer neuron generation in the AP2 γ mutant cortex were region-specific, being restricted to occipital regions as emphasized by the transcriptional changes at caudal but not rostral levels. Several transcripts differentially regulated in the AP2 γ mutant compared to WT cortices are involved in regionalization. For example, Emx1 was decreased in the cortex of AP2 γ mutant mice and appears to be involved to some extent in regionalization of the cortical primordium promoting medial fates (Muzio and Mallamaci, 2003). Emx1 shows a gradient of expression in the cortex caudal high to rostral low and thus its downregulation in the AP2 γ mutant cortex may contribute to the strong phenotype in caudal regions observed in this mutant. Further interesting genes regulated by AP2 γ at the molecular level were found to be important for regionalization, such as Tcf3 and PRMT8. Indeed, the T-cell factor TCF3 is known as a caudalizing factor operating in the context of

Wnt/beta-catenin signalling to induce gene expression in discrete compartments along the rostral-caudal axis of the developing vertebrate nervous system. Interestingly, in zebrafish, basal repression of caudal genes is achieved through the function of Headless (Hdl), a Tcf3 homolog. (Dorsky et al., 2003). Loss of Tcf3 function in the Hdl mutant reveals that Hdl represses Wnt target genes, providing genetic evidence that a component of the Wnt signalling pathway is essential in vertebrate head formation and patterning (Kim et al., 2000). In addition, the protein PRMT8 was recently identified and shown to be distributed in brain tissue (Lee et al., 2005a). PRMT8 shows a highly distinct expression pattern in the neurons of the mouse brain. PRMT8-positive cells showed stronger labelling especially in the sensory system, such as auditory, visual and vestibular systems. The strong expression of PRMT8 transcript in these regions, reveal a probable functional involvement of PRMT8 in caudal regionalization. Taken together, several genes regulated by AP2 γ at the molecular level are actually very important for arealization, specifically regulating caudal regions of the developing cortex that may very well contribute to the region-specificity of AP2 γ functions in the cortex.

Notably, AP2 γ is regulated by Pax6 thereby providing a positive feed-back mechanism and possibly explaining the gradient of AP2 γ expression that mirrors the gradient of Pax6 expression (lateral and rostral high). As Pax6 expression is high rostrally and very low to absent in the occipital regions of the cortex, AP2 γ possibly can be less compensated by Pax6 in occipital regions of the cortex. Thus, the transcriptional network interacting with AP2 γ in the cerebral cortex is crucial to control the functions of AP2 γ in a region specific manner.

8.2.5 Functional relevance of the regulation of upper layer neuron numbers by AP2 γ

The striking specificity of the phenotype in the AP2 γ ^{-/-} cortex to occipital regions gave us the good possibility of studying the role of upper layer neurons in the function of the visual cortex. Indeed, exclusively in the occipital cortex, Cux1/2-positive upper layer neurons were reduced by about 40% and callosal projection neurons were also greatly affected after loss of AP2 γ . This neurodevelopmental deficit of upper layer neurons in the occipital cortex of the adult AP2 γ mutant mice had strong functional consequences in the visual performance of these mice. The visual acuity (cortical spatial resolution evaluated by VEPs) was abnormally low in AP2 γ mutant mice as well as the ratio between contralateral and ipsilateral (C-I) that measures cortical binocularity by VEPs. There was also a trend for increased delay in the latency of visual responses. Indeed, visual acuity is a well-established measurement of the overall visual function in mammals (Fagiolini et al., 1994; Gianfranceschi et al., 1999). These

observations might be related with the reduction of callosal projections observed in these mice. *Lmo4* is significantly downregulated in the AP2 γ mutant cortex and it is known to be expressed in callosal neurons of layers II/III and in layer V (Arlotta et al., 2005; Bulchand et al., 2003), suggesting a role of this factor in the specification of callosal neurons. Furthermore, *Lmo4* plays a key role in mediating Ca²⁺ activation (Kashani et al., 2006) and may thereby impair important signalling pathways mediating functional neuronal maturation in the cerebral cortex. Importantly, *Homer2*, similarly downregulated in the AP2 γ mutant, was shown to be expressed in pyramidal neurons of cortical layers II/III and V (Brakeman et al., 1997). Moreover, *Emx1* was reported to be important for the proper formation of the corpus callosum. Consistently, *Emx1* mutant mice lack most or all of their corpus callosum and the callosal commissure axons are stacked and failed to cross the midline into the opposite hemisphere (Hong et al., 2007; Qiu et al., 1996). Thus, *Lmo4*, *Homer2* and *Emx1* downregulation might contribute to the reduction of callosal neurons observed in this mutant. Taken together, the reduction in callosal connections in these mutant mice could play a role in their visual acuity capacities, further supporting the previous evidence for the importance of callosal projections in the development of visual acuity during the critical period in rats (Caleo et al., 2007).

Interestingly, visual acuity, binocularity and response latency develop progressively during maturation of the visual cortex. Indeed, the ratio between contralateral and ipsilateral is usually lower in juvenile mice as compared to adults (Frenkel and Bear, 2004; Sawtell et al., 2003). Moreover, response latency is higher in young versus fully mature animals ((Fagiolini et al., 1997). Thus, the lower C-I ratio in the adult AP2 γ mutant mice might reflect an impairment in functional maturation of the cortex. The trend for an increased latency in the visual response in the AP2 γ mutant is also consistent with an altered functional development. For example, similar functional deficits (low acuity, greater binocularity and increased latency) are observed when development is disturbed by rearing animals in the dark (Fagiolini et al., 1997). This data therefore prompt the hypothesis that the AP2 γ mutant cortex might remain more plastic in the adult.

In agreement with this prediction, at the transcriptome level several genes upregulated by AP2 γ at embryonic stages seem to be involved in plasticity. The pentraxin Ptx3, up-regulated in the E14 AP2 γ mutant cortices at the transcriptome level, was already shown to have a protective role in seizure-induced neurodegeneration (Ravizza et al., 2001) and might contribute to synaptic plasticity (Xu et al., 2003). Indeed, some long pentraxins are expressed in the brain and some are involved in neuronal plasticity and degeneration. In addition, we

found the PDZ domain containing RING finger 3 (PDZRN3) being up-regulated in this mutant cortices. So far, there is no evidence for the function of PDZRN3 in the cortex, however, PDZRN3 was shown to function as a synapse-associated E3 ubiquitin ligase to regulate the postsynaptic development in other systems. Strikingly, this ubiquitin–proteasome pathway has been implicated in synaptic development and plasticity (Lu et al., 2007). Thus, the up-regulation of Ptx3 and PDZRN3 in the AP2 γ mutant cortices at caudal levels may contribute to an increased plasticity in the adult visual cortex of these mutants, as suggested by the electrophysiology tests described above.

Strikingly, the neural cell recognition molecule Close Homolog of L1 (Chl1), up-regulated in the AP2 γ mutant cortices at the transcriptome level, displays an interesting graded pattern of expression with highest levels caudally in the visual cortex, moderate levels in the somatosensory region, and low levels rostrally in the motor region (Liu et al., 2000). In the posterior cortical regions, Chl1 is higher expressed in the cortical plate and subventricular zone (Liu et al., 2000). Chl1 is required for neuronal positioning and dendritic growth of pyramidal neurons in the posterior regions of the developing mouse neocortex. Moreover, Chl1 is expressed in pyramidal neurons in a high-caudal to low-rostral gradient within the developing cortex (Demyanenko et al., 2004). Interestingly, deep layer pyramidal neurons of Chl1 knock-out mice are shifted to lower laminar positions in the visual and somatosensory cortex and developed misoriented. A downward shift in position of DiI-labelled callosal neurons in the middle layers (III/IV) was shown to occur in Chl1 mutants (Demyanenko et al., 2004). Thus, the restriction of Chl1 expression and the effects of its deletion in posterior neocortical areas suggest that Chl1 may regulate area-specific neuronal connectivity and have an important function in the visual cortex. Possibly, Chl1 is one candidate downstream target of AP2 γ mediating its important neuronal functions in the visual cortex.

8.2.6 Phylogenetic considerations on the regulation of upper layer neurons by AP2 γ

Consistent with a role of AP2 γ in regulating the number of upper layer neurons in the visual cortex, we observed a higher expression of AP2 γ in the VZ/SVZ progenitors of the primate visual area 17 compared to area 18 and in the human developing occipital cortex. AP2 γ expression also persists into the adult human cortex suggesting later functions in neurons in higher mammals. Indeed, in primate cortices there is a pronounced difference in the number of upper layer neurons between area 17 and 18 (Dehay et al., 1993; Lukaszewicz et al., 2005). Most strikingly, the SVZ and the proportion of non-apically dividing cells becomes very large in the cerebral cortex of primates where it reaches more than 90% of the progenitor

pool during mid-neurogenesis (Rakic, 2002; Smart et al., 2002). These observations also prompt speculations about the specific role of basal progenitors in the specification of upper layer neurons in the developing cerebral cortex during phylogeny (Kriegstein et al., 2006; Martinez-Cerdeno et al., 2006; Pontious et al., 2008; Rakic, 1995). The higher expression of AP2 γ in the area 17 of primates may suggest a role of this transcription factor on the specification of basal progenitors and upper layer neuron generation in higher mammals. Taken together, AP2 γ is a novel key transcription factor important for the specification of upper layer neurons in a region specific manner during mouse cortical development that may also play a crucial role in the expansion of upper layer neurons during phylogeny.

9 References

- Abramova, N., Charniga, C., Goderie, S.K., Temple, S., 2005. Stage-specific changes in gene expression in acutely isolated mouse CNS progenitor cells. *Dev Biol* 283, 269-281.
- Alvarez-Buylla, A., 1990. Mechanism of neurogenesis in adult avian brain. *Experientia* 46, 948-955.
- Alvarez-Buylla, A., Garcia-Verdugo, J.M., Tramontin, A.D., 2001. A unified hypothesis on the lineage of neural stem cells. *Nat Rev Neurosci* 2, 287-293.
- Arkell, R., Beddington, R.S., 1997. BMP-7 influences pattern and growth of the developing hindbrain of mouse embryos. *Development* 124, 1-12.
- Arlotta, P., Molyneaux, B.J., Chen, J., Inoue, J., Kominami, R., Macklis, J.D., 2005. Neuronal subtype-specific genes that control corticospinal motor neuron development in vivo. *Neuron* 45, 207-221.
- Aschner, M., Cherian, M.G., Klaassen, C.D., Palmiter, R.D., Erickson, J.C., Bush, A.I., 1997. Metallothioneins in brain--the role in physiology and pathology. *Toxicol Appl Pharmacol* 142, 229-242.
- Auman, H.J., Nottoli, T., Lakiza, O., Winger, Q., Donaldson, S., Williams, T., 2002. Transcription factor AP-2gamma is essential in the extra-embryonic lineages for early postimplantation development. *Development* 129, 2733-2747.
- Backman, M., Machon, O., Mygland, L., van den Bout, C.J., Zhong, W., Taketo, M.M., Krauss, S., 2005. Effects of canonical Wnt signalling on dorso-ventral specification of the mouse telencephalon. *Dev Biol* 279, 155-168.
- Baker, K.M., Wei, G., Schaffner, A.E., Ostrowski, M.C., 2003. Ets-2 and components of mammalian SWI/SNF form a repressor complex that negatively regulates the BRCA1 promoter. *J Biol Chem* 278, 17876-17884.
- Batardiere, A., Barone, P., Dehay, C., Kennedy, H., 1998. Area-specific laminar distribution of cortical feedback neurons projecting to cat area 17: quantitative analysis in the adult and during ontogeny. *J Comp Neurol* 396, 493-510.
- Batista-Brito, R., Close, J., Machold, R., Fishell, G., 2008. The distinct temporal origins of olfactory bulb interneuron subtypes. *J Neurosci* 28, 3966-3975.
- Bayer, S.A., Altman, J., Russo, R.J., Dai, X.F., Simmons, J.A., 1991. Cell migration in the rat embryonic neocortex. *J Comp Neurol* 307, 499-516.
- Belluzzi, O., Benedusi, M., Ackman, J., LoTurco, J.J., 2003. Electrophysiological differentiation of new neurons in the olfactory bulb. *J Neurosci* 23, 10411-10418.
- Benjamini, Y., Hochberg, Y., 1997. Multiple hypotheses testing with weights. *Scand. J. Stat.* 24, 407-418.
- Bennett, M.V., Contreras, J.E., Bukauskas, F.F., Saez, J.C., 2003. New roles for astrocytes: gap junction hemichannels have something to communicate. *Trends Neurosci* 26, 610-617.
- Bentivoglio, M., Mazzarello, P., 1999. The history of radial glia. *Brain Res Bull* 49, 305-315.
- Berninger, B., Guillemot, F., Gotz, M., 2007. Directing neurotransmitter identity of neurones derived from expanded adult neural stem cells. *Eur J Neurosci* 25, 2581-2590.
- Berninger, B., Guillemot, F. and Götz, M., 2007. Directing neurotransmitter identity of neurons derived from expanded adult neural stem cells. *Eur J Neurosci* Volume 25.
- Bibel, J.R., Emmanuel Lacroix & Yves-Alain Barde, 2007. Generation of a defined and uniform population of CNS neurons from mouse embryonic stem cells. *Nature Protocols* Manuscript submitted for publication.
- Bibel, M., Richter, J., Lacroix, E., Barde, Y.A., 2007. Generation of a defined and uniform population of CNS progenitors and neurons from mouse embryonic stem cells. *Nat Protoc* 2, 1034-1043.
- Bibel, M., Richter, J., Schrenk, K., Tucker, K.L., Staiger, V., Korte, M., Goetz, M., Barde, Y.A., 2004. Differentiation of mouse embryonic stem cells into a defined neuronal lineage. *Nat Neurosci* 7, 1003-1009.

- Bishop, K.M., Goudreau, G., O'Leary, D.D., 2000. Regulation of area identity in the mammalian neocortex by *Emx2* and *Pax6*. *Science* 288, 344-349.
- Bittman, K., Owens, D.F., Kriegstein, A.R., LoTurco, J.J., 1997. Cell coupling and uncoupling in the ventricular zone of developing neocortex. *J Neurosci* 17, 7037-7044.
- Blass-Kampmann, S., Reinhardt-Maelicke, S., Kindler-Rohrborn, A., Cleaves, V., Rajewsky, M.F., 1994. In vitro differentiation of E-N-CAM expressing rat neural precursor cells isolated by FACS during prenatal development. *J Neurosci Res* 37, 359-373.
- Bosher, J.M., Williams, T., Hurst, H.C., 1995. The developmentally regulated transcription factor AP-2 is involved in c-erbB-2 overexpression in human mammary carcinoma. *Proc Natl Acad Sci U S A* 92, 744-747.
- Braganca, J., Eloranta, J.J., Bamforth, S.D., Ibbitt, J.C., Hurst, H.C., Bhattacharya, S., 2003. Physical and functional interactions among AP-2 transcription factors, p300/CREB-binding protein, and CITED2. *J Biol Chem* 278, 16021-16029.
- Braganca, J., Swingler, T., Marques, F.I., Jones, T., Eloranta, J.J., Hurst, H.C., Shioda, T., Bhattacharya, S., 2002. Human CREB-binding protein/p300-interacting transactivator with ED-rich tail (CITED) 4, a new member of the CITED family, functions as a co-activator for transcription factor AP-2. *J Biol Chem* 277, 8559-8565.
- Brakeman, P.R., Lanahan, A.A., O'Brien, R., Roche, K., Barnes, C.A., Huganir, R.L., Worley, P.F., 1997. Homer: a protein that selectively binds metabotropic glutamate receptors. *Nature* 386, 284-288.
- Britanova, O., Akopov, S., Lukyanov, S., Gruss, P., Tarabykin, V., 2005. Novel transcription factor *Satb2* interacts with matrix attachment region DNA elements in a tissue-specific manner and demonstrates cell-type-dependent expression in the developing mouse CNS. *Eur J Neurosci* 21, 658-668.
- Buffo, A., Vosko, M.R., Erturk, D., Hamann, G.F., Jucker, M., Rowitch, D., Gotz, M., 2005. Expression pattern of the transcription factor *Olig2* in response to brain injuries: implications for neuronal repair. *Proc Natl Acad Sci U S A* 102, 18183-18188.
- Bulchand, S., Subramanian, L., Tole, S., 2003. Dynamic spatiotemporal expression of LIM genes and cofactors in the embryonic and postnatal cerebral cortex. *Dev Dyn* 226, 460-469.
- Cai, L., Morrow, E.M., Cepko, C.L., 2000. Misexpression of basic helix-loop-helix genes in the murine cerebral cortex affects cell fate choices and neuronal survival. *Development* 127, 3021-3030.
- Calegari, F., Haubensak, W., Haffner, C., Huttner, W.B., 2005. Selective lengthening of the cell cycle in the neurogenic subpopulation of neural progenitor cells during mouse brain development. *J Neurosci* 25, 6533-6538.
- Caleo, M., Restani, L., Gianfranceschi, L., Costantin, L., Rossi, C., Rossetto, O., Montecucco, C., Maffei, L., 2007. Transient synaptic silencing of developing striate cortex has persistent effects on visual function and plasticity. *J Neurosci* 27, 4530-4540.
- Cameron, R.S., Rakic, P., 1991. Glial cell lineage in the cerebral cortex: a review and synthesis. *Glia* 4, 124-137.
- Campbell, K., Götz, M., 2002. Radial glia: multi-purpose cells for vertebrate brain development. *Trends Neurosci* 25, 235-238.
- Cappello, S., Attardo, A., Wu, X., Iwasato, T., Itohara, S., Wilsch-Brauninger, M., Eilken, H.M., Rieger, M.A., Schroeder, T.T., Huttner, W.B., Brakebusch, C., Gotz, M., 2006. The Rho-GTPase *cdc42* regulates neural progenitor fate at the apical surface. *Nat Neurosci* 9, 1099-1107.
- Carleton, A., Petreanu, L.T., Lansford, R., Alvarez-Buylla, A., Lledo, P.M., 2003. Becoming a new neuron in the adult olfactory bulb. *Nat Neurosci* 6, 507-518.
- Carrasco, J., Penkowa, M., Hadberg, H., Molinero, A., Hidalgo, J., 2000. Enhanced seizures and hippocampal neurodegeneration following kainic acid-induced seizures in metallothionein-I + II-deficient mice. *Eur J Neurosci* 12, 2311-2322.

Caviness, V.S., Jr., Goto, T., Tarui, T., Takahashi, T., Bhide, P.G., Nowakowski, R.S., 2003. Cell output, cell cycle duration and neuronal specification: a model of integrated mechanisms of the neocortical proliferative process. *Cereb Cortex* 13, 592-598.

Chanas-Sacre, G., Rogister, B., Moonen, G., Leprince, P., 2000. Radial glia phenotype: origin, regulation, and transdifferentiation. *J Neurosci Res* 61, 357-363.

Chazaud, C., Oulad-Abdelghani, M., Bouillet, P., Decimo, D., Chambon, P., Dolle, P., 1996. AP-2.2, a novel gene related to AP-2, is expressed in the forebrain, limbs and face during mouse embryogenesis. *Mech Dev* 54, 83-94.

Chen, H.H., Schock, S.C., Xu, J., Safarpour, F., Thompson, C.S., Stewart, A.F., 2007. Extracellular ATP-dependent upregulation of the transcription cofactor LMO4 promotes neuron survival from hypoxia. *Exp Cell Res* 313, 3106-3116.

Chenn, A., Walsh, C.A., 2002. Regulation of cerebral cortical size by control of cell cycle exit in neural precursors. *Science* 297, 365-369.

Chenn, A., Zhang, Y.A., Chang, B.T., McConnell, S.K., 1998. Intrinsic polarity of mammalian neuroepithelial cells. *Mol Cell Neurosci* 11, 183-193.

Cleveland, W.S., 1981. Lowess: A program for smoothing scatterplots by robust locally weighted regression. *The American Statistician* 35, 54.

Coelho, D.J., Sims, D.J., Ruegg, P.J., Minn, I., Muench, A.R., Mitchell, P.J., 2005. Cell type-specific and sexually dimorphic expression of transcription factor AP-2 in the adult mouse brain. *Neuroscience* 134, 907-919.

Conti, L., Cattaneo, E., 2008. Novel and immortalization-based protocols for the generation of neural CNS stem cell lines for gene therapy approaches. *Methods Mol Biol* 438, 319-332.

Conti, L., Pollard, S.M., Gorba, T., Reitano, E., Toselli, M., Biella, G., Sun, Y., Sanzone, S., Ying, Q.L., Cattaneo, E., Smith, A., 2005. Niche-independent symmetrical self-renewal of a mammalian tissue stem cell. *PLoS Biol* 3, e283.

Conti, L., Reitano, E., Cattaneo, E., 2006. Neural stem cell systems: diversities and properties after transplantation in animal models of diseases. *Brain Pathol* 16, 143-154.

Cowley, G.P., Smith, M.E., 1996. Cadherin expression in melanocytic naevi and malignant melanomas. *J Pathol* 179, 183-187.

Cross, J.C., Baczyk, D., Dobric, N., Hemberger, M., Hughes, M., Simmons, D.G., Yamamoto, H., Kingdom, J.C., 2003. Genes, development and evolution of the placenta. *Placenta* 24, 123-130.

D'Arcangelo, G., Nakajima, K., Miyata, T., Ogawa, M., Mikoshiba, K., Curran, T., 1997. Reelin is a secreted glycoprotein recognized by the CR-50 monoclonal antibody. *J Neurosci* 17, 23-31.

Dehay, C., Giroud, P., Berland, M., Smart, I., Kennedy, H., 1993. Modulation of the cell cycle contributes to the parcellation of the primate visual cortex. *Nature* 366, 464-466.

Demyanenko, G.P., Schachner, M., Anton, E., Schmid, R., Feng, G., Sanes, J., Maness, P.F., 2004. Close homolog of L1 modulates area-specific neuronal positioning and dendrite orientation in the cerebral cortex. *Neuron* 44, 423-437.

den Hollander, A.I., Ghiani, M., de Kok, Y.J., Wijnholds, J., Ballabio, A., Cremers, F.P., Broccoli, V., 2002. Isolation of Crb1, a mouse homologue of *Drosophila* crumbs, and analysis of its expression pattern in eye and brain. *Mech Dev* 110, 203-207.

Desai, A.R., McConnell, S.K., 2000. Progressive restriction in fate potential by neural progenitors during cerebral cortical development. *Development* 127, 2863-2872.

Doetsch, F., Caille, I., Lim, D.A., Garcia-Verdugo, J.M., Alvarez-Buylla, A., 1999a. Subventricular zone astrocytes are neural stem cells in the adult mammalian brain. *Cell* 97, 703-716.

Doetsch, F., Garcia-Verdugo, J.M., Alvarez-Buylla, A., 1997. Cellular composition and three-dimensional organization of the subventricular germinal zone in the adult mammalian brain. *J Neurosci* 17, 5046-5061.

Doetsch, F., Garcia-Verdugo, J.M., Alvarez-Buylla, A., 1999b. Regeneration of a germinal layer in the adult mammalian brain. *Proc Natl Acad Sci U S A* 96, 11619-11624.

Doetsch, F., Petreanu, L., Caille, I., Garcia-Verdugo, J.M., Alvarez-Buylla, A., 2002. EGF converts transit-amplifying neurogenic precursors in the adult brain into multipotent stem cells. *Neuron* 36, 1021-1034.

Dorsky, R.I., Itoh, M., Moon, R.T., Chitnis, A., 2003. Two *tcf3* genes cooperate to pattern the zebrafish brain. *Development* 130, 1937-1947.

Easterday, M.C., Dougherty, J.D., Jackson, R.L., Ou, J., Nakano, I., Paucar, A.A., Roobini, B., Dianati, M., Irvin, D.K., Weissman, I.L., Terskikh, A.V., Geschwind, D.H., Kornblum, H.I., 2003. Neural progenitor genes. Germinal zone expression and analysis of genetic overlap in stem cell populations. *Dev Biol* 264, 309-322.

El-Hashash, A.H., Esbrit, P., Kimber, S.J., 2005. PTHrP promotes murine secondary trophoblast giant cell differentiation through induction of endocycle, upregulation of giant-cell-promoting transcription factors and suppression of other trophoblast cell types. *Differentiation* 73, 154-174.

Englund, C., Fink, A., Lau, C., Pham, D., Daza, R.A., Bulfone, A., Kowalczyk, T., Hevner, R.F., 2005. Pax6, Tbr2, and Tbr1 are expressed sequentially by radial glia, intermediate progenitor cells, and postmitotic neurons in developing neocortex. *J Neurosci* 25, 247-251.

Fagiolini, M., Pizzorusso, T., Berardi, N., Domenici, L., Maffei, L., 1994. Functional postnatal development of the rat primary visual cortex and the role of visual experience: dark rearing and monocular deprivation. *Vision Res* 34, 709-720.

Fagiolini, M., Pizzorusso, T., Porciatti, V., Cenni, M., Maffei, L., 1997. Transplant of Schwann cells allows normal development of the visual cortex of dark-reared rats. *Eur J Neurosci* 9, 102-112.

Fawcett, J.W., Asher, R.A., 1999. The glial scar and central nervous system repair. *Brain Res Bull* 49, 377-391.

Fode, C., Ma, Q., Casarosa, S., Ang, S.L., Anderson, D.J., Guillemot, F., 2000. A role for neural determination genes in specifying the dorsoventral identity of telencephalic neurons. *Genes Dev* 14, 67-80.

Frenkel, M.Y., Bear, M.F., 2004. How monocular deprivation shifts ocular dominance in visual cortex of young mice. *Neuron* 44, 917-923.

Frotscher, M., 1997. Dual role of Cajal-Retzius cells and reelin in cortical development. *Cell Tissue Res* 290, 315-322.

Furuta, Y., Piston, D.W., Hogan, B.L., 1997. Bone morphogenetic proteins (BMPs) as regulators of dorsal forebrain development. *Development* 124, 2203-2212.

Gabay, L., Lowell, S., Rubin, L.L., Anderson, D.J., 2003. Deregulation of dorsoventral patterning by FGF confers trilineage differentiation capacity on CNS stem cells in vitro. *Neuron* 40, 485-499.

Gage, F.H., 2002. Neurogenesis in the adult brain. *J Neurosci* 22, 612-613.

Gaiano, N., Nye, J.S., Fishell, G., 2000. Radial glial identity is promoted by Notch1 signalling in the murine forebrain. *Neuron* 26, 395-404.

Gal, J.S., Morozov, Y.M., Ayoub, A.E., Chatterjee, M., Rakic, P., Haydar, T.F., 2006. Molecular and morphological heterogeneity of neural precursors in the mouse neocortical proliferative zones. *J Neurosci* 26, 1045-1056.

Gardner, R.L., Davies, T.J., 2003. The basis and significance of pre-patterning in mammals. *Philos Trans R Soc Lond B Biol Sci* 358, 1331-1338; discussion 1338-1339.

Gaubatz, S., Imhof, A., Dosch, R., Werner, O., Mitchell, P., Buettner, R., Eilers, M., 1995. Transcriptional activation by Myc is under negative control by the transcription factor AP-2. *EMBO J* 14, 1508-1519.

Gauchat, D., Escriva, H., Miljkovic-Licina, M., Chera, S., Langlois, M.C., Begue, A., Laudet, V., Galliot, B., 2004. The orphan COUP-TF nuclear receptors are markers for neurogenesis from cnidarians to vertebrates. *Dev Biol* 275, 104-123.

Gentilini, M., and Santoni, F., 2006. FlagTrap, a bioinformatic pipeline to identify membrane proteins. CRS4 Technical Report 10.

Geschwind, D.H., Ou, J., Easterday, M.C., Dougherty, J.D., Jackson, R.L., Chen, Z., Antoine, H., Terskikh, A., Weissman, I.L., Nelson, S.F., Kornblum, H.I., 2001. A genetic analysis of neural progenitor differentiation. *Neuron* 29, 325-339.

Gianfranceschi, L., Fiorentini, A., Maffei, L., 1999. Behavioural visual acuity of wild type and bcl2 transgenic mouse. *Vision Res* 39, 569-574.

Gotz, M., Hartfuss, E., Malatesta, P., 2002. Radial glial cells as neuronal precursors: a new perspective on the correlation of morphology and lineage restriction in the developing cerebral cortex of mice. *Brain Res Bull* 57, 777-788.

Götz, M., Hartfuss, E., Malatesta, P., 2002. Radial glial cells as neuronal precursors: a new perspective on the correlation of morphology and lineage restriction in the developing cerebral cortex of mice. *Brain Res Bull* 57, 777-788.

Götz, M., Huttner, W.B., 2005. The cell biology of neurogenesis. *Nat Rev Mol Cell Biol* 6, 777-788.

Götz, M., Stoykova, A., Gruss, P., 1998. Pax6 controls radial glia differentiation in the cerebral cortex. *Neuron* 21, 1031-1044.

Grove, E.A., Fukuchi-Shimogori, T., 2003. Generating the cerebral cortical area map. *Annu Rev Neurosci* 26, 355-380.

Grove, E.A., Williams, B.P., Li, D.Q., Hajihosseini, M., Friedrich, A., Price, J., 1993. Multiple restricted lineages in the embryonic rat cerebral cortex. *Development* 117, 553-561.

Gulisano, M., Broccoli, V., Pardini, C., Boncinelli, E., 1996. Emx1 and Emx2 show different patterns of expression during proliferation and differentiation of the developing cerebral cortex in the mouse. *Eur J Neurosci* 8, 1037-1050.

Hack, M.A., Saghatelian, A., de Chevigny, A., Pfeifer, A., Ashery-Padan, R., Lledo, P.M., Gotz, M., 2005. Neuronal fate determinants of adult olfactory bulb neurogenesis. *Nature neuroscience* 8, 865-872.

Hack, M.A., Sugimori, M., Lundberg, C., Nakafuku, M., Gotz, M., 2004. Regionalization and fate specification in neurospheres: the role of Olig2 and Pax6. *Mol Cell Neurosci* 25, 664-678.

Hajihosseini, M., Iavachev, L., Price, J., 1993. Evidence that retroviruses integrate into post-replication host DNA. *Embo J* 12, 4969-4974.

Hand, R., Bortone, D., Mattar, P., Nguyen, L., Heng, J.I., Guerrier, S., Boutt, E., Peters, E., Barnes, A.P., Parras, C., Schuurmans, C., Guillemot, F., Polleux, F., 2005. Phosphorylation of Neurogenin2 specifies the migration properties and the dendritic morphology of pyramidal neurons in the neocortex. *Neuron* 48, 45-62.

Haremak, T., Tanaka, Y., Hongo, I., Yuge, M., Okamoto, H., 2003. Integration of multiple signal transducing pathways on Fgf response elements of the *Xenopus* caudal homologue Xcad3. *Development* 130, 4907-4917.

Hartfuss, E., Forster, E., Bock, H.H., Hack, M.A., LePrince, P., Luque, J.M., Herz, J., Frotscher, M., Gotz, M., 2003. Reelin signalling directly affects radial glia morphology and biochemical maturation. *Development* 130, 4597-4609.

Hartfuss, E., Galli, R., Heins, N., Gotz, M., 2001. Characterization of CNS precursor subtypes and radial glia. *Dev Biol* 229, 15-30.

Haubensak, W., Attardo, A., Denk, W., Huttner, W.B., 2004. Neurons arise in the basal neuroepithelium of the early mammalian telencephalon: a major site of neurogenesis. *Proc Natl Acad Sci U S A* 101, 3196-3201.

Haubst, N., Berger, J., Radjendirane, V., Graw, J., Favor, J., Saunders, G.F., Stoykova, A., Gotz, M., 2004. Molecular dissection of Pax6 function: the specific roles of the paired domain and homeodomain in brain development. *Development* 131, 6131-6140.

Heins, N., Malatesta, P., Cecconi, F., Nakafuku, M., Tucker, K.L., Hack, M.A., Chapouton, P., Barde, Y.A., Gotz, M., 2002. Glial cells generate neurons: the role of the transcription factor Pax6. *Nat Neurosci* 5, 308-315.

Hermanson, O., Sugihara, T.M., Andersen, B., 1999. Expression of LMO-4 in the central nervous system of the embryonic and adult mouse. *Cell Mol Biol (Noisy-le-grand)* 45, 677-686.

Hidalgo, J., Aschner, M., Zatta, P., Vasak, M., 2001. Roles of the metallothionein family of proteins in the central nervous system. *Brain Res Bull* 55, 133-145.

Hilger-Eversheim, K., Moser, M., Schorle, H., Buettner, R., 2000. Regulatory roles of AP-2 transcription factors in vertebrate development, apoptosis and cell-cycle control. *Gene* 260, 1-12.

Hirabayashi, Y., Itoh, Y., Tabata, H., Nakajima, K., Akiyama, T., Masuyama, N., Gotoh, Y., 2004. The Wnt/beta-catenin pathway directs neuronal differentiation of cortical neural precursor cells. *Development* 131, 2791-2801.

Hodge, R.D., Kowalczyk, T.D., Wolf, S.A., Encinas, J.M., Rippey, C., Enikolopov, G., Kempermann, G., Hevner, R.F., 2008. Intermediate progenitors in adult hippocampal neurogenesis: Tbr2 expression and coordinate regulation of neuronal output. *J Neurosci* 28, 3707-3717.

Holm, P.C., Mader, M.T., Haubst, N., Wizenmann, A., Sigvardsson, M., Gotz, M., 2007. Loss- and gain-of-function analyses reveal targets of Pax6 in the developing mouse telencephalon. *Mol Cell Neurosci* 34, 99-119.

Hong, S.M., Liu, Z., Fan, Y., Neumann, M., Won, S.J., Lac, D., Lum, X., Weinstein, P.R., Liu, J., 2007. Reduced hippocampal neurogenesis and skill reaching performance in adult Emx1 mutant mice. *Exp Neurol* 206, 24-32.

Iwasato, T., Datwani, A., Wolf, A.M., Nishiyama, H., Taguchi, Y., Tonegawa, S., Knopfel, T., Erzurumlu, R.S., Itoharu, S., 2000. Cortex-restricted disruption of NMDAR1 impairs neuronal patterns in the barrel cortex. *Nature* 406, 726-731.

Jager, R., Werling, U., Rimpf, S., Jacob, A., Schorle, H., 2003. Transcription factor AP-2gamma stimulates proliferation and apoptosis and impairs differentiation in a transgenic model. *Mol Cancer Res* 1, 921-929.

Jean, D., Gershenwald, J.E., Huang, S., Luca, M., Hudson, M.J., Tainsky, M.A., Bar-Eli, M., 1998. Loss of AP-2 results in up-regulation of MCAM/MUC18 and an increase in tumor growth and metastasis of human melanoma cells. *J Biol Chem* 273, 16501-16508.

Jung, C.G., Kim, H.J., Kawaguchi, M., Khanna, K.K., Hida, H., Asai, K., Nishino, H., Miura, Y., 2005. Homeotic factor ATBF1 induces the cell cycle arrest associated with neuronal differentiation. *Development* 132, 5137-5145.

Kasai, M., Satoh, K., Akiyama, T., 2005. Wnt signalling regulates the sequential onset of neurogenesis and gliogenesis via induction of BMPs. *Genes Cells* 10, 777-783.

Kashani, A.H., Qiu, Z., Jurata, L., Lee, S.K., Pfaff, S., Goebbels, S., Nave, K.A., Ghosh, A., 2006. Calcium activation of the LMO4 transcription complex and its role in the patterning of thalamocortical connections. *J Neurosci* 26, 8398-8408.

Kee, Y., Bronner-Fraser, M., 2001. Temporally and spatially restricted expression of the helix-loop-helix transcriptional regulator Id1 during avian embryogenesis. *Mech Dev* 109, 331-335.

Kee, Y., Bronner-Fraser, M., 2005. To proliferate or to die: role of Id3 in cell cycle progression and survival of neural crest progenitors. *Genes Dev* 19, 744-755.

- Kessarlis, N., Fogarty, M., Iannarelli, P., Grist, M., Wegner, M., Richardson, W.D., 2006. Competing waves of oligodendrocytes in the forebrain and postnatal elimination of an embryonic lineage. *Nat Neurosci* 9, 173-179.
- Key, G., Kubbutat, M.H., Gerdes, J., 1994. Assessment of cell proliferation by means of an enzyme-linked immunosorbent assay based on the detection of the Ki-67 protein. *J Immunol Methods* 177, 113-117.
- Kim, A.S., Anderson, S.A., Rubenstein, J.L., Lowenstein, D.H., Pleasure, S.J., 2001a. Pax-6 regulates expression of SFRP-2 and Wnt-7b in the developing CNS. *J Neurosci* 21, RC132.
- Kim, A.S., Lowenstein, D.H., Pleasure, S.J., 2001b. Wnt receptors and Wnt inhibitors are expressed in gradients in the developing telencephalon. *Mech Dev* 103, 167-172.
- Kim, C.H., Oda, T., Itoh, M., Jiang, D., Artinger, K.B., Chandrasekharappa, S.C., Driever, W., Chitnis, A.B., 2000. Repressor activity of Headless/Tcf3 is essential for vertebrate head formation. *Nature* 407, 913-916.
- Kosaka, K., Kosaka, T., 2007. Chemical properties of type 1 and type 2 periglomerular cells in the mouse olfactory bulb are different from those in the rat olfactory bulb. *Brain Res* 1167, 42-55.
- Kriegstein, A., Noctor, S., Martinez-Cerdeno, V., 2006. Patterns of neural stem and progenitor cell division may underlie evolutionary cortical expansion. *Nat Rev Neurosci* 7, 883-890.
- Kriegstein, A.R., Götz, M., 2003. Radial glia diversity: a matter of cell fate. *Glia* 43, 37-43.
- Kudoh, T., Wilson, S.W., Dawid, I.B., 2002. Distinct roles for Fgf, Wnt and retinoic acid in posteriorizing the neural ectoderm. *Development* 129, 4335-4346.
- Lagenaur, C., Schachner, M., 1981. Monoclonal antibody (M2) to glial and neuronal cell surfaces. *J Supramol Struct Cell Biochem* 15, 335-346.
- Lee, J., Sayegh, J., Daniel, J., Clarke, S., Bedford, M.T., 2005a. PRMT8, a new membrane-bound tissue-specific member of the protein arginine methyltransferase family. *J Biol Chem* 280, 32890-32896.
- Lee, M.K., Tuttle, J.B., Rebhun, L.I., Cleveland, D.W., Frankfurter, A., 1990. The expression and posttranslational modification of a neuron-specific beta-tubulin isotype during chick embryogenesis. *Cell Motil Cytoskeleton* 17, 118-132.
- Lee, S.K., Jurata, L.W., Nowak, R., Lettieri, K., Kenny, D.A., Pfaff, S.L., Gill, G.N., 2005b. The LIM domain-only protein LMO4 is required for neural tube closure. *Mol Cell Neurosci* 28, 205-214.
- Li, H., Goswami, P.C., Domann, F.E., 2006. AP-2gamma induces p21 expression, arrests cell cycle, and inhibits the tumor growth of human carcinoma cells. *Neoplasia* 8, 568-577.
- Li, M., Naidu, P., Yu, Y., Berger, N.A., Kannan, P., 2004. Dual regulation of AP-2alpha transcriptional activation by poly(ADP-ribose) polymerase-1. *Biochem J* 382, 323-329.
- Li, W., Cogswell, C.A., LoTurco, J.J., 1998. Neuronal differentiation of precursors in the neocortical ventricular zone is triggered by BMP. *J Neurosci* 18, 8853-8862.
- Liepelt, U., Kindler-Rohrborn, A., Lennartz, K., Reinhardt-Maelicke, S., Rajewsky, M.F., 1990. Differentiation potential of a monoclonal antibody-defined neural progenitor cell population isolated from prenatal rat brain by fluorescence-activated cell sorting. *Brain Res Dev Brain Res* 51, 267-278.
- Lin, X., Shah, S., Bulleit, R.F., 1996. The expression of MEF2 genes is implicated in CNS neuronal differentiation. *Brain Res Mol Brain Res* 42, 307-316.
- Lindsell, C.E., Boulter, J., diSibio, G., Gossler, A., Weinmaster, G., 1996. Expression patterns of Jagged, Delta1, Notch1, Notch2, and Notch3 genes identify ligand-receptor pairs that may function in neural development. *Mol Cell Neurosci* 8, 14-27.
- Liu, Q., Dwyer, N.D., O'Leary, D.D., 2000. Differential expression of COUP-TFI, CHL1, and two novel genes in developing neocortex identified by differential display PCR. *J Neurosci* 20, 7682-7690.

Lledo, P.M., Merkle, F.T., Alvarez-Buylla, A., 2008. Origin and function of olfactory bulb interneuron diversity. *Trends Neurosci*.

Lledo, P.M., Saghatelian, A., 2005. Integrating new neurons into the adult olfactory bulb: joining the network, life-death decisions, and the effects of sensory experience. *Trends Neurosci* 28, 248-254.

Lu, Q.R., Sun, T., Zhu, Z., Ma, N., Garcia, M., Stiles, C.D., Rowitch, D.H., 2002. Common developmental requirement for Olig function indicates a motor neuron/oligodendrocyte connection. *Cell* 109, 75-86.

Lu, X.P., Salbert, G., Pfahl, M., 1994. An evolutionary conserved COUP-TF binding element in a neural-specific gene and COUP-TF expression patterns support a major role for COUP-TF in neural development. *Mol Endocrinol* 8, 1774-1788.

Lu, Z., Je, H.S., Young, P., Gross, J., Lu, B., Feng, G., 2007. Regulation of synaptic growth and maturation by a synapse-associated E3 ubiquitin ligase at the neuromuscular junction. *J Cell Biol* 177, 1077-1089.

Lukaszewicz, A., Savatier, P., Cortay, V., Giroud, P., Huissoud, C., Berland, M., Kennedy, H., Dehay, C., 2005. G1 phase regulation, area-specific cell cycle control, and cytoarchitectonics in the primate cortex. *Neuron* 47, 353-364.

Lupo, G., Harris, W.A., Lewis, K.E., 2006. Mechanisms of ventral patterning in the vertebrate nervous system. *Nat Rev Neurosci* 7, 103-114.

Luskin, M.B., Parnavelas, J.G., Barfield, J.A., 1993. Neurons, astrocytes, and oligodendrocytes of the rat cerebral cortex originate from separate progenitor cells: an ultrastructural analysis of clonally related cells. *J Neurosci* 13, 1730-1750.

Luskin, M.B., Pearlman, A.L., Sanes, J.R., 1988. Cell lineage in the cerebral cortex of the mouse studied in vivo and in vitro with a recombinant retrovirus. *Neuron* 1, 635-647.

Lyons, G.E., Micales, B.K., Schwarz, J., Martin, J.F., Olson, E.N., 1995. Expression of *mef2* genes in the mouse central nervous system suggests a role in neuronal maturation. *J Neurosci* 15, 5727-5738.

Mabie, P.C., Mehler, M.F., Kessler, J.A., 1999. Multiple roles of bone morphogenetic protein signalling in the regulation of cortical cell number and phenotype. *J Neurosci* 19, 7077-7088.

Mabie, P.C., Mehler, M.F., Marmur, R., Papavasiliou, A., Song, Q., Kessler, J.A., 1997. Bone morphogenetic proteins induce astroglial differentiation of oligodendroglial-astroglial progenitor cells. *J Neurosci* 17, 4112-4120.

Malatesta, P., Hack, M.A., Hartfuss, E., Kettenmann, H., Klinkert, W., Kirchhoff, F., Gotz, M., 2003. Neuronal or glial progeny: regional differences in radial glia fate. *Neuron* 37, 751-764.

Malatesta, P., Hartfuss, E., Gotz, M., 2000. Isolation of radial glial cells by fluorescent-activated cell sorting reveals a neuronal lineage. *Development* 127, 5253-5263.

Mallamaci, A., Iannone, R., Briata, P., Pintonello, L., Mercurio, S., Boncinelli, E., Corte, G., 1998. EMX2 protein in the developing mouse brain and olfactory area. *Mech Dev* 77, 165-172.

Mallamaci, A., Muzio, L., Chan, C.H., Parnavelas, J., Boncinelli, E., 2000. Area identity shifts in the early cerebral cortex of *Emx2*^{-/-} mutant mice. *Nat Neurosci* 3, 679-686.

Maric, D., Maric, I., Chang, Y.H., Barker, J.L., 2003. Prospective cell sorting of embryonic rat neural stem cells and neuronal and glial progenitors reveals selective effects of basic fibroblast growth factor and epidermal growth factor on self-renewal and differentiation. *J Neurosci* 23, 240-251.

Martinez-Cerdeno, V., Noctor, S.C., Kriegstein, A.R., 2006. The role of intermediate progenitor cells in the evolutionary expansion of the cerebral cortex. *Cereb Cortex* 16 Suppl 1, i152-161.

Mason, H.A., Rakowiecki, S.M., Gridley, T., Fishell, G., 2006. Loss of notch activity in the developing central nervous system leads to increased cell death. *Dev Neurosci* 28, 49-57.

Matsumoto, S., Banine, F., Struve, J., Xing, R., Adams, C., Liu, Y., Metzger, D., Chambon, P., Rao, M.S., Sherman, L.S., 2006. Brg1 is required for murine neural stem cell maintenance and gliogenesis. *Dev Biol* 289, 372-383.

Mattar, P., Britz, O., Johannes, C., Nieto, M., Ma, L., Rebeyka, A., Klenin, N., Polleux, F., Guillemot, F., Schuurmans, C., 2004. A screen for downstream effectors of Neurogenin2 in the embryonic neocortex. *Dev Biol* 273, 373-389.

Mayer-Proschel, M., Kalyani, A.J., Mujtaba, T., Rao, M.S., 1997. Isolation of lineage-restricted neuronal precursors from multipotent neuroepithelial stem cells. *Neuron* 19, 773-785.

McConnell, S.K., 1995. Strategies for the generation of neuronal diversity in the developing central nervous system. *J Neurosci* 15, 6987-6998.

Mehler, M.F., Mabie, P.C., Zhu, G., Gokhan, S., Kessler, J.A., 2000. Developmental changes in progenitor cell responsiveness to bone morphogenetic proteins differentially modulate progressive CNS lineage fate. *Dev Neurosci* 22, 74-85.

Merkle, F.T., Tramontin, A.D., Garcia-Verdugo, J.M., Alvarez-Buylla, A., 2004. Radial glia give rise to adult neural stem cells in the subventricular zone. *Proc Natl Acad Sci U S A* 101, 17528-17532.

Misson, J.P., Edwards, M.A., Yamamoto, M., Caviness, V.S., Jr., 1988a. Identification of radial glial cells within the developing murine central nervous system: studies based upon a new immunohistochemical marker. *Brain Res Dev Brain Res* 44, 95-108.

Misson, J.P., Edwards, M.A., Yamamoto, M., Caviness, V.S., Jr., 1988b. Mitotic cycling of radial glial cells of the fetal murine cerebral wall: a combined autoradiographic and immunohistochemical study. *Brain Res* 466, 183-190.

Miyata, T., 2007. Asymmetric Cell Division During Brain Morphogenesis. *Progress in Molecular and Subcellular Biology*.

Miyata, T., Kawaguchi, A., Okano, H., Ogawa, M., 2001. Asymmetric inheritance of radial glial fibers by cortical neurons. *Neuron* 31, 727-741.

Miyata, T., Kawaguchi, A., Saito, K., Kawano, M., Muto, T., Ogawa, M., 2004. Asymmetric production of surface-dividing and non-surface-dividing cortical progenitor cells. *Development* 131, 3133-3145.

Mizuguchi, R., Sugimori, M., Takebayashi, H., Kosako, H., Nagao, M., Yoshida, S., Nabeshima, Y., Shimamura, K., Nakafuku, M., 2001. Combinatorial roles of olig2 and neurogenin2 in the coordinated induction of pan-neuronal and subtype-specific properties of motoneurons. *Neuron* 31, 757-771.

Mizutani, K., Yoon, K., Dang, L., Tokunaga, A., Gaiano, N., 2007. Differential Notch signalling distinguishes neural stem cells from intermediate progenitors. *Nature* 449, 351-355.

Mlodzik, M., 1999. Planar polarity in the Drosophila eye: a multifaceted view of signalling specificity and cross-talk. *EMBO J* 18, 6873-6879.

Molnar, Z., Metin, C., Stoykova, A., Tarabykin, V., Price, D.J., Francis, F., Meyer, G., Dehay, C., Kennedy, H., 2006. Comparative aspects of cerebral cortical development. *Eur J Neurosci* 23, 921-934.

Molyneaux, B.J., Arlotta, P., Menezes, J.R., Macklis, J.D., 2007. Neuronal subtype specification in the cerebral cortex. *Nat Rev Neurosci* 8, 427-437.

Mori, T., Buffo, A., Gotz, M., 2005. The novel roles of glial cells revisited: the contribution of radial glia and astrocytes to neurogenesis. *Curr Top Dev Biol* 69, 67-99.

Moser, M., Pscherer, A., Roth, C., Becker, J., Mucher, G., Zerres, K., Dixkens, C., Weis, J., Guay-Woodford, L., Buettner, R., Fassler, R., 1997. Enhanced apoptotic cell death of renal epithelial cells in mice lacking transcription factor AP-2beta. *Genes Dev* 11, 1938-1948.

Mukouyama, Y.S., Deneen, B., Lukaszewicz, A., Novitch, B.G., Wichterle, H., Jessell, T.M., Anderson, D.J., 2006. Olig2⁺ neuroepithelial motoneuron progenitors are not multipotent stem cells in vivo. *Proc Natl Acad Sci U S A* 103, 1551-1556.

Munoz-Sanjuan, I., A, H.B., 2001. Early posterior/ventral fate specification in the vertebrate embryo. *Dev Biol* 237, 1-17.

Muzio, L., DiBenedetto, B., Stoykova, A., Boncinelli, E., Gruss, P., Mallamaci, A., 2002. Conversion of cerebral cortex into basal ganglia in Emx2(-/-) Pax6(Sey/Sey) double-mutant mice. *Nat Neurosci* 5, 737-745.

Muzio, L., Mallamaci, A., 2003. Emx1, emx2 and pax6 in specification, regionalization and arealization of the cerebral cortex. *Cereb Cortex* 13, 641-647.

Nakamura, K., Hioki, H., Fujiyama, F., Kaneko, T., 2005. Postnatal changes of vesicular glutamate transporter (VGluT)1 and VGluT2 immunoreactivities and their colocalization in the mouse forebrain. *J Comp Neurol* 492, 263-288.

Nakashima, K., Takizawa, T., Ochiai, W., Yanagisawa, M., Hisatsune, T., Nakafuku, M., Miyazono, K., Kishimoto, T., Kageyama, R., Taga, T., 2001. BMP2-mediated alteration in the developmental pathway of fetal mouse brain cells from neurogenesis to astrocytogenesis. *Proc Natl Acad Sci U S A* 98, 5868-5873.

Nieto, M., Monuki, E.S., Tang, H., Imitola, J., Haubst, N., Khoury, S.J., Cunningham, J., Gotz, M., Walsh, C.A., 2004. Expression of Cux-1 and Cux-2 in the subventricular zone and upper layers II-IV of the cerebral cortex. *J Comp Neurol* 479, 168-180.

Nieto, M., Schuurmans, C., Britz, O., Guillemot, F., 2001. Neural bHLH genes control the neuronal versus glial fate decision in cortical progenitors. *Neuron* 29, 401-413.

Nikoletopoulou, V., Plachta, N., Allen, N.D., Pinto, L., Gotz, M., Barde, Y.A., 2007. Neurotrophin Receptor-Mediated Death of Misspecified Neurons Generated from Embryonic Stem Cells Lacking Pax6. *Cell Stem Cell* 1, 529-540.

Ninkovic, J., Götz, M., 2007. Signalling in adult neurogenesis: from stem cell niche to neuronal networks. *Curr Opin Neurobiol* 17, 338-344.

Noctor, S.C., Flint, A.C., Weissman, T.A., Dammerman, R.S., Kriegstein, A.R., 2001. Neurons derived from radial glial cells establish radial units in neocortex. *Nature* 409, 714-720.

Noctor, S.C., Flint, A.C., Weissman, T.A., Wong, W.S., Clinton, B.K., Kriegstein, A.R., 2002. Dividing precursor cells of the embryonic cortical ventricular zone have morphological and molecular characteristics of radial glia. *J Neurosci* 22, 3161-3173.

Noctor, S.C., Martinez-Cerdeno, V., Ivic, L., Kriegstein, A.R., 2004. Cortical neurons arise in symmetric and asymmetric division zones and migrate through specific phases. *Nat Neurosci* 7, 136-144.

Nolte, C., Matyash, M., Pivneva, T., Schipke, C.G., Ohlemeyer, C., Hanisch, U.K., Kirchhoff, F., Kettenmann, H., 2001. GFAP promoter-controlled EGFP-expressing transgenic mice: a tool to visualize astrocytes and astrogliosis in living brain tissue. *Glia* 33, 72-86.

Nosaka, T., Kawashima, T., Misawa, K., Ikuta, K., Mui, A.L., Kitamura, T., 1999. STAT5 as a molecular regulator of proliferation, differentiation and apoptosis in hematopoietic cells. *Embo J* 18, 4754-4765.

Ohba, H., Chiyoda, T., Endo, E., Yano, M., Hayakawa, Y., Sakaguchi, M., Darnell, R.B., Okano, H.J., Okano, H., 2004. Sox21 is a repressor of neuronal differentiation and is antagonized by YB-1. *Neurosci Lett* 358, 157-160.

Ohtsuka, T., Sakamoto, M., Guillemot, F., Kageyama, R., 2001. Roles of the basic helix-loop-helix genes Hes1 and Hes5 in expansion of neural stem cells of the developing brain. *J Biol Chem* 276, 30467-30474.

Olenik, C., Aktories, K., Meyer, D.K., 1999. Differential expression of the small GTP-binding proteins RhoA, RhoB, Cdc42u and Cdc42b in developing rat neocortex. *Brain Res Mol Brain Res* 70, 9-17.

Ono, K., Takebayashi, H., Ikeda, K., Furusho, M., Nishizawa, T., Watanabe, K., Ikenaka, K., 2008. Regional- and temporal-dependent changes in the differentiation of Olig2 progenitors in the forebrain, and the impact on astrocyte development in the dorsal pallium. *Dev Biol*.

Parras, C.M., Galli, R., Britz, O., Soares, S., Galichet, C., Battiste, J., Johnson, J.E., Nakafuku, M., Vescovi, A., Guillemot, F., 2004. Mash1 specifies neurons and oligodendrocytes in the postnatal brain. *Embo J* 23, 4495-4505.

Paul Horton, K.-J.P., Takeshi Obayashi & Kenta Nakai, 2006. Protein Subcellular Localization Prediction with WoLF PSORT. *Proceedings of the 4th Annual Asia Pacific Bioinformatics Conference APBC06*, Taipei, Taiwan, pp. 39-48.

Perissi, V., Menini, N., Cottone, E., Capello, D., Sacco, M., Montaldo, F., De Bortoli, M., 2000. AP-2 transcription factors in the regulation of ERBB2 gene transcription by oestrogen. *Oncogene* 19, 280-288.

Pimentel, D.O., Margrie, T.W., 2008. Glutamatergic transmission and plasticity between olfactory bulb mitral cells. *J Physiol* 586, 2107-2119.

Pinto, L., Gotz, M., 2007. Radial glial cell heterogeneity--the source of diverse progeny in the CNS. *Prog Neurobiol* 83, 2-23.

Pinto, L., Mader, M.T., Irmeler, M., Gentilini, M., Santoni, F., Drechsel, D., Blum, R., Stahl, R., Bulfone, A., Malatesta, P., Beckers, J., Gotz, M., 2008. Prospective isolation of functionally distinct radial glial subtypes--lineage and transcriptome analysis. *Mol Cell Neurosci* 38, 15-42.

Piper, M., Nurcombe, V., Reid, K., Bartlett, P., Little, M., 2002. N-terminal Slit2 promotes survival and neurite extension in cultured peripheral neurons. *Neuroreport* 13, 2375-2378.

Plachta, N., Bibel, M., Tucker, K.L., Barde, Y.A., 2004. Developmental potential of defined neural progenitors derived from mouse embryonic stem cells. *Development* 131, 5449-5456.

Pollard, S., Conti, L., Smith, A., 2006. Exploitation of adherent neural stem cells in basic and applied neurobiology. *Regen Med* 1, 111-118.

Pontious, A., Kowalczyk, T., Englund, C., Hevner, R.F., 2008. Role of intermediate progenitor cells in cerebral cortex development. *Dev Neurosci* 30, 24-32.

Porciatti, V., Pizzorusso, T., Maffei, L., 1999. The visual physiology of the wild type mouse determined with pattern VEPs. *Vision Res* 39, 3071-3081.

Price, J., Thurlow, L., 1988. Cell lineage in the rat cerebral cortex: a study using retroviral-mediated gene transfer. *Development* 104, 473-482.

Qian, X., Goderie, S.K., Shen, Q., Stern, J.H., Temple, S., 1998. Intrinsic programs of patterned cell lineages in isolated vertebrate CNS ventricular zone cells. *Development* 125, 3143-3152.

Qian, X., Shen, Q., Goderie, S.K., He, W., Capela, A., Davis, A.A., Temple, S., 2000. Timing of CNS cell generation: a programmed sequence of neuron and glial cell production from isolated murine cortical stem cells. *Neuron* 28, 69-80.

Qiu, M., Anderson, S., Chen, S., Meneses, J.J., Hevner, R., Kuwana, E., Pedersen, R.A., Rubenstein, J.L., 1996. Mutation of the Emx-1 homeobox gene disrupts the corpus callosum. *Dev Biol* 178, 174-178.

Rahaman, S.O., Harbor, P.C., Chernova, O., Barnett, G.H., Vogelbaum, M.A., Haque, S.J., 2002. Inhibition of constitutively active Stat3 suppresses proliferation and induces apoptosis in glioblastoma multiforme cells. *Oncogene* 21, 8404-8413.

Rainer, J., Sanchez-Cabo, F., Stocker, G., Sturn, A., Trajanoski, Z., 2006. CARMAweb: comprehensive R- and bioconductor-based web service for microarray data analysis. *Nucleic Acids Res* 34, W498-503.

- Rakic, P., 1995. A small step for the cell, a giant leap for mankind: a hypothesis of neocortical expansion during evolution. *Trends Neurosci* 18, 383-388.
- Rakic, P., 2002. Neurogenesis in adult primate neocortex: an evaluation of the evidence. *Nat Rev Neurosci* 3, 65-71.
- Ramalho-Santos, M., Yoon, S., Matsuzaki, Y., Mulligan, R.C., Melton, D.A., 2002. "Stemness": transcriptional profiling of embryonic and adult stem cells. *Science* 298, 597-600.
- Rao, M.S., 1999. Multipotent and restricted precursors in the central nervous system. *Anat Rec* 257, 137-148.
- Rash, J.E., Davidson, K.G., Kamasawa, N., Yasumura, T., Kamasawa, M., Zhang, C., Michaels, R., Restrepo, D., Ottersen, O.P., Olson, C.O., Nagy, J.I., 2005. Ultrastructural localization of connexins (Cx36, Cx43, Cx45), glutamate receptors and aquaporin-4 in rodent olfactory mucosa, olfactory nerve and olfactory bulb. *J Neurocytol* 34, 307-341.
- Ravizza, T., Moneta, D., Bottazzi, B., Peri, G., Garlanda, C., Hirsch, E., Richards, G.J., Mantovani, A., Vezzani, A., 2001. Dynamic induction of the long pentraxin PTX3 in the CNS after limbic seizures: evidence for a protective role in seizure-induced neurodegeneration. *Neuroscience* 105, 43-53.
- Reid, C.B., Walsh, C.A., 2002. Evidence of common progenitors and patterns of dispersion in rat striatum and cerebral cortex. *J Neurosci* 22, 4002-4014.
- Ridet, J.L., Malhotra, S.K., Privat, A., Gage, F.H., 1997. Reactive astrocytes: cellular and molecular cues to biological function. *Trends Neurosci* 20, 570-577.
- Ross, S.E., Greenberg, M.E., Stiles, C.D., 2003. Basic helix-loop-helix factors in cortical development. *Neuron* 39, 13-25.
- Ruiz i Altaba, A., 1998. Neural patterning. Deconstructing the organizer. *Nature* 391, 748-749.
- Russ, A.P., Wattler, S., Colledge, W.H., Aparicio, S.A., Carlton, M.B., Pearce, J.J., Barton, S.C., Surani, M.A., Ryan, K., Nehls, M.C., Wilson, V., Evans, M.J., 2000. Eomesodermin is required for mouse trophoblast development and mesoderm formation. *Nature* 404, 95-99.
- Sakamoto, K., Yoshida, S., Ikegami, K., Minakami, R., Kato, A., Udo, H., Sugiyama, H., 2007. Homer1c interacts with Hippi and protects striatal neurons from apoptosis. *Biochem Biophys Res Commun* 352, 1-5.
- Sapin, V., Bouillet, P., Oulad-Abdelghani, M., Dastugue, B., Chambon, P., Dolle, P., 2000. Differential expression of retinoic acid-inducible (Stra) genes during mouse placentation. *Mech Dev* 92, 295-299.
- Sauer, F.C., 1935a. Mitosis in the neural tube. *J. Comp. Neurol.* 62, 377-405.
- Sauer, F.C., 1935b. Mitosis in the neural tube. *J. Comp. Neurol.* 62, 377-405.
- Sawtell, N.B., Frenkel, M.Y., Philpot, B.D., Nakazawa, K., Tonegawa, S., Bear, M.F., 2003. NMDA receptor-dependent ocular dominance plasticity in adult visual cortex. *Neuron* 38, 977-985.
- Schorle, H., Meier, P., Buchert, M., Jaenisch, R., Mitchell, P.J., 1996. Transcription factor AP-2 essential for cranial closure and craniofacial development. *Nature* 381, 235-238.
- Schreiber, J., Enderich, J., Sock, E., Schmidt, C., Richter-Landsberg, C., Wegner, M., 1997. Redundancy of class III POU proteins in the oligodendrocyte lineage. *J Biol Chem* 272, 32286-32293.
- Schuurmans, C., Armant, O., Nieto, M., Stenman, J.M., Britz, O., Klenin, N., Brown, C., Langevin, L.M., Seibt, J., Tang, H., Cunningham, J.M., Dyck, R., Walsh, C., Campbell, K., Polleux, F., Guillemot, F., 2004. Sequential phases of cortical specification involve Neurogenin-dependent and -independent pathways. *Embo J* 23, 2892-2902.
- Schwartz, B., Melnikova, V.O., Tellez, C., Mourad-Zeidan, A., Blehm, K., Zhao, Y.J., McCarty, M., Adam, L., Bar-Eli, M., 2007. Loss of AP-2alpha results in deregulation of E-

cadherin and MMP-9 and an increase in tumorigenicity of colon cancer cells in vivo. *Oncogene* 26, 4049-4058.

Seri, B., Garcia-Verdugo, J.M., Collado-Morente, L., McEwen, B.S., Alvarez-Buylla, A., 2004. Cell types, lineage, and architecture of the germinal zone in the adult dentate gyrus. *J Comp Neurol* 478, 359-378.

Seri, B., Garcia-Verdugo, J.M., McEwen, B.S., Alvarez-Buylla, A., 2001. Astrocytes give rise to new neurons in the adult mammalian hippocampus. *J Neurosci* 21, 7153-7160.

Shen, Q., Wang, Y., Dimos, J.T., Fasano, C.A., Phoenix, T.N., Lemischka, I.R., Ivanova, N.B., Stifani, S., Morrissey, E.E., Temple, S., 2006. The timing of cortical neurogenesis is encoded within lineages of individual progenitor cells. *Nat Neurosci* 9, 743-751.

Shi, D., Kellems, R.E., 1998. Transcription factor AP-2gamma regulates murine adenosine deaminase gene expression during placental development. *J Biol Chem* 273, 27331-27338.

Shiraishi, Y., Mizutani, A., Yuasa, S., Mikoshiba, K., Furuichi, T., 2004. Differential expression of Homer family proteins in the developing mouse brain. *J Comp Neurol* 473, 582-599.

Shou, J., Rim, P.C., Calof, A.L., 1999. BMPs inhibit neurogenesis by a mechanism involving degradation of a transcription factor. *Nat Neurosci* 2, 339-345.

Sif, S., Stukenberg, P.T., Kirschner, M.W., Kingston, R.E., 1998. Mitotic inactivation of a human SWI/SNF chromatin remodeling complex. *Genes Dev* 12, 2842-2851.

Simone, C., 2006. SWI/SNF: the crossroads where extracellular signalling pathways meet chromatin. *J Cell Physiol* 207, 309-314.

Sivak, J.M., West-Mays, J.A., Yee, A., Williams, T., Fini, M.E., 2004. Transcription Factors Pax6 and AP-2alpha Interact To Coordinate Corneal Epithelial Repair by Controlling Expression of Matrix Metalloproteinase Gelatinase B. *Mol Cell Biol* 24, 245-257.

Smart, I.H., Dehay, C., Giroud, P., Berland, M., Kennedy, H., 2002. Unique morphological features of the proliferative zones and postmitotic compartments of the neural epithelium giving rise to striate and extrastriate cortex in the monkey. *Cereb Cortex* 12, 37-53.

Soriano, E., Del Rio, J.A., 2005. The cells of cajal-retzius: still a mystery one century after. *Neuron* 46, 389-394.

Stenman, J., Toresson, H., Campbell, K., 2003a. Identification of two distinct progenitor populations in the lateral ganglionic eminence: implications for striatal and olfactory bulb neurogenesis. *J Neurosci* 23, 167-174.

Stenman, J.M., Wang, B., Campbell, K., 2003b. Tlx controls proliferation and patterning of lateral telencephalic progenitor domains. *J Neurosci* 23, 10568-10576.

Stewart, H.J., Brennan, A., Rahman, M., Zoidl, G., Mitchell, P.J., Jessen, K.R., Mirsky, R., 2001. Developmental regulation and overexpression of the transcription factor AP-2, a potential regulator of the timing of Schwann cell generation. *Eur J Neurosci* 14, 363-372.

Stoykova, A., Treichel, D., Hallonet, M., Gruss, P., 2000. Pax6 modulates the dorsoventral patterning of the mammalian telencephalon. *J Neurosci* 20, 8042-8050.

Sugimori, M., Nagao, M., Bertrand, N., Parras, C.M., Guillemot, F., Nakafuku, M., 2007. Combinatorial actions of patterning and HLH transcription factors in the spatiotemporal control of neurogenesis and gliogenesis in the developing spinal cord. *Development* 134, 1617-1629.

Sun, Y., Nadal-Vicens, M., Misono, S., Lin, M.Z., Zubiaga, A., Hua, X., Fan, G., Greenberg, M.E., 2001. Neurogenin promotes neurogenesis and inhibits glial differentiation by independent mechanisms. *Cell* 104, 365-376.

Tabor, R., Friedrich, R.W., 2008. Pharmacological analysis of ionotropic glutamate receptor function in neuronal circuits of the zebrafish olfactory bulb. *PLoS ONE* 3, e1416.

Takahashi, T., Nowakowski, R.S., Caviness, V.S., Jr., 1995. The cell cycle of the pseudostratified ventricular epithelium of the embryonic murine cerebral wall. *J Neurosci* 15, 6046-6057.

Tanaka, S., Kunath, T., Hadjantonakis, A.K., Nagy, A., Rossant, J., 1998. Promotion of trophoblast stem cell proliferation by FGF4. *Science* 282, 2072-2075.

Tarabykin, V., Stoykova, A., Usman, N., Gruss, P., 2001. Cortical upper layer neurons derive from the subventricular zone as indicated by *Svet1* gene expression. *Development* 128, 1983-1993.

Temple, S., Alvarez-Buylla, A., 1999. Stem cells in the adult mammalian central nervous system. *Curr Opin Neurobiol* 9, 135-141.

Temple, S., Qian, X., 1995. bFGF, neurotrophins, and the control of cortical neurogenesis. *Neuron* 15, 249-252.

Tokunaga, A., Kohyama, J., Yoshida, T., Nakao, K., Sawamoto, K., Okano, H., 2004. Mapping spatio-temporal activation of Notch signalling during neurogenesis and gliogenesis in the developing mouse brain. *J Neurochem* 90, 142-154.

Tramontin, A.D., Garcia-Verdugo, J.M., Lim, D.A., Alvarez-Buylla, A., 2003. Postnatal development of radial glia and the ventricular zone (VZ): a continuum of the neural stem cell compartment. *Cereb Cortex* 13, 580-587.

Tripodi, M., Filosa, A., Armentano, M., Studer, M., 2004. The COUP-TF nuclear receptors regulate cell migration in the mammalian basal forebrain. *Development* 131, 6119-6129.

Tse, E., Smith, A.J., Hunt, S., Lavenir, I., Forster, A., Warren, A.J., Grutz, G., Foroni, L., Carlton, M.B., Colledge, W.H., Boehm, T., Rabbitts, T.H., 2004. Null mutation of the *Lmo4* gene or a combined null mutation of the *Lmo1/Lmo3* genes causes perinatal lethality, and *Lmo4* controls neural tube development in mice. *Mol Cell Biol* 24, 2063-2073.

Turner, D.L., Cepko, C.L., 1987. A common progenitor for neurons and glia persists in rat retina late in development. *Nature* 328, 131-136.

Walsh, C., Cepko, C.L., 1993. Clonal dispersion in proliferative layers of developing cerebral cortex. *Nature* 362, 632-635.

Wang, D., Shin, T.H., Kudlow, J.E., 1997. Transcription factor AP-2 controls transcription of the human transforming growth factor- α gene. *J Biol Chem* 272, 14244-14250.

Weigmann, A., Corbeil, D., Hellwig, A., Huttner, W.B., 1997. Prominin, a novel microvilli-specific polytopic membrane protein of the apical surface of epithelial cells, is targeted to plasmalemmal protrusions of non-epithelial cells. *Proc Natl Acad Sci U S A* 94, 12425-12430.

Werling, U., Schorle, H., 2002a. Conditional inactivation of transcription factor AP-2gamma by using the Cre/loxP recombination system. *Genesis* 32, 127-129.

Werling, U., Schorle, H., 2002b. Transcription factor gene AP-2 gamma essential for early murine development. *Mol Cell Biol* 22, 3149-3156.

Williams, B.P., Price, J., 1995. Evidence for multiple precursor cell types in the embryonic rat cerebral cortex. *Neuron* 14, 1181-1188.

Wu, S.X., Goebbels, S., Nakamura, K., Nakamura, K., Kometani, K., Minato, N., Kaneko, T., Nave, K.A., Tamamaki, N., 2005. Pyramidal neurons of upper cortical layers generated by NEX-positive progenitor cells in the subventricular zone. *Proc Natl Acad Sci U S A* 102, 17172-17177.

Xu, D., Hopf, C., Reddy, R., Cho, R.W., Guo, L., Lanahan, A., Petralia, R.S., Wenthold, R.J., O'Brien, R.J., Worley, P., 2003. Narp and NP1 form heterocomplexes that function in developmental and activity-dependent synaptic plasticity. *Neuron* 39, 513-528.

Yadav, A., Kalita, A., Dhillon, S., Banerjee, K., 2005. JAK/STAT3 pathway is involved in survival of neurons in response to insulin-like growth factor and negatively regulated by suppressor of cytokine signalling-3. *J Biol Chem* 280, 31830-31840.

Yoon, K., Gaiano, N., 2005. Notch signalling in the mammalian central nervous system: insights from mouse mutants. *Nat Neurosci* 8, 709-715.

Young, K.M., Merson, T.D., Sotthibundhu, A., Coulson, E.J., Bartlett, P.F., 2007. p75 neurotrophin receptor expression defines a population of BDNF-responsive neurogenic precursor cells. *J Neurosci* 27, 5146-5155.

Zhou, Q., Anderson, D.J., 2002. The bHLH transcription factors OLIG2 and OLIG1 couple neuronal and glial subtype specification. *Cell* 109, 61-73.

Zimmer, C., Tiveron, M.C., Bodmer, R., Cremer, H., 2004. Dynamics of Cux2 expression suggests that an early pool of SVZ precursors is fated to become upper cortical layer neurons. *Cereb Cortex* 14, 1408-1420.

10 Acknowledgements

I would like to thank to:

Magdalena Götz, for being my excellent supervisor. I thank her for sharing always with me her knowledge, enthusiasm, creativity and great ideas. She helped me modulating my scientific way of thinking, encouraged me and supported me.

Mücella Öcallan, Markus Körbs, Annette Bust, Angelika Waiser, Andrea Steiner, Detlef Franzen and Timucin Öztürk for excellent technical assistance.

Marie-Theres Schmid, Jovica Ninkovic, Pratibha Tripathi, Leanne Godinho, Dilek Ertürk, Franziska Weinandy, Christian Böhringer, Benedikt Berninger, Monika Brill, Marcos Costa, Ruth Beckervordersandforth-Bonk, Maki Asami, Tessa Walcher, Ronny Stahl, Robert Blum for great scientific discussions and for creating a happy lab environment.

Daniela Dreschel and Marion Betizeau for being great students and for their help on my projects.

Portuguese Fundação para a Ciência e Tecnologia/European Social Fund for their money support.

My parents and my husband for supporting me always and in every regard.

No duty is more urgent than that of returning thanks!

"We cannot live only for ourselves. A thousand fibers connect us with our fellowmen; and along those fibers, as sympathetic threads, our actions run as causes, and they come back to us as effects."

Herman Melville

"Happiness lies in the joy of achievement and the thrill of creative effort."

Franklin D. Roosevelt

11 Curriculum vitae

PERSONAL DATA

Name:

Luísa Alexandra Meireles Pinto

Place of Work:

Helmholtz Zentrum München German Research Center for Environment and
Health (GmbH)

ISF – Institute of Stem Cell

Ingolstädter Landstr. 1

D-85764 Neuherberg

Munich

Germany

Address (private):

Riesstr. 65, App. 243

80993 - Munich

Germany

Email: lampinto@clix.pt; luisa.pinto@helmholtz-muenchen.de

Age:

Born March 10th, 1981

Marital Status:

Married

Birth Place:

Vila Verde, Portugal

EDUCATION

Finished the High School with the average score of 18 (scale 0 to 20) in July 1999.

Finished my diploma (estágio), with the supervision of Dr. Ernest Arenas, in the Laboratory of Molecular Neurobiology, Medical Biochemistry and Biophysics, Karolinska Institute, Stockholm, with the average score of 19 (scale 0 to 20), from October 2003 to June 2004

Finished the Biochemistry Course in the Department of Biochemistry of the University of Coimbra with the average score of 16 (scale 0 to 20) in July 2004

Finishing the PhD (doctor degree), with the supervision of Dr. Magdalena Götz, in the Institute of Stem Cell, Helmholtz Zentrum München German Research Center for Environment and Health (GmbH), Munich, Germany - supported by the Portuguese Fundação para a Ciência e Tecnologia/European Social Fund.

FOREIGN LANGUAGES

Good knowledge of English – English course of the Universal English-BBC London (not finished); and English lessons for seven years

Has some knowledge of French and Spanish

PERSONAL INTERESTS AND OTHER ACTIVITIES

Playing piano (lessons for 3 years).

Singing lessons for 4 years

Practice some sports: Volleyball, badminton, dance, aerobics, hydro gymnastic

Member of the Biochemistry Students Group of the Academic Association of Coimbra in 2003

Member of the National Association of Biochemistry (ANBioq)

Organization of the I National Meeting of Biochemistry Students in Coimbra, 2003

CONGRESSES AND CONFERENCES

2000:

XII NATIONAL MEETING OF BIOCHEMISTRY, September 28-30, Póvoa do Varzim, Portugal

2001:

II PROFESSIONAL JOURNIES, by ANBIOQ (National Association of Biochemistry), October 1-3, Coimbra University
(Attended lectures — personal interest)

2002:

JORNADAS ALBERT NETTER – GENETICS AND BIOTECHNOLOGY IN GENECOLOGY, 1-2 March, Coimbra, Portugal

XIII NATIONAL BIOCHEMISTRY CONGRESS, 5-7 December, Lisboa, Portugal.

MOLECULAR CELL BIOLOGY-lectures, November 18-22, IBILI, Coimbra, Portugal (personal interest)

2003:

I NATIONAL MEETING OF BIOCHEMISTRY STUDENTS, April 25-27, Coimbra, Portugal

2004:

MEDICAL BIOCHEMISTRY AND BIOPHYSICS CONFERENCE, March 11-12, Stockholm, Sweden

4th FORUM OF EUROPEAN NEUROSCIENCE - FENS, July 10-14, Lisbon, Portugal

2005

3rd Munich Symposium on “Cell dynamics: from molecular structure to cellular motility”, October 5-7, Biocenter of the Ludwig-Maximilians-University, Munich, Germany

2006

International Conference “EMBRYONIC AND SOMATIC STEM CELLS – REGENERATIVE SYSTEMS FOR CELL AND TISSUE REPAIR“ 2nd Biennial Leopoldina Conference, September 24-27, Dresden, Germany

2007

IBRO Satellite Meeting on Neural Development “Stem cells, axon guidance and cell migration in the developing and adult brain”, July 8-12, Cairns, Australia

7th IBRO World Congress of Neuroscience, July 12-17, Melbourne, Australia

2008

International Conference “Cortical Development Meeting”, May 22-25, Crete, Greece

POSTER PRESENTATION

2004:

From stem cells to midbrain dopaminergic neurons

Anita Hall, Julianna Kele Olovsson, Luisa Pinto, Carmen Ramirez, Carmen Salto and Ernest Arenas.

Laboratory of Molecular Neurobiology, Medical Biochemistry and Biophysics, Karolinska Institute, 17177 Stockholm, Sweden.

(Presented in the MBB (Medical Biochemistry and Biophysics) Conference, March 11-12th, Stockholm, 2004)

2005:

Ventral midbrain glia modulate dopaminergic neuron development by secreting Wnts

Gonçalo Castelo-Branco, Kyle Sousa, Vitezslav Bryja, Luisa Pinto, Joseph Wagner and Ernest Arenas

Laboratory of Molecular Neurobiology, Medical Biochemistry and Biophysics, Karolinska Institute, 17177 Stockholm, Sweden.

(Presented in the “Stem Cells Keystone”, Canadá, 2005)

2007:

Transcriptional profile of neurogenic versus non-neurogenic radial glial cells in the developing cortex

Luisa Pinto¹, Michael Mader¹, Martin Irmeler², Alessandro Bulfone³ and Magdalena Götz¹

¹ GSF -Institute of Stem cell Research, Neuherberg-Munich, Germany

² GSF - Institute of Experimental Genetics, Neuherberg, Germany

³ Stem Cell Research Institute, Dibrat, H.S. Raffaele, Milan, Italy

(Presented in the IBRO Satellite Meeting on Neural Development, Cairns, and IBRO World Congress of Neuroscience, Melbourne, Australia, 2007)

2008:

AP2 γ regulates basal progenitor fate and upper layer neuron specification in the mouse cerebral cortex

Luisa Pinto, Daniela Drechsel, Marie-Theres Schmid, Jovica Ninkovic, Martin Irmeler, Francois Guillemot, Johannes Beckers, Colette Dehay, Nada Zecevic, Hubert Schorle and Magdalena Götz

Helmholtz Center Munich, Institute for Stem Cell Research, Neuherberg/Munich, Germany

(Presented in the Cortical Development Meeting, Crete, 2008)

PUBLICATIONS

Gonçalo Castelo-Branco, Kyle Sousa, Vitezslav Bryja, **Luísa Pinto**, Joseph Wagner and Ernest Arenas (2005), “Ventral midbrain glia express region-specific transcription factors and regulate dopaminergic neurogenesis through Wnt-5a secretion”. *Mol Cell Neurosci*. 2006 Feb;31(2):251-62. Epub 2005 Oct 21

Luisa Pinto, Magdalena Götz, “Radial Glial cell heterogeneity-The source of diverse progeny in the CNS”, *Prog Neurobiol*. 2007 Sep;83(1):2-23. Epub 2007 March 7

Vassiliki Nikolettou, Nicolas Plachta, Nicolas D. Allen, **Luisa Pinto**, Magdalena Götz and Yves-Alain Barde, “Neurotrophin receptor-mediated death of misspecified neurons derived from embryonic stem cells lacking Pax6”, *Cell Stem Cell*, Vol 1, 529-540, 15 November 2007

Luisa Pinto, Michael T. Mader, Martin Irmeler, Marco Gentilini, Federico Santoni, Daniela Drechsel, Robert Blum, Ronny Stahl, Alessandro Bulfone, Paolo Malatesta, Johannes Beckers, and Magdalena Götz, “Prospective isolation of functionally distinct radial glial subtypes – lineage and transcriptome analysis”, *Mol Cell Neurosci*, Vol 38, 15-42, May 2008

Anita C. Hall, Sonia Bonilla, **Luisa Pinto**, Alessio Attardo, Magdalena Götz, Wieland B. Huttner, and Ernest Arenas, “Identification of floor plate radial glia as neurogenic progenitors of midbrain dopaminergic neurons”, *Glia*, Vol 56(8), 809-20, Jun2 2008

Luisa Pinto, Daniela Drechsel, Marie-Theres Schmid, Jovica Ninkovic, Martin Irmeler, Monika Brill, Laura Restani, Laura Gianfranceschi, Johannes Beckers, Francois Guillemot, Matteo Caleo, Victor Tarabykin, Kristin Baer, Colette Dehay, Nada Zecevic, Hubert Schorle and Magdalena Götz, “The transcription factor AP2 γ regulates basal progenitor fate and affects both the number of layer II/III neurons and function in the visual cortex”, manuscript submitted for publication to *Neuron*